PETROGENESIS OF DUNITE, WEHRLITE AND WEBSTERITE XENOLITHS FROM KIMBERLEY, SOUTH AFRICA: ORIGIN AS MANTLE PERIDOTITES OR CUMULATES

Dissertation

zur Erlangung des Grades

Doktor der Naturwissenschaften

am Fachbereich

Chemie, Pharmazie und Geowissenschaften

der Johannes Gutenberg-Universität Mainz

Tatjana Rehfeldt

geboren am 16. Juli 1975 in Berlin

Mainz, 2007

A dissertation submitted to the

Geosciences Institute of the Johannes Gutenberg University Mainz

in fulfilment of the requirements for the degree of

Doctor rerum naturalium

Dekan:

1. Berichterstatter:

2. Berichterstatter:

Tag der mündlichen Prüfung:

PREFACE

This doctoral thesis includes results of my research at the University of Mainz in cooperation with the Carnegie Institution of Washington, Institution of Terrestrial Magnetism and the Department of Geology of the Royal Holloway University of London between 2003-2007.

The second part of the thesis is published in the Journal of Petrology:

Rehfeldt, T., Jacob, D.E., Carlson R.W. and Foley, S.F. (2007): Fe-rich dunite xenoliths from south African kimberlites: Cumulates from Karoo flood basalts. Journal of Petrology, doi: 10.1093/petrology/egm023.

This part has co-authors as listed above, their contributions are mentioned in the acknowledgments of this thesis.

CONTENTS

SUMMARY

Dunite, wehrlite and websterite xenoliths occur amongst a large abundance of mantle xenoliths in kimberlites of the Kimberley cluster in South Africa. They have mostly been neglected for the study of mantle petrology up to know. On the basis of texture, major and trace elements, oxygen isotopes as well as Re-Os isotope characteristics, they can be subdivided into two groups. A coarse-grained mantle peridotite group, comprising dunite, wehrlite and websterite xenoliths, that are similar to fertile peridotites and represent upper mantle assemblages that are differently stong influenced by mantle metasomatism. And a cumulate group, containing fine-grained Fe-rich dunite xenoliths that represent cumulates of flood basalt magmatism related to the ~183 Ma Karoo and the ~2.7 Ga Ventersdorp events in southern Africa.

Dunite, wehrlite and websterite xenoliths have preserved a complex history of melt depletion and metasomatic re-enrichment events, which gives not only information about the different re-enrichment stages of the subcratonic lithospheric mantle, but also about spatial differences within the Kaapvaal craton upper mantle. Websterite xenoliths comprise orthopyroxene (40-85 Vol. %), clinopyroxene (5-42 Vol. %), garnet (4-10 Vol. %) and subordinately olivine (0-33 Vol. %), while dunite and wehrlite xenoliths contain predominantly olivine (65-100 Vol %) and subordinately orthopyroxene, clinopyroxene and garnet. High melt depletion and a dunitic to harzburgitic protolith composition are reflected by high forsterite (Fo_{90-92}) and high olivine NiO contents (2800-5000 ppm) in dunite, wehrlite and websterite xenoliths and high orthopyroxene Mg# (Mg/(Mg+Fe)) of 0.91-0.93 in dunite and wehrlite xenoliths. Re-depletion ages of predominantly 2.9 Ga reflect a minimum age of melt depletion. Melt depletion ceased in conjunction with collision of the Kimberley block with the Witwatersrand block ~2.9 Ga ago. Subduction related re-fertilisation of the previously depleted mantle xenoliths is documented by i) amoeboid textured orthopyroxene, clinopyroxene and garnet, which crystallized in schlieren along olivine grain boundaries, ii) high whole-rock SiO_2, Al_2O_3, CaO, TiO_2, FeO contents, iii) low oxygen isotope ratios in clinopyroxene and garnet of 4.8-5.4 ‰ and 4.7-5.3 ‰, respectively and iv) trace element compositions of wehrlitic clinopyroxene and garnet in equilibrium with high-pressure partial melts of eclogite. Trace element disequilibrium of orthopyroxene with clinopyroxene and garnet indicates a separate origin for orthopyroxene, on the one side as primary mantle orthopyroxene in dunite and wehrlite xenoliths and on the other side as reaction product with Si-rich melts produced by low temperature partial melting of eclogite. This reaction triggered the replacement of olivine by orthopyroxene in the surrounding mantle and produces the typical Si-rich composition of Kaapvaal mantle peridotites. Partial melting of eclogite at higher temperatures produced a second metasomatic melt with lower SiO_2, but higher Al_2O_3, CaO,

FeO, Ti, Zr, Hf and a low oxygen isotope ratio. This melt triggered clinopyroxene and locally garnet and rutile crystallization in percolation veins, replacing olivine and orthopyroxene in large parts of the Kaapvaal upper mantle. Additionally, websterite xenoliths have experienced late stage cryptic metasomatism by a hybrid silico-carbonatite melt (kimberlite), changing the trace element composition of clinopyroxene, orthopyroxene and garnet to different extents. Hence websterite and most fertile lherzolite xenoliths have experienced three metasomatic events: i) reaction with high-Si melt (>60 wt. % SiO_2), ii) percolation of subduction related silica melt with lower SiO_2 content and iii) cryptic metasomatism by kimberlite. In contrast, dunite and wehrlite xenoliths have only experienced the second metasomatic event. They represent mantle lithologies further away from metasomatising agents.

The Fe-rich dunites mainly comprise olivine neoblasts with subordinate olivine porphyroclasts and parallel-orientated needles of ilmenite, which enclose spinel in some samples. The lower forsterite and NiO contents of olivine in Fe-rich dunites compared to mantle peridotite xenoliths (Fo_{87-89} vs. Fo_{93-95} and 1300-2800ppm vs. 2200-3900 ppm, respectively), rules out a restitic origin. Cr-rich spinels are remnants of the original cumulate mineralogy that survived a late stage metasomatic overprint related to the production of the host kimberlite, producing ilmenite and phlogopite in some samples. Olivine porphyroclasts and neoblasts have different trace element compositions, the latter having higher Ti, V, Cr and Ni and lower Zn, Zr and Nb contents, indicating contrasting origins for neoblasts and porphyroclasts. The dunites have high $^{187}Os/^{188}Os$ ratios (0.11-0.15) indicating young (Phanerozoic) model ages for most samples, whereas three samples show isotopic mixtures between Phanerozoic neoblasts and ancient porphyroclastic material. Most Fe-rich dunite xenoliths can be interpreted as cumulates of fractional crystallization of Karoo flood basalt magmatism, whereas the porphyroclasts are interpreted to be remnants from the much earlier Archaean Ventersdorp magmatic episode.

ACKNOWLEDGMENTS

This work has only been accomplished because of the help and friendship of many different people all around the world. They inspired my work on mantle xenoliths, geochemistry and mantle petrology and always supported me during the course of the study of geology in Greifswald and the spezialisation in mantle petrology in Mainz. Here I acknowledge the help of my most important sopporters.

INTRODUCTION

1. Archaean cratons

Cratons are the oldest and tectonically most stable parts of the continents. They are surrounded by younger mobile belts, amalgamating continental crust to the cratonic continent cores. Archaean cratons occur within all continents, e.g. in North America the Slave, Superior and Wyoming Cratons, in South America the Amazonian Craton, in Africa the Kaapvaal and Zimbabwe Cratons and the Kongo Craton, in northern Europe the Karelian-Belomorian-Kola, Volgo-Uralian and Sarmatian Cratons, in eastern Russia the Siberian Craton, in China the Tarim, Yangtze and Sino-Korean Craton and in Australia the Yilgarn and Pilbara Cratons. These cratons comprise typical Archaean magmatic rocks, such as tonalite – trondhjemite - granodiorite complexes (TTGs), picritic basalts and komatiites. Additionally greenstone-belts are unique to the Archaean, comprising Archaean sedimentary rocks. The development of such for millions of years tectonically stable crust early in the Earth's history has been intensely debated in literature (see Kröner, 1985) and two kinds of evolutionary models are discussed, a uniformitarian, postulating plate-tectonics to have worked upon the Earth back to the earliest Archaean (Drummond and Defant, 1990; Nutman et al., 1993) and evolutionary models unique to the Archaean. The latter may involve many different processes: i) delamination of lower eclogitic crust and crust formation due to upwelling mantle material (Zegers and van Keken, 2001; van Thienen et al., 2004), ii) large convection and periodic mantle overturn leading to massive melting and strong depletion of the upper mantle (Griffin et al., 2003b; van Thienen et al., 2004) and iii) widespread plume activity causing large scale melting and crustal growth (Pearson et al., 1995a; Windley, 1998; van Thienen et al., 2004). These Archaean cratonic areas are economically important due to the occurrence of diamonds within kimberlite diatremes, which are volatile-rich magmas that penetrate the cratonic upper mantle and crust during highly explosive eruptions, picking up wall-rocks (amongst others diamonds from more than 120 km depth) along the way to the Earth's surface (e.g. Skinner, 1989).

2. Evolution of the Kaapvaal Craton

The Kaapvaal Craton is an Archaean Craton in southern Africa covering an area of about 1.2 million km^2, occupying large areas of South Africa, Swaziland, Lesotho and extending into Botswana, Zimbabwe and Mozambique. It is surrounded by several mobile belts, on the eastern side the Jurassic Lebombo monocline, to the south the Namaqua-Natal mobile belt (ca. 1.1-1.9 Ga) and to the west the Kheis over thrust belt (ca. 2.0 Ga; de Wit et al., 1992). To the north the Kaapvaal craton experienced a himalayan-type continent-

continent collision with the Zimbabwe craton at 2.68±0.05 Ga (de Wit et al., 1992), which evolved the Limpopo mobile belt that was pressed between the two cratons. While the crust beneath the Kaapvaal craton is about 35 km thick (James et al., 2003), the crust beneath the surrounding mobile belts has a thickness of about 42 km (de Wit et al., 1992). Above the Moho the crust of the Kaapvaal craton has a density of about 2.86 g/cm^3, appropriate for felsic and intermediate rock compositions. This is different in younger crust, where mafic rock compositions dominate the lower crust. The craton is characterized by low heat flow (~45 mW/m^2) and diamondiferous kimberlites, while the surrounding mobile belts have higher heat flow (~80 mW/m^2) and diamond-barren kimberlites which indicates a lithosphere thickness underneath the craton of >120 km (de Wit et al., 1992).

The Kaapvaal Craton consists of several sub-domains, that become younger from east to west and were welded together during several periods of continental crust formation and collision. The oldest sub-domain is the Ancient Gneiss Complex of the Barberton terrains (~3.5 Ga; Tegtmeyer and Kröner, 1987). It represents a piece of early oceanic lithosphere, which was obducted onto a volcanic arc-like terrain. According to mantle xenoliths (Dokolowayo kimberlite, Swaziland) from this area the lithospheric mantle of the oldest part of the Kaapvaal craton consisted of metasomatic peridotites and basalts (eclogite). The overlying crust was a mixture of mafic (greenstone), and tonalitic-trondhjemitic (granite) rocks (Tankard et al., 1982). The youngest Archaean stabilization event of the Kaapvaal craton juxtaposed two main domains, an eastern domain (Witwatersrand Block) ca. 3.5 Ga old and a younger western domain (Kimberley Block) which is mostly post 3.2 Ga old (de Wit et al., 1992). They were juxtaposed by an episode of subduction and terrain collision at about 2.9 Ga. Subduction occurred beneath the Kimberley block culminating in collisional suturing in the vicinity of the Colesberg lineament (Schmitz et al., 2004). The amalgamation of the Kimberley Block and Witwatersrand Block can be seen in the episodic diamond genesis of diamonds from Kimberley (Richardson et al. 2001, Shirey et al. 2003), Koffifontein (Pearson et al. 1998, Shirey et al. 2003), Jwaneng, Orapa (Shirey et al. 2003) and Pretoria. Here diamonds have Re-Os modal ages culminating in a twofold evolution (Proterozoic ca. 1.5 Ga and Archaean ca. 2.9 Ga) of the Kaapvaal craton near the Colesberg lineament. The Kaapvaal Craton has been essentially stable since 2.6 Ga (de Wit et al., 1992). There are some areas within the Kaapvaal Craton, which have also experienced younger tectonic events, for example the north-central part was disturbed ca. 2.05 Ga ago by the major intracratonic Bushvelt plutonic event (Hoal, 2003; Grégoire et al., 2005).

Two periods of flood basalt magmatism have been identified in southern Africa, penetrating and probably overprinting the cratonic upper mantle (Griffin et al., 2005). One of those events is the Archaean Ventersdorp flood basalt magmatism (~2.7 Ga; Crow and Condie, 1988), which produced a fractionated rock series comprising from bottom to top

basaltic to felsic volcanics (Crow and Condie, 1987). The much younger Karoo flood basalt event occurred within a relative short time period in the late Jurassic (184 to 179 Ma; Duncan et al., 1997) and covered large areas. Igneous rocks of the Karoo flood basalt event have been identified all over southern Africa, in Antarctica and Australia, which made up the Gondwana supercontinent at that time. It comprises voluminous volcanic basalt sequences (e.g. Lesotho; Marsh et al., 1997) and plutonic feeder dyke series (e.g. Lebombo-Nuanetsi region; Ellam and Cox, 1989; Sweeney et al., 1994).

The youngest volcanic event that penetrated the Kaapvaal cratonic upper mantle and crust is the kimberlite volcanism. In southern Africa two kimberlite types can be distinguished according to their isotopic signature, petrography, content of xenoliths/xenocrysts and whole-rock chemistry (Skinner, 1989). Group I kimberlites (basaltic) are 1600 to 50 Ma old and developed from a relatively poorly light rare earth element (LREE) enriched lithosphere. Group II kimberlites (micaceous), which are up to know only identified in South Africa (Verwoerd, 1992), have ages of 200 to 110 Ma and are generated in a more LREE-enriched lithosphere (Allsopp and Barrett, 1975; Davis, 1977). This indicates that the mantle source is undifferentiated to slightly depleted relative to bulk earth (Smith, 1983; Pearson et al., 1995b). While the Group I kimberlites are widely distributed, Group II kimberlites occur only in a belt between Sutherland and Swaziland.

3. Sampling the Earth's upper mantle

The mantle comprises 80 % by volume of the Earth and is amongst other things essentially important for understanding the composition of the Earth's crust. To study the composition and physical processes of the Earth's mantle geologists use indirect and direct methods. On the one hand, seismic models, analysis of gravity anomalies and heat flow measurements help to identify different rock domains within the Earth's mantle and crust (e.g. Tankard et al., 1982; de Wit et al., 1992; Priestley et al., 2006). On the other hand, analysis of mantle samples that were brought to the Earth's surface via many different processes provides means to analyse the mantle directly.

Despite modern methods large areas of the Earth's mantle remain inaccessible for geologists. The Earth's crust has an average thickness of ~5 km underneath the oceans and ~35 km underneath the continents. Up to know, the Earth's upper mantle is only accessible at slow mid-ocean spreading ridges such as the Gakkel Ridge north of Iceland (e.g. Hellebrand et al., 2002). The deepest bore-hole made in a continental setting is ~12 km deep and has just reached the upper crust lower crust transition zone (Kola peninsula). Other mantle pieces accessible for geologists are found in orogenic settings, in ophiolites or as xenoliths in basaltic and kimberlitic volcanic rocks. In orogenic settings the upper mantle is

squeezed up during mountain building processes as seen in the Ronda and Beni Bousera peridotite complexes in Spain and Marocco, the Lherz orogenic peridotite in the Pyrenees, which is the type locality for lherzolite, and the Horoman peridotite in Japan. Ophiolites such as the Oman ophiolite, the Troodos and Othris ophiolites in Greece or the Bay of Islands ophiolite in Newfoundland are blocks of oceanic crust and upper mantle that were obducted during plate collision. Usually they have preserved the complete oceanic crust-mantle section, comprising pelagic sediments on top and further down pillow lavas, sheeted gabbro dykes, mafic gabbro cumulates, ultramafic cumulates and depleted and fertile mantle peridotites. Especially on the Oman ophiolite extensive studies of the well exposed mantle section has lead to the theory of melt percolation in dunite and websterite veins within the peridotitic mantle (Kelemen et al., 1992). Orogenic peridotite massifs and ophiolite complexes represent large pieces, many kilometres long, of the cratonic and oceanic crust and mantle, respectively. Their upper mantle mineralogy is often strongly altered; olivine is totally serpentinized. Due to slow ascent rates during obduction these complexes show intensive metamorphic re-equilibration to lower pressures and temperatures.

Small pieces of the upper Earth's mantle have also been brought to the Earth's surface by fast ascending melts and can be found in volcanic settings all over the world. They are carried to the Earth's surface by mantle-derived basaltic or kimberlitic melts. Compared to orogenic peridotites and ophiolites, mantle peridotite xenoliths have the advantage of fresh and unaltered compositions, due to the fast ascent within the host melt. A disadvantage is their small sample size (few centimetres). Basalt-borne and kimberlite-borne mantle xenoliths differ in the dominance of spinel-bearing assemblages in basalt and garnet-bearing assemblages in kimberlite. This indicates, that basaltic melts rather sample shallower levels of the upper mantle since spinel is stable to up to 60 km depth, while kimberlitic melts come from higher depth and sample the upper mantle at deeper levels.

4. Xenoliths in kimberlites of the Kaapvaal Craton

An important contribution to decipher the evolution of the Kaapvaal craton has been made by studying xenoliths in kimberlites (e.g. Nixon and Boyd, 1973; MacGregor, 1975; Gurney and Harte, 1980; Boyd and Mertzman, 1987; Gurney et al., 1991; Pearson et al., 1995a; Stiefenhofer et al., 1997; Konzett et al., 1998; Menzies et al., 1999; Zhang et al., 2000; Irvine et al., 2001; Carlson and Moore, 2004; Griffin et al., 2004). Kimberlites are very abundant within the Kaapvaal craton and have penetrated and sampled the cratonic upper mantle and crust 200 to 50 Ma ago (e.g. Allsopp and Barrett, 1975; Davis, 1977). Such ultramafic xenoliths, identified in the kimberlites of the Kaapvaal craton are peridotites (lherzolites, harzburgites, websterites, wehrlites and dunite), eclogites, mica - amphibole -

rutile - ilmenite - diopside (MARID) suite and phlogopite - ilmenite - clinopyroxene (PIC) suite xenoliths and megacrysts (clinopyroxene, olivine, garnet and ilmenite).

Peridotite xenoliths comprise olivine, orthopyroxene, clinopyroxene and garnet in different amounts and are the most abundant ultramafic xenolith type found in the Kimberley kimberlite cluster (Gurney and Harte, 1980). Their chemical composition is mostly depleted in basaltic elements (e.g. Al_2O_3, FeO, CaO, TiO_2), but often a re-enrichment in compatible trace elements has been reported. Peridotite xenoliths are interpreted to represent mantle rocks, which have experienced high degree of partial melting and afterwards several episodes of metasomatic re-enrichment (Gurney et al., 1991; Stiefenhofer et al., 1997; Konzett et al., 2000; Zhang et al., 2001; Simon et al., 2002; Grégoire et al., 2003; Rehfeldt et al., 2007; Simon et al., 2007; page 78 of this thesis).

Eclogite xenoliths are mainly bimineralic, comprising garnet and clinopyroxene. They can be totally absent in kimberlite diatrems or may dominate the xenolith suite (e.g. Roberts Victor). They have mostly basaltic bulk-rock compositions (Coleman et al., 1965). Eclogite xenoliths originate either as subducted altered oceanic crust, having a plagioclase-bearing protolith that was transformed into eclogite at high pressure (e.g. Jagoutz et al., 1984; Neal et al., 1990; Yaxley and Green, 1998b; Jacob and Foley, 1999; Jacob, 2004; Kogiso and Hirschmann, 2006). Sometimes additional depletion by partial melting of these eclogites within the upper mantle gives rise to TTG melts (e.g. Barth et al., 2001; Aulbach et al., 2002; Barth et al., 2002a). On the other hand a cumulatic origin from subduction-related melts within the Earth's mantle has been proposed (e.g. McCandless and Gurney, 1986; Barth et al., 2002b; Schulze et al., 2003; Schmickler et al., 2004). Archaean oceanic crust was probably thicker than modern-day oceanic crust, due to a higher heat-flow, which produced higher influx of melt (Bickle et al., 1994). The thought, that such a thick oceanic crust could not subduct into the Earth's mantle gave rise to the delamination theory for Archaean tectonics (e.g. Zegers and van Keken, 2001; Foley et al., 2003a; Bédard, 2006) and may hint at the existence of subducted lower oceanic crust cumulates, that are preserved next to eclogite xenoliths since the Archaean within the upper mantle (Foley et al., 2003b). Such oceanic cumulates might be represented by dunite, wehrlite or websterite xenoliths, as found within the Kimberley kimberlite cluster. This was one working hypothesis for the present thesis.

MARID and PIC xenoliths mainly comprise secondary metasomatic minerals such as phlogopite, ilmenite, diopside, K-richterite and rutile (e.g. Dawson and Smith, 1977; Gurney and Harte, 1980). They are enriched in incompatible elements such as Mg, Fe, Ti, K, Rb and LREE, but depleted in Al (Dawson, 1987a). They are related to metasomatised mantle peridotites in which a similar secondary mineral paragenesis can be found, having higher Al and Mg contents inherited from the primary mantle assemblage (Waters et al., 1989;

Grégoire et al., 2003). MARID suite xenoliths have U-Pb model ages in zircon of 80 to 140 Ma (Konzett et al., 1998) older than the host group I kimberlite, similar to group II kimberlites. The presence of amphibole in these xenoliths suggests crystallization at low pressure (<100 km) from a kimberlitic melt in veinlets under oxidizing conditions (Dawson and Smith, 1977) by olivine fractionation and exsolution of a carbonatitic component (Konzett et al., 1998).

Megacrysts or discrete nodules are large crystals (>1 cm) of olivine, garnet, clinopyroxene, orthopyroxene, ilmenite or phlogopite often found in kimberlites (e.g. Gurney et al., 1979; Gurney and Harte, 1980; Hops et al., 1986; Schulze, 1987). Megacrysts are interpreted to represent kimberlite phenocrysts which crystallized at high pressure from a proto-kimberlitic melt, fractionating a parent kimberlitic magma (e.g. Mitchell, 1987). They can be subdivided into a Cr-rich and a Cr-poor group (Gurney and Harte, 1980). The Cr-rich suite represents high-pressure cumulates, which fractionate the kimberlite melt and leads to crystallization of Cr-poor megacrysts consecutively (e.g. Moore, 1987; Schulze, 1987). Their close relationship with deformed peridotites suggest crystallization within the thermal aureole of the kimberlite magma (Mercier, 1979; Moore and Belousova, 2005). Ilmenite megacrysts have often intensive exsolution textures indicating different redox conditions within the upper Earth's mantle (Haggerty and Tompkins, 1983) or high-temperature deformation and recrystallisation during initial stages of kimberlite formation (Mitchell, 1973). Both, clinopyroxene-ilmenite and clinopyroxene-phlogopite intergrowth and garnet exsolution from clinopyroxene are interpreted to be due to fragmentation of the kimberlitic cumulates and remixing during transport in the host magma (Mitchell, 1987). In the second part of this study, Fe-rich dunite xenoliths, interpreted to be cumulates of flood basalt magmatism, are compared in detail with the cumulatic kimberlite olivine megacrysts.

Ultramafic xenoliths of the present study have been collected from the Yachts Club Dump in 2002 and the Boshof Road Dump in 2004. These dumps are produced during extensive diamond extraction from kimberlites of the Kimberley kimberlite cluster, comprising of large amounts of crustal and mantle xenoliths. The Kimberley kimberlites are located close to the town of Kimberley in the Orange Free State, Republic of South Africa. They have sampled large amounts of upper mantle material of the Archaean Kaapvaal cratonic mantle. The petrological and geochemical composition of dunite, wehrlite and websterite xenoliths of this study is summarized in the Appendix.

CONTRASTING TYPES OF METASOMATISM IN DUNITE, WEHRLITE AND WEBSTERITE XENOLITHS FROM KIMBERLEY, SOUTH AFRICA

Abstract

Dunite, wehrlite and websterite xenoliths are rare members of the mantle xenolith suite within the Kimberley kimberlites of the Kaapvaal craton in Southern Africa. They can be ordered together with fertile peridotite xenoliths in a sequence of decreasing metasomatism: websterite, fertile peridotite, wehrlite and dunite xenoliths, respectively. Websterite xenoliths comprise high proportions of orthopyroxene and subordinately clinopyroxene, garnet and olivine, while dunite and wehrlite xenoliths comprise predominantly olivine and subordinately, clinopyroxene, garnet and orthopyroxene. Clinopyroxene, orthopyroxene and garnet in dunite, wehrlite and websterite xenoliths have clear metasomatic amoeboid textures, replacing olivine and/or orthopyroxene. The higher their abundance in mantle xenoliths, the closer the rock is situated to metasomatising agents such as veins of melt percolation.

Mineral major element compositions in dunite, wehrlite and websterite xenoliths are similar to Kaapvaal mantle peridotite xenoliths. The xenoliths experienced a high degree of partial melting (>30 %) prior to metasomatism, indicated by a high Mg# (Mg/(Mg+Fe)) of silicate minerals (Fo_{89-93}, pyroxene Mg# 0.88-0.93 and garnet Mg# 0.72-0.85), high Cr# (Cr/(Cr+Al)) of spinel (0.53-0.84) and mostly low whole-rock SiO_2, CaO and Al_2O_3 contents. Re-Os systematics indicate melt depletion ~2.9 Ga ago. It produced refractory dunites and harzburgites, precursory rocks of the studied dunite, wehrlite and webtserite xenoliths.

Subduction of oceanic crust shortly before collision of the western Kimberley block and eastern Witwatersrand block at ~2.9 Ga produced Si-rich melts (>60 wt. % SiO_2), which originated from partial melting of eclogite at low temperatures (<1300 °C). This melt reacted with the surrounding refractory mantle changing olivine into orthopyroxene and producing the typical orthopyroxene rich mantle lithology of the Kaapvaal craton. Oxygen isotope compositions of clinopyroxene and garnet in dunite, wehrlite and websterite xenoliths are lighter than typical mantle, also indicating a subduction related metasomatic origin. Partial melting of eclogite at higher temperature changes the melt composition, higher amounts of melt are produced, percolating larger areas of the mantle, enriching it in CaO, Al_2O_3, FeO and high field strength elements and crystallizing clinopyroxene and garnet, which have positive Zr-Hf and slight negative to positive Ti anomalies; this indicates subalkaline melt compositions.

In contrast, low HFSE and high REE compositions of clinopyroxene and garnet in websterite and most fertile peridotite xenoliths reflect late stage cryptic metasomatism by peralkaline melt (kimberlite) only affecting assemblages close to the metasomatising melt.

1. Introduction

Mantle xenoliths retrieved from kimberlites in southern Africa have helped to understand the different processes that have changed and modified the Kaapvaal subcratonic lithospheric mantle. Dunite, wehrlite and websterite xenoliths are rare but important members of the xenolith suite found in the Kimberley kimberlites of the Kaapvaal Craton. They represent two end-members of metasomatic re-enrichment of a former strongly depleted sublithospheric upper mantle (e.g. Gurney and Harte, 1980; Boyd and Mertzman, 1987; Pearson et al., 1995a; Griffin et al., 1999a; Carlson and Moore, 2004; Schmitz et al., 2004). Websterites represent assemblages close to metasomatising agents such as subducted oveanic crust or veins of melt percolation. They have experienced several metasomatic overprints. Dunite and wehrlite xenoliths exhibit only a slight metasomatic overprint and represent more distal mantle lithologies. Fertile mantle peridotites, dominating the xenolith suite at Kimberely (Nixon and Boyd, 1973; Gurney and Harte, 1980), are very similar to the websterite xenoliths of this study, also representing strongly metasomatised lithologies of the Kaapvaal sublithospheric upper mantle (Erlank et al., 1987; Konzett et al., 2000; Grégoire et al., 2003; Simon et al., 2003; Simon et al., 2007). Several features of Kaapvaal mantle peridotites and their origin are controversially discussed in literature, the overall SiO_2 or orthopyroxene-rich nature, compared to mantle peridotites from oceanic settings (Boyd, 1989b; Boyd et al., 1997) and the possibility of silicate melt (Stachel and Harris, 1997; van Achterbergh et al., 2001; Simon et al., 2007) and/or carbonatitic/kimberlitic melt metasomatism (Griffin et al., 1999b; van Achterbergh, 2004). Metasomatism is interpreted to have refertilized the whole mantle section beneath the Kaapvaal Craton (e.g. Griffin et al., 2003b).

We report mineral major and trace element compositions, whole-rock major elements, oxygen isotopes in silicate minerals and olivine, furthermore whole-rock Re/Os systematics in dunite, wehrlite and websterite xenoliths found in the kimberlites of the Kimberley cluster. A sequence of near vein assemblages to assemblages away from veins can be established (websterite, fertile peridotite, wehrlite, dunite), that reflect complex and spatially distributed re-enrichment processes within the Kaapvaal Craton, documenting modal metasomatism by high silicate to moderately silicate melts and cryptic metasomatism by a kimberlite precursor melt. This metasomatism triggered diverse refertilisation of the Kaapvaal upper mantle.

2. Geological setting of the Kimberley area

The creation of the western Kaapvaal cratonic nucleus is manifested in 3.2 Ga old harzburgitic diamond inclusions from Kimberley (e.g. Richardson et al., 2004). Mantle peridotites of the Kimberley block have Re-Os model ages that culminate at 2.5-3.0 Ga (Pearson et al., 1995a; Carlson et al., 1999; Irvine et al., 2001; Simon et al., 2003), indicating strong depletion of the protolith during that time, related to mantle wedge melting (Stachel et al., 1998; Schmitz et al., 2004) or partial melting at low pressure in an intraoceanic rift setting (Simon et al., 2007). Subduction of oceanic crust has been well-constrained to have occurred at 2.9 Ga from eclogite xenoliths of the Kimberley kimberlites (Jagoutz et al., 1984; Menzies et al., 1999; Richardson et al., 2001). At this time two main domains of the Kaapvaal Craton were juxtaposed onto each other, the western Kimberley Block onto the eastern Witwatersrand Block close to the Colesberg lineament (de Wit et al., 1992; Schmitz et al., 2004).

2.1. Metasomatism in relation to magmatic events in the Kimberley area

The sublithospheric upper mantle of the Kaapvaal Craton has a complex metasomatic history. The cause and effect of the metasomatic overprint is intensely debated in literature: if fluid or melt and if carbonatitic, kimberlitic or silicate melt. An enrichment of the upper mantle in Ti, Fe, K, light rare earth elements (LREE) and other large ion lithophile elements (LILE) due to metasomatism is widely accepted (e.g. Menzies et al., 1987). But this enrichement can cause two kinds of metasomatism: i) cryptic metasomatism, changing the chemical composition of the primary minerals (Dawson, 1984) or ii) modal metasomatism by crystallization of new phases (Harte, 1983), such as pyroxene, garnet, phlogopite, amphibole, rutile or ilmenite at the expense of the primary phases (Mitchell, 1973; Carswell, 1975; Harte et al., 1987; Hawkesworth et al., 1990; Winterburn et al., 1990; Simon et al., 2002; Grégoire et al., 2003; Simon et al., 2003). Metasomatic features in Kaapvaal mantle peridotites can be related to several geological events within the Kaapvaal craton.

1) The above described subduction event at ~2.9 Ga has been related to several metasomatic features found in Kaapvaal mantle peridotites: i) orthopyroxene, clinopyroxene, garnet and phlogopite crystallization in the mantle wegde from Si-rich rhyodacitic melts released at low pressure from subducted basalt in equilibrium with carbonated eclogite (Green, 2000; Simon et al., 2003), ii) garnet modification or precipitation from highly fractionated melts or fluids, that are derived from the asthenosphere or from recycled oceanic crust (e.g. Griffin et al., 1999b; Simon et al., 2003; van Achterbergh, 2004) and iii) cryptic overprint of clinopyroxene and garnet or crystallisation of clinopyroxene in the peridotite wall-rock caused by carbonatitic melts

released during melting of carbonated eclogite of the subducted slab at high pressure (Green, 2000; van Achterbergh, 2004).

2) The ~200 Ma Karoo flood basalt magmatism (Duncan et al., 1997) has been identified as a metasomatic event (Erlank et al., 1980; Hawkesworth et al., 1990; Griffin et al., 2003a). Additionally, Fe-rich dunite xenoliths found in kimberlites of the Kimberley area are interpreted to be cumulates of large igneous province magmatism (Dawson et al., 1981; Rehfeldt et al., 2007 page 78 in this thesis).

3) Kimberlite production within the upper mantle (at ~200 Ma Group II kimberlites and at ~90 Ma Goup I kimberlites; Smith, 1983; Skinner, 1989) lead to the crystallization of secondary phlogopite, K-richterite, diopside and Lindsleyite-Mathiasite (LIMA) minerals (e.g. Erlank et al., 1980; Hawkesworth et al., 1990). Cumulatic mica-amphibole-rutile-ilmenite-diopside (MARID) suite and phlogopite-ilmenite-clinopyroxene (PIC) suite xenoliths are interpreted to have crystallized directly from these kimberlitic melts (e.g. Dawson and Smith, 1977; Konzett et al., 1998). Additionally, they have been identified inducing metasomatism within the sublithospheric upper mantle (e.g. Dawson, 1987a; Waters et al., 1989; Griffin et al., 2003a; Rehfeldt et al., 2007). From such high alkaline silicate melts, that are precursory melts of kimberlites, clinopyroxene has crystallized. It is enriched in LREE and LILE and depleted in Ti, Nb, Ta, Zr and Hf (e.g. Dawson, 1987b; Konzett et al., 2000; Grégoire et al., 2003; Simon et al., 2003).

On the one hand, chemical zonation of silicate minerals can account for a young overprint of the xenoliths (Glaser et al., 1999). With incorporation of mantle peridotite xenoliths within Group I kimberlites (~86 Ma; Allsopp and Barrett, 1975; Davis, 1977) in the Kimberley area a last overprint of kimberlite infiltration along grain boundaries occurred. On the other hand, how long textural disequilibrium can persist in the sublithospheric upper mantle has not been resolved yet.

3. Samples and analytical methods

For this study six dunite, eight wehrlite and four websterite xenoliths have been analysed petrographically and geochemically. They are a few centimetres to up to 30 cm large and show small brownish reaction rims (1 mm – 1 cm) and veins penetrating the samples (1 – 2 mm wide to up to 2 cm long) due to the high reactivity of the host kimberlite. These alteration areas were avoided during sample preparation. The samples are part of a new collection from the Boshof Road dump, Northern Cape Province, South Africa. Except samples AJE362, AJE400 and AJE401 that were provided by the University of Cape Town (RSA) and are part of the A.J.Erlank collection. The samples are by-products of diamond mining at the DuToitspan, Bultfontein and Kimberley kimberlite pipes. The Kimberley group

of kimberlites is found close to the town of Kimberley, RSA and was emplaced during the Cretaceous at 86 ± 3 Ma (Allsopp and Barrett, 1975; Davis, 1977). All kimberlites of the Kimberley cluster are Group I kimberlites (Smith, 1983; LeRoex et al., 2003). Apart from the dunite, wehrlite and websterite xenoliths, Kimberley kimberlites contain lherzolitic and harzburgitic mantle xenoliths (e.g. Carswell and Dawson, 1970; Gurney and Harte, 1980; Erlank et al., 1987; Hawkesworth et al., 1990; Schulze, 1995; Griffin et al., 1999b; Dawson, 2004), eclogite xenoliths (e.g. Boyd and Nixon, 1978; MacGregor and Manton, 1986; Jacob et al., 2005), MARID xenoliths (e.g. Dawson and Smith, 1977; Waters et al., 1989; Konzett et al., 1998; Grégoire et al., 2003), as well as cumulate dunite xenoliths (e.g. Dawson et al., 1981; Rehfeldt et al., 2007 page 81 in this thesis).

The modal composition of dunite, wehrlite and websterite xenoliths has been determined in two ways: i) graphically using a grey scale image of the samples and the free software ScionImage (Table 1) and ii) by mass balanced calculation using mineral major element compositions (determined with an electron microprobe) and whole-rock major element compositions (determined by X-ray fluorescence analysis; XRF). The results of the second method were used to check that minor phases, such as rutile, ilmenite and phlogopite, had not been overestimated during the graphical modal composition determination.

The major element composition of olivine, clinopyroxene, orthopyroxene, garnet, spinel, ilmenite, rutile and phlogopite was analysed on polished thin sections with a JEOL JXA 8900 RL electron microprobe at the Department of Geosciences, Johannes Gutenberg-University of Mainz, Germany, and the Centre of Earth Sciences of the Georg-August-University Göttingen, Germany, using wavelength dispersive analysis and a range of natural and synthetic standards (Table 2 to Table 7). The data were corrected using the CITZAF procedure (Armstrong, 1995), and detection limits were between 0.01 and 0.07 wt. %. Fluorine in phlogopite had detection limits of 0.17 wt. %.

The whole-rock major element composition was calculated using the modal and mineral major element compositions of the xenolith samples (data from Table 1 to Table 7). Additionally, major elements of some samples were measured on fused discs by standard X-ray fluorescence (MagiXPro) spectrometry at the Department of Geosciences, Johannes Gutenberg-University of Mainz, Germany. Since the xenoliths are kimberlite-borne and kimberlite melt is highly mobile, contamination along grain boundaries can never be ruled out. The totally different composition of kimberlite compared to mantle xenoliths can change the xenoliths composition, especially in trace elements and can lead to different conclusions for petrogenesis. Hence, only the recalculated whole-rock composition obtained from fresh mineral cores has been used for further interpretation (Table 8).

Table 1: Texture and modal composition [vol. %] of dunite, wehrlite and websterite xenoliths (cpx=clinopyroxene, cr=chromian spinel, grt=garnet, ilm=ilmenite, ol=olivine, opx=orthopyroxene, phl=phlogopite, rt=rutile)

sample	ol	opx	cpx	grt	phl	oxide		texture	and comments	reaction features
dunite										
DJ0223	92	3	-	-	3	2	rt	coarse	with phl-opx-glass patches	phl+glass along grain margins
DJ0259	100	-	+	+	+	+	ilm	porphyro-clastic	66% recrystallized; ol zoned	ol zoned
DJ0273	91	1	1	-	5	2	cr	coarse	with phl+opx+glass patches	phl+glass along grain margins
DJ0274	91	4	1	-	3	1	cr	coarse	with phl+opx+glass patches	phl+glass along grain margins
DJ0297	98	-	1	-	-	1	ilm	coarse	granular	-
DJ02100	100	-	+	-	-			coarse	granular	-
wehrlite										
AJE362	65	-	32	-	1.5	1.5	ilm cr	coarse	with amoeboid cpx	cpx replacing ol
AJE400	80	-	16	-	2	2	cr	coarse	with amoeboid cpx	cpx replacing ol
AJE401	94	-	3	1	2	+	cr	porphyro-clastic	foliated, 72% recrystallized; ol zoned	cpx+grt+phl replacing ol porphyroclastic ol zoned
DJ0214	94	+	4	-	+	2	rut ilm cr	porphyro-clastic	65% recrystallized, with amoeboid cpx and rt	cpx+rt replacing ol recrystallization of ol
DJ0256	89	2	6	1	1	1	rut cr	porphyro-clastic	25% recrystallized, with opx+cpx+grt patches	ol+grt replacing ol opx replacing cpx+grt kelyphitisation of grt
DJ0258A	88	-	11	-	-	1	cr	coarse	with amoeboid cpx	cpx replacing ol
DJ0271	90	-	4	4	1	1	rut ilm cr	coarse	with grt+cpx+spl patches	cpr+rt replacing ol
DJ0275	94	-	5	-	1	-		coarse	with amoeboid cpx; ol zoned	cpx+phl replacing ol porphyroclastic ol zoned
DJ0276	96	-	3	-	1	-		porphyro-clastic	50% recrystallized, foliated, with amoeboid cpx	cpx+phl replacing ol
websterite										
DJ0215	-	60	32	8	-	-		coarse	with amoeboid cpx and fine-grained grt along pyroxene grain boundaries	opx replacing cpx grt recrystallization from cpx+opx
DJ0216	33	40	23	4	+	+	spl	coarse	with amoeboid cpx and grt	cpx+grt+opx replacing ol
DJ0217	-	85	5	10	+	+	spl ilm	coarse	with amoeboid cpx and grt	cpx+grt+opx replaced ol
DJ0218	-	49	42	9	+	+	spl	coarse	with amoeboid cpx and fine-grained grt along pyroxene grain boundaries	opx replacing cpx grt recrystallized from cpx kelyphitisation of grt

The trace element composition of the constituting minerals has been determined with a laser ablation – inductively coupled plasma – mass spectrometry system (LA-ICP-MS) at the Institute of Geosciences at Mainz University using a New Wave Research UP-213 laser ablation system coupled with an Agilent 7500ce quadrupole ICP-MS (Table 2 to Table 7). Measurements were carried out on polished thick section of ~100 µm thickness, with laser energy densities of ~6.5 J/cm^2. Spot sizes ranged from 25 µm to 100 µm, depending on the grain size. Clinopyroxene, garnet and phlogopite were measured with Ar as carrier gas; the concentrations of rare earth elements (REE), high field strength elements (HFSE), some transition metals (V, Mn, Co, Ni, Zn) and large ion lithophile elements (LILE: Rb, Sr, Cs, B) were analysed. Olivine and orthopyroxene were measured using He as carrier gas, since they have low trace element concentrations and the material is better ablated with He. Ar was added to the mix of He and ablated material just shortly before the plasma. In spinel,

Table 2: Average major element, oxygen isotope and trace element compositions of olivine in dunite, wehrlite and websterite xenoliths (Abbreviations: as in Table 1 plus Cr#=Cr/(Cr+Al); dl detection limit; IST=internal standard; Mg#=Mg/(Mg+Fe); n=number of measurements; nd=not determined; repl.=replacing).

olivine

Major element composition [wt. %]

	dunit									
sample	**DJ0223**		**DJ0259**				**DJ0273**		**DJ0274**	
comment			porphyroclasts			neoblasts				
n	**3**	*1σ*	**3**	*1σ*	**3**	*1σ*	**3**	*1σ*	**5**	*1σ*
SiO_2	**41.50**	*0.06*	**40.95**	*0.68*	**40.44**	*0.10*	**41.14**	*0.11*	**41.05**	*0.20*
FeO	**7.59**	*0.10*	**9.44**	*2.21*	**12.90**	*0.49*	**10.54**	*0.13*	**10.30**	*0.15*
MgO	**50.58**	*0.26*	**49.35**	*1.80*	**46.86**	*0.53*	**48.34**	*0.28*	**48.92**	*0.13*
MnO	**0.14**	*0.02*	**0.13**	*0.004*	**0.15**	*0.02*	**0.19**	*0.02*	**0.19**	*0.03*
NiO	**0.32**	*0.00*	**0.38**	*0.02*	**0.25**	*0.07*	**0.26**	*0.01*	**0.29**	*0.02*
total	**100.13**		**100.25**		**100.61**		**100.47**		**100.75**	
Mg #	**0.92**		**0.90**		**0.87**		**0.89**		**0.89**	

Oxygen isotope composition [‰]

$\delta^{18}O$	**nd**		**5.03**			**nd**		**5.02**		**nd**
replicate	**nd**		**5.08**			**nd**		**4.91**		**nd**

Trace element composition [ppm]

comment			porphyroclasts				neoblasts			
			core		rim					
n	**12**	*1σ*	**11**	*1σ*	**7**	*1σ*	**6**	*1σ*	**15**	*1σ*
Al	**4.97**	*6.19*	**61.9**	*11.3*	**3.42**	*2.94*	**54.6**	*11.4*	**0.705**	*0.316*
Ca	**72.3**	*8.3*	**167**	*55*	**82.3**	*21.3*	**552**	*162*	**51.0**	*26.6*
Cr	**90.1**	*12.5*	**243**	*41*	**43.9**	*9.7*	**211**	*31*	**39.5**	*2.2*
Co	**131**	*5*	**134**	*14*	**151**	*7*	**177**	*5*	**123**	*6*
Cu	**0.394**	*0.227*	**2.24**	*0.31*	**0.255**	*0.160*	**3.10**	*0.22*	**0.0420**	*0.0014*
Zn	**58.8**	*3.2*	**60.3**	*21.1*	**93.0**	*13.0*	**102**	*6*	**98.5**	*9.1*
Ga	**0.0289**	*0.0223*	**0.0849**	*0.0405*	**0.0252**	*0.0071*	**0.118**	*0.027*	**0.0099**	*0.0020*
Ti	**146**	*7*	**108**	*86*	**131**	*16*	**242**	*34*	**88.3**	*5.5*
V	**3.37**	*0.49*	**5.46**	*0.55*	**2.33**	*0.08*	**4.42**	*0.74*	**1.73**	*0.10*
Zr	**0.267**	*0.068*	**0.277**	*0.130*	**0.283**	*0.056*	**0.454**	*0.096*	**0.132**	*0.023*
Nb	**0.123**	*0.025*	**0.124**	*0.022*	**0.993**	*0.213*	**0.0894**	*0.0293*	**0.752**	*0.202*
Hf	**0.0113**	*0.0049*	**0.0154**	*0.0052*	**<dl**		**0.0298**	*0.0143*	**0.0259**	*0.0199*
Ta	**0.0041**	*0.0010*	**0.0074**	*0.0012*	**0.0422**	*0.0139*	**0.0111**	*0.0060*	**0.0145**	*0.0061*
Ce	**<dl**		**<dl**		**0.0090**	*0.0073*	**<dl**		**0.0037**	*0.0010*
Sc	**2.27**	*0.12*	**2.34**	*0.56*	**2.16**	*0.31*	**3.13**	*0.41*	**1.29**	*0.24*
Rb										
Sr	**<dl**		**0.0064**	*0.0028*	**<dl**		**0.0107**	*0.0031*	**0.0156**	*0.0073*
Y	**0.0058**	*0.0018*	**0.0094**	*0.0058*	**0.0041**	*0.0001*	**0.0251**	*0.0058*	**0.0055**	*0.0013*
Ba	**0.0517**	*0.0107*	**<dl**		**0.0250**	*0.0042*	**0.103**	*0.106*	**0.0269**	*0.0107*
Li	**1.91**	*0.17*	**1.60**	*0.70*	**2.47**	*0.26*	**2.76**	*0.55*	**2.62**	*0.43*
B	**0.632**	*0.106*	**0.819**	*0.182*	**0.837**	*0.134*	**0.978**	*0.288*	**0.799**	*0.318*

olivine and orthopyroxene all transition metals, the high field strength elements, Ca, Al, Li, B, Rb, Ba, Ce and Th were measured. In olivine and spinel REE were mostly neglected because their concentration was close to or below the detection limit. Glitter software has been used for data reduction using the NIST 612 standard for silicate minerals and NIST 610 for oxides as external standards (Pearce et al., 1997). As internal standard ^{28}Si was used for olivine, orthopyroxene and phlogopite, ^{42}Ca for clinopyroxene and garnet, ^{52}Cr for spinel, and ^{47}Ti for ilmenite and rutile and normalized to the corresponding electron microprobe results. The USGS reference glass BCR-2G was measured after every seventh measurement as an unknown (for the results on BCR-2G and detection limits obtained with this LA-ICP-MS

Table 2: continued.

olivine

Major element composition [wt. %]

	dunite				*wehrlite*							
sample	**DJ0297**		**DJ02100**		**AJE362**		**AJE400**				**AJE401**	
comment							porphyroclasts		neoblasts		porphyroclasts	
n	**6**	*1σ*	**7**	*1σ*	**7**	*1σ*	**6**	*1σ*	**3**	*1σ*	**12**	*1σ*
SiO_2	**40.21**	*0.11*	**40.51**	*0.19*	**40.60**	*0.09*	**40.41**	*0.19*	**40.46**	*0.09*	**40.86**	*0.17*
FeO	**9.73**	*0.12*	**9.43**	*0.12*	**8.53**	*0.12*	**9.29**	*0.04*	**9.22**	*0.08*	**7.50**	*0.09*
MgO	**49.47**	*0.13*	**49.50**	*0.20*	**50.20**	*0.16*	**49.90**	*0.29*	**49.86**	*0.19*	**50.98**	*0.16*
MnO	**0.14**	*0.02*	**0.13**	*0.02*	**0.10**	*0.01*	**0.13**	*0.02*	**0.09**	*0.01*	**0.12**	*0.02*
NiO	**0.27**	*0.02*	**0.39**	*0.02*	**0.31**	*0.02*	**0.36**	*0.04*	**0.35**	*0.02*	**0.34**	*0.03*
total	**99.82**		**99.98**		**99.74**		**100.08**		**99.97**		**99.80**	
Mg #	**0.91**		**0.91**		**0.92**		**0.92**		**0.92**		**0.93**	

Oxygen isotope composition [‰]

$\delta^{18}O$	**5.12**		**5.61**		**5.16**		**4.92**		**nd**		**5.18**	
replicate	**5.02**		**5.33**		**5.11**		**5.17**		**nd**		**5.04**	

Trace element composition [ppm]

comment											porphyroclasts core	
n	**23**	*1σ*	**14**	*1σ*	**4**	*1σ*	**15**	*1σ*			**7**	*1σ*
Al	**30.8**	*1.7*	**60.8**	*4.3*	**46.7**	*2.5*	**59.3**	*4.4*			**72.6**	*16.7*
Ca	**139**	*39*	**166**	*13*	**152**	*15*	**152**	*26*			**177**	*43*
Cr	**116**	*7*	**123**	*11*	**173**	*9*	**190**	*11*			**301**	*11*
Co	**140**	*4*	**153**	*6*	**126**	*4*	**144**	*9*			**123**	*2*
Cu	**1.11**	*0.05*	**1.93**	*0.21*	**1.75**	*0.06*	**1.95**	*0.14*			**1.66**	*0.17*
Zn	**83.8**	*16.0*	**85.5**	*12.9*	**66.8**	*3.2*	**78.8**	*5.3*			**50.9**	*2.1*
Ga	**0.0954**	*0.0128*	**0.149**	*0.024*	**0.108**	*0.011*	**0.169**	*0.025*			**0.113**	*0.02*
Ti	**204**	*11*	**202**	*10*	**198**	*10*	**203**	*15*			**212**	*15*
V	**4.44**	*0.22*	**5.39**	*0.17*	**4.48**	*0.17*	**5.64**	*0.31*			**4.99**	*0.75*
Zr	**0.405**	*0.054*	**0.379**	*0.057*	**0.270**	*0.037*	**0.249**	*0.023*			**0.318**	*0.05*
Nb	**0.156**	*0.019*	**0.110**	*0.019*	**0.0892**	*0.0145*	**0.0837**	*0.0131*			**0.103**	*0.02*
Hf	**0.0126**	*0.0022*	**0.0112**	*0.0042*	**0.0082**	*0.0007*	**0.0075**	*0.0025*			**0.013**	*0.01*
Ta	**0.0113**	*0.0032*	**0.0066**	*0.0012*	**0.0064**	*0.0017*	**0.0066**	*0.0025*			**0.0065**	*0.00*
Ce	**0.0119**	*0.0077*	**0.0025**	*0.0016*	**0.0060**	*0.0035*	**0.0024**	*0.0006*			**0.0046**	*0.00*
Sc	**2.25**	*0.11*	**2.11**	*0.06*	**3.05**	*0.35*	**2.80**	*0.37*			**2.38**	*0.21*
Rb	**0.0680**	*0.0114*	**<dl**		**<dl**		**0.0076**	*0.0048*			**nd**	
Sr	**0.0094**	*0.0017*	**0.0068**	*0.0012*	**0.0102**	*0.0035*	**0.0041**	*0.0021*			**0.0111**	*0.00*
Y	**0.0063**	*0.0021*	**0.0055**	*0.0011*	**0.0054**	*0.0031*	**0.0052**	*0.0013*			**0.0055**	*0.00*
Ba	**0.0448**	*0.0272*	**<dl**		**0.0412**	*0.0376*	**0.132**	*0.025*			**0.0528**	*0.04*
Li	**2.14**	*0.07*	**2.01**	*0.05*	**2.48**	*0.05*	**2.35**	*0.13*			**2.08**	*0.08*
B	**1.09**	*0.25*	**0.460**	*0.125*	**0.719**	*0.171*	**0.882**	*0.404*			**1.311**	*0.25*

Rehfeldt et al., 2007 page 78 in this thesis). Detection limits in olivine are generally lower than in clinopyroxene, orthopyroxene, garnet, phlogopite and oxide minerals. To test the sensitivity of the LA-ICP-MS system for trace element analysis on olivine and orthopyroxene the MPI DING peridotite standard BM90/21-G has been measured several times with NIST 612 as external standard. Except of Ta the measured trace element concentrations are at least one order of magnitude above the detection limit; all are within the literature data range of BM90/21-G (Jochum et al., 2000).

Optically clean mineral separates of olivine, orthopyroxene, clinopyroxene, garnet and phlogopite were prepared for oxygen isotope measurements by handpicking under a binocular microscope. The grains were rinsed in water and ethanol, and analysed by laser-

Table 2: continued.

olivine

Major element composition [wt. %]

	wehrlite									
sample	**AJE401**			**DJ0214**			**DJ0256**		**DJ0258A**	
comment	porphyroclasts	neoblasts		porphyroclasts		neoblasts				
n		**9**	*1σ*	**12**	*1σ*	**8**	*1σ*	**28** *1σ*	**3**	*1σ*
SiO_2		**40.90**	*0.19*	**40.67**	*0.11*	**40.72**	*0.14*	**40.39** *0.18*	**41.14**	*0.30*
FeO		**7.49**	*0.16*	**7.96**	*0.10*	**7.93**	*0.10*	**8.73** *0.40*	**7.53**	*0.07*
MgO		**50.94**	*0.17*	**50.57**	*0.19*	**50.99**		**49.97** *0.37*	**50.95**	*0.10*
MnO		**0.10**	*0.02*	**0.12**	*0.02*	**0.10**	*0.02*	**0.11** *0.03*	**0.10**	*0.004*
NiO		**0.33**	*0.02*	**0.33**	*0.02*	**0.32**	*0.02*	**0.34** *0.03*	**0.35**	*0.02*
total		**99.76**		**99.66**		**100.06**		**99.55**	**100.07**	
Mg #		**0.93**		**0.93**		**0.93**		**0.92**	**0.93**	

Oxygen isotope composition [‰]

$\delta^{18}O$		**3.91**		**5.36**		**nd**		**5.39**	**5.30**	
replicate		**4.27**		**5.16**		**nd**		**5.45**	**5.11**	

Trace element composition [ppm]

comment	porphyroclasts rim		neoblasts							
n	**7**	*1σ*	**8**	*1σ*	**22**	*1σ*	**28**	*1σ*	**21**	*1σ*
Al	**89.7**	*22.3*	**86.7**	*7.1*	**54.2**	*5.8*	**96.6**	*19.7*	**64.6**	*3.0*
Ca	**214**	*34*	**191**	*45*	**175**	*59*	**217**	*71*	**186**	*33*
Cr	**297**	*11*	**285**	*15*	**268**	*19*	**279**	*35*	**241**	*7*
Co	**131**	*11*	**127**	*3*	**125**	*3*	**143**	*11*	**128**	*7*
Cu	**1.73**	*0.28*	**1.73**	*0.12*	**1.52**	*0.17*	**2.40**	*0.39*	**2.73**	*0.25*
Zn	**52.8**	*5.7*	**50.5**	*1.4*	**59.0**	*3.5*	**74.8**	*9.7*	**61.8**	*3.9*
Ga	**0.149**	*0.046*	**0.119**	*0.026*	**0.110**	*0.016*	**0.220**	*0.039*	**0.174**	*0.057*
Ti	**197**	*21*	**167**	*16*	**196**	*21*	**209**	*26*	**229**	*44*
V	**5.19**	*0.72*	**5.65**	*0.47*	**4.36**	*0.35*	**7.21**	*0.92*	**6.21**	*1.29*
Zr	**0.280**	*0.075*	**0.236**	*0.029*	**0.283**	*0.060*	**0.306**	*0.095*	**0.374**	*0.113*
Nb	**0.106**	*0.082*	**0.0575**	*0.0183*	**0.0961**	*0.0296*	**0.0594**	*0.0338*	**0.0963**	*0.0380*
Hf	**<dl**		**0.0078**	*0.0075*	**0.0108**	*0.0030*	**0.0376**	*0.0524*	**0.0134**	*0.0046*
Ta	**0.0130**	*0.0032*	**0.0066**	*0.0034*	**0.0064**	*0.0019*	**0.0059**	*0.0006*	**0.0061**	*0.0014*
Ce	**<dl**		**0.0031**	*0.0018*	**0.0044**	*0.0024*	**0.0039**	*0.0015*	**<dl**	
Sc	**2.20**	*0.54*	**3.32**	*0.24*	**2.73**	*0.28*	**2.32**	*0.45*	**3.10**	*1.72*
Rb	**nd**		**nd**		**nd**		**nd**		**0.0667**	*0.0483*
Sr	**<dl**		**0.0062**	*0.0023*	**0.0104**	*0.0067*	**0.0103**	*0.0073*	**<dl**	
Y	**<dl**		**0.0044**	*0.0018*	**0.0079**	*0.0047*	**0.0073**	*0.0017*	**0.0062**	*0.0020*
Ba	**<dl**		**<dl**		**<dl**		**0.0380**	*0.0192*	**<dl**	
Li	**2.03**	*0.32*	**1.99**	*0.17*	**2.22**	*0.21*	**2.48**	*0.44*	**2.58**	*0.17*
B	**1.06**	*0.14*	**2.61**	*0.41*	**1.14**	*0.67*	**0.83**	*0.27*	**0.63**	*0.16*

assisted fluorination mass-spectrometry at the Department of Geology, Royal Holloway University of London (following the method of Mattey and Macpherson, 1993 and Mattey, 1997). All values are reported as $\delta^{18}O$ relative to Vienna – Standard Mean Ocean Water (Table 2 to Table 5 and Table 7). San Carlos Olivine (SC OL) and Gore Mountain Garnet (GMG II) were measured as standards and were reproducible within ± 0.08 ‰ (1σ, n=21). Replicate measurements yielded external precisions of 0.005-0.36 ‰.

Whole-rock powders and olivine separates of dunite, wehrlite and websterite xenoliths were analysed for Re-Os isotope composition at the Department of Terrestrial Magnetism, Carnegie Institution of Washington, USA and additionally, whole-rock powders of samples DJ0214 and DJ0256 were analysed at the Max-Planck-Institut für Chemie, Mainz, Germany

Table 2: continued.

olivine

Major element composition [wt. %]

	wehrlite								***websterite***	
sample	**DJ0271**		**DJ0275**		**DJ0276**				**DJ0216**	
comment					porphyroclasts		neoblasts			
n	**6**	*1σ*	**6**	*1σ*	**4**	*1σ*	**3**	*1σ*	**6**	*1σ*
SiO_2	**40.45**	*0.18*	**40.22**	*0.11*	**40.19**	*0.10*	**40.21**	*0.15*	**40.16**	*0.15*
FeO	**8.50**	*0.07*	**10.71**	*0.18*	**10.75**	*0.07*	**10.69**	*0.05*	**11.04**	*0.06*
MgO	**50.37**	*0.16*	**48.60**	*0.20*	**48.54**	*0.21*	**48.75**	*0.23*	**48.38**	*0.16*
MnO	**0.12**	*0.02*	**0.14**	*0.03*	**0.12**	*0.05*	**0.12**	*0.02*	**0.12**	*0.01*
NiO	**0.36**	*0.02*	**0.22**	*0.02*	**0.24**	*0.04*	**0.21**	*0.02*	**0.39**	*0.02*
total	**99.79**		**99.88**		**99.84**		**99.98**		**100.08**	
Mg #	**0.93**		**0.90**		**0.90**		**0.90**		**0.90**	

Oxygen isotope composition [‰]

$\delta^{18}O$	**5.24**		**5.10**		**nd**		**nd**		**4.79**	
replicate	**4.99**		**5.05**		**nd**		**nd**		**5.12**	

Trace element composition [ppm]

comment			cores		rims					
n	**9**	*1σ*	**8**	*1σ*	**8**	*1σ*	**21**	*1σ*	**10**	*1σ*
Al	**63.5**	*6.1*	**12.8**	*0.6*	**13.2**	*0.5*	**23.0**	*2.7*	**20.5**	*3.4*
Ca	**166**	*15*	**141**	*7*	**149**	*32*	**154**	*15*	**66.1**	*9.3*
Cr	**243**	*18*	**54.6**	*2.8*	**53.2**	*1.2*	**62.1**	*7.7*	**33.9**	*2.9*
Co	**128**	*5*	**131**	*1*	**136**	*8*	**139**	*4*	**153**	*10*
Cu	**1.75**	*0.26*	**0.613**	*0.012*	**0.655**	*0.108*	**1.13**	*0.21*	**0.139**	*0.011*
Zn	**68.4**	*3.6*	**86.1**	*0.8*	**94.9**	*10.7*	**86.0**	*3.7*	**60.3**	*4.8*
Ga	**0.147**	*0.022*	**0.0791**	*0.0107*	**0.0915**	*0.0135*	**0.120**	*0.026*	**0.0349**	*0.0105*
Ti	**204**	*8*	**31.7**	*13.9*	**135**	*22*	**183**	*19*	**128**	*8*
V	**5.47**	*0.36*	**4.09**	*0.20*	**4.13**	*0.12*	**4.69**	*0.41*	**2.58**	*0.17*
Zr	**0.331**	*0.032*	**0.258**	*0.050*	**0.379**	*0.039*	**0.413**	*0.073*	**0.192**	*0.030*
Nb	**0.0995**	*0.0208*	**0.507**	*0.170*	**0.254**	*0.033*	**0.153**	*0.030*	**0.538**	*0.041*
Hf	**0.0116**	*0.0053*	**0.0079**	*0.0028*	**<dl**		**0.0150**	*0.0032*	**<dl**	
Ta	**0.0079**	*0.0017*	**0.0196**	*0.0056*	**0.0159**	*0.0029*	**0.0088**	*0.0032*	**0.0171**	*0.0067*
Ce	**<dl**				**<dl**		**0.0070**	*0.0014*	**<dl**	
Sc	**2.23**	*0.19*	**2.74**	*0.57*	**2.19**	*0.12*	**2.55**	*0.35*	**2.37**	*0.10*
Rb	**nd**		**0.0251**	*0.0108*						
Sr	**0.0081**	*0.0028*	**<dl**		**0.0037**	*0.0001*	**0.0106**	*0.0058*	**0.0048**	*0.0011*
Y	**0.0053**	*0.0011*	**0.0048**	*0.0018*	**0.0042**	*0.0011*	**0.0078**	*0.0037*	**0.0071**	*0.0003*
Ba	**<dl**		**0.0093**	*0.0040*	**<dl**		**0.0975**	*0.0742*	**0.0329**	*0.0222*
Li	**2.34**	*0.12*	**2.25**	*0.02*	**2.12**	*0.10*	**2.07**	*0.30*	**1.96**	*0.41*
B	**0.541**	*0.148*	**0.417**	*0.100*	**0.857**	*0.555*	**1.16**	*0.38*	**0.952**	*0.367*

(following the procedure of Carlson et al., 1999 and Rehfeldt et al., 2007, page 78 in this thesis, in both institutions). Laboratory blanks of 2 pg Os and 1 pg Re were obtained during the measurements and subtracted from the values summarized in Table 9.

4. Results

4.1. Petrography and mineral composition

4.1.1. Dunite xenoliths

Dunite xenoliths comprise almost exclusively olivine (DJ0259, DJ02100; Fig. 1 a) and minor amounts of clinopyroxene (1-5 vol. %), orthopyroxene, garnet, phlogopite or oxide minerals

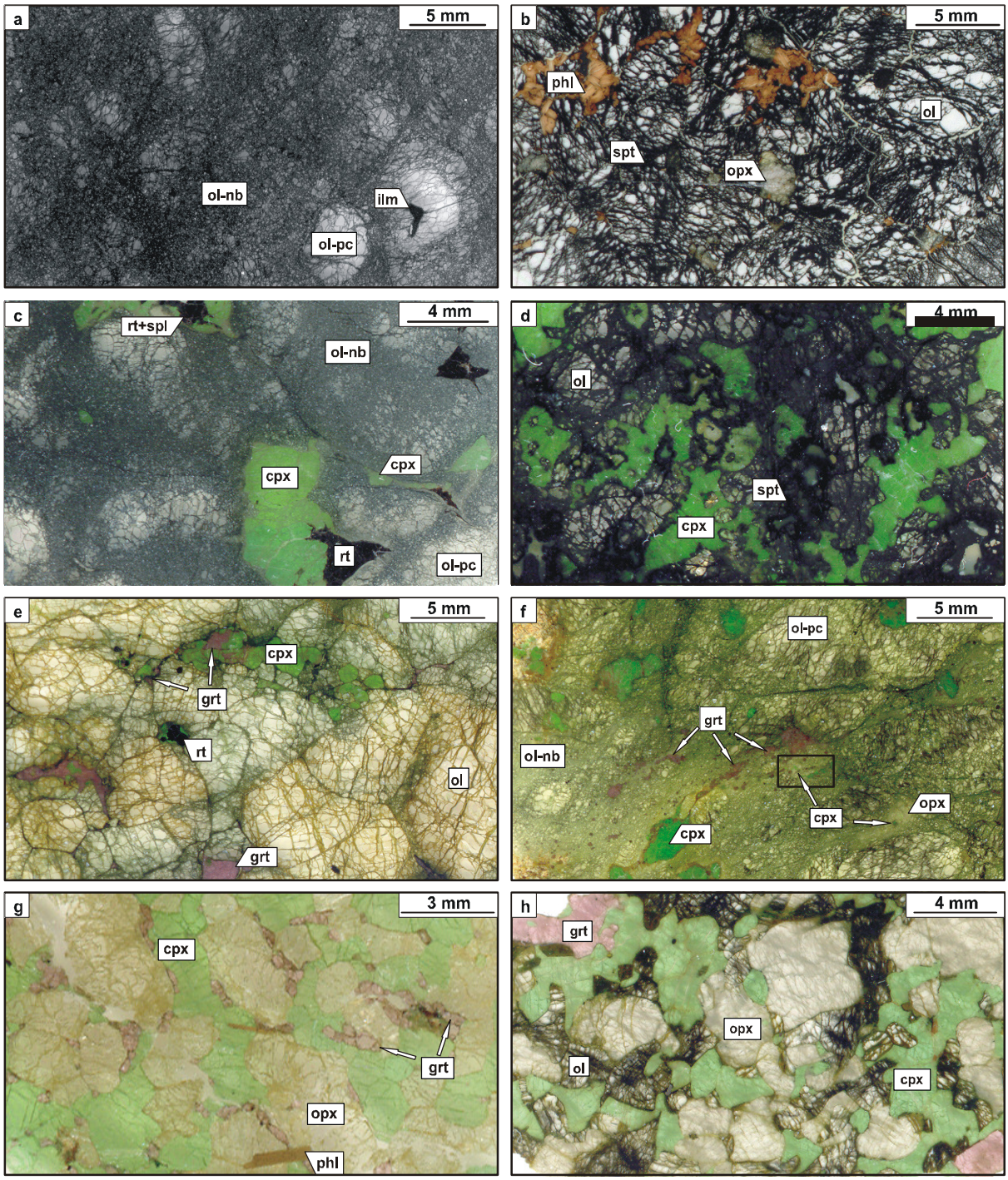

Fig. 1: Photomicrographs of dunite, wehrlite and websterite xenoliths ordered from (a) to (h) according to increasing amount of modal metasomatism: (a) porphyroclastic dunite DJ0259 comprising olivine porphyroclasts surrounded by olivine neoblasts and ilmenite in minor amounts, (b) granular dunite DJ0223 containing slightly serpentinized olivine, as well as orthopyroxene and phlogopite, (c) porphyroclastic wehrlite DJ0214 with olivine porphyroclasts surrounded by olivine neoblasts; vermicular clinopyroxene rutile patches replace olivine, (d) granular wehrlite AJE362 comprising coarse olivine and amoeboid clinopyroxene, (e) granular wehrlite DJ0271 comprising coarse olivine and amoeboid patches of clinopyroxene garnet and oxide minerals along olivine margins, (f) porphyroclastic wehrlite DJ0256 with olivine porphyroclasts and neoblasts and clinopyroxene, garnet and orthopyroxene schlieren (black square is enlarged in Fig. 5 a); (g) heterogranular websterite DJ0218 containing orthopyroxene that is consumed by clinopyroxene and necklace garnets crystallized at pyroxene margins and (h) granular coarse grained websterite DJ0216 comprising slightly serpentinized olivine that is consumed by coarse orthopyroxene, clinopyroxene and garnet. Abbreviations same as in Table 1.

(DJ0223, DJ0259, DJ0273, DJ0274 and DJ0297; Fig. 1 b). Most dunite xenoliths are coarse-grained granular containing large olivine crystals (38 mm – 300 µm). Only dunite xenolith DJ0259 has a porphyroclastic texture with coarse olivine porphyroclasts (13 mm – 500 µm) that merge into and are surrounded by fine-grained olivine neoblasts (1 mm – 50 µm; Fig. 1 a). Except of olivine and orthopyroxene, all other minerals seem to have crystallized in cracks and along olivine grain boundaries exhibiting an amoeboid, veined texture (Fig. 1 b).

Olivine in the dunite xenoliths is coarse-grained and has forsterite contents of Fo_{89-93}, intermediate between olivine in restitic dunites (Fo_{93-95} and NiO 0.3-0.4 wt. %; Gurney and Harte, 1980) and olivine in cumulatic dunites (Fo_{87-90}; Gurney and Harte, 1980; Clague, 1988; Rehfeldt, et al. 2007 Fe-rich dunite xenolilths chapter p. 77; Fig. 2). Olivine in mantle peridotites is often coarse-grained, similar to olivine in the studied dunite xenoliths, while olivine in cumulatic dunites are finer grained (Gurney and Harte, 1980; Rehfeldt et al., 2007 Fe-rich dunite xenolilths chapter p. 77). Additionally, olivine in the studied dunite xenoliths has similar high NiO contents of 0.3-0.4 wt. % as olivine in mantle xenoliths (0.3-0.5; e.g. Boyd and Mertzman, 1987), while cumulatic olivine has lower NiO contents of 0.2-0.3 wt. % (Fig. 3). Porphyroclastic dunite DJ0259 has olivine neoblasts with lower forsterite (Fo_{87}) and lower NiO contents (0.25 wt. %) than olivine in granular dunite xenoliths.

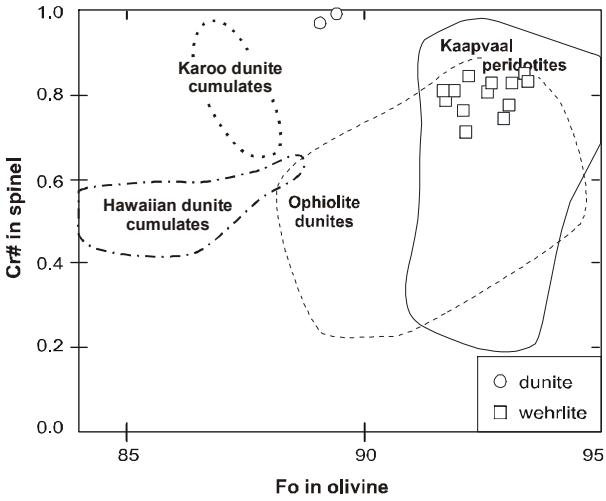

Fig. 2: Spinel Cr# versus forsterite content of coexisting olivine in dunite and wehrlite xenoliths compared to olivine in Kaapvaal mantle xenoliths and cumulate xenoliths, ophiolitic channel dunites and Hawaiian dunite cumulates (Kaapvaal peridotite: Carswell et al., 1979; Simon, 2004; Kaapvaal dunite cumulates: Dawson et al., 1981 ; Rehfeldt et al., 2007 Fe-rich dunite xenolilths chapter p. 77; ophiolitic channel dunites: Suhr, 1999; Koga et al., 2001; Hawaiian dunite cumulates: Clague, 1988).

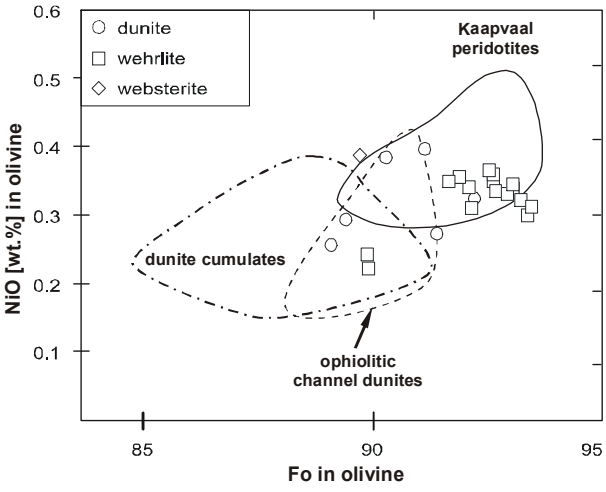

Fig. 3: NiO versus forsterite in olivine of dunite, wehrlite and websterite xenoliths compared to olivine in mantle peridotites, ophiolitic peridotites and cumulatic dunites (references as in Fig. 2).

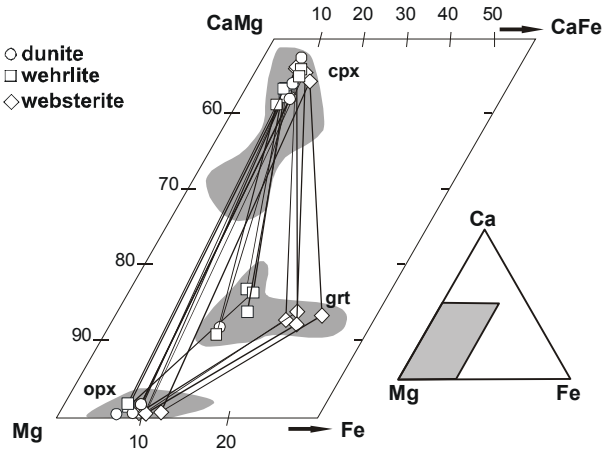

Fig. 4: Fe-Mg-Ca diagram displaying major element compositions of clinopyroxene, orthopyroxene and garnet in dunite, wehrlite and websterite xenoliths compared to Kaapvaal mantle peridotite xenoliths (Carswell et al., 1979; Hervig et al., 1986; Boyd and Mertzman, 1987).

Orthopyroxene, clinopyroxenes, as well as garnet in dunite xenoliths have Mg# of 0.90-0.93 and 0.85, respectively (Table 3 to Table 5), plotting towards high MgO compositions within the Kaapvaal mantle peridotite field (Fig. 4; Carswell et al., 1979; Hervig et al., 1986; Boyd and Mertzman, 1987). Of these, the clinopyroxene lies at the high Ca end of the compositional field of clinopyroxene in Kaapvaal mantle peridotites. Garnet, on the other hand, lies towards high Mg#, having a chrome-pyrope composition (G9 according to Dawson and Stephens, 1975).

Spinel in dunite samples DJ0273 and DJ0274 has a pure chromite composition with high Cr# (0.98-0.99) and low Mg# (0.35-0.40;Fig. 2; Table 6). They have crystallized together with phlogopite along olivine grain boundaries. Ilmenite in dunite xenoliths occurs without the presence of any other oxide mineral and has Cr_2O_3 contents of 0.88-3.2 wt. %, which is indicative of crystallization from percolating kimberlite (Wyatt et al., 2004).

Phlogopite can be subdivided texturally and chemically into primary and secondary phlogopites. Primary phlogopite is euhedral to subhedral and crystallizes along olivine grain boundaries (Fig. 1 b), while secondary phlogopite is mostly anhedral and occurs in dunite xenoliths replacing ilmenite. Compared to primary phlogopite, it has high TiO_2 contents (0.4-0.7 wt. % versus 2.6-4.1 wt.%, respectively) and low Cr_2O_3 contents (0.2-0.5 wt. % versus 1.0-1.1 wt. %, respectively; Table 7).

4.1.2. Wehrlite xenoliths

Wehrlite has a similar mineralogy and texture as dunite xenoliths with high modal olivine contents (96-65 vol. %; Table 1). Orthopyroxene is rare in wehrlite xenoliths, occurring in schlieren together with euhedral garnet or as granular grains together with olivine. Clinopyroxene (32-3 vol. %) crystallized as amoeboid grains in schlieren in some samples intergrown with garnet, phlogopite and oxide minerals (Fig. 1 c and d). The secondary texture

Table 3: Average major element, oxygen isotope and trace element compositions of orthopyroxene in dunite, wehrlite and websterite xenoliths (Abbreviations same as in Table 1 and 2).

orthopyroxene

Major element composition [wt. %]

	dunite						***wehrlite***				***websterite***	
sample	**DJ0223**		**DJ0273**		**DJ0274**		**DJ0214**		**DJ0256**		**DJ0215**	
comment	in patches		in patches		in patches		secondary					
n	**8**	*1σ*	**3**	*1σ*	**3**	*1σ*	**5**	*1σ*	**12**	*1σ*	**9**	*1σ*
SiO_2	**57.81**	*0.50*	**57.41**	*0.66*	**57.37**	*0.22*	**55.68**	*1.27*	**56.66**	*0.43*	**56.97**	*0.19*
TiO_2	**0.08**	*0.01*	**0.17**	*0.02*	**0.15**	*0.04*	**0.20**	*0.04*	**0.22**	*0.04*	**0.04**	*0.02*
Al_2O_3	**0.03**	*0.01*	**0.26**	*0.23*	**0.17**	*0.04*	**1.21**	*0.57*	**1.43**	*0.29*	**0.67**	*0.03*
Cr_2O_3	**0.13**	*0.02*	**0.52**	*0.20*	**0.61**	*0.23*	**1.15**	*0.36*	**0.75**	*0.13*	**0.17**	*0.03*
CaO	**0.27**	*0.01*	**0.92**	*0.37*	**0.96**	*0.24*	**0.99**	*0.13*	**0.78**	*0.09*	**0.32**	*0.01*
FeO	**4.62**	*0.08*	**6.15**	*0.31*	**6.13**	*0.54*	**4.97**	*0.07*	**5.14**	*0.13*	**6.74**	*0.05*
MgO	**36.20**	*0.62*	**33.84**	*0.67*	**34.69**	*1.11*	**34.79**	*0.58*	**34.83**	*0.44*	**34.68**	*0.44*
MnO	**0.14**	*0.02*	**0.15**	*0.04*	**0.15**	*0.04*	**0.13**	*0.01*	**0.12**	*0.03*	**0.15**	*0.03*
NiO	**0.08**	*0.02*	**0.10**	*0.02*	**0.11**	*0.02*	**0.12**	*0.05*	**0.11**	*0.04*	**0.11**	*0.02*
Na_2O	**0.04**	*0.01*	**0.12**	*0.03*	**0.19**	*0.05*	**0.23**	*0.07*	**0.20**	*0.04*	**0.04**	*0.02*
total	**99.39**		**99.65**		**100.5**		**99.46**		**100.25**		**99.88**	
Mg#	**0.93**		**0.91**		**0.91**		**0.93**		**0.92**		**0.90**	

Oxygen isotope composition [‰]

$\delta^{18}O$	**nd**		**nd**		**nd**		**nd**		**nd**		**5.39**	
replicate	**nd**		**nd**		**nd**		**nd**		**nd**		**6.06**	

Trace element composition [ppm]

sample	**DJ0223**								**DJ0256**		**DJ0215**	
n	**8**	*1σ*							**5**	*1σ*	**3**	*1σ*
Co	**50.5**	*1.6*							**63.4**	*1.0*	**nd**	
Cu	**<dl**								**2.11**	*0.34*	**nd**	
Zn	**37.2**	*2.1*							**45.8**	*2.1*	**nd**	
Ga	**nd**								**8.57**	*1.94*	**nd**	
Ti	**520**	*22*							**1623**	*235*	**230**	*2*
V	**13.2**	*0.5*							**104**	*18*	**41.1**	*1.0*
Zr	**0.183**	*0.087*							**1.58**	*0.42*	**0.249**	*0.011*
Nb	**<dl**								**<dl**		**0.197**	*0.019*
Hf	**<dl**								**0.138**	*0.019*	**0.0089**	*0.0006*
Ta	**<dl**								**<dl**		**0.0341**	*0.0064*
La	**0.0560**								**0.0747**	*0.0752*	**0.0199**	*0.0069*
Ce	**0.0590**	*0.0028*							**0.0427**	*0.0075*	**0.0836**	*0.0107*
Pr	**<dl**								**0.0385**	*0.0219*	**<dl**	
Nd	**0.285**	*0.035*							**<dl**		**0.0354**	*0.0035*
Sm	**<dl**								**<dl**		**<dl**	
Eu	**<dl**								**<dl**		**<dl**	
Gd	**<dl**								**<dl**		**<dl**	
Tb	**nd**								**nd**		**<dl**	
Dy	**<dl**								**0.0945**	*0.0346*	**<dl**	
Ho	**nd**								**nd**		**0.0013**	*0.0004*
Er	**<dl**								**<dl**		**0.0079**	*0.0006*
Tm	**nd**								**nd**		**<dl**	
Yb	**0.184**	*0.050*							**<dl**		**<dl**	
Lu	**<dl**								**<dl**		**<dl**	
Sc	**3.02**	*0.42*							**5.92**	*0.84*	**6.19**	*0.19*
Rb	**0.114**	*0.020*							**0.143**	*0.062*	**<dl**	
Sr	**0.206**	*0.039*							**0.292**	*0.025*	**0.130**	*0.024*
Y	**nd**								**0.134**	*0.042*	**0.0156**	*0.0101*
Ba	**0.970**	*0.226*							**0.537**	*0.186*	**<dl**	
Th	**nd**								**nd**		**0.0079**	*0.0006*
U	**nd**								**nd**		**0.0020**	*0.0005*
Li	**<dl**								**1.66**	*0.29*	**nd**	
B	**nd**								**<dl**		**nd**	

of clinopyroxene and garnet indicates a dunitic to harzburgitic protolith composition, similar to the studied dunite xenoliths. Almost all dunite and wehrlite xenoliths have high modal olivine contents compared to Archaean lherzolite and harzburgite xenoliths (80-100 Vol. % versus 40-82 Vol. %, respectively; Boyd, 1974). Most of them lie at the high end of the oceanic mantle depletion trend (Boyd, 1974), due to high forsterite contents. Wehrlite xenoliths AJE362, AJE400, DJ0258A and DJ0271 are coarse-grained granular comprising large, anhedral olivine crystals (18 mm - 200 µm), while wehrlites AJE401, DJ0214, DJ0256 and DJ0276 are porphyroclastic, slightly foliated with olivine porphyroclasts (20 mm - 300 µm) surrounded by fine grained recrystallised olivine neoblasts (1.3 mm - 5 µm). Additionally, anhedral, amoeboid clinopyroxene (12 mm - 90 µm), in some samples orthopyroxene (1.5 mm - 5 µm) and phlogopite (5.4 mm – 10 µm) as well as garnet (4.4 mm- 20 µm) and oxide minerals such as spinel, ilmenite and rutile (2 mm – 2 µm) occur in the wehrlite xenoliths together with clinopyroxene crystallizing along veins and grain boundaries of large olivines (Fig. 1 c-f). The secondary minerals exhibit schlieren in some samples together with orthopyroxene, that are oriented

Table 3: continued.

orthopyroxene

Major element composition [wt. %]

	websterite					
sample	**DJ0216**		**DJ0217**		**DJ0218**	
comment						
n	**6**	*1σ*	**6**	*1σ*	**11**	*1σ*
SiO_2	**56.93**	*0.18*	**56.64**	*0.17*	**57.10**	*0.51*
TiO_2	**0.08**	*0.03*	**0.09**	*0.01*	**0.03**	*0.04*
Al_2O_3	**0.64**	*0.03*	**0.64**	*0.02*	**0.69**	*0.03*
Cr_2O_3	**0.14**	*0.03*	**0.21**	*0.03*	**0.17**	*0.03*
CaO	**0.26**	*0.02*	**0.35**	*0.01*	**0.31**	*0.03*
FeO	**6.84**	*0.06*	**7.88**	*0.07*	**6.30**	*0.11*
MgO	**34.62**	*0.12*	**33.37**	*0.12*	**35.04**	*0.36*
MnO	**0.15**	*0.03*	**0.15**	*0.03*	**0.15**	*0.02*
NiO	**0.09**	*0.02*	**0.13**	*0.02*	**0.11**	*0.02*
Na_2O	**0.08**	*0.02*	**0.09**	*0.01*	**0.05**	*0.04*
total	**99.84**		**99.56**		**99.94**	
Mg#	**0.90**		**0.88**		**0.91**	

Oxygen isotope composition [‰

$\delta^{18}O$	**5.60**		**6.00**		**5.44**	
replicate	**6.21**		**6.40**		**5.76**	

Trace element composition [ppm]

sample	**DJ0216**		**DJ0217**		**DJ0218**	
n	**16**	*1σ*	**4**	*1σ*	**3**	*1σ*
Co	**63.7**	*2.3*	**nd**		**nd**	
Cu	**0.181**	*0.077*	**nd**		**nd**	
Zn	**41.0**	*4.1*	**nd**		**nd**	
Ga	**2.35**	*0.19*	**nd**		**nd**	
Ti	**434**	*38*	**511**	*17*	**104**	*4*
V	**30.1**	*2.2*	**36.6**	*0.5*	**29.9**	*0.3*
Zr	**0.315**	*0.085*	**0.482**	*0.061*	**0.274**	*0.069*
Nb	**0.110**	*0.113*	**0.166**	*0.025*	**0.188**	*0.023*
Hf	**0.0097**	*0.0046*	**0.0149**	*0.0021*	**<dl**	
Ta	**0.0070**	*0.0049*	**0.0208**	*0.0034*	**0.0201**	*0.0045*
La	**0.0338**	*0.0314*	**0.0143**	*0.0065*	**0.0345**	*0.0030*
Ce	**0.0926**	*0.0430*	**0.0567**	*0.0159*	**0.0918**	*0.0120*
Pr	**0.0104**	*0.0069*	**0.0143**	*0.0017*	**0.0134**	*0.0035*
Nd	**0.0545**	*0.0106*	**0.0733**	*0.0237*	**0.0529**	*0.0017*
Sm	**0.0181**	*0.0064*	**0.0260**	*0.0014*	**0.0108**	*0.0023*
Eu	**0.0083**	*0.0015*	**0.0135**	*0.0046*	**0.0036**	*0.0004*
Gd	**<dl**		**0.0289**	*0.0065*	**0.0082**	*0.0005*
Tb	**<dl**		**0.0050**	*0.0008*	**0.0020**	*0.0005*
Dy	**0.0111**	*0.0035*	**0.0164**	*0.0056*	**<dl**	
Ho	**0.0029**	*0.0002*	**0.0044**	*0.0008*	**<dl**	
Er	**0.0096**	*0.0015*	**0.0101**	*0.0037*	**<dl**	
Tm	**0.0025**	*0.0009*	**0.0029**	*0.0015*	**<dl**	
Yb	**0.0136**	*0.0061*	**0.0120**	*0.0041*	**<dl**	
Lu	**0.0128**	*0.0144*	**0.0021**	*0.0010*	**<dl**	
Sc	**5.62**	*1.33*	**7.39**	*0.21*	**5.18**	*0.04*
Rb	**<dl**		**<dl**		**0.0216**	*0.0163*
Sr	**0.239**	*0.200*	**0.339**	*0.059*	**0.187**	*0.025*
Y	**0.0633**	*0.0196*	**0.0793**	*0.0105*	**0.0305**	*0.0051*
Ba	**0.121**	*0.117*	**<dl**		**0.107**	*0.071*
Th	**0.0062**	*0.0021*	**0.0030**	*0.0011*	**0.0132**	*0.0025*
U	**0.0024**	*0.0022*	**0.0048**	*0.0011*	**0.0031**	*0.0005*
Li	**0.880**	*0.059*	**nd**		**nd**	
B	**1.36**	*0.68*	**nd**		**nd**	

parallel a foliation (AJE401, DJ0256 and DJ0276; Fig. 1 e-f and Fig. 5 a). Wehrlite sample DJ0256 contains next to the above described schlieren, euhedral garnet that occurs together with orthopyroxene and breaks down to kelyphite comprising phlogopite and chromite (Fig. 5 b). This is a feature due to temperature rise and decompression, that is often described in mantle peridotites (e.g. Boyd et al., 1997; Grégoire et al., 2003; Zheng et al., 2005; Foley et al., 2006). Similarly, in sample DJ0214 clinopyroxene breaks down, producing a rim comprising of secondary orthopyroxene and spinel (Fig. 5 c). It also contains 2 Vol. % rutile that crystallized as anhedral amoeboid minerals together with clinopyroxene (Fig. 1 c) and breaks down to chromite (Fig. 5 d).

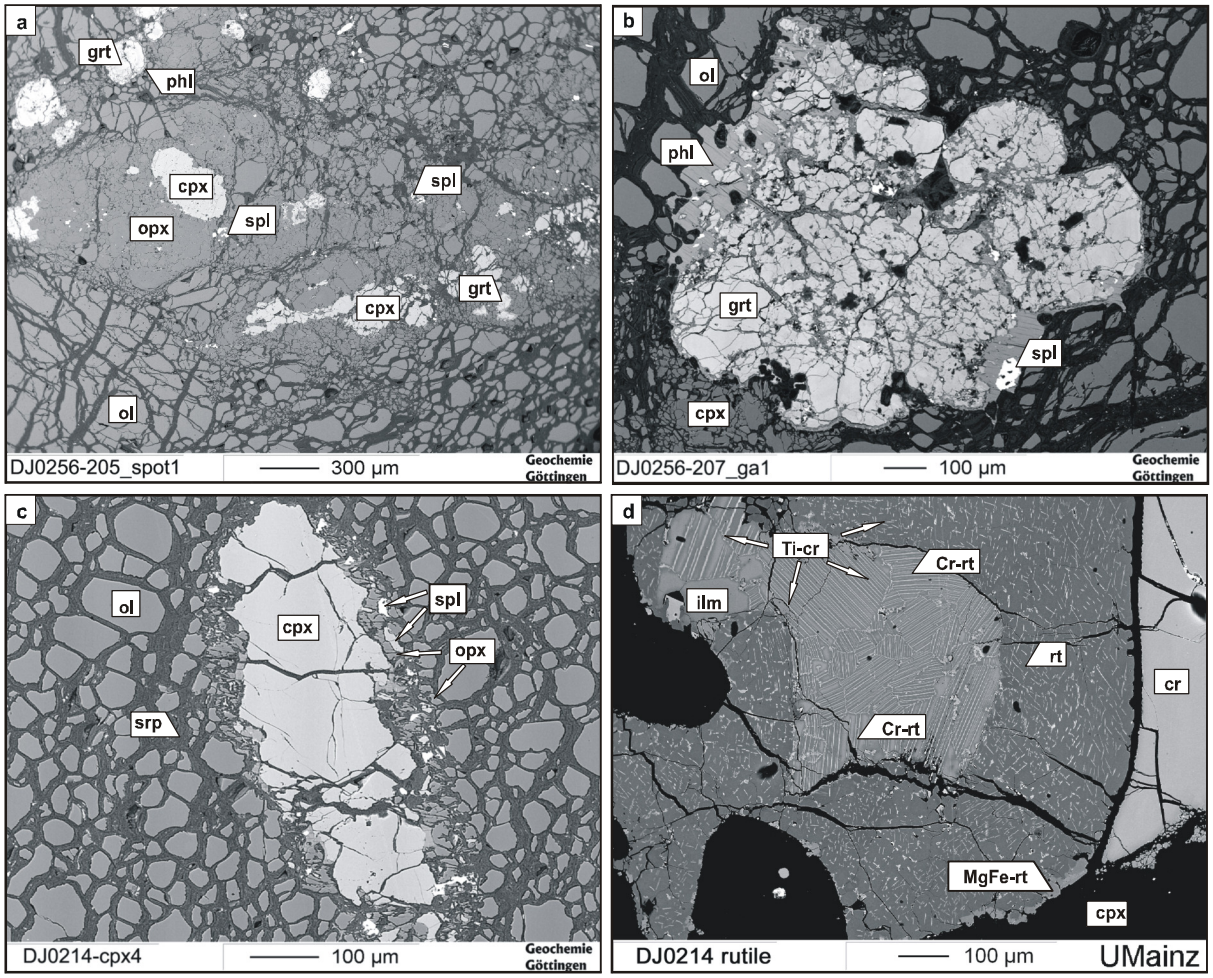

Fig. 5: Backscattered electron microprobe pictures of (a) clinopyroxene, orthopyroxene and garnet schlieren in wehrlite DJ0256 surrounded by fine grained olivine neoblasts, (b) garnet in wehrlite DJ0256 with a kelyphite rim breaking down into phlogopite and spinel, (c) clinopyroxene in wehrlite DJ0214 that breaks down to fine grained orthopyroxene and spinel and (d) rutile in wehrlite DJ0214 that has exsolution lamellae of Ti-rich chromite. Abbreviations same as in Table 1.

Table 4: Average major element, oxygen isotope and trace element compositions of clinopyroxene in dunite, wehrlite and websterite xenoliths (Abbreviations: as in Table 1 and 2).

clinopyroxene

Major element composition [wt. %]

	dunite											
sample	**DJ0259**		**DJ0273**		**DJ0274**				**DJ0297**		**DJ02100**	
comment							resorbed					
n	**3**	*1σ*	**5**	*1σ*	**3**	*1σ*	**3**	*1σ*	**4**	*1σ*	**6**	*1σ*
SiO_2	**56.30**	*0.34*	**53.71**	*0.56*	**54.37**	*0.36*	**54.81**	*0.58*	**55.98**	*0.20*	**55.91**	*0.28*
TiO_2	**0.10**	*0.02*	**0.71**	*0.30*	**0.72**	*0.33*	**0.74**	*0.06*	**0.34**	*0.02*	**0.33**	*0.02*
Al_2O_3	**0.12**	*0.03*	**0.41**	*0.12*	**0.29**	*0.13*	**0.48**	*0.20*	**1.85**	*0.20*	**2.44**	*0.11*
Cr_2O_3	**1.27**	*0.42*	**1.04**	*0.17*	**1.30**	*0.27*	**1.17**	*0.41*	**1.91**	*0.48*	**1.52**	*0.18*
CaO	**22.72**	*0.27*	**20.54**	*0.39*	**20.53**	*0.71*	**20.00**	*0.81*	**19.22**	*0.38*	**18.42**	*0.13*
FeO	**2.65**	*0.40*	**3.58**	*0.31*	**3.46**	*0.36*	**3.49**	*0.32*	**2.80**	*0.05*	**2.85**	*0.04*
MgO	**16.51**	*0.10*	**18.14**	*0.41*	**18.36**	*0.76*	**17.80**	*0.05*	**15.90**	*0.50*	**16.45**	*0.10*
MnO	**0.10**	*0.01*	**0.13**	*0.02*	**0.16**	*0.04*	**0.12**	*0.00*	**0.08**	*0.02*	**0.10**	*0.04*
Na_2O	**1.10**	*0.13*	**0.95**	*0.09*	**1.00**	*0.07*	**1.10**	*0.06*	**2.37**	*0.29*	**2.32**	*0.08*
total	**100.87**		**99.21**		**100.19**		**99.71**		**100.44**		**100.34**	
Mg#	**0.92**		**0.90**		**0.90**		**0.90**		**0.91**		**0.91**	

Oxygen isotope composition [‰]

$\delta^{18}O$	**nd**		**4.89**		**nd**		**nd**		**nd**		**nd**	
replicate	**nd**		**5.07**		**nd**		**nd**		**nd**		**nd**	

Trace element composition [ppm]

n	**6**	*1σ*							**6**	*1σ*	**8**	*1σ*
Co	**17.5**	*1.8*							**nd**		**nd**	
Zn	**12.2**	*2.8*							**nd**		**nd**	
Ni	**216**	*113*							**nd**		**nd**	
Ti	**623**	*72*							**2218**	*159*	**1925**	*73*
V	**253**	*28*							**338**	*29*	**249**	*24*
Zr	**39.3**	*16.8*							**66.5**	*13.0*	**47.4**	*7.9*
Nb	**0.197**	*0.025*							**0.250**	*0.170*	**0.272**	*0.200*
Hf	**1.95**	*0.86*							**3.97**	*0.65*	**2.77**	*0.52*
Ta	**0.0099**	*0.0022*							**0.0180**	*0.0044*	**0.0254**	*0.0084*
La	**11.0**	*7.8*							**1.55**	*0.39*	**1.98**	*0.30*
Ce	**45.4**	*33.5*							**6.40**	*1.89*	**8.36**	*1.07*
Pr	**8.31**	*6.15*							**1.27**	*0.32*	**1.62**	*0.18*
Nd	**39.7**	*26.5*							**6.99**	*1.90*	**8.81**	*0.96*
Sm	**7.15**	*3.79*							**1.91**	*0.48*	**2.37**	*0.28*
Eu	**1.77**	*0.75*							**0.576**	*0.129*	**0.725**	*0.083*
Gd	**4.70**	*2.08*							**1.68**	*0.26*	**2.01**	*0.26*
Tb	**0.497**	*0.217*							**0.217**	*0.042*	**0.246**	*0.036*
Dy	**2.22**	*0.96*							**1.10**	*0.22*	**1.24**	*0.19*
Ho	**0.306**	*0.135*							**0.162**	*0.026*	**0.171**	*0.017*
Er	**0.599**	*0.246*							**0.308**	*0.056*	**0.357**	*0.023*
Tm	**0.0585**	*0.0220*							**0.0295**	*0.0051*	**0.0385**	*0.0080*
Yb	**0.290**	*0.100*							**0.141**	*0.033*	**0.167**	*0.026*
Lu	**0.0339**	*0.0140*							**0.0152**	*0.0037*	**0.0197**	*0.0036*
Sc	**79.1**	*16.4*							**44.7**	*2.4*	**29.2**	*2.5*
Rb	**0.0335**	*0.0332*							**nd**		**nd**	
Sr	**631**	*372*							**117**	*30*	**123**	*9*
Y	**7.26**	*3.54*							**3.61**	*0.54*	**4.01**	*0.33*
Ba	**0.278**	*0.092*							**0.334**	*0.154*	**0.131**	*0.041*
Th	**0.0315**	*0.0128*							**0.0251**	*0.0085*	**0.0351**	*0.0178*
U	**0.0045**	*0.0055*							**0.0054**	*0.0016*	**0.0052**	*0.0031*
Li	**0.301**	*0.069*							**0.847**	*0.207*	**0.920**	*0.098*

Table 4: continued.

clinopyroxene

Major element composition [wt. %]

	wehrlite									
sample	**AJE362**		**AJE400**		**AJE401**		**DJ0214**			**DJ0256**
comment								neoblasts		
n	**9**	*1σ*	**5**	*1σ*	**21**	*1σ*	**14**	*1σ*	**5** *1σ*	**26** *1σ*
SiO_2	**54.60**	*0.20*	**54.40**	*0.10*	**54.11**	*0.39*	**54.24**	*0.40*	**52.84** *0.48*	**54.35** *0.35*
TiO_2	**0.39**	*0.03*	**0.39**	*0.04*	**0.48**	*0.18*	**0.39**	*0.03*	**0.40** *0.04*	**0.40** *0.04*
Al_2O_3	**2.44**	*0.19*	**2.05**	*0.29*	**2.61**	*0.24*	**2.45**	*0.10*	**2.63** *0.10*	**2.47** *0.33*
Cr_2O_3	**2.14**	*0.36*	**2.16**	*0.06*	**3.36**	*0.65*	**3.44**	*0.12*	**3.25**	**2.96** *0.13*
CaO	**18.63**	*0.36*	**18.61**	*0.55*	**18.13**	*0.46*	**18.09**	*0.24*	**17.48** *0.12*	**18.11** *0.40*
FeO	**2.66**	*0.06*	**2.91**	*0.16*	**2.33**	*0.17*	**2.39**	*0.08*	**2.54** *0.01*	**2.58** *0.15*
MgO	**16.22**	*0.48*	**16.52**	*0.26*	**15.64**	*0.67*	**15.52**	*0.13*	**16.14** *0.25*	**15.89** *0.34*
MnO	**0.10**	*0.02*	**0.09**	*0.02*	**0.09**	*0.02*	**0.07**	*0.02*	**0.09** *0.03*	**0.09** *0.03*
Na_2O	**2.51**	*0.20*	**2.40**	*0.16*	**2.86**	*0.40*	**2.90**	*0.07*	**2.74** *0.09*	**2.73** *0.17*
total	**99.69**		**99.53**		**99.60**		**99.49**		**98.12**	**99.57**
Mg#	**0.92**		**0.91**		**0.92**		**0.92**		**0.92**	**0.92**

Oxygen isotope composition [‰]

$\delta^{18}O$	**5.17**		**5.32**		**5.02**		**5.26**		**nd**	**5.22**
replicate	**5.39**		**5.43**		**5.17**		**5.06**		**nd**	**5.80**

Trace element composition [ppm]

n	**5**	*1σ*	**4**	*1σ*	**5**	*1σ*	**5**	*1σ*	**7** *1σ*
Co	**nd**		**nd**		**nd**		**nd**		**14.1** *0.6*
Zn	**nd**		**nd**		**nd**		**nd**		**10.3** *0.9*
Ni	**243**	*3*	**265**	*1*	**240**	*5*	**228**	*22*	**232** *9*
Ti	**2711**	*118*	**2592**	*343*	**2596**	*143*	**2766**	*156*	**2764** *133*
V	**273**	*5*	**233**	*48*	**270**	*10*	**264**	*10*	**267** *13*
Zr	**68.6**	*7.3*	**59.9**	*13.9*	**61.1**	*5.6*	**88.1**	*6.6*	**72.4** *4.9*
Nb	**0.434**	*0.104*	**0.252**	*0.016*	**0.498**	*0.237*	**0.403**	*0.074*	**1.03** *0.11*
Hf	**3.71**	*0.62*	**3.44**	*1.44*	**3.40**	*0.28*	**4.56**	*0.58*	**4.16** *0.41*
Ta	**0.0369**	*0.0074*	**0.0222**	*0.0055*	**0.0302**	*0.0163*	**0.0481**	*0.0271*	**0.0738** *0.0139*
La	**1.70**	*0.07*	**1.48**	*0.03*	**1.50**	*0.04*	**1.41**	*0.08*	**2.24** *0.13*
Ce	**6.53**	*0.41*	**5.55**	*0.13*	**5.65**	*0.26*	**5.57**	*0.17*	**6.82** *0.31*
Pr	**1.30**	*0.09*	**1.20**	*0.05*	**1.13**	*0.06*	**1.21**	*0.05*	**1.45** *0.14*
Nd	**7.60**	*0.46*	**7.24**	*0.41*	**7.46**	*1.07*	**7.77**	*0.86*	**8.01** *0.34*
Sm	**2.14**	*0.12*	**2.02**	*0.16*	**1.96**	*0.23*	**2.25**	*0.20*	**2.21** *0.12*
Eu	**0.667**	*0.043*	**0.593**	*0.072*	**0.591**	*0.041*	**0.682**	*0.068*	**0.670** *0.028*
Gd	**1.97**	*0.15*	**1.86**	*0.24*	**1.74**	*0.09*	**2.06**	*0.13*	**2.07** *0.09*
Tb	**0.238**	*0.019*	**0.236**	*0.038*	**0.223**	*0.015*	**0.259**	*0.017*	**0.264** *0.015*
Dy	**1.27**	*0.10*	**1.19**	*0.22*	**1.12**	*0.09*	**1.32**	*0.12*	**1.31** *0.08*
Ho	**0.179**	*0.017*	**0.171**	*0.036*	**0.151**	*0.006*	**0.196**	*0.006*	**0.187** *0.014*
Er	**0.360**	*0.042*	**0.341**	*0.058*	**0.323**	*0.021*	**0.392**	*0.014*	**0.366** *0.023*
Tm	**0.0345**	*0.0047*	**0.0294**	*0.0061*	**0.0305**	*0.0056*	**0.0384**	*0.0052*	**0.0399** *0.0041*
Yb	**0.174**	*0.020*	**0.177**	*0.047*	**0.153**	*0.019*	**0.186**	*0.018*	**0.190** *0.023*
Lu	**0.0182**	*0.0031*	**0.0163**	*0.0031*	**0.0182**	*0.0034*	**0.0208**	*0.0023*	**0.0180** *0.0048*
Sc	**37.3**	*1.2*	**28.3**	*2.6*	**32.2**	*1.0*	**36.4**	*0.7*	**36.6** *1.5*
Rb	**0.0347**	*0.0075*	**<dl**		**0.144**	*0.088*	**0.243**	*0.292*	**0.528** *0.148*
Sr	**100**	*3*	**100**	*10*	**98.7**	*8.7*	**101**	*6*	**107** *2*
Y	**4.22**	*0.30*	**4.03**	*0.80*	**3.68**	*0.19*	**4.70**	*0.35*	**4.32** *0.14*
Ba	**0.974**	*0.096*	**0.047**	*0.004*	**2.46**	*1.88*	**0.125**	*0.014*	**6.29** *0.39*
Th	**0.0315**	*0.0019*	**0.0197**	*0.0014*	**0.0451**	*0.0197*	**0.0193**	*0.0094*	**0.133** *0.007*
U	**0.0090**	*0.0009*	**0.0043**	*0.0016*	**0.0118**	*0.0040*	**0.0066**	*0.0012*	**0.0220** *0.0047*
Li	**nd**		**nd**		**nd**		**nd**		**nd**

Table 4: continued.

clinopyroxene

Major element composition [wt. %]

	wehrlite								*websterite*	
sample	**DJ0258A**		**DJ0271**		**DJ0275**		**DJ0276**		**DJ0215**	
comment										
n	**6**	*1σ*	**6**	*1σ*	**5**	*1σ*	**3**	*1σ*	**7**	*1σ*
SiO_2	**54.54**	*1.02*	**54.15**	*0.26*	**54.72**	*0.14*	**54.40**	*0.07*	**54.32**	*0.32*
TiO_2	**0.41**	*0.03*	**0.41**	*0.03*	**0.24**	*0.04*	**0.29**	*0.01*	**<dl**	
Al_2O_3	**2.71**	*0.17*	**2.80**	*0.15*	**1.05**	*0.05*	**1.45**	*0.06*	**1.43**	*0.12*
Cr_2O_3	**2.53**	*0.39*	**3.35**	*0.29*	**0.91**	*0.07*	**1.52**	*0.83*	**0.83**	*0.03*
CaO	**17.62**	*0.39*	**17.90**	*0.23*	**21.78**	*0.14*	**20.60**	*0.46*	**22.29**	*0.32*
FeO	**2.43**	*0.15*	**2.63**	*0.02*	**3.07**	*0.08*	**3.13**	*0.19*	**2.72**	*0.09*
MgO	**16.38**	*0.55*	**15.52**	*0.26*	**16.63**	*0.12*	**16.29**	*0.33*	**16.90**	*0.26*
MnO	**0.10**	*0.04*	**0.08**		**0.08**	*0.02*	**0.08**	*0.01*	**0.08**	*0.04*
Na_2O	**2.77**	*0.22*	**2.99**	*0.16*	**1.50**	*0.05*	**1.91**	*0.28*	**1.14**	*0.07*
total	**99.48**		**99.82**		**99.99**		**99.67**		**99.71**	
Mg#	**0.92**		**0.91**		**0.91**		**0.90**		**0.92**	

Oxygen isotope composition [‰]

$\delta^{18}O$	**5.09**		**4.92**		**5.00**		**nd**		**4.82**	
replicate	**5.05**		**5.05**		**4.93**		**nd**		**5.22**	

Trace element composition [ppm]

n	**9**	*1σ*	**12**	*1σ*	**4**	*1σ*	**10**	*1σ*	**4**	*1σ*
Co	**22.9**	*1.0*	**21.0**	*2.5*	**nd**		**21.0**	*1.5*	**nd**	
Zn	**12.9**	*2.6*	**13.1**	*3.0*	**nd**		**14.6**	*3.1*	**nd**	
Ni	**329**	*27*	**369**	*71*	**183**	*7*	**207**	*20*	**334**	*7*
Ti	**2796**	*225*	**2817**	*179*	**1693**	*33*	**1965**	*148*	**359**	*11*
V	**296**	*31*	**326**	*24*	**397**	*14*	**410**	*25*	**239**	*9*
Zr	**54.8**	*7.0*	**66.5**	*10.3*	**113**	*6*	**90.8**	*8.9*	**15.8**	*1.4*
Nb	**0.322**	*0.091*	**0.294**	*0.147*	**0.252**	*0.020*	**0.225**	*0.019*	**0.328**	*0.044*
Hf	**2.87**	*0.56*	**4.14**	*0.67*	**7.41**	*0.34*	**5.61**	*0.79*	**0.558**	*0.029*
Ta	**0.0304**	*0.0074*	**0.0380**	*0.0115*	**0.0224**	*0.0009*	**0.0197**	*0.0048*	**0.0411**	*0.0035*
La	**1.55**	*0.12*	**1.71**	*0.31*	**2.03**	*0.39*	**2.28**	*0.17*	**16.8**	*1.2*
Ce	**6.09**	*0.40*	**6.78**	*0.83*	**8.54**	*1.79*	**9.69**	*0.72*	**37.4**	*1.9*
Pr	**1.14**	*0.08*	**1.31**	*0.24*	**1.77**	*0.36*	**1.91**	*0.15*	**3.89**	*0.34*
Nd	**6.47**	*0.65*	**7.51**	*0.99*	**10.2**	*1.9*	**10.6**	*0.7*	**12.3**	*1.6*
Sm	**1.74**	*0.21*	**2.11**	*0.28*	**2.78**	*0.45*	**3.00**	*0.27*	**1.29**	*0.21*
Eu	**0.569**	*0.088*	**0.638**	*0.053*	**0.844**	*0.124*	**0.893**	*0.065*	**0.270**	*0.049*
Gd	**1.70**	*0.19*	**1.75**	*0.28*	**2.42**	*0.30*	**2.38**	*0.19*	**0.634**	*0.102*
Tb	**0.253**	*0.044*	**0.247**	*0.023*	**0.300**	*0.032*	**0.282**	*0.021*	**0.0490**	*0.0105*
Dy	**1.19**	*0.20*	**1.13**	*0.20*	**1.48**	*0.12*	**1.43**	*0.10*	**0.183**	*0.035*
Ho	**0.172**	*0.016*	**0.167**	*0.030*	**0.204**	*0.011*	**0.205**	*0.030*	**0.0216**	*0.0046*
Er	**0.369**	*0.058*	**0.380**	*0.042*	**0.394**	*0.028*	**0.388**	*0.077*	**0.0472**	*0.0081*
Tm	**0.0392**	*0.0067*	**0.0445**	*0.0113*	**0.0395**	*0.0033*	**nd**		**0.0044**	*0.0008*
Yb	**0.187**	*0.014*	**0.163**	*0.026*	**0.184**	*0.009*	**0.180**	*0.064*	**0.0167**	*0.0036*
Lu	**0.0219**	*0.0068*	**0.0255**	*0.0084*	**0.0186**	*0.0024*	**0.0169**	*0.0108*	**0.0032**	*0.0013*
Sc	**26.8**	*2.6*	**29.5**	*1.5*	**56.5**	*2.1*	**45.7**	*4.5*	**28.1**	*1.3*
Rb	**0.0057**	*0.0003*	**0.0694**	*0.1072*	**0.0242**	*0.0169*	**<dl**		**<dl**	
Sr	**91.6**	*2.0*	**105**	*5*	**131**	*16*	**137**	*11*	**341**	*28*
Y	**4.14**	*0.50*	**4.03**	*0.36*	**4.52**	*0.21*	**4.50**	*0.19*	**0.582**	*0.106*
Ba	**0.0674**	*0.0103*	**0.336**	*0.238*	**0.209**	*0.243*	**0.142**	*0.096*	**0.119**	*0.052*
Th	**0.0310**	*0.0128*	**0.0547**	*0.0296*	**0.0164**	*0.0016*	**0.0183**	*0.0123*	**0.528**	*0.045*
U	**0.0083**	*0.0024*	**0.0079**	*0.0015*	**0.0033**	*0.0003*	**0.0041**	*0.0162*	**0.0264**	*0.0019*
Li	**0.901**	*0.077*	**1.49**	*0.19*	**nd**		**0.509**	*0.121*	**nd**	

Olivine in wehrlite xenoliths has a major element composition similar to olivine in Kaapvaal mantle peridotites (Fo_{92-93} versus Fo_{89-93} and NiO 0.3 to 0.4 wt. % and 0.3 to 0.5 wt. %, respectively; Table 2; e.g. Boyd and Mertzman, 1987; Simon et al., 2007). No compositional difference exists between olivine porphyroclasts and olivine neoblasts in porphyroclastic wehrlites (Table 2). Wehrlitic olivine has similar to slightly higher forsterite contents than dunitic olivine (Fig. 2 and Fig. 3) and a smaller range in NiO contents (0.31-0.36 wt.% versus 0.27-0.39 wt. %), excluding wehrlites DJ0275 and DJ0276, which have lower NiO (0.3-0.4 wt. % versus 0.2 wt. %, respectively) and lower forsterite contents (Fo_{92-93} versus Fo_{90}, respectively). Clinopyroxene and orthopyroxene in wehrlites have Mg# of 0.90-0.92 and 0.92-0.93, respectively (Table 3), and garnet has Mg# of 0.83-0.85 (Table 5), all similar to clinopyroxene, orthopyroxene and garnet in the studied dunites. Clinopyroxene is rich in CaO, lying within the Ca-rich end of the Kaapvaal mantle peridotite clinopyroxene compositional field (Fig. 4). Orthopyroxene in wehrlite has higher TiO_2, Al_2O_3, Cr_2O_3 and Na_2O contents than orthopyroxene in dunite. Garnet has a major element composition higher in TiO_2, Cr_2O_3, CaO and lower in Al_2O_3 compared to garnet in dunite DJ0259. They can be classified as titanian-pyrope to titanian uvarovite-pyrope garnets

Table 4: continued.

clinopyroxene

Major element composition [wt. %]						
	websterite					
sample	**DJ0216**		**DJ0217**		**DJ0218**	
comment						
n	**7**	*1σ*	**7**	*1σ*	**11**	*1σ*
SiO_2	**54.38**	*0.17*	**54.18**	*0.16*	**54.44**	*0.35*
TiO_2	**0.17**	*0.02*	**0.22**	*0.02*	**<dl**	
Al_2O_3	**2.47**	*0.14*	**2.63**	*0.11*	**1.68**	*0.07*
Cr_2O_3	**1.04**	*0.16*	**1.66**	*0.12*	**0.95**	*0.05*
CaO	**20.51**	*0.19*	**19.33**	*0.33*	**21.90**	*0.32*
FeO	**3.32**	*0.05*	**3.84**	*0.05*	**2.69**	*0.09*
MgO	**15.57**	*0.17*	**15.09**	*0.13*	**16.75**	*0.20*
MnO	**0.09**	*0.02*	**0.11**	*0.04*	**0.08**	*0.03*
Na_2O	**2.12**	*0.09*	**2.53**	*0.14*	**1.40**	*0.05*
total	**99.67**		**99.58**		**99.89**	
Mg#	**0.89**		**0.88**		**0.92**	
Oxygen isotope composition [‰]						
$\delta^{18}O$	**4.94**		**5.39**		**4.93**	
replicate	**5.55**		**5.47**		**4.92**	
Trace element composition [ppm]						
n	**4**	*1σ*	**5**	*1σ*	**4**	*1σ*
Co	**nd**		**nd**		**nd**	
Zn	**nd**		**nd**		**nd**	
Ni	**217**	*51*	**292**	*10*	**333**	*17*
Ti	**977**	*262*	**1506**	*41*	**188**	*9*
V	**267**	*66*	**313**	*6*	**197**	*5*
Zr	**40.8**	*10.6*	**77.5**	*3.5*	**18.6**	*4.4*
Nb	**0.254**	*0.081*	**0.728**	*0.078*	**0.442**	*0.042*
Hf	**1.36**	*0.38*	**2.60**	*0.10*	**0.436**	*0.143*
Ta	**0.0235**	*0.0063*	**0.0932**	*0.0046*	**0.0363**	*0.0067*
La	**18.8**	*4.9*	**5.99**	*0.45*	**23.3**	*0.9*
Ce	**52.3**	*12.7*	**22.3**	*1.3*	**46.8**	*4.8*
Pr	**6.24**	*1.55*	**4.82**	*0.26*	**5.94**	*1.01*
Nd	**20.4**	*5.4*	**27.8**	*1.4*	**21.7**	*4.2*
Sm	**2.29**	*0.60*	**5.93**	*0.25*	**2.37**	*0.54*
Eu	**0.522**	*0.126*	**1.45**	*0.03*	**0.480**	*0.129*
Gd	**1.55**	*0.35*	**3.67**	*0.15*	**1.21**	*0.30*
Tb	**0.194**	*0.051*	**0.347**	*0.015*	**0.101**	*0.022*
Dy	**0.978**	*0.245*	**1.46**	*0.06*	**0.405**	*0.121*
Ho	**0.152**	*0.041*	**0.204**	*0.010*	**0.0506**	*0.0138*
Er	**0.372**	*0.029*	**0.408**	*0.028*	**0.0946**	*0.0206*
Tm	**0.0322**	*0.0080*	**0.0409**	*0.0053*	**0.0077**	*0.0025*
Yb	**0.168**	*0.047*	**0.189**	*0.005*	**0.0264**	*0.0108*
Lu	**0.0174**	*0.0041*	**0.0233**	*0.0022*	**0.0046**	*0.0022*
Sc	**47.6**	*12.6*	**59.7**	*1.5*	**25.5**	*0.6*
Rb	**<dl**		**<dl**		**<dl**	
Sr	**460**	*114*	**395**	*22*	**470**	*67*
Y	**3.73**	*0.96*	**4.86**	*0.05*	**1.21**	*0.36*
Ba	**0.107**	*0.089*	**0.581**	*0.412*	**0.0753**	*0.0181*
Th	**0.311**	*0.108*	**0.0721**	*0.0088*	**0.769**	*0.045*
U	**0.0256**	*0.0093*	**0.0157**	*0.0024*	**0.0496**	*0.0035*
Li	**nd**		**nd**		**nd**	

(G11; after Dawson & Stephens 1976). In wehrlite xenoliths spinel has a slightly lower Cr# (0.67-0.84) and higher Mg# (0.57-0.68) than spinel in dunites (Table 6). The high TiO_2 content of spinel in dunite and wehrlite xenoliths (1.6-3.7 wt. %) compared to primary spinel in Kaapvaal mantle peridotites (0.0-2.0 wt. %; Carswell et al., 1979; Hervig et al., 1986; Boyd and Mertzman, 1987) reflects a secondary origin as break down product of rutile (e.g.

Table 5: Average major element, oxygen isotope and trace element compositions of garnet in dunite, wehrlite and websterite xenoliths (Abbreviations same as in Table 1 and 2).

garnet

Major element composition [wt. %]												
	dunite		***wehrlite***								***websterite***	
sample	**DJ0259**		**AJE401**		**DJ0256**		**DJ0258A**		**DJ0271**		**DJ0215**	
comment												
n	**2**	*1σ*	**4**	*1σ*	**26**	*1σ*	**3**	*1σ*	**8**	*1σ*	**6**	*1σ*
SiO_2	**43.35**	*0.43*	**41.10**	*0.27*	**41.01**	*0.39*	**42.78**	*0.48*	**40.94**	*0.20*	**41.00**	*0.09*
TiO_2	**0.27**	*0.07*	**1.03**	*0.26*	**1.00**	*0.20*	**0.63**	*0.05*	**0.60**	*0.05*	**<dl**	
Al_2O_3	**19.97**	*0.45*	**18.17**	*1.11*	**18.31**	*0.78*	**18.37**	*1.38*	**18.03**	*0.64*	**20.93**	*0.20*
Cr_2O_3	**4.40**	*0.49*	**5.34**	*1.18*	**5.32**	*0.88*	**6.13**	*1.63*	**6.11**	*0.82*	**2.69**	*0.14*
CaO	**4.71**	*0.04*	**6.77**	*0.65*	**6.54**	*0.60*	**5.31**	*0.51*	**5.52**	*0.32*	**5.49**	*0.12*
FeO	**6.44**	*0.29*	**6.53**	*0.22*	**7.24**	*0.11*	**6.53**	*0.20*	**7.52**	*0.09*	**10.41**	*0.14*
MgO	**21.22**	*0.28*	**19.90**	*0.76*	**19.64**	*0.65*	**20.41**	*0.62*	**20.09**	*0.36*	**18.32**	*0.17*
MnO	**0.33**	*0.01*	**0.34**	*0.05*	**0.32**	*0.03*	**0.33**	*0.03*	**0.38**	*0.02*	**0.57**	*0.05*
Na_2O	**0.07**	*0.02*	**0.09**	*0.03*	**0.09**	*0.02*	**0.10**	*0.04*	**0.09**	*0.02*	**0.03**	*0.01*
total	**100.73**		**99.28**		**99.48**		**100.58**		**99.29**		**99.43**	
Mg#	**0.85**		**0.84**		**0.83**		**0.85**		**0.83**		**0.76**	
Oxygen isotope composition [‰]												
$\delta^{18}O$	**nd**		**nd**		**4.96**		**nd**		**4.70**		**4.74**	
replicate	**nd**		**nd**		**5.49**		**nd**		**4.58**		**4.82**	
Trace element composition [ppm]												
n	**4**	*1σ*	**8**	*1σ*	**10**	*1σ*	**4**	*1σ*	**12**	*1σ*	**4**	*1σ*
Co	**37.7**	*1.1*	**54.3**	*11.1*	**43.3**	*3.2*	**44.5**	*6.0*	**nd**		**nd**	
Zn	**9.83**	*1.20*	**35.2**	*12.7*	**40.4**	*21.4*	**14.6**	*2.0*	**nd**		**nd**	
Ni	**42.1**	*0.4*	**73.9**	*23.4*	**81.5**	*20.7*	**59.4**	*8.9*	**65.4**	*6.6*	**25.8**	*0.6*
Ti	**1801**	*261*	**7500**	*1598*	**7353**	*1926*	**4350**	*319*	**4253**	*259*	**417**	*16*
V	**218**	*9*	**409**	*103*	**449**	*88*	**206**	*23*	**262**	*14*	**167**	*6*
Zr	**68.0**	*10.7*	**314**	*112*	**366**	*155*	**111**	*14*	**155**	*24*	**37.2**	*7.6*
Nb	**0.305**	*0.092*	**0.912**	*0.619*	**0.981**	*0.573*	**0.179**	*0.041*	**0.170**	*0.061*	**0.297**	*0.087*
Hf	**1.06**	*0.11*	**7.93**	*2.59*	**9.76**	*3.60*	**2.30**	*0.49*	**3.54**	*0.62*	**0.371**	*0.106*
Ta	**0.0303**	*0.0024*	**0.0532**	*0.0145*	**0.0663**	*0.0280*	**0.0188**	*0.0096*	**0.0445**	*0.0333*	**0.0129**	*0.0012*
La	**0.0673**	*0.0444*	**0.225**	*0.141*	**0.397**	*0.306*	**0.0134**	*0.0062*	**0.0542**	*0.0478*	**0.0823**	*0.0283*
Ce	**0.568**	*0.268*	**1.18**	*1.11*	**1.23**	*0.67*	**0.136**	*0.001*	**0.234**	*0.068*	**0.436**	*0.037*
Pr	**0.205**	*0.054*	**0.215**	*0.111*	**0.442**	*0.315*	**0.0694**	*0.0301*	**0.0942**	*0.0298*	**0.139**	*0.018*
Nd	**2.11**	*0.34*	**2.55**	*1.85*	**2.68**	*0.58*	**0.899**	*0.045*	**0.943**	*0.192*	**1.00**	*0.13*
Sm	**1.78**	*0.30*	**2.22**	*1.70*	**2.18**	*0.62*	**1.01**	*0.11*	**1.02**	*0.15*	**0.574**	*0.104*
Eu	**0.750**	*0.118*	**1.07**	*0.50*	**1.07**	*0.32*	**0.522**	*0.048*	**0.576**	*0.088*	**0.224**	*0.033*
Gd	**2.84**	*0.65*	**5.16**	*2.54*	**5.27**	*1.70*	**2.59**	*0.27*	**2.81**	*0.26*	**0.893**	*0.221*
Tb	**0.442**	*0.106*	**1.00**	*0.29*	**1.10**	*0.37*	**0.611**	*0.094*	**0.704**	*0.079*	**0.171**	*0.023*
Dy	**3.01**	*0.80*	**8.06**	*1.85*	**8.88**	*2.82*	**5.50**	*0.43*	**6.19**	*0.65*	**1.32**	*0.19*
Ho	**0.64**	*0.15*	**1.83**	*0.49*	**1.93**	*0.58*	**1.36**	*0.12*	**1.44**	*0.13*	**0.292**	*0.046*
Er	**1.89**	*0.36*	**5.43**	*1.72*	**5.38**	*1.63*	**4.36**	*0.43*	**4.49**	*0.49*	**0.898**	*0.111*
Tm	**0.294**	*0.049*	**0.787**	*0.274*	**0.709**	*0.186*	**0.654**	*0.091*			**0.136**	*0.008*
Yb	**2.08**	*0.25*	**4.75**	*1.56*	**4.16**	*1.34*	**4.60**	*0.38*	**4.00**	*0.39*	**0.968**	*0.054*
Lu	**0.350**	*0.028*	**0.688**	*0.242*	**0.571**	*0.172*	**0.715**	*0.059*	**0.593**	*0.069*	**0.161**	*0.014*
Sc	**98.6**	*3.8*	**156**	*32*	**118**	*27*	**93.9**	*11.5*	**89.5**	*6.8*	**129**	*2*
Rb	**0.0172**		**0.0853**	*0.0356*	**3.14**	*1.17*	**0.0295**	*0.0049*	**0.175**	*0.132*	**0.0195**	*0.0021*
Sr	**2.11**	*1.70*	**1.97**	*1.33*	**15.3**	*10.6*	**0.388**	*0.288*	**0.527**	*0.283*	**0.287**	*0.092*
Y	**17.0**	*4.0*	**43.8**	*11.4*	**44.1**	*14.2*	**33.4**	*2.9*	**35.8**	*2.5*	**8.09**	*0.81*
Ba	**0.109**	*0.099*	**0.350**	*0.289*	**10.78**	*7.07*	**0.138**	*0.125*	**0.202**	*0.082*	**0.167**	*0.039*
Th	**0.0029**	*0.0021*	**0.0187**	*0.0114*	**0.0846**	*0.0565*	**0.0053**	*0.0026*	**0.0203**	*0.0091*	**0.0219**	*0.0089*
U	**0.0173**	*0.0016*	**0.0342**	*0.0169*	**0.0508**	*0.0236*	**0.0067**	*0.0014*	**0.0146**	*0.0056*	**0.0309**	*0.0024*
Li	**0.0801**	*0.0172*	**1.07**	*0.29*	**nd**		**0.250**	*0.050*	**0.497**	*0.137*	**nd**	

DJ0214), in kelyphite rims of garnet (e.g. DJ0256) or in glass patches occurring together with phlogopite (e.g. DJ0274). Rutile occurs only in wehrlite xenoliths DJ0214, DJ0256 and DJ0271 and is intergrown with clinopyroxene. It has high Cr_2O_3 contents (3.9-5.8 wt. %). In sample DJ0214 it occurs next to chromite, has a Cr-rich core and breaks down into ilmenite and Ti-rich chromite lamellae and patches (Fig. 5 d). Ilmenite in these rutile-bearing samples has higher Cr_2O_3 content (5.8-10.6 wt. %) than ilmenite in dunite xenoliths. Most phlogopites in wehrlite xenoliths are secondary, occurring in kelyphite rims of garnet (Fig. 5 b), together with ilmenite or as crystals consuming clinopyroxene. Secondary phlogopite has high TiO_2 and Cr_2O_3 contents compared to primary phlogopite (TiO_2 = 1.2-4.1 wt. % versus 0.9 wt. % and Cr_2O_3 = 0.25-2.5 wt. % versus 0.2 wt. %, respectively; Table 7). It can be chemically subdivided into phlogopite replacing garnet in kelyphite rims,

Table 5: continued.

garnet

Major element composition [wt. %]						
	websterite					
sample	**DJ0216**		**DJ0217**		**DJ0218**	
comment						
n	**5**	*1σ*	**7**	*1σ*	**9**	*1σ*
SiO_2	**41.19**	*0.09*	**40.61**	*0.20*	**41.33**	*0.19*
TiO_2	**0.11**	*0.01*	**0.18**	*0.02*	**<dl**	
Al_2O_3	**21.12**	*0.25*	**19.94**	*0.18*	**21.37**	*0.19*
Cr_2O_3	**2.35**	*0.25*	**3.51**	*0.07*	**2.30**	*0.21*
CaO	**4.84**	*0.13*	**5.26**	*0.11*	**5.10**	*0.09*
FeO	**10.82**	*0.09*	**11.91**	*0.08*	**10.13**	*0.13*
MgO	**18.66**	*0.12*	**17.53**	*0.09*	**19.06**	*0.01*
MnO	**0.56**	*0.02*	**0.47**	*0.04*	**0.53**	*0.05*
Na_2O	**<dl**		**0.05**	*0.02*	**<dl**	
total	**99.66**		**99.45**		**99.81**	
Mg#	**0.75**		**0.72**		**0.77**	
Oxygen isotope composition [‰]						
$\delta^{18}O$	**4.90**		**5.26**		**4.80**	
replicate	**5.29**		**5.14**		**4.80**	
Trace element composition [ppm]						
n	**4**	*1σ*	**4**	*1σ*	**4**	*1σ*
Co	**nd**		**nd**		**nd**	
Zn	**nd**		**nd**		**nd**	
Ni	**26.8**	*11.1*	**30.1**	*0.8*	**29.8**	*5.6*
Ti	**974**	*476*	**1286**	*23*	**200**	*14*
V	**147**	*69*	**182**	*5*	**111**	*10*
Zr	**28.0**	*14.0*	**43.7**	*5.4*	**12.2**	*5.0*
Nb	**0.122**	*0.053*	**0.244**	*0.028*	**0.279**	*0.038*
Hf	**0.210**	*0.111*	**0.629**	*0.043*	**0.0362**	*0.0071*
Ta	**0.0106**	*0.0045*	**0.0206**	*0.0032*	**0.0128**	*0.0007*
La	**<dl**		**0.0314**	*0.0014*	**0.0491**	*0.0258*
Ce	**0.620**	*0.315*	**0.571**	*0.020*	**0.533**	*0.084*
Pr	**0.189**	*0.077*	**0.308**	*0.027*	**0.142**	*0.005*
Nd	**1.42**	*0.81*	**3.31**	*0.20*	**1.20**	*0.20*
Sm	**0.818**	*0.429*	**1.90**	*0.16*	**0.572**	*0.132*
Eu	**0.417**	*0.217*	**0.717**	*0.104*	**0.204**	*0.057*
Gd	**2.15**	*1.13*	**2.72**	*0.31*	**0.713**	*0.187*
Tb	**0.596**	*0.309*	**0.544**	*0.030*	**0.125**	*0.020*
Dy	**6.35**	*3.57*	**4.59**	*0.23*	**1.14**	*0.24*
Ho	**1.79**	*1.00*	**1.14**	*0.08*	**0.262**	*0.041*
Er	**6.27**	*3.50*	**3.75**	*0.21*	**0.811**	*0.109*
Tm	**1.06**	*0.63*	**0.578**	*0.046*	**0.116**	*0.007*
Yb	**7.93**	*4.78*	**3.97**	*0.29*	**0.950**	*0.055*
Lu	**1.30**	*0.75*	**0.680**	*0.048*	**0.151**	*0.018*
Sc	**206**	*109*	**156**	*4*	**120**	*5*
Rb	**<dl**		**0.0254**	*0.0076*	**<dl**	
Sr	**0.473**	*0.145*	**0.896**	*0.514*	**0.372**	*0.355*
Y	**48.6**	*26.5*	**30.6**	*1.7*	**8.30**	*1.77*
Ba	**0.0805**	*0.0187*	**<dl**		**0.124**	*0.081*
Th	**0.0189**	*0.0141*	**0.0152**	*0.0055*	**0.0227**	*0.0055*
U	**0.0205**	*0.0102*	**0.0302**	*0.0098*	**0.0440**	*0.0118*
Li	**nd**		**nd**		**nd**	

having high Al_2O_3 and Cr_2O_3 contents (12.9-14.5 wt. % and 1.3-2.5 wt. %; Delaney et al., 1980) and phlogopite replacing clinopyroxene having intermediate Al_2O_3 (11.9-13.3 wt. %) and Cr_2O_3 contents (0.3-1.8 wt. %) between garnet breakdown phlogopite and primary phlogopite.

4.1.3. Websterite xenoliths

Websterite xenoliths comprise mainly orthopyroxene (40-85 vol. %), clinopyroxene (5-42 vol. %) and garnet (4-10 vol. %; Fig. 1 g-h). Additionally phlogopite occurs in minor amounts. Since up to 33 Vol. % intensely serpentinized olivine is present in sample DJ0216 it should rather be classified as lherzolite (Fig. 1 h), but its unusual low olivine content compared to typical mantle lherzolites (80-48 vol. %; e.g. Nixon and Boyd, 1973; Boyd and Mertzman, 1987; Boyd, 1989b; Simon et al., 2007) and its petrographic and compositional similarity with websterite xenoliths DJ0215, DJ0217 and DJ0218, have led us to classify this sample as websterite too. It can be seen has a link between websterites and fertile lherzolites.

The websterite xenoliths may also have dunitic or harzburgitic protoliths (as seen in sample DJ0216), but are totally overprinted by crystallization of secondary minerals, predominantly orthopyroxene. They have the highest amount of metasomatically added minerals (66-100 Vol. %). Websterite xenoliths are coarse-grained granular with large anhedral, amoeboid orthopyroxene (15 mm - 200 µm), clinopyroxene (6 mm - 35 µm) and garnet minerals that could have crystallized at the expense of olivine (6 - 1 mm in DJ0216; Fig. 1 h). Samples DJ0215 and DJ0218 contain fine grained garnets (2 mm - 70 µm), that have crystallised as small chains along pyroxene grain boundaries (Fig. 1 g), while DJ0216 and DJ0217 have coarse amoeboid garnets 6 mm – 250 µm large (Fig. 1 h). Euhedral primary phlogopite (2 mm - 80 µm) and anhedral oxide minerals (750 - 5 µm) occur in minor amounts.

Olivine in websterite DJ0216 has an intermediate forsterite content of Fo_{90} and a high NiO content of 0.4 wt. %, compared to olivine in dunite and wehrlite xenoliths (Fig. 3; Table 2), lying within the range of olivine in Kaapvaal mantle peridotites. Additionally, websterite xenoliths comprise clinopyroxene, orthopyroxene and garnet with similar to slightly lower Mg# compared to dunite and wehrlite xenoliths (clinopyroxene Mg# 0.88-0.92, orthopyroxene 0.88-0.91 and garnet 0.72-0.77; Table 3 to Table 5). Clinopyroxene has a similar to slightly higher CaO content than clinopyroxene in dunite and wehrlite xenoliths (19.3-22.3 wt. % and 17.5-21.8 wt. %, respectively). Orthopyroxene has low TiO_2, CaO, Na_2O and intermediate Al_2O_3 contents compared to dunitic and wehrlitic orthopyroxene. Next to the lower MgO content (Fig. 4), garnet in websterite xenoliths has lower TiO_2, Cr_2O_3, and higher Al_2O_3, FeO, MnO and Na_2O contents compared to garnet in dunite and wehrlite xenoliths (Table 5). It has a chrome-pyrope composition (G9; Dawson and Stephens, 1975) similar to garnet found in dunite DJ0259. Phlogopites in websterite xenoliths occur mostly as large minerals within orthopyroxenes (Fig. 1 g) and have major element compositions similar to primary phlogopite (Delaney et al., 1980). In websterite DJ0217 phlogopite replaces garnet and has higher TiO_2

and Cr_2O_3 contents (Table 7). Phlogopite in websterite xenoliths has high BaO contents compared to phlogopite in dunite and wehrlite xenoliths (0.2-0.5 wt. % versus 0.1 wt. %, respectively). Spinel in websterite sample DJ0217 has similar Mg# as spinel in wehrlite xenoliths, but the lowest Cr# (0.57 and 0.53, respectively).

In dunite, wehrlite and websterite xenoliths coarse-grained minerals such as olivine porphyroclasts and olivine in coarse granular samples as well as pyroxene and garnet minerals are intensely cracked, while olivine neoblasts are fresh and unaltered. Due to weathering, olivine porphyroclasts and neoblasts are serpentinized along grain margins and cracks with sulphide minerals and magnetite crystallizing within serpentine.

Table 6: Average major element and trace element compositions of oxide minerals in dunite, wehrlite and websterite xenoliths (Abbreviations same as in Table 1 and 2, plus Ilm = $(2xFe^{2+})/(Ti+Fe^{2+}+Fe^{3+}+Mg)$; Gk = geikielite = $(2xMg)/(Ti+Fe^{2+}+Fe^{3+}+Mg)$). Fe^{2+} and Fe^{3+} in ilmenite has been calculated stoichiometrically (Droop, 1987).

oxide minerals

Major element composition [wt. %]

	dunite								***wehrlite***		
sample	**DJ0223**	**DJ0259**		**DJ0273**		**DJ0274**		**DJ0297**		**AJE362**	**AJE400**	
comment	rt	ilm		cr		cr		ilm		cr	cr	
n	**1**	**4**	*1σ*	**9**	*1σ*	**3**	*1σ*	**2**	*1σ*	**1**	**2**	*1σ*
TiO_2	**96.70**	**53.30**	*0.33*	**3.68**	*0.43*	**3.59**	*0.02*	**53.93**	*0.05*	**1.57**	**3.24**	*0.23*
Al_2O_3	**nd**	**0.19**	*0.01*	**0.53**	*0.17*	**0.44**	*0.01*	**0.31**	*0.01*	**13.06**	**8.40**	*4.55*
Cr_2O_3	**3.30**	**4.09**	*0.30*	**50.11**	*0.45*	**50.87**	*0.12*	**3.24**	*0.06*	**52.03**	**52.11**	*5.22*
V_2O_3	**nd**	**nd**		**0.28**	*0.15*	**0.22**	*0.03*	**0.09**	*0.03*	**0.33**	**0.23**	*0.06*
FeO	**0.47**	**29.05**	*0.09*	**35.25**	*1.90*	**35.73**	*0.37*	**26.70**	*0.31*	**16.48**	**21.93**	*0.74*
MgO	**0.16**	**12.65**	*0.11*	**8.15**	*1.07*	**7.09**	*0.41*	**14.45**	*0.28*	**14.67**	**12.28**	*0.83*
MnO	**nd**	**0.30**	*0.02*	**0.34**	*0.09*	**0.40**	*0.05*	**0.30**	*0.004*	**0.25**	**0.25**	*0.04*
NiO	**nd**	**0.23**	*0.01*	**0.19**	*0.04*	**0.14**	*0.03*	**0.21**	*0.05*	**0.09**	**0.18**	*0.01*
ZnO	**nd**	**0.05**	*0.01*	**0.15**	*0.05*	**0.18**	*0.01*	**nd**		**nd**	**nd**	
total	**100.63**	**99.87**		**98.68**		**98.65**		**99.22**		**98.48**	**98.61**	
Mg#	**-**	**-**		**0.40**		**0.35**		**-**		**0.68**	**0.57**	
Cr#	**-**	**-**		**0.98**		**0.99**		**-**		**0.73**	**0.81**	
Ilm	**-**	**0.49**		**-**		**-**		**0.44**		**-**	**-**	
Gk	**-**	**0.45**		**-**		**-**		**0.51**		**-**	**-**	

Trace element composition [ppm]

	ilm	
n	**4**	*1σ*
Cr	**20904**	*301*
Co	**200**	*3*
Ni	**1686**	*28*
Cu	**21.6**	*1.1*
Ga	**10.9**	*0.4*
Ge	**0.913**	*0.104*
Mo	**0.472**	*0.031*
Sn	**8.77**	*0.16*
Sb	**<dl**	
W	**0.0675**	*0.0079*
Zr	**581**	*4*
Nb	**734**	*19*
Hf	**19.8**	*0.1*
Ta	**107**	*2*
Sc	**22.0**	*0.4*
Y	**0.0910**	*0.0082*
Ba	**<dl**	
Pb	**0.557**	*0.090*
Th	**0.0018**	*0.0012*
U	**0.0170**	*0.0045*
Li	**2.14**	*0.09*

Table 6: continued.

oxide minerals

Major element composition [wt. %]

	wehrlite										
sample	**AJE401**		**DJ0214**					**DJ0256**			
comment	cr		spl	ilm		rt		cr		cr	
n	**9**	*1σ*	**1**	**2**	*1σ*	**13**	*1σ*	**5**	*1σ*	**2**	*1σ*
TiO_2	**2.76**	*0.28*	**3.32**	**49.50**	*1.80*	**90.73**	*1.73*	**2.82**	*0.82*	**3.64**	*0.09*
Al_2O_3	**11.22**	*2.08*	**7.08**	**0.37**	*0.22*	**0.10**	*0.07*	**17.10**	*7.07*	**6.81**	*0.38*
Cr_2O_3	**52.40**	*2.15*	**54.72**	**11.36**	*0.30*	**5.83**	*1.10*	**44.91**	*5.36*	**54.78**	*0.13*
V_2O_3	**0.25**	*0.03*	**0.18**	**0.04**	*0.01*	**0.06**	*0.04*	**0.30**	*0.03*	**0.19**	*0.21*
FeO	**17.80**	*0.34*	**20.89**	**24.18**	*2.04*	**0.40**	*0.46*	**18.50**	*1.90*	**20.79**	*0.09*
MgO	**14.36**	*0.50*	**12.71**	**14.16**	*0.92*	**<dl**		**14.65**	*1.17*	**12.63**	*0.21*
MnO	**0.23**	*0.02*	**0.25**	**0.15**	*0.01*	**<dl**		**0.20**	*0.03*	**0.19**	*0.05*
NiO	**0.17**	*0.02*	**0.12**	**0.30**	*0.02*	**<dl**		**0.19**	*0.02*	**0.19**	*0.001*
ZnO	**nd**		**nd**	**0.35**	*0.02*	**0.28**	*0.10*	**nd**		**nd**	
total	**99.19**		**99.28**	**100.40**		**97.39**		**98.66**		**99.22**	
Mg#	**0.65**		**0.58**	**-**		**-**		**0.65**		**0.58**	
Cr#	**0.76**		**0.84**	**-**		**-**		**0.64**		**0.84**	
Ilm	**-**		**-**	**0.38**		**-**		**-**		**-**	
Gk	**-**		**-**	**0.54**		**-**		**-**		**-**	

Trace element composition [ppm]

	spl		rt	
n	**2**	*1σ*	**10**	*1σ*
Cr	**IST**		**49825**	*3076*
Co	**296**	*2*	**3.86**	*1.81*
Ni	**1512**	*38*	**44.1**	*11.1*
Cu	**29.2**	*0.4*	**8.83**	*1.77*
Ga	**85.2**	*0.2*	**3.03**	*0.78*
Ge	**1.00**	*0.04*	**0.443**	*0.135*
Mo	**0.146**	*0.026*	**13.6**	*0.7*
Sn	**1.64**	*0.24*	**34.1**	*1.9*
Sb	**0.734**	*0.363*	**0.293**	*0.047*
W	**0.0165**	*0.0007*	**12.4**	*0.6*
Zr	**5.38**	*0.78*	**3639**	*171*
Nb	**2.20**	*1.41*	**12828**	*494*
Hf	**0.240**	*0.010*	**129**	*6*
Ta	**0.204**	*0.185*	**1766**	*81*
Sc	**2.52**	*0.36*	**9.34**	*0.47*
Y	**0.0390**	*0.0255*	**0.0520**	*0.0091*
Ba	**1.85**		**<dl**	
Pb	**29.8**	*4.3*	**6.19**	*4.02*
Th	**0.0078**	*0.0011*	**0.0017**	*0.0005*
U	**0.0042**	*0.0013*	**3.01**	*0.15*
Li	**1.23**	*0.12*	**0.451**	*0.217*

Table 6: continued.

oxide minerals

Major element composition [wt. %]

	wehrlite								*websterite*		
sample	**DJ0256**		**DJ0258A**	**DJ0271**					**DJ0217**		
comment	rt		cr	spl		rt	ilm		cr		ilm
n	**4**	*1σ*	**1**	**3**	*1σ*	**1**	**2**	*1σ*	**3**	*1σ*	**1**
TiO_2	**90.80**	*4.73*	**2.27**	**3.37**	*0.17*	**91.81**	**50.34**	*3.94*	**1.65**	*0.40*	**46.78**
Al_2O_3	**0.56**	*1.12*	**15.44**	**8.52**	*0.87*	**0.00**	**0.27**	*0.01*	**22.52**	*5.29*	**0.49**
Cr_2O_3	**4.57**	*2.01*	**49.35**	**52.70**		**3.94**	**10.65**	*2.10*	**38.02**	*4.99*	**5.78**
V_2O_3	**0.07**	*0.09*	**0.05**	**0.16**	*0.14*	**0.09**	**0.14**	*0.20*	**0.06**	*0.01*	**0.38**
FeO	**0.82**	*1.15*	**17.03**	**21.70**	*0.35*	**0.18**	**25.09**	*1.31*	**24.38**	*1.01*	**35.16**
MgO	**0.48**	*0.86*	**15.35**	**12.64**	*0.13*	**0.02**	**13.13**	*1.40*	***12.36***	*0.97*	***9.97***
MnO	**0.03**	*0.03*	**0.18**	**0.22**	*0.05*	**0.00**	**0.16**	*0.03*	**0.29**	*0.05*	**0.23**
NiO	**0.01**	*0.01*	**0.19**	**0.17**	*0.03*	**0.00**	**0.31**	*0.01*	**0.23**	*0.05*	**0.26**
ZnO	**nd**		**0.30**	**0.09**		**nd**	**nd**		**0.23**	*0.04*	**0.07**
total	**97.34**		**100.16**	**99.57**		**96.04**	**100.09**		**99.74**		**99.13**
Mg#	**-**		**0.70**	**0.58**		**-**	**-**		**0.57**		**-**
Cr#	**-**		**0.68**	**0.81**		**-**	**-**		**0.53**		**-**
Ilm	**-**		**-**	**-**		**-**	**0.46**		**-**		**0.49**
Gk	**-**		**-**	**-**		**-**	**0.50**		**-**		**0.37**

Trace element composition [ppm]

	spl		rt		ilm
n	**6**	*1σ*	**2**	*1σ*	**1**
Cr	**IST**		**45367**	*282*	**90503**
Co	**253**	*20*	**6.13**	*3.68*	**210**
Ni	**1595**	*143*	**39.2**	*10.6*	**3770**
Cu	**25.4**	*2.9*	**8.08**	*0.83*	**40.3**
Ga	**100**	*14*	**1.26**	*0.33*	**23.1**
Ge	**1.05**	*0.31*	**0.422**	*0.182*	**<dl**
Mo	**<dl**		**14.4**	*1.5*	**<dl**
Sn	**1.42**	*0.19*	**34.7**	*2.2*	**14.5**
Sb	**0.163**	*0.093*	**0.338**	*0.035*	**<dl**
W	**<dl**		**10.7**	*0.2*	**<dl**
Zr	**4.15**	*1.00*	**4254**	*18*	**416**
Nb	**0.891**	*0.163*	**9346**	*113*	**350**
Hf	**0.198**	*0.045*	**140**	*3*	**17.1**
Ta	**0.183**	*0.080*	**1412**	*16*	**96.2**
Sc	**1.72**	*0.20*	**9.46**	*0.11*	**29.3**
Y	**<dl**		**0.0374**	*0.0090*	**<dl**
Ba	**<dl**		**<dl**		**<dl**
Pb	**23.9**	*8.4*	**4.25**	*2.08*	**74.3**
Th	**<dl**		**<dl**		**<dl**
U	**0.0115**	*0.0133*	**2.98**	*0.06*	**<dl**
Li	**0.848**	*0.142*	**0.513**	*0.103*	**3.85**

4.2. Oxygen isotope composition of the constituent minerals

Dunite, wehrlite and websterite xenoliths have oxygen isotope compositions similar to mantle peridotites in olivine (4.9-5.6 ‰ in the studied xenoliths versus 4.8-5.5 ‰ in mantle peridotites; Mattey et al., 1994; Fig. 6 and Table 2) and slightly lower than mantle peridotites in clinopyroxene (5.3-5.9 ‰ versus 4.8-5.8 ‰, respectively, Table 4) and garnet (4.9-5.6 ‰ versus 4.6-5.5 ‰, respectively, Table 5). The olivine oxygen isotope composition reflects a primary mantle origin from dunitic to harzburgitic protoliths. Due to serpentine and spinel along olivine neoblast margins, wehrlite sample AJE401 has lower $\delta^{18}O$ values (3.9-4.3 ‰) in olivine neoblasts than in olivine porphyroclasts (5.0-5.2 ‰; spinel has low $\delta^{18}O$ values; Lowry et al., 2003). Orthopyroxene in dunite and websterite xenoliths has $\delta^{18}O$ values similar to

slightly higher than orthopyroxene in mantle peridotites (5.4-6.4 ‰ and 5.4-6.1 ‰, respectively), while orthopyroxene in wehrlite DJ0256 has much lower $\delta^{18}O$ values (4.2 ‰; Table 3), also due to serpentine and spinel in cracks and along grain margins. Phlogopite has $\delta^{18}O$ values typical for metasomatic phlogopite in Kaapvaal mantle peridotites (5.1-6.4 ‰ versus 4.9-7.0, respectively; Table 7; Lowry personal communication).

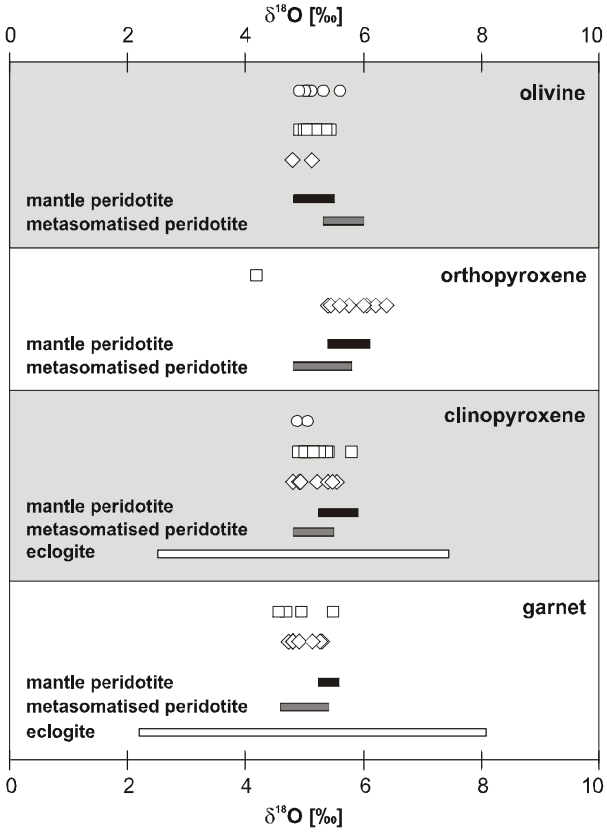

Fig. 6: Oxygen isotope composition of constituent silicate minerals in dunite, wehrlite and websterite xenoliths compared to literature oxygen isotope data (mantle peridotites: Mattey et al., 1994, metasomatised peridotites: Zhang et al., 2003; Perkins et al., 2006, eclogites: MacGregor and Manton, 1986; Jacob et al., 1994; Jacob and Foley, 1999). Symbols as in Fig. 4.

Table 7: Average major element, oxygen isotope and trace element compositions of phlogopite in dunite, wehrlite and websterite xenoliths (Abbreviations same as in Table 1 and 2).

phlogopite

Major element composition [wt. %]

	dunite								***wehrlite***			
sample	**DJ0223**			**DJ0259**		**DJ0273**		**DJ0274**		**AJE362**		**AJE400**	
comment	secondary		primary	repl. ilm		primary		primary		repl. cpx		repl. cpx	
n	**2**	*1σ*	**1**	**4**	*1σ*	**3**	*1σ*	**3**	*1σ*	**5**	*1σ*	**3**	*1σ*
SiO_2	**41.00**	*1.18*	**43.27**	**39.11**	*0.34*	**42.15**	*0.25*	**42.08**	*0.15*	**39.20**	*0.48*	**41.03**	*0.24*
TiO_2	**2.56**	*1.87*	**0.73**	**4.12**	*0.12*	**0.40**	*0.01*	**0.42**	*0.01*	**4.09**	*0.35*	**1.93**	*0.02*
Al_2O_3	**12.35**	*0.72*	**10.62**	**13.19**	*0.27*	**10.38**	*0.02*	**10.19**	*0.15*	**13.34**	*0.48*	**12.78**	*0.12*
Cr_2O_3	**1.02**	*0.54*	**0.53**	**1.06**	*0.04*	**0.20**	*0.04*	**0.32**	*0.21*	**1.64**	*0.22*	**0.77**	*0.08*
BaO	**<dl**		**0.09**	**<dl**		**<dl**		**<dl**		**0.10**	*0.05*	**<dl**	
FeO	**3.94**	*0.39*	**3.26**	**5.13**	*0.16*	**5.05**	*0.07*	**5.10**	*0.25*	**3.44**	*0.39*	**3.53**	*0.17*
MgO	**24.18**	*1.76*	**26.69**	**22.22**	*0.30*	**26.36**	*0.10*	**26.54**	*0.27*	**22.30**	*0.63*	**24.36**	*0.54*
NiO	**nd**			**nd**		**nd**		**nd**		**0.10**	*0.05*	**nd**	
K_2O	**10.20**	*0.05*	**10.67**	**9.76**	*0.30*	**10.46**	*0.12*	**10.20**	*0.09*	**10.14**	*0.32*	**10.02**	*0.24*
Na_2O	**0.38**	*0.04*	**0.09**	**0.34**	*0.03*	**0.16**	*0.04*	**0.14**	*0.03*	**0.50**	*0.08*	**0.36**	*0.13*
Cl	**0.02**	*<0.0*	**0.04**	**0.02**	*<0.01*	**<dl**		**0.02**	*<0.0*	**0.02**	*0.01*	**0.05**	*0.01*
F	**0.49**	*0.03*	**0.74**	**0.52**	*0.07*	**0.64**	*0.14*	**0.81**	*0.08*	**0.36**	*0.08*	**0.44**	*0.01*
total	**96.12**		**96.73**	**95.47**		**95.81**		**95.82**		**95.22**		**95.27**	
Mg#	**0.92**		**0.94**	**0.89**		**0.90**		**0.90**		**0.92**		**0.92**	

Oxygen isotope composition [‰]

$\delta^{18}O$	**nd**	**nd**	**nd**	**5.68**	**nd**	**5.50**	**nd**
replicate	**nd**	**nd**	**nd**	**nd**	**nd**	**5.65**	**nd**

Table 7: continued.

phlogopite

Major element composition [wt. %]

	wehrlite													
sample	**AJE401**				**DJ0214**		**DJ0256**				**DJ0271**		**DJ0275**	
comment	secondary		repl. garnet		repl. cpx		repl. cpx		repl. garnet		repl. cpx		primary	
n	**9**	*1σ*	**3**	*1σ*	**3**	*1σ*	**7**	*1σ*	**13**	*1σ*	**2**	*1σ*	**4**	*1σ*
SiO_2	**40.25**	*0.52*	**38.70**	*0.26*	**40.74**	*0.67*	**39.37**	*0.22*	**38.72**	*0.89*	**40.01**	*1.00*	**41.48**	*0.19*
TiO_2	**1.86**	*0.36*	**2.66**	*0.05*	**2.87**	*0.26*	**3.80**	*0.20*	**3.12**	*0.49*	**2.28**	*0.83*	**0.91**	*0.03*
Al_2O_3	**12.93**	*0.38*	**14.45**	*0.72*	**12.42**	*0.31*	**13.21**	*0.50*	**14.09**	*0.97*	**12.98**	*0.83*	**11.49**	*0.08*
Cr_2O_3	**1.25**	*0.12*	**2.02**	*0.14*	**1.60**	*0.14*	**1.83**	*0.08*	**2.52**	*0.72*	**1.18**	*0.42*	**0.19**	*0.01*
BaO	**<dl**		**0.15**	*0.12*	**<dl**		**<dl**		**0.06**	*0.06*	**0.06**		**<dl**	
FeO	**2.88**	*0.09*	**2.99**	*0.04*	**3.07**	*0.04*	**3.37**	*0.10*	**3.64**	*0.39*	**3.31**	*0.01*	**3.89**	*0.09*
MgO	**24.09**	*0.37*	**22.89**	*0.47*	**23.98**	*0.42*	**22.50**	*0.24*	**22.44**	*0.82*	**23.70**	*1.22*	**25.17**	*0.11*
NiO	**0.18**	*0.01*	**0.16**		**0.16**	*<0.0*	**0.18**	*0.02*	**0.13**	*0.04*	**0.21**	*0.03*	**0.13**	*0.02*
K_2O	**10.38**	*0.18*	**9.39**	*0.70*	**9.92**	*0.35*	**10.26**	*0.29*	**9.68**	*0.67*	**10.19**	*0.23*	**10.98**	*0.16*
Na_2O	**0.20**	*0.06*	**0.68**	*0.28*	**0.49**	*0.04*	**0.41**	*0.05*	**0.48**	*0.16*	**0.35**	*0.35*	**0.15**	*0.04*
Cl	**0.04**	*0.01*	**0.03**	*0.02*	**0.11**	*0.17*	**0.02**	*0.01*	**0.02**	*0.01*	**0.04**	*0.04*	**0.03**	*0.01*
F	**0.34**	*0.02*	**0.26**	*0.05*	**0.51**	*0.09*	**0.38**	*0.07*	**0.35**	*0.12*	**0.31**	*0.02*	**0.49**	*0.03*
total	**94.40**		**94.38**		**95.87**		**95.33**		**95.23**		**94.59**		**94.90**	
Mg#	**0.94**		**0.93**		**0.93**		**0.92**		**0.92**		**0.93**		**0.92**	

Oxygen isotope composition [‰]

$\delta^{18}O$	**5.30**		**nd**		**5.40**		**nd**		**nd**		**5.46**		**5.11**	
replicate	**5.46**		**nd**		**6.12**		**nd**		**nd**		**nd**		**nd**	

Trace element composition [ppm]

comment	secondary												primary	
n	**4**	*1σ*											**4**	*1σ*
Ti	**10941**	*744*											**5699**	*424*
V	**86.1**	*9.4*											**74.3**	*2.2*
Zr	**4.61**	*0.68*											**3.17**	*0.76*
Nb	**5.02**	*0.08*											**5.78**	*0.38*
Hf	**0.157**	*0.022*											**0.131**	*0.025*
Ta	**0.320**	*0.027*											**0.486**	*0.022*
La	**<dl**												**0.0194**	*0.0018*
Ce	**<dl**												**0.0517**	*0.0620*
Pr	**0.0177**	*0.0046*											**0.0087**	*0.0113*
Nd	**0.0547**	*0.0280*											**0.0317**	*0.0248*
Sm	**<dl**												**<dl**	
Eu	**0.0148**	*0.0044*											**0.0098**	*0.0066*
Gd	**<dl**												**0.0158**	*0.0081*
Tb	**<dl**												**0.0015**	*0.0011*
Ho	**<dl**												**0.0028**	*0.0007*
Er	**<dl**												**0.0043**	*0.0004*
Tm	**<dl**												**0.0033**	*0.0003*
Yb	**0.0077**	*0.0028*											**<dl**	
Lu	**<dl**												**0.0012**	*0.0007*
Sc	**3.93**	*0.25*											**3.06**	*0.35*
Rb	**525**	*29*											**729**	*49*
Sr	**7.87**	*0.86*											**2.59**	*0.43*
Y	**0.0141**	*0.0023*											**0.0071**	*0.0138*
Ba	**192**	*9*											**111**	*9*
Th	**0.0086**	*0.0014*											**0.0119**	*0.0038*
U	**<dl**												**0.0048**	*0.0032*

Table 7: continued.

phlogopite

Major element composition [wt. %]

	wehrlite		*websterite*					
sample	**DJ0276**		**DJ0216**		**DJ0217**		**DJ0218**	
comment	repl. cpx		primary		repl. garnet		primary	
n	**2**	*1σ*	**2**	*1σ*	**2**	*1σ*	**2**	*1σ*
SiO_2	**41.39**	*0.07*	**40.45**	*0.01*	**38.26**	*0.86*	**40.70**	*0.07*
TiO_2	**1.17**	*<0.01*	**0.61**	*0.01*	**1.86**	*0.48*	**0.16**	*0.06*
Al_2O_3	**11.94**	*0.01*	**13.06**	*0.11*	**12.94**	*2.30*	**12.98**	*0.17*
Cr_2O_3	**0.25**	*<0.01*	**0.43**	*0.01*	**1.23**	*0.07*	**0.59**	*0.03*
BaO	**0.07**	*<0.01*	**0.50**	*0.03*	**0.22**	*0.07*	**0.31**	*0.03*
FeO	**3.94**	*0.04*	**3.87**	*0.11*	**5.08**	*0.37*	**3.59**	*0.08*
MgO	**24.64**	*<0.01*	**24.51**	*0.01*	**23.46**	*2.55*	**25.17**	*0.24*
NiO	**0.09**	*0.03*	**0.21**	*0.003*	**0.19**	*0.08*	**0.27**	*0.00*
K_2O	**10.84**	*0.14*	**9.36**	*0.38*	**7.29**	*0.84*	**10.28**	*0.01*
Na_2O	**0.14**	*0.01*	**0.73**	*0.02*	**0.88**	*0.33*	**0.42**	*0.00*
Cl	**0.05**	*0.01*	**0.07**	*0.01*	**0.04**	*0.02*	**0.09**	*0.01*
F	**0.53**	*0.02*	**0.24**	*0.09*	**0.27**	*0.07*	**<dl**	
total	**95.04**		**94.03**		**91.69**		**94.55**	
Mg#	**0.92**		**0.92**		**0.89**		**0.93**	

Oxygen isotope composition [‰]

$\delta^{18}O$	**nd**		**6.43**		**5.73**		**5.38**	
replicate	**nd**		**5.88**		**5.60**		**nd**	

Trace element composition [ppm]

comment					repl. grt		primary	
n					**3**	*1σ*	**4**	*1σ*
Ti					**11435**	*4426*	**989**	*95*
V					**187**	*68*	**84.8**	*2.4*
Zr					**16.0**	*5.5*	**1.64**	*0.32*
Nb					**24.5**	*10.9*	**32.0**	*3.5*
Hf					**0.550**	*0.191*	**0.0762**	*0.0094*
Ta					**2.08**	*0.78*	**1.62**	*0.28*
La					**0.369**	*0.096*	**0.0129**	*0.0060*
Ce					**0.755**	*0.640*	**0.0185**	*0.0111*
Pr					**0.118**	*0.038*	**<dl**	
Nd					**0.322**	*0.270*	**<dl**	
Sm					**0.0663**	*0.0624*	**<dl**	
Eu					**0.151**	*0.096*	**0.104**	*0.009*
Gd					**<dl**		**0.0195**	*0.0107*
Tb					**<dl**		**0.0082**	*0.0069*
Ho					**0.0047**	*0.0008*	**<dl**	
Er					**<dl**		**<dl**	
Tm					**<dl**		**<dl**	
Yb					**0.0180**	*0.0021*	**<dl**	
Lu					**0.0126**	*0.0093*	**<dl**	
Sc					**12.17**	*3.42*	**3.52**	*0.10*
Rb					**173**	*62*	**203**	*16*
Sr					**101**	*11*	**91.2**	*13.3*
Y					**0.106**	*0.082*	**0.0237**	*0.0080*
Ba					**1895**	*688*	**2450**	*280*
Th					**0.0482**	*0.0610*	**5.30**	*0.98*
U					**0.0207**	*0.0005*	**0.229**	*0.057*

These oxygen isotope values indicate a twofold trend for silicate minerals in dunite, wehrlite and websterite xenoliths. While olivine has typical primary mantle oxygen isotope compositions, clinopyroxene and garnet have oxygen isotope compositions indicating interaction with low $\delta^{18}O$ melt (Zhang et al., 2003; Perkins et al., 2006). Oxygen isotope fractionation can only occure at low pressures (Clayton et al., 1975), hence the low $\delta^{18}O$ values indicate the presence of altered oceanic crust within the Kaapvaal mantle, which is responsible for the oxygen isotope composition of clinopyroxene and garnet. Similarly, the large range in oxygen isotope composition of orthopyroxene in websterite xenoliths, may indicate interaction with subduction related metasomatising melts.

The oxygen isotope composition of the constituting silicate minerals in dunite, wehrlite and websterite xenoliths has been determined to test the possibility of a cumulate origin within the lower oceanic crust or in the lower parts of oceanic plateaus (Foley et al., 2003b; Foley et al., 2003a). A large range in oxygen isotope compositions reflects hydrothermal alteration within the oceanic crust, similar to eclogite xenoliths (2.2-8.0 ‰; e.g. MacGregor and Manton, 1986; Jacob, 2004) and oceanic crust and ophiolite complexes (e.g. Gregory and Taylor, 1981; Alt et al., 1989) and would be a good proof for a lower crust cumulate origin. Such hydrothermal alteration can reach deep into the oceanic crust (Hart et al., 1999). But the small range and oxygen isotope composition of the silicate minerals makes a cumulatic origin for the dunite, wehrlite and websterite xenoliths questionable (Fig. 6).

4.3. Recalculated whole-rock major element composition

The major element composition of the studied dunite, wehrlite and websterite xenoliths has been plotted in Fig. 7. Most dunite and wehrlite xenoliths are refractory with low SiO_2, Al_2O_3, CaO and high MgO and FeO contents. Websterite xenoliths are more fertile than the dunite and wehrlite xenoliths, showing a trend towards higher SiO_2, Al_2O_3, CaO and lower MgO and FeO* compositions. This trend can also be seen in some wehrlite xenoliths (AJE362 and AJE400). They exhibit the highest SiO_2, Al_2O_3, CaO, Na_2O and the lowest FeO and MgO content of all dunite and wehrlite xenoliths (Table 8). Overall, the dunite and wehrlite xenoliths have similar SiO_2, CaO, similar to lower Al_2O_3 and higher MgO whole-rock contents than Kaapvaal mantle peridotites (e.g. Boyd and Mertzman, 1987; Grégoire et al., 2002; 2003; van Achterbergh, 2004). Their trend towards higher FeO* and MgO is similar to peridotites that are interpreted to have experienced carbonatite melt metasomatism (e.g. Yaxley et al., 1991; Rudnick et al., 1993; Gorring and Kay, 2000).

High loss on ignition values (LOI) in Table 8 reflect high serpentine abundances in the whole-rocks, due to weathering.

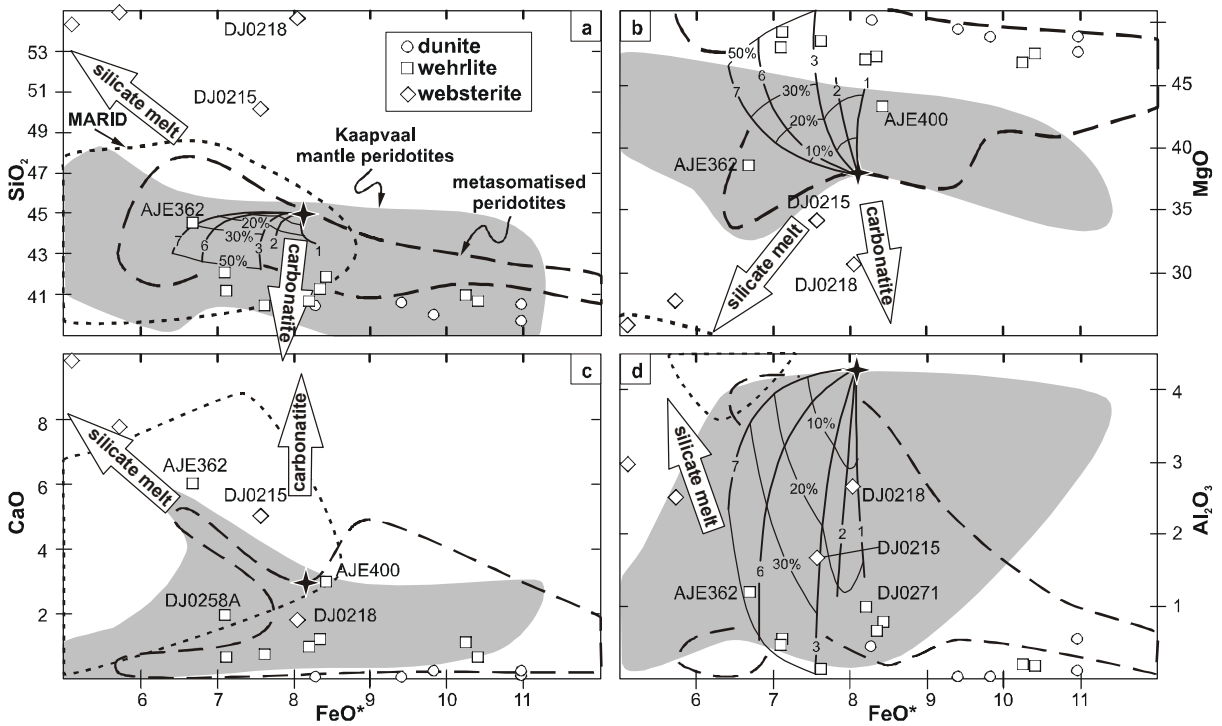

Fig. 7: Recalculated whole-rock major element composition of dunite, wehrlite and websterite xenoliths compared to Kaapvaal mantle peridotite xenoliths (Nixon et al., 1981; Boyd and Mertzman, 1987; Grégoire et al., 2002; 2003; van Achterbergh, 2004; Simon et al., 2007), metasomatised peridotite xenoliths interpreted to be overprinted by carbonatite metasomatism (Yaxley et al., 1991; Rudnick et al., 1993; Gorring and Kay, 2000) and MARID xenoliths (Dawson, 1987a; Grégoire et al., 2002): (a) SiO_2, (b) MgO, (c) TiO_2, (d) Al_2O_3 versus FeO* (total Fe as ferrous iron). Arrows show towards the composition of silicate and carbonatite melt inclusions in diamonds and peridotite xenoliths (silicate melt: Schiano and Clocchiatti, 1994; Frezzotti et al., 2002, carbonatite: Klein-BenDavid et al., 2004; van Achterbergh et al., 2004; Klein-BenDavid et al., 2007). Primitive mantle composition is shown with a star (McDonough and Sun, 1995). From there petrogenetic grids of increasing melt depletion (± vertical lines in %) are plotted reflecting residual mantle compositions at different pressure (± horizontal lines in GPa; redrawn after Walter, 2005).

Table 8: Whole-rock major element composition [wt. %] of dunite, wehrlite and websterite xenoliths measured and recalculated using modal compositions (Table 1) and mineral major element compositions (Table 2 to Table 7).

rock-type	dunite								wehrlite
sample	DJ0223	DJ0259		DJ0273	DJ0297		DJ02100		AJE362
method	calculated	calculated	measured	calculated	calculated	measured	calculated	measured	calculated
SiO_2	40.40	40.47	37.27	39.67	39.96	37.36	40.55	37.96	44.51
TiO_2	0.33	0.17	0.18	0.14	0.57	0.05	0.02	0.05	0.24
Al_2O_3	0.45	0.09	0.22	0.54	0.03	0.16	0.02	0.16	1.20
Cr_2O_3	0.61	0.07	0.04	1.01	0.07	0.01	0.02	0.02	1.49
CaO	0.04	0.10	0.11	0.22	0.22	0.02	0.06	0.04	5.99
FeO*	8.29	10.97	11.51	10.97	9.83	8.67	9.42	8.30	6.69
MgO	50.20	48.81	42.75	47.63	48.79	44.64	49.42	44.11	38.51
MnO	0.12	0.15	0.14	0.19	0.14	0.11	0.13	0.11	0.10
NiO	0.30	0.37	0.27	0.26	0.27	0.25	0.39	0.38	0.21
K_2O	0.32	0.03	0.05	0.53	-	0.01	-	0.01	0.16
Na_2O	-	0.03	<0.02	0.04	0.03	<0.04	0.02	<0.04	0.82
P_2O_5	-	-	0.04	-	-	0.01	-	0.00	-
LOI	-	-	6.76	-	-	7.48	-	8.03	-
total	101.03	101.27	100.60	101.21	99.89	99.71	100.06	100.04	99.91
Mg#	0.82	0.78	0.74	0.77	0.79	0.80	0.80	0.80	0.82

rock-type	wehrlite									
sample	AJE400		AJE401		DJ0214		DJ0256		DJ0258A	
method	calculated	measured	calculated	measured	calculated	measured	calculated	measured	calculated	measured
SiO_2	41.86	38.08	41.17	38.70	40.43	37.66	41.26	38.80	42.05	39.13
TiO_2	0.20	0.06	0.09	0.35	1.63	0.79	0.19	0.09	0.10	0.13
Al_2O_3	0.76	0.32	0.54	0.42	0.13	0.28	0.66	0.42	0.46	0.49
Cr_2O_3	1.43	0.09	0.24	0.24	0.42	0.15	0.61	0.17	0.76	0.32
CaO	3.00	0.69	0.65	0.45	0.75	0.26	1.21	0.50	1.97	1.55
FeO*	8.43	8.29	7.13	6.66	7.63	7.75	8.35	7.41	7.10	6.39
MgO	43.29	43.98	49.22	45.64	48.47	45.25	47.30	44.25	47.97	44.07
MnO	0.12	0.10	0.11	0.09	0.10	0.10	0.11	0.10	0.12	0.09
NiO	0.30	0.37	0.33	0.31	0.30	0.55	0.31	0.29	0.28	0.28
K_2O	0.21	0.01	0.21	0.09	-	0.07	0.10	0.02	0.00	0.01
Na_2O	0.41	0.00	0.11	0.01	0.13	<0.01	0.18	0.03	0.32	0.19
P_2O_5	-	0.01	-	0.01	-	0.00	-	0.00	-	0.01
LOI	-	7.41	-	6.55	-	6.36	-	7.63	-	6.57
total	100.00	100.32	99.79	100.26	100.00	100.07	100.29	100.54	101.12	99.93
Mg#	0.80	0.80	0.84	0.84	0.83	0.82	0.81	0.82	0.82	0.84

rock-type	wehrlite						websterite			
sample	DJ0271		DJ0275		DJ0276		DJ0215	DJ0216	DJ0217	DJ0218
method	calculated	measured	calculated	measured	calculated	measured	calculated	calculated	calculated	calculated
SiO_2	40.60	38.55	40.95	38.24	40.64	37.86	54.90	50.18	54.63	54.32
TiO_2	0.80	0.07	0.03	0.06	0.05	0.05	0.04	0.08	0.10	0.02
Al_2O_3	0.97	0.21	0.18	0.29	0.17	0.22	2.51	1.67	2.67	2.98
Cr_2O_3	0.50	0.06	0.06	0.09	0.06	0.05	0.58	0.39	0.62	0.68
CaO	0.96	0.08	1.10	1.51	0.64	0.45	7.76	5.02	1.79	9.81
FeO*	8.22	8.00	10.26	9.21	10.42	9.39	5.72	7.58	8.04	5.09
MgO	47.06	46.71	46.76	42.92	47.45	43.91	27.79	34.14	30.70	25.80
MnO	0.12	0.10	0.14	0.12	0.12	0.12	0.16	0.14	0.18	0.16
NiO	0.33	0.35	0.21	0.23	0.21	0.23	0.08	0.17	0.11	0.09
K_2O	0.11	0.01	0.11	0.05	0.11	0.03	-	-	-	-
Na_2O	0.14	<0.03	0.09	0.02	0.07	0.00	0.39	0.52	0.21	0.61
P_2O_5	-	0.01	-	0.04	-	0.02	-	-	-	-
LOI	-	4.73	-	6.18	-	7.21	-	-	-	-
total	99.81	99.74	99.89	99.99	99.94	100.60	99.94	99.90	99.06	99.56
Mg#	0.82	0.82	0.78	0.78	0.78	0.78	0.79	0.78	0.75	0.80

4.4. Mineral trace element composition

In Fig. 8 key trace elements in olivine are plotted against the olivine MgO content and compared to olivine in mantle peridotites from abyssal and cratonic settings. Most olivines in dunite, wehrlite and websterite xenoliths cover the same range of Cr and Zr contents, a similar to slightly lower range in Ni content and a lower range in Al and Ca contents than mantle peridotites. The low Al content may indicate a high degree of partial melting, while the low Ca content indicates high equilibration pressures (Köhler and Brey, 1990). Disregarding olivine in samples DJ0259, which is zoned and shows more complicated patterns, olivines in the studied xenoliths exhibit a positive trend of MgO with Cr and Al as well as a slightly

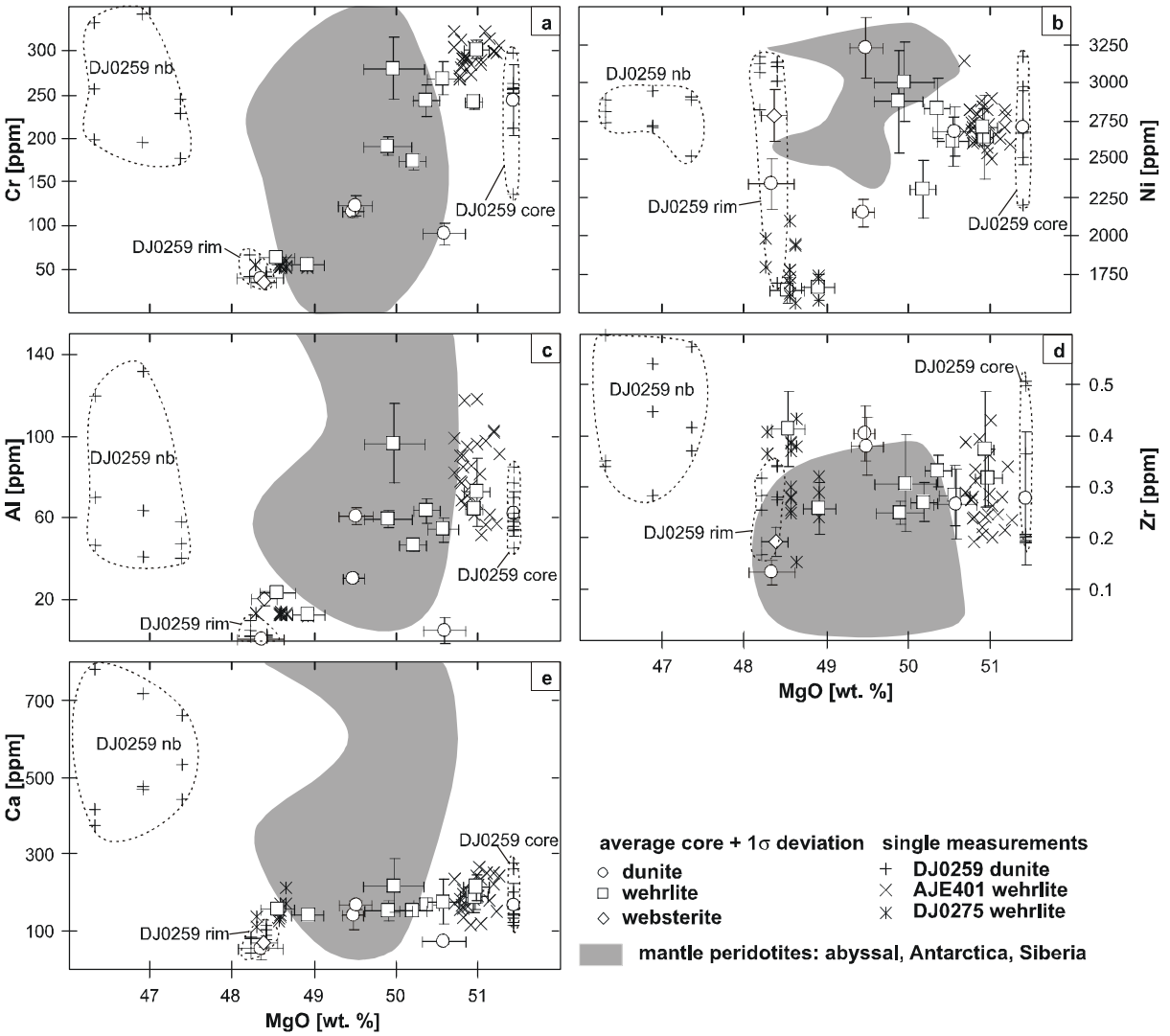

Fig. 8: Trace element composition of olivine (a) Cr, (b) Ni, (c) Al, (d) Zr and (e) Ca versus MgO in dunite, wehrlite and websterite xenoliths compared to olivine in peridotites from Antarctica (Foley et al., 2006), Siberia (Glaser et al., 1999) and to olivine in abyssal peridotites (Grégoire et al., 2000; Grégoire et al., 2001). Large open symbols as in Fig. 4 are average trace element core compositions with 1σ error bars, crosses, hatches and stars are single trace element measurements illustrating the absence or presence of zonation.

positive trend with Ca (Table 2). Olivine in websterite DJ0216 has lower Ca contents than olivine in wehrlite xenoliths (60-80 ppm versus 140-220 ppm, respectively). On the contrary, dunite xenoliths have olivine covering almost the whole range of Ca contents (50-180 ppm) shown by wehrlite and websterite xenoliths. This indicates that olivine in websterite DJ0216 equilibrated at lower pressure than olivine in wehrlite and most dunite xenoliths. For most samples olivine porphyroclasts and olivine neoblasts have homogeneous trace element contents. Only samples DJ0259 and DJ0275 show zonation between olivine core and rims and olivine porphyroclasts and neoblasts displaying a large scatter of single olivine trace element contents as shown in Fig. 8. In contrast, single measurements of the homogeneous olivines in AJE401 show restricted ranges in trace element composition. While the granular wehrlite xenolith DJ0275 has olivine with just slight core-rim zonation, showing a slight increase of Ti, Zr, Ni, Zn towards the olivine rims (Table 2), DJ0259 has large zonation profiles from olivine core to rim to neoblast (Fig. 8). In this sample two kinds of olivine zonation profiles exist, one with a rim core zonation more or less homogeneous in Ni, depleted in Ca and Zr and enriched in Cr (Fig. 9 a), the other depleted in Ca, Zr and Cr and enriched in Ni (Fig. 9 b). The first kind of pattern indicates the presence of a former spinel inclusion (Fig. 1 a) enriching the olivine porphyroclast in Cr and Ni. Generally olivine porphyroclasts have lower Ca contents than olivine neoblasts indicating lower equilibration pressures during olivine recrystallisation.

Orthopyroxene in dunite, wehrlite and websterite xenoliths has typical low trace element compositions and additionally negative Sr and positive Ti anomalies (Fig. 10 a and b; Table 3). The Ti anomaly is counterbalanced by a negative Ti anomaly in clinopyroxene (Fig. 10 c and d). In contrast, the negative Zr anomaly in clinopyroxene is not counterbalanced by a positive Zr anomaly in coexisting orthopyroxene, which should be the case for primary pyroxene pairs in mantle xenoliths (Rampone et al., 1991).

Clinopyroxene in dunite, wehrlite and websterite xenoliths have two distinct trace element patterns: a wehrlitic and a websteritic. Wehrlitic clinopyroxene has a negative Ti and a positive Hf anomaly and a slight enrichment in middle rare earth elements (MREE) compared to LREE and heavy rare earth elements (HREE). This is reflected in low chondrite normalized (McDonough and Sun, 1995) La over Yb ratios of $(La/Yb)_{CN}$ = 5-9 and is similar to clinopyroxene trace element patterns of other Kaapvaal wehrlite and polymict peridotite xenoliths (Zhang et al., 2001; Grégoire et al., 2002; Table 4). On the contrary, websteritic clinopyroxene has trace element patterns with strong negative Ti and Zr-Hf anomalies and a steep decrease from LREE to HREE, resulting in high $(La/Yb)_{CN}$ ratios of 22-680, which are

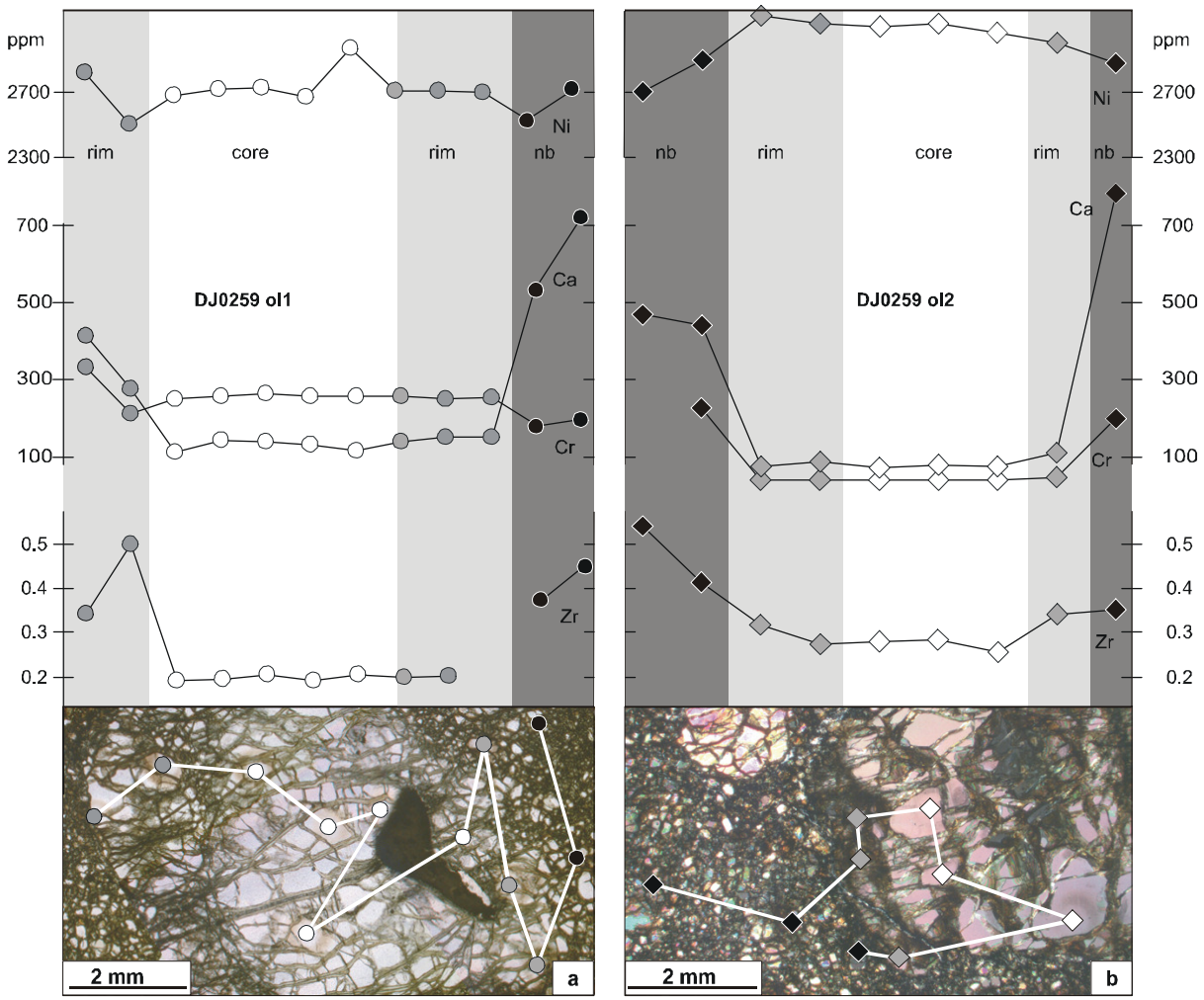

Fig. 9: Zonation profiles of Ni, Ca, Cr and Zr in olivine porphyroclast cores (white symbols), rims (grey) towards olivine neoblasts (black) in dunite sample DJ0259.

similar to clinopyroxene in Kaapvaal garnet peridotites (Grégoire et al., 2002; 2003; van Achterbergh, 2004; Simon et al., 2007). Clinopyroxene in dunite xenolith DJ0259 has also a "websteritic" trace element pattern with high $(La/Yb)_{CN}$ = 26, while clinopyroxene in dunite xenoliths DJ0297 and DJ02100 have "wehrlitic" trace element patterns with low $(La/Yb)_{CN}$ = 7-8.

Similar wehrlitic and websteritic trace element patterns are also present in garnet (Fig. 10 e and f; Table 5). Garnet in wehrlite xenoliths has a strong positive Zr-Hf anomaly and a slight negative Ti anomaly, while garnet in websterite xenoliths displays strong negative Hf and Ti anomalies. Garnet in dunite xenolith DJ0259 has a similar pattern as garnet in websterite xenoliths. Similar to clinopyroxene, the trace element composition of wehrlitic garnets is comparable with light coloured garnets in polymict peridotites (Zhang et al., 2001), while the trace element composition of websteritic garnets is similar to dark colored garnet in polymict peridotites and garnet in Kaapvaal peridotite xenoliths (Grégoire et al., 2002; 2003; van Achterbergh, 2004; Zhang et al., 2001; Simon et al., 2007).

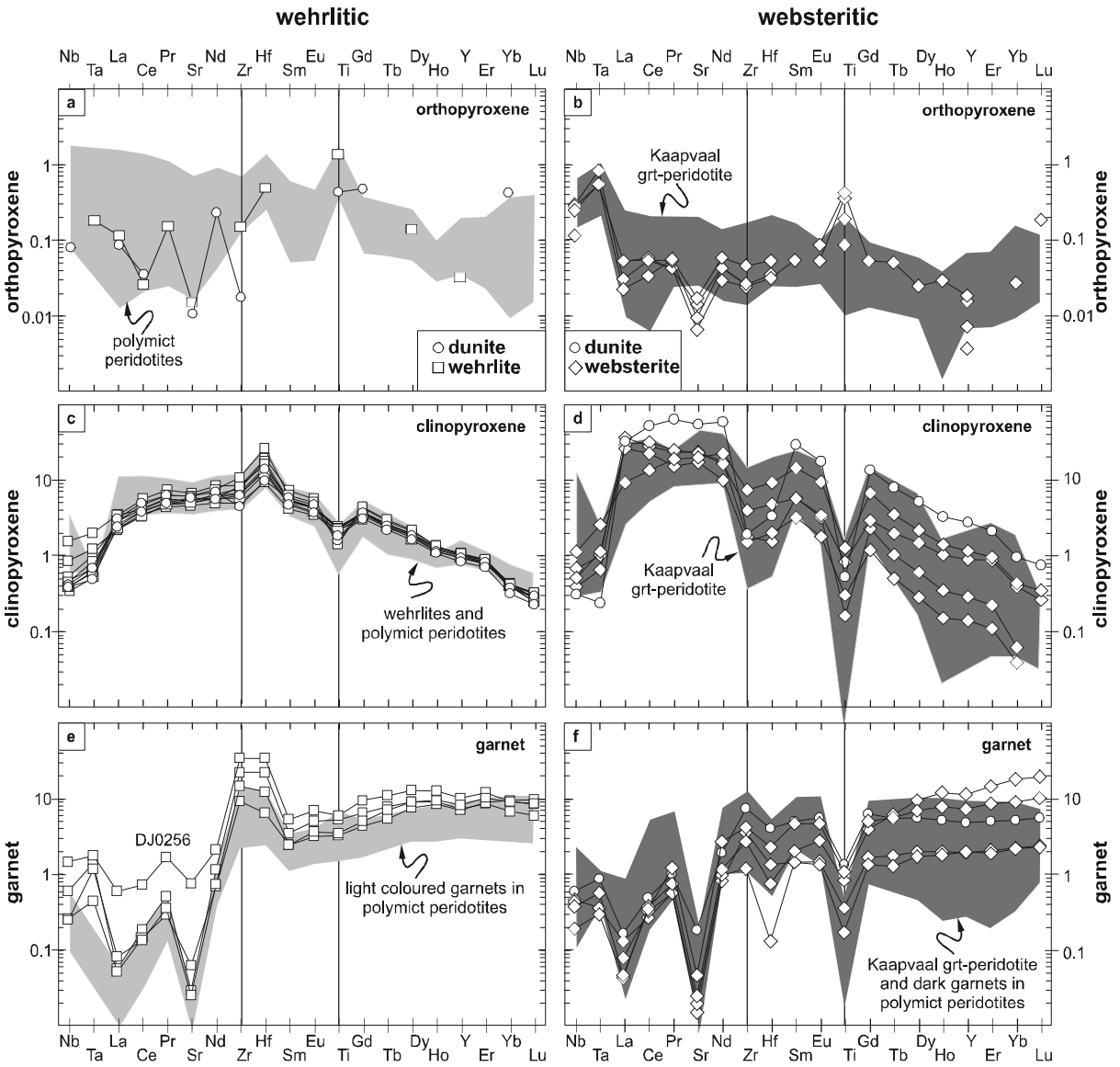

Fig. 10: Mineral trace element composition normalized to the primitive mantle (McDonough and Sun, 1995) of orthopyroxene (a) and (b), clinopyroxene (c) and (d) and garnet (e) and (f) in dunite, wehrlite and websterite xenoliths. Wehrlitic patterns with positive Zr-Hf anomaly are shown in (a), (c) and (e) and compared to polymict peridotites and wehrlite xenoliths from the literature (Zhang et al., 2000; Grégoire et al., 2002; Zhang et al., 2003). Websteritic patterns with negative Zr-Hf anomaly are shown in (b), (d) and (f) and compared to Kaapvaal mantle peridotites (Simon et al., 2003; Simon, 2004; van Achterbergh, 2004). Note different scales for orthopyroxene.

Normalization of the trace element composition of pyroxene and garnet of dunite, wehrlite and websterite xenoliths to pyroxene and garnet in primitive peridotite xenolith Vi313-6 (Ionov, 2004) yields again two types of trace element patterns (Fig. 11). Vi313-6 is a Siberian garnet peridotite xenolith with a bulk trace element composition similar to primitive mantle. Orthopyroxene in wehrlite DJ0256 has a similar to slightly enriched trace element pattern as primitive Vi313-6 orthoyproxene, while orthopyroxene in websterite xenoliths is mostly depleted, except for Nb and LREE in comparison to primitive orthopyroxene (Fig. 11 a, b). Wehrlitic clinopyroxene has normalized trace element compositions of ~1 for most of

the elements. Only a slight positive Zr-Hf anomaly and a slight negative Ti anomaly (Fig. 11 c) make them different to the primitive clinopyroxene in Vi313-6. In contrast, websteritic clinopyroxene are stronger depleted in Ti and enriched in LREE, while Zr-Hf and the other REE are slightly enriched to slightly depleted compared to the Vi313-6 clinopyroxene (Fig. 11 d). Similar patterns are displayed by garnets in wehrlite and websterite xenoliths when normalized to Vi313-6 garnet (Fig. 11 e and f). Wehrlitic garnet has positive Zr-Hf and Ti peaks, higher LREE and only slightly higher HREE compositions compared to primitiv garnet, while websteritic garnet is slightly depleted to slightly enriched in Zr-Hf, Ti, MREE and HREE, enriched in LREE, displaying slight negative peaks for Zr-Hf and Ti.

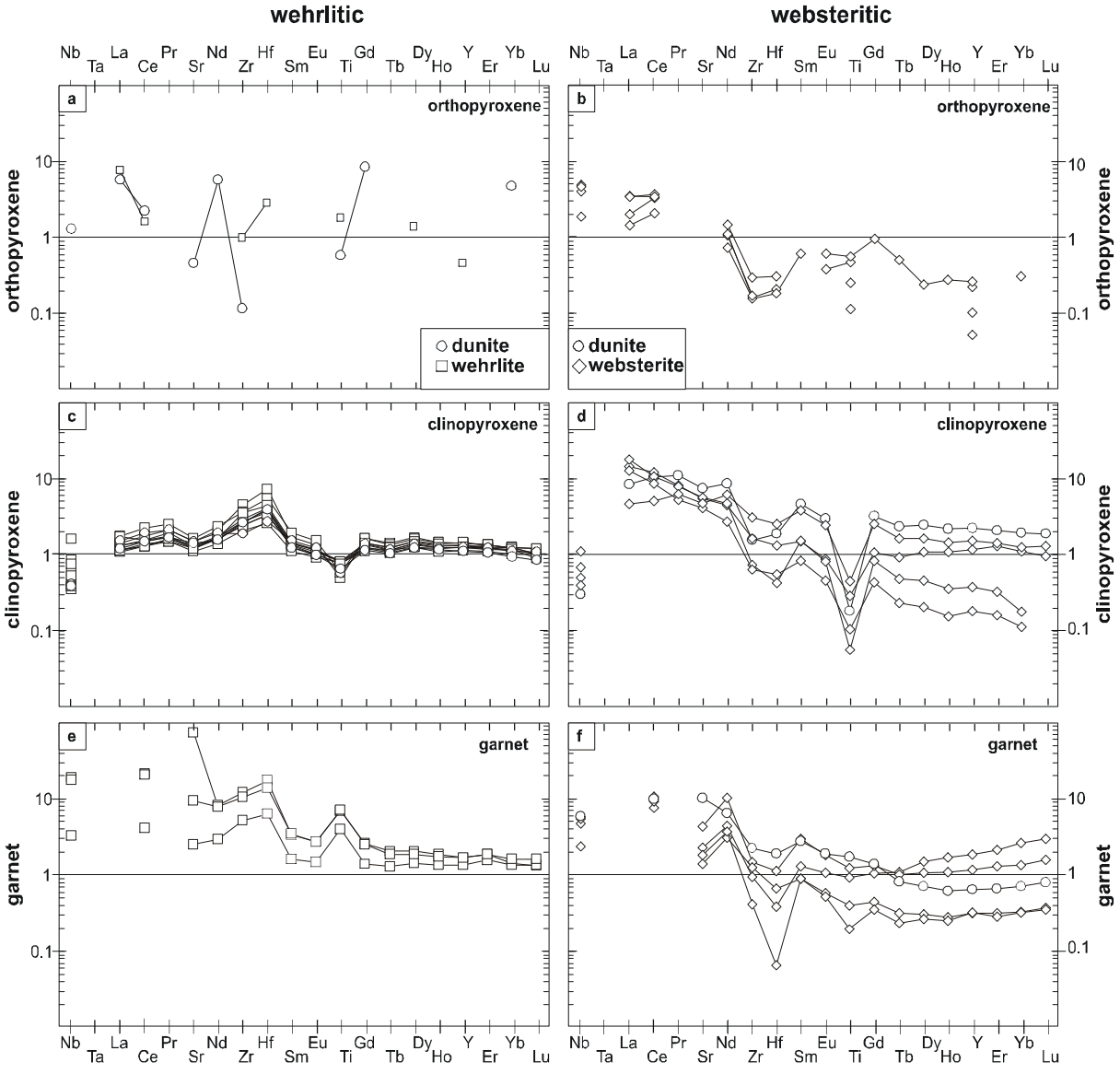

Fig. 11: Mineral trace element composition of (a) and (b) orthopyroxene, (c) and (d) clinopyroxene and (e) and (f) garnet in dunite, wehrlite and websterite xenoliths normalized to the trace element compositions of orthopyroxene, clinopyroxene and garnet of primitive mantle peridotite Vi313-6 (Ionov, 2004). Wehrlitic patterns in the left column (a), (c) and (e) and websteritic patterns in the right column (b), (d) and (f).

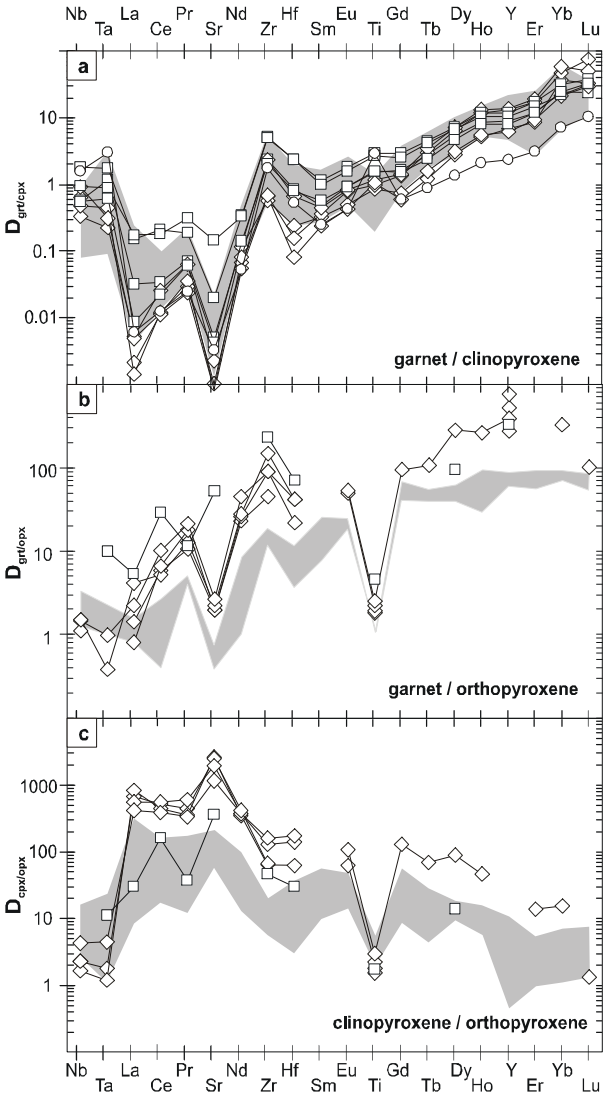

Fig. 12: Calculated mineral/mineral partition coefficients compared to equilibrium partition coefficients shown in grey shading (a) $D_{grt/cpx}$, (b) $D_{grt/opx}$ and (c) $D_{cpx/opx}$ (Zack et al., 1997; Glaser et al., 1999; Green et al., 2000; Ionov, 2004).

By calculating mineral/mineral trace element partition coefficients, a close relationship of garnet and clinopyroxene is evident (Fig. 12). The garnet clinopyroxene trace element partition coefficients ($D_{grt/cpx}$) have similar values in dunite, wehrlite and websterite xenoliths in agreement with equilibrium $D_{grt/cpx}$ in other mantle xenoliths worldwide (Fig. 12 a; e.g. Glaser et al., 1999). Keeping the two different trace element patterns of wehrlitic and websteritic clinopyroxene and garnet (Fig. 10) in mind, these similar trace element partition coefficients justify the assumption that wehrlitic and websteritic garnet and clinopyroxene have crystallized or equilibrated together. Only wehrlite sample DJ0256 has $D_{grt/cpx}$ with Ce, Pr and Sr more enriched in garnet than clinopyroxene and dunite xenolith DJ0259 has $D_{grt/cpx}$ with Tb, Dy, Ho and Y slightly enriched in clinopyroxene over garnet compared to equilibrium mantle peridotite $D_{grt/cpx}$. On the other hand, garnet orthopyroxene trace element partition coefficients ($D_{grt/opx}$) and clinopyroxene orthopyroxene trace element partition coefficients ($D_{cpx/opx}$) in wehrlite and websterite xenoliths do not agree with equilibrium $D_{grt/opx}$ and $D_{cpx/opx}$ in mantle peridotites worldwide (Fig. 12 b and c). This indicates for both, websterite xenoliths

and wehrlite DJ0256, that orthopyroxene has a different petrogenetic history than clinopyroxene and garnet.

The trace element composition of coexisting Ti-oxides and Cr-rich spinel has been analysed in wehrlite xenoliths DJ0271 and DJ0214, where spinel and ilmenite occur as disintegration minerals of rutile (Fig. 5 d). As typical for rutile (Green and Pearson, 1987), it is enriched in HFSE and depleted in transition metals such as Ga, Co, Cu, Zn, Cr and Mn, compared to ilmenite and spinel (Fig. 13; Table 6). A sequence of decreasing HFSE and increasing transition metals can be established from rutile to ilmenite to spinel. The trace element composition of spinel is similar to spinel in abyssal mantle peridotites (e.g. Grégoire et al., 2000). In contrast, ilmenite in wehrlite xenoliths has slightly higher Cr, Sc and Ni contents (Cr 21000-91000 ppm, Sc 22-29 ppm, Ni 1700-3800 ppm), than mantle-derived ilmenite (Cr 640-11000 ppm, Sc 5-14 ppm, Ni 950-2000 ppm; Barth et al., 2002b; Zack and Brumm, 1998; Fig. 13. Rutile from wehrlite xenoliths DJ0214 and DJ0271 has a similar trace element compositions as eclogitic rutiles having subchondritic Nb/Ta ratios of 6.6-7.3 (chondritic Nb/Ta=17.4, McDonough and Sun, 1995). Both rutile and ilmenite are enriched in Cr, while spinel is enriched in Ti, reflecting the close relationship of rutile, ilmenite and spinel.

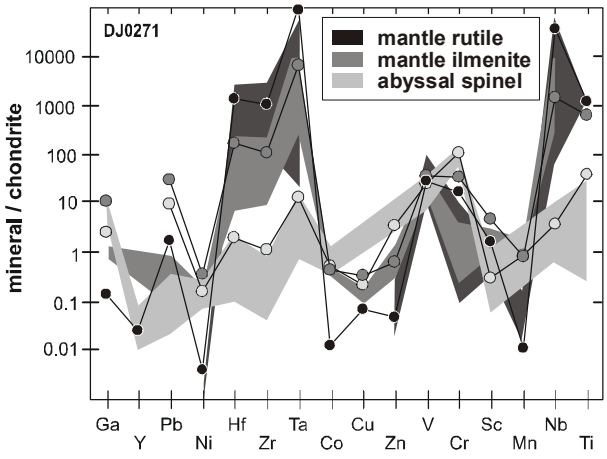

Fig. 13: Chondrite normalized trace element composition (McDonough and Sun, 1995) of coexisting oxide minerals in wehrlite xenolith DJ0271 with compositional fields of eclogitic rutile (black; Rudnick et al., 2000), mantle ilmenite (grey; Zack and Brumm, 1998; Barth et al., 2002b) and spinel in abyssal peridotites (light grey; Grégoire et al., 2000; Grégoire et al., 2001; Moine et al., 2001) as comparison.

Phlogopite in wehrlite and websterite xenoliths have trace element compositions typical for metasomatic phlogopite (Grégoire et al., 2002; van Achterbergh, 2004) with high Sr and HFSE contents (Table 7). In detail phlogopite in websterite xenoliths has higher Nb, Ta, Sr, Ba, Y and LREE compositions than phlogopite in wehrlite xenoliths, which may reflect the rarity of oxide phases in the websteritic xenoliths in comparison to wehrlitic xenoliths (Table 1). Additionally, phlogopite replacing garnet is more enriched in HFSE.

4.5. Re/Os systematics of dunite, wehrlite and websterite xenoliths

Dunite, wehrlite and websterite xenoliths have Re concentrations and Os isotope compositions similar to Kaapvaal mantle peridotites (Fig. 14). They have similarly low Re concentrations of mostly <0.3 ppb (versus <0.4 ppb Re for mantle peridotites; Fig. 14 a). Only wehrlite DJ0214 has higher Re content of 0.9 ppb. In contrast, dunite and wehrlite xenoliths have a smaller range and slightly lower Os contents of 0.03-6.6 ppb (with an average of 2.6 ppb) than mantle peridotites (0.14-18 ppb, average ~4 ppb; Fig. 14 b; Walker et al., 1989; Pearson et al., 1995c; Carlson et al., 1999; Menzies et al., 1999; Irvine et al., 2001; Meisel et al., 2001; Carlson and Moore, 2004; Simon et al., 2007). Websterite

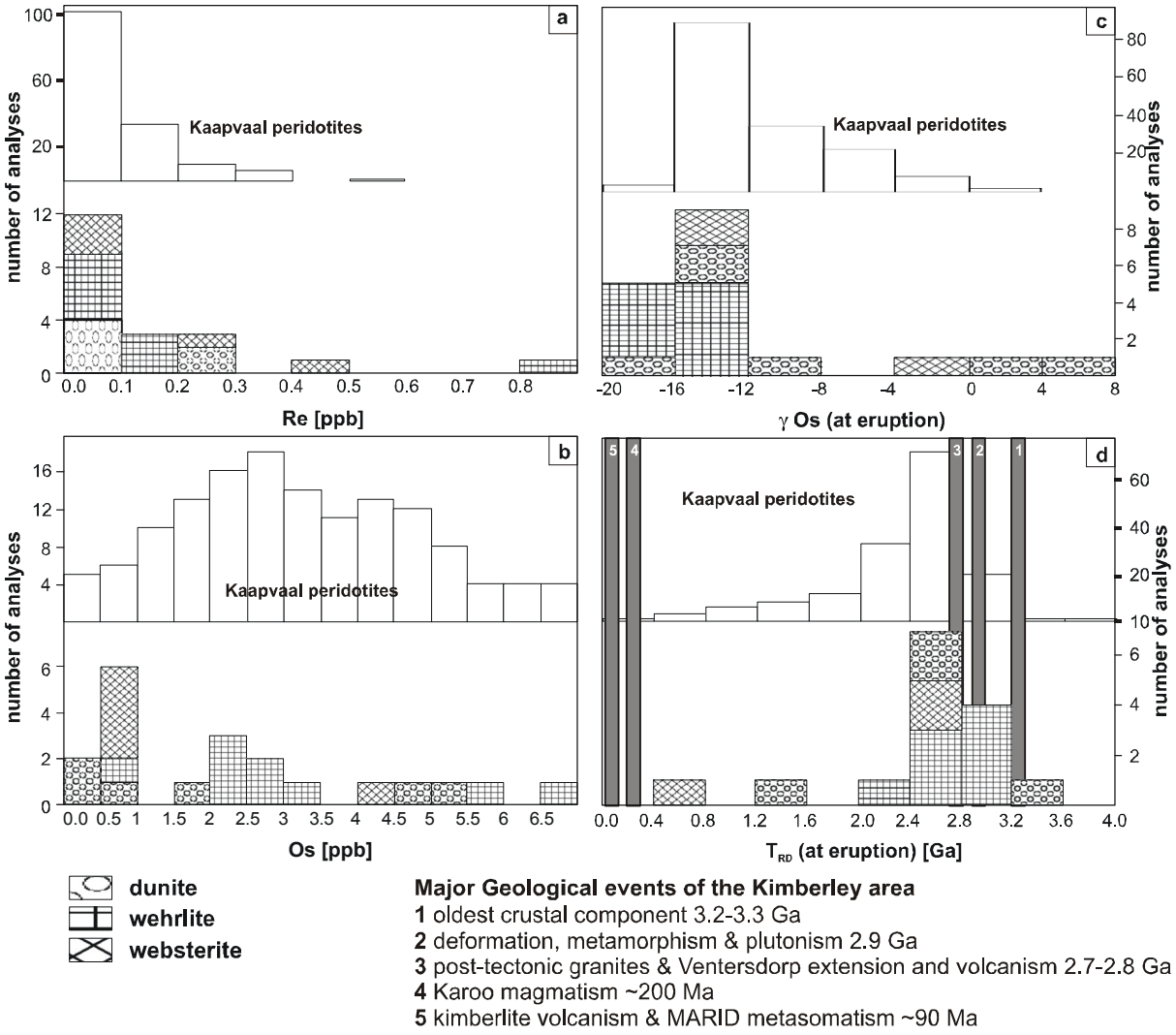

Fig. 14: Re-Os systematics of whole-rock dunite, wehrlite and websterite xenoliths (a) Re content [ppb], (b) Os content [ppb], (c) γOs calculated back to 86 Ma the time of kimberlite eruption and (d) Re-depletion age (T_{RD}) [Ga] compared to Kaapvaal craton mantle peridotites (upper histograms with open bars; Walker et al., 1989; Pearson et al., 1995a; Carlson et al., 1999; Menzies et al., 1999; Irvine et al., 2001; Meisel et al., 2001; Carlson and Moore, 2004; Simon, 2004) and major geological events of the Kimberley area (Davis, 1977; Schulze, 1995; Duncan et al., 1997; Konzett et al., 2000). Calculation of T_{RD} and γOs as described in header of Table 9.

xenoliths have lower Os contents than mantle peridotites (mostly <1 ppb; DJ0216 has 4 ppb). The $^{187}Os/^{188}Os$ ratio of wehrlite, most dunites and websterites DJ0215 and DJ0218 calculated back to the time of the kimberlite eruption 86 Ma (Table 9) is also similar to mantle peridotites (γOs from -18 to -8 versus -18 to 3 with most below -12 in mantle peridotites; Fig. 14 c; Walker et al., 1989; Pearson et al., 1995c; Carlson et al., 1999; Menzies et al., 1999; Irvine et al., 2001; Meisel et al., 2001; Carlson and Moore, 2004; Simon et al., 2007). Most dunite, wehrlite and websterite xenoliths have low $^{187}Re/^{188}Os$ ratios of 0.02-0.5. In contrast, dunite DJ02100 and wehrlite DJ0214 have high $^{187}Re/^{188}Os$ ratios of 1.5-1.9, which can be explained by kimberlite infiltration, since kimberlites have $^{187}Re/^{188}Os$ of 1.5±1.44 (Pearson et al., 1995b). DJ0297 has an extremely high $^{187}Re/^{188}Os$ ratio of 25. Dunite samples DJ02100 and DJ0297, as well as websterite DJ0216 have more radiogenic γOs ratios of -3 to 8 (Table 9) and websterite DJ0217 has an highly radiogenic γOs ratio.

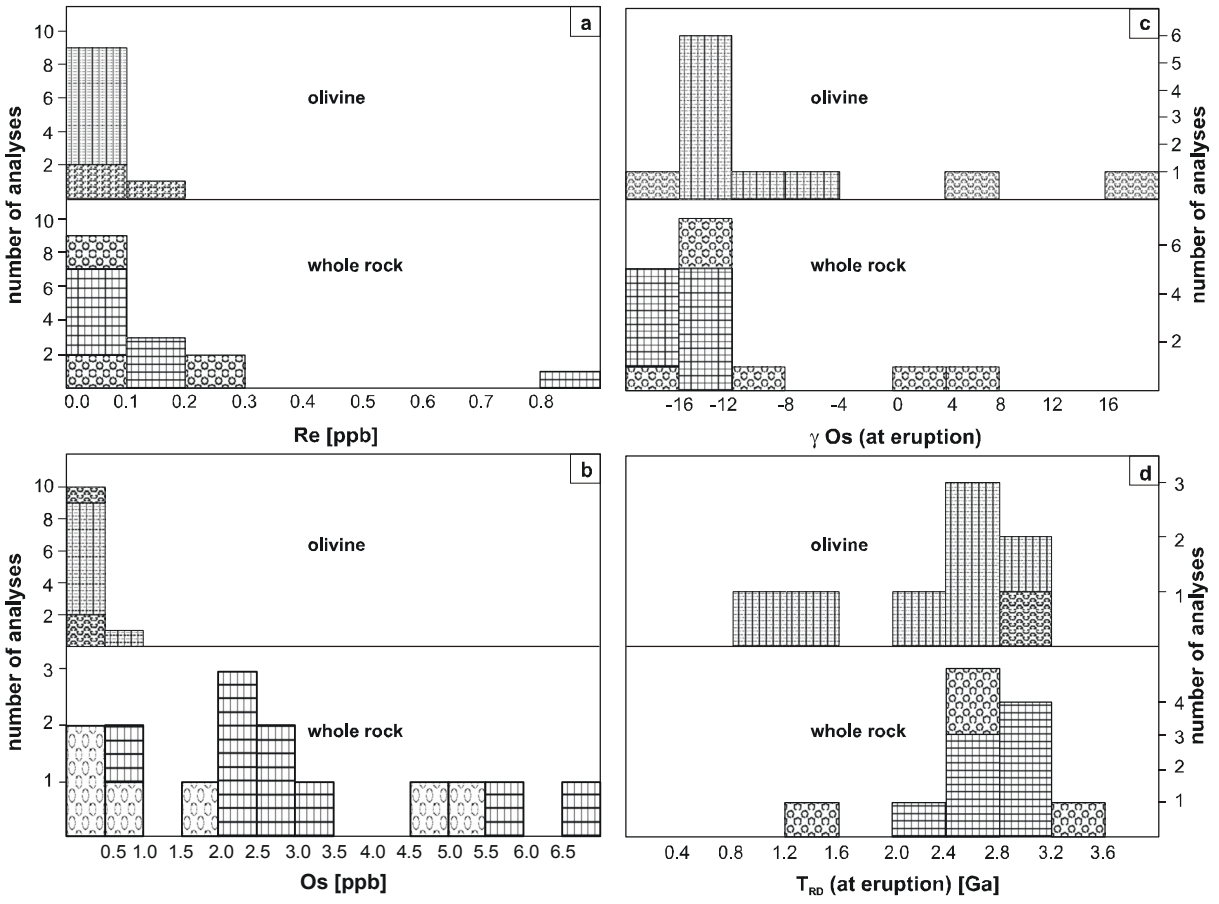

Fig. 15: Comparison of Re-Os systematics of whole-rocks (lower histograms) and olivine seperates (upper histograms) of dunite and wehrlite xenoliths (a) Re content [ppb], (b) Os content [ppb], (c) γOs and (d) T_{RD} [Ga] (T_{RD} and γOs calculated as in Table 9).

Table 9: Re-Os isotope composition of whole-rocks and olivine separates (italic) of dunite, wehrlite and websterite xenoliths. (Abbreviations same as in Table 1, plus wr=whole-rock). Re depletion ages (T_{RD}), model ages (T_{MA}) and γOs were calculated using present day bulk silicate earth (BSE) values of $^{187}Os/^{188}Os_{BSE}$=0.1296 and $^{187}Re/^{188}Os_{BSE}$=0.4353 (Walker et al., 1989; Meisel et al., 2001). The γOs(86 Ma) ratio is time corrected to a mean Kimberley kimberlite eruption age of 86 Ma.

rock type	***dunite***									***wehrlite***
sample	**DJ0223**	**DJ0259**		**DJ0273**	**DJ0274**	**DJ0297**		**DJ02100**		**AJE362**
fraction	wr	wr	*ol*	wr	wr	wr	*ol*	wr	*ol*	wr
Re [ppb]	**0.02650**	**0.01570**	***0.01740***	**0.22270**	**0.22230**	**0.01400**	***0.03160***	**0.07220**	***0.00320***	**0.02230**
2σ	*0.00050*	*0.00050*	*0.00130*	*0.00060*	*0.00060*	*0.00060*	*0.00120*	*0.00060*	*0.00100*	*0.00050*
Os [ppb]	**1.60380**	**0.62940**	***0.15980***	**4.74760**	**5.07950**	**0.00280**	***0.00340***	**0.18680**	***0.03820***	**3.00690**
2σ	*0.00080*	*0.00060*	*0.00130*	*0.00140*	*0.00150*	*0.00060*	*0.00120*	*0.00060*	*0.00100*	*0.00100*
$^{187}Re/^{188}Os$	**0.07950**	**0.12001**	***0.52694***	**0.22553**	**0.21047**	**25.18266**	***45.67484***	**1.86652**	***0.40458***	**0.03564**
2σ	*0.00150*	*0.00382*	*0.03960*	*0.00061*	*0.00057*	*5.50315*	*16.21357*	*0.01663*	*0.12687*	*0.00080*
$^{187}Os/^{188}Os$	**0.10550**	**0.11830**	***0.15480***	**0.11060**	**0.11060**	**0.17530**	***0.17170***	**0.13660**	***0.13640***	**0.10880**
2σ	*0.00002*	*0.00005*	*0.00015*	*0.00001*	*0.00001*	*0.00136*	*0.00135*	*0.00013*	*0.00097*	*0.00001*
γOs (86 Ma)	**-18.29**	**-8.41**	***19.44***	**-14.50**	**-14.48**	**7.92**	***-17.65***	**3.84**	***5.31***	**-15.68**
T_{RD} [Ga]	**3.25**	**1.56**	***-3.47***	**2.61**	**2.60**	**-1.34**	***3.14***	**-0.60**	***-0.86***	**2.81**
uncertainty	*0.04*	*0.09*	*0.25*	*0.06*	*0.06*	*0.36*	*0.22*	*0.16*	*0.29*	*0.05*
T_{MA} [Ga]	**3.93**	**2.11**	***14.58***	**5.20**	**4.87**	**0.11**	***0.06***	**0.29**	***-15.02***	**3.05**
uncertainty	*0.01*	*0.06*	*4.52*	*-0.04*	*-0.02*	*0.02*	*0.02*	*-0.03*	*-18.67*	*0.04*

rock type	***wehrlite***									
sample	**AJE362**	**AJE400**	**AJE401**		**DJ0214**		**DJ0256**		**DJ0258A**	
fraction	*ol*	wr	wr	*ol*	wr	*ol*	wr	*ol*	wr	*ol*
Re [ppb]	***0.02980***	**0.11600**	**0.02560**	***0.00480***	**0.87500**	***0.00480***	**0.11200**	***0.00300***	**0.06090**	***0.00560***
2σ	*0.00110*	*0.00050*	*0.00050*	*0.00110*	*-*	*0.00100*	*-*	*0.00110*	*0.00050*	*0.00110*
Os [ppb]	***0.26100***	**2.29790**	**5.98320**	***0.19260***	**2.79680**	***0.02750***	**2.03090**	***0.08210***	**0.73510**	***0.36550***
2σ	*0.00110*	*0.00090*	*0.00160*	*0.00110*	*-*	*0.00100*	*-*	*0.00110*	*0.00070*	*0.00120*
$^{187}Re/^{188}Os$	***0.54858***	**0.24268**	**0.02061**	***0.11981***	**1.49500**	***0.83390***	**0.26400**	***0.17790***	**0.39851**	***0.07331***
2σ	*0.02038*	*0.00105*	*0.00040*	*0.02746*	*0.00000*	*0.17636*	*0.00000*	*0.06527*	*0.00329*	*0.01440*
$^{187}Os/^{188}Os$	***0.11040***	**0.10960**	**0.10970**	***0.11020***	**0.10800**	***0.11950***	**0.10970**	***0.12330***	**0.11360**	***0.11200***
2σ	*0.00026*	*0.00002*	*0.00001*	*0.00035*	*0.00017*	*0.00203*	*0.00017*	*0.00068*	*0.00004*	*0.00018*
γOs (86 Ma)	***-15.01***	**-15.29**	**-14.97**	***-14.69***	**-17.93**	**-6.27**	**-15.24**	***-4.60***	**-12.36**	***-13.24***
T_{RD} [Ga]	***2.69***	**2.74**	**2.69**	***2.64***	**3.19**	***1.54***	**2.73**	***0.90***	**2.24**	***2.39***
uncertainty	*0.09*	*0.05*	*0.05*	*0.10*	*0.06*	*0.37*	*0.08*	*0.20*	*0.07*	*0.09*
T_{MA} [Ga]	***-11.15***	**5.93**	**2.81**	***3.58***	**-1.24**	***-1.54***	**6.60**	***1.45***	**21.67**	***2.85***
uncertainty	*-2.90*	*-0.11*	*0.05*	*-0.37*	*-0.05*	*-0.38*	*-0.18*	*-0.53*	*-9.22*	*-0.09*

rock type	***wehrlite***						***websterite***				
sample	**DJ0271**		**DJ0275**		**DJ0276**		**DJ0215**	**DJ0216**	**DJ0217**		**DJ0218**
fraction	wr	*ol*	wr	*ol*	wr	*ol*	wr	wr	wr	wr	wr
Re [ppb]	**0.06100**	***0.00390***	**0.06400**	***0.00800***	**0.12140**	***0.00690***	**0.01260**	**0.29470**	**0.51410**	**0.08100**	**0.01970**
2σ	*0.00050*	*0.00100*	*0.00050*	*0.00100*	*0.00050*	*0.00100*	*0.00050*	*0.00050*	*0.00050*	*0.00050*	*0.00050*
Os [ppb]	**6.64300**	***0.79900***	**2.25950**	***0.18630***	**2.55180**	***0.07690***	**0.81460**	**4.05020**	**0.75150**	**0.75540**	**0.95370**
2σ	*0.00170*	*0.00110*	*0.00090*	*0.00110*	*0.00100*	*0.00110*	*0.00060*	*0.00120*	*0.00070*	*0.00060*	*0.00070*
$^{187}Re/^{188}Os$	**0.04416**	***0.02374***	**0.13612**	***0.20594***	**0.22860**	***0.43344***	**0.07445**	**0.35069**	**3.46125**	**0.54211**	**0.09922**
2σ	*0.00036*	*0.00609*	*0.00106*	*0.02577*	*0.00095*	*0.06312*	*0.00295*	*0.00060*	*0.00466*	*0.00337*	*0.00252*
$^{187}Os/^{188}Os$	**0.10720**	***0.10880***	**0.10710**	***0.10960***	**0.10720**	***0.11100***	**0.10940**	**0.12580**	**0.50680**	**0.50470**	**0.10970**
2σ	*0.00001*	*0.00008*	*0.00002*	*0.00035*	*0.00001*	*0.00086*	*0.00004*	*0.00001*	*0.00024*	*0.00023*	*0.00004*
γOs (86 Ma)	**-16.93**	***-15.67***	**-17.11**	***-15.25***	**-17.14**	***-14.42***	**-15.26**	**-2.85**	**289.09**	**290.71**	**-15.06**
T_{RD} [Ga]	**3.02**	***2.81***	**3.05**	***2.74***	**3.05**	***2.59***	**2.74**	**0.59**	**-115.96**	**-117.98**	**2.70**
uncertainty	*0.05*	*0.06*	*0.05*	*0.10*	*0.05*	*0.17*	*0.06*	*0.11*	*11.30*	*11.78*	*0.06*
T_{MA} [Ga]	**3.34**	***2.96***	**4.35**	***5.02***	**6.18**	***143.83***	**3.27**	**2.64**	**7.05**	**90.44**	**3.45**
uncertainty	*0.04*	*-0.01*	*0.00*	*-0.76*	*-0.11*	*161.65*	*0.01*	*0.29*	*0.02*	*5.73*	*0.01*

Measured olivine separates of dunite and wehrlite xenoliths have a narrower range and lower Re and Os concentrations than whole-rocks (Fig. 15). In most wehrlite xenoliths the γOs ratio is only slightly lower in olivine than in the corresponding whole-rocks (Fig. 15). For these xenoliths the tie-lines between Re/Os and Os isotope composition of olivine separates and whole-rocks (not shown) yield a small range of initial $^{187}Os/^{188}Os$ (0.1171-0.1022). In contrast, olivine in wehrlite samples DJ0214 and DJ0256 has more radiogenic γOs ratios than in whole-rocks, yielding initial $^{187}Os/^{188}Os$ ratios larger than the mantle value (0.1340 and 0.1510 vs. 0.1296, respectively; Meisel et al., 2001). Similarly, olivines in dunite

xenoliths DJ0259, DJ0297 and DJ02100 have more heterogeneous Os isotope compositions compared to whole-rocks, with γOs in olivine from -18 to 20 and in the corresponding whole-rock from -8 to 8. This leads to initial $^{187}Os/^{188}Os$ ratios higher than the mantle value for samples DJ0297 (0.1797) and DJ02100 (0.1363), but similar to most wehrlite xenoliths for sample DJ0259 (0.1075). The $^{187}Re/^{188}Os$ ratio of dunite sample DJ0297 is even higher in the olivine separates (46) than in the whole-rock analyses. In contrast, olivine in dunite DJ02100 and wehrlite DJ0214 have lower $^{187}Re/^{188}Os$ ratios (0.4-0.8), similar to the other dunite, wehrlite and websterite xenoliths, which indicates that kimberlite infiltration did not affect the olivine. The high $^{187}Re/^{188}Os$ of dunite DJ0297 can be explained by percolating Re-rich melts, which are even more enriched in Re than kimberlite.

5. Thermobarometry

Equilibration temperatures and pressures have been calculated for wehrlite and websterite xenoliths. Application of thermobarometers on dunite xenoliths yielded mostly unrealistic temperatures and pressures, since the thermobarometers are based on element partitioning between garnet, clinopyroxene and/or orthopyroxene, which are minor phases in dunites and are often in disequilibrium with olivine.

Generally, temperatures and pressures are calculated using major element compositions, which equilibrate much faster than trace elements (Van Orman et al., 2001). All of the studied xenoliths have olivine in textural disequilibrium with the other silicate minerals either due to recrystallisation (porphyroclastic texture, Fig. 1 a, c and e) or due to the consumption of olivine during crystallization of secondary pyroxene and garnet (Fig. 1 e-g). Therefore, calibrated thermometers and barometer requiring equilibrium between olivine and other silicate minerals give mostly unrealistic values and cannot be applied. Since the clinopyroxene composition in garnet-bearing and garnet-free wehrlite and websterite xenoliths is similar, e.g. being HREE depleted (Fig. 10), we assume that wehrlites and websterites have crystallized in the presence of garnet. Hence thermobarometers calibrated on garnet-bearing assemblages can be applied.

Brey and Köhler (1990) analysed four-phase lherzolites and favoured four thermobarometer pairs: the two-pyroxene Fe-Mg exchange thermometer $T(2px)_{BKN}$ combined with the Al in orthopyroxene barometer P_{BKN} (Brey and Köhler, 1990), $T(2px)_{BKN}$ combined with the Ca in olivine barometer P_{KB} (Köhler and Brey, 1990), the garnet-clinopyroxene Fe-Mg exchange thermometer T_{Krogh} (Krogh, 1988) combined with P_{BKN} and the olivine-garnet Fe-Mg exchange thermometer $T_{O'Neill}$ in combination with P_{BKN} (O'Neill and Wood, 1979). Other recommendation of thermobarometers (Xu et al., 1998) are the Ca in orthopyroxene thermometer $T_{Ca\text{-}in\text{-}opx}$ (Brey and Köhler, 1990) in combination with the Al in orthopyroxene

and garnet barometer P_{NG} (Nickel and Green, 1985) in addition to $T(2px)_{BKN}/P_{BKN}$,. Since these thermobarometric combinations are not applicable to all xenoliths of this study, due to lack of garnet or orthopyroxene, further thermobarometers have been applied: the single clinopyroxene thermobarometer T_{NT}/P_{NT}, that uses the Cr-in-clinopyroxene content as barometer and the enstatite-in-clinopyroxene content as thermometer (Nimis and Taylor, 2000) and the garnet-orthopyroxene Fe-Mg exchange thermobarometer T_{GH}/P_{GH} (Harley, 1984 as calibrated by Glebovitsky et al., 2004).

For the thermobarometric calculations ferrous iron has been used as total iron, since no big difference occur when calculating the equilibration temperature and pressure with ferric or ferrous iron (Schmickler et al., 2004). Equilibration temperatures and pressures were calculated using the homogeneous core composition of minerals lying in direct contact with each other. For wehrlite and websterite xenoliths $T(2px)_{BKN}$ extrapolated upon the Kalahari geotherm (Rudnick and Nyblade, 1999) and T_{NT}/P_{NT} and T_{GH}/P_{GH} give the most convincing results (Table 10).

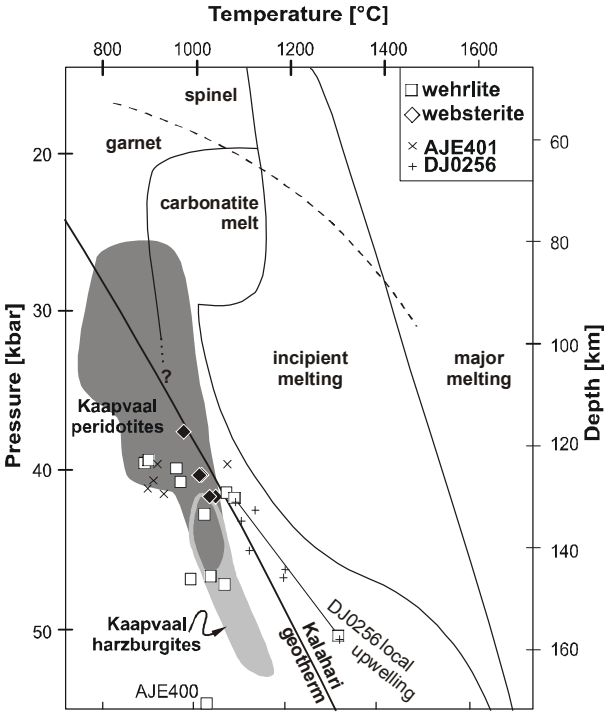

Fig. 16: Upper mantle phase diagram with calculated equilibration temperatures and pressures of wehrlite and websterite xenoliths (Table 4; Green and Falloon, 1998). Open symbols are average temperatures and pressures or maximum and minimum pressures and temperatures in case of wehrlite DJ0256; crosses and hatches are temperatures and pressures calculated from neighbouring mineral pairs in wehrlites AJE401 and DJ0256. Compositional fields: Kaapvaal peridotites (van Achterbergh, 2004; Simon et al., 2007) and Kaapvaal harzburgites (Schulze, 1995; Saltzer et al., 2001), Kalahari geotherm (Rudnick and Nyblade, 1999). The question mark indicates, that carbonatite can also be stable towards higher pressures (Sweeney et al., 1995; Dalton and Wood, 1993).

Wehrlite xenoliths have a large range in equilibration temperatures and pressures (T_{NT} 890-1080 °C and P_{NT} 38-55 kbar), while websterite xenoliths have a smaller range and similar to slightly lower equilibration temperatures and pressures (T_{GH} 970-1040 °C and P_{GH} 38-42 kbar). Both lie close to the Kalahari geotherm (Rudnick and Nyblade, 1999). Especially websterite xenoliths lie within the pressure temperature fields of low-temperature Kaapvaal mantle peridotites (e.g. Grégoire et al., 2003; van Achterbergh, 2004; Simon et al., 2007), while some wehrlite xenoliths (AJE362, AJE400, DJ0258A) have higher pressures and

temperatures lying within the PT-field of strongly depleted Kaapvaal harzburgite xenoliths (Fig. 16; e.g. Schulze, 1995; Griffin et al., 1999a; Saltzer et al., 2001). Especially in sample DJ0256 a number of schlieren, with orthopyroxene, clinopyroxene and garnet lying in direct contact to each other, were analysed leading to a wide range of equilibration temperatures and pressures (ΔT ~ 200 °C and ΔP ~ 10 kbar; Fig. 16) lying off the Kalahari geotherm, towards higher temperatures and pressures. Similarly wehrlite AJE401 has a wide range in equilibration temperatures ΔT ~ 150°C, but a small range in equilibration pressure (P_{NT} = 40±1 kbar).

Table 10: Temperature [°C] and pressure [kbar] of equilibration of dunite, wehrlite and websterite xenoliths using T_{BKN}(2px) (Brey and Köhler, 1990) extrapolated to the Kalahari geotherm (Rudnick and Nyblade, 1999), T_{NT} and P_{NT} (Nimis and Taylor, 2000) and T_{GH} and P_{GH} (Harley, 1984; Glebovitsky et al., 2004). Temperatures outside the calibration of the thermometers (as quoted in last line) are in parentheses. Abbreviations are as in Table 1.

	T_{BKN}(2px)	P	T_{NT}	P_{NT}	T_{GH}	P_{GH}
	cpx-opx	geotherm	En-in-cpx	Cr-in-cpx	grt-opx	grt-opx
wehrlite						
AJE362	no opx		**990**	**47.0**	no grt and opx	
AJE400	no opx		**1025**	**54.8**	no grt and opx	
AJE401	no opx		**894-1064**	**39.6-41.5**	no grt and opx	
DJ0214	1114-1170	46.5-50.4	**961-1018**	**39.9-42.8**	no grt and opx	
DJ0256	1060-1229	43-55	918-1076	38.3-49.9	**1081-1302**	**41.9-50.6**
DJ0258A	no opx		**1032-1063**	**46.7-47.3**	no grt and opx	
DJ0271	no opx		**901-968**	**39.4-40.8**	no grt and opx	
websterite						
DJ0215	(772)	25.9	(765)	39.2	**1010**	**40.3**
DJ0216	915-842	29.2-32.8	876	49.3	**1007-1040**	**40.2-41.7**
DJ0217	904	32.3	(832)	47.1	**971**	**37.6**
DJ0218	909	32.5	888	40.0	**1026**	**41.7**
equilibration conditions	four-phase peridotites 900-1400 °C 10-60 kbar ±31°C		Garnet-peridotite 850-1500°C <60 kbar ±2.3 kbar ±30°C		Garnet-orthopyroxene paragenesis 700-1500°C 5-60 kbar T=±10% P=±5%	

6. Discussion

The petrogenetic history of the sublithospheric upper mantle underneath the Kaapvaal craton has been studied for a long time (e.g. Nixon and Boyd, 1973; MacGregor, 1975; Gurney and Harte, 1980; Boyd and Mertzman, 1987; Gurney et al., 1991; Pearson et al., 1995a; Konzett et al., 2000) and can be subdivided into three periods: i) strong melt depletion in the late Archaean producing refractory harzburgites and dunites (e.g. Gurney and Harte, 1980; Schulze, 1995), ii) re-fertilisation during multiple metasomatic events (Gurney and Harte, 1980; Dawson, 1987b; Griffin et al., 1999b; Konzett et al., 2000; Zhang et al., 2001; Grégoire et al., 2003; Dawson, 2004; Simon et al., 2007) and iii) interaction with kimberlitic magma prior to incorporation and ascent to the Earth's surface as xenoliths within the host kimberlite

(Konzett et al., 1998; Grégoire et al., 2002). These periods are documented by the different textures and compositions of ultramafic mantle xenoliths found in kimberlites of the Kaapvaal Craton, i) coarse-grained granular dunites and harzburgites, ii) metasomatically enriched websterites, lherzolites and wehrlites and iii) MARID and PIC xenoliths. The mantle peridotite suite of the Kaapvaal kimberlites is dominated by harzburgites and fertile lherzolites (e.g. Harte, 1983; Grégoire et al., 2003). Dunite and wehrlite xenoliths are rare, but can be closely related to harzburgites and lherzolites due to similar textures (Fig. 15), as well as similar major and trace element compositions (Fig. 2 to Fig. 4, Fig. 7 and Fig. 10). Dunite and wehrlite xenoliths have a refractory mineralogy with only low abundances of secondary minerals such as clinopyroxene. They reflect mantle xenolith assemblages that have not been as intensely percolated by infiltrating melts as websterites and lherzolites.

6.1. Archaean melt depletion

Melt depletion, as seen on Re-depletion ages and Re-Os model ages of most Kaapvaal mantle peridotites, occurred in the Kimberley region predominantly between 3.2 Ga, the time of the oldest components found in the Kimberley area, and 2.9 Ga, the time of juxtaposition of the western Kimberley block and the eastern Witwatersrand block (e.g. de Wit et al., 1992; Carlson and Moore, 2004; Schmitz et al., 2004; Simon et al., 2007). It may have happened in a suboceanic arc setting (Simon et al., 2007) or during subduction due to mantle wedge melting (Stachel et al., 1998; Schmitz et al., 2004). There are several indications found in dunite, wehrlite and websterite xenoliths that extensive melt depletion of the Kaapvaal lithospheric mantle occurred prior to metasomatism: i) a refractory whole-rock major element composition lying towards up to 40-50 % melt depletion according to the petrogenetic grid plotted in Fig. 7, deduced from partial melting experiments (Walter, 2005), ii) high abundances of olivine in dunite and wehrlite xenoliths (65-100 Vol. %; Table 1) with high forsterite contents (mostly Fo_{90-93}; Table 2), iii) high Cr# (0.64-0.84) of spinel and high forsterite contents of Fo_{90-93} (Fig. 2) in wehrlite xenoliths indicate partial melting of 30-40 % (Arai, 1994) and iv) Archaean Re-depletion ages of wehrlite, as well as most dunite and websterite xenoliths (2.9±0.3 Ga; Table 9). Similar features are often described from Kaapvaal mantle peridotites, indicating a depleted protolithic mantle (e.g. Zhang et al., 2001; Grégoire et al., 2003; Simon et al., 2007). Because T_{RD} is calculated assuming that a melt-depletion event occurred removing all Re from the sample and hence the ^{187}Os did not grow due to radioactive decay of ^{187}Re since the depletion event, it represents a minimum age of melt depletion.

Different Re-depletion ages are seen in dunite DJ0259 and websterite DJ0216, as well as dunites DJ0297, DJ02100 and websterite DJ0217. The former two samples have low Re-depletion ages of 1.3±0.6 Ga, but average model ages of T_{MA}=2.3±0.3 Ga, which lies in

the same range as Kaapvaal peridotite Re-depletion ages. These samples seem to reflect a mixed age between an old (Archaean) and a young (Phanerozoic) depletion event. The latter three have future Re-depletion ages with the dunite samples having model ages of T_{MA}=290-110 Ma (similar to Group II kimberlites), while DJ0217 has an extremely radiogenic γOs ratio with T_{MA} older than the earth.

Overall, the protoliths of dunite, wehrlite, fertile lherzolite and websterite xenoliths are highly refractory dunites and harzburgites.

6.2. Modelling hypothetical melts in equilibrium with pyroxene and garnet

In Fig. 17 the $(La/Yb)_{CN}$ ratio, which indicates the extent of REE fractionation in clinopyroxene, is plotted versus the Ti/Eu ratio, which indicates HFSE decoupling from REE. Additionally, basanitic and carbonatitic melts are plotted. The HFSE are strongly incompatible with carbonatitic melts, while silicate melts contain HFSE. During mantle melting HFSE are usually incompatible and go into the melt, except when a Ti-mineral such as rutile is present in the mantle and retains them. The REE are generally incompatible in basaltic magma, with slight increase in compatibility from La to Lu. Mantle melting produces LREE depletion in the restitic mantle assemblage. But since clinopyroxenes in dunite, wehrlite and websterite xenoliths are enriched in LREE (websteritic more than wehrlitic; Fig. 11), they must be metasomatic either by modal metasomatism or by cryptic re-enrichment. Wehrlitic clinopyroxene has high Ti/Eu but low $(La/Yb)_{CN}$ ratios displaying a trend towards silicate melts (e.g. basanite). Websteritic clinopyroxene has low Ti/Eu and high $(La/Yb)_{CN}$ ratios, similar to the majority of Kaapvaal peridotites, displaying a trend towards highly alkaline melts (e.g. carboantite; Fig. 17).

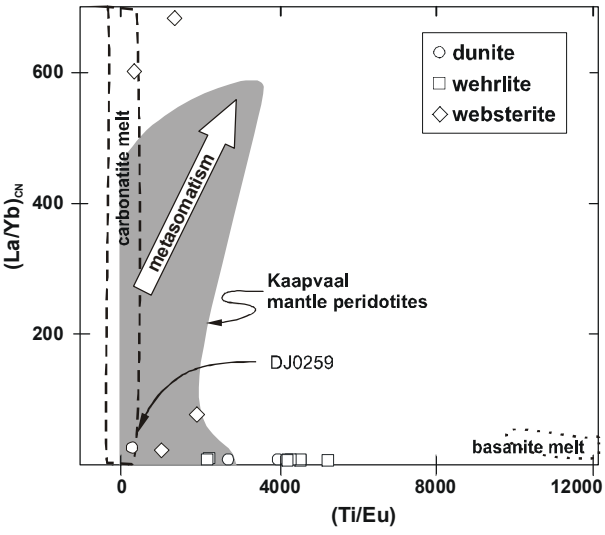

Fig. 17: Chondrite normalized La/Yb versus Ti/Eu in clinopyroxene of dunite, wehrlite and websterite xenoliths separating silica from carbonatite melt metasomatism (Coltorti et al., 1999) plotted together with trace element composition of crustal carbonatite (broken line; Bizimis et al., 2003) and basanite melt (dotted line; Frey et al., 1978) and typical clinopyroxene in metasomatised Kaapvaal mantle peridotite xenoliths (grey field; Grégoire et al., 2002; 2003; Simon et al., 2003; van Achterbergh, 2004; Simon et al., 2007).

Calculating hypothetical melts in equilibrium with clinopyroxene, orthopyroxene and garnet helps to identify possible melts that have infiltrated and metasomatised the Kaapvaal craton upper mantle. For these calculations mineral/melt partition coefficients obtained from natural basaltic rocks and experiments were used (Table 11). Wehrlitic clinopyroxene and garnet have hypothetical equilibrium melts with an overall smooth trace element pattern, having a slight positive Zr-Hf anomaly (Fig. 18 a and b). In contrast, websteritic clinopyroxene and garnet have hypothetical equilibrium melts with a steeper REE pattern than wehrlitic equilibrium melts and additionally a strong negative Ti anomaly and in some cases a negative Zr-Hf anomaly (Fig. 18 d and e). Especially clinopyroxene in dunite DJ0259 has both negative Zr-Hf and Ti anomalies. Orthopyroxene has different equilibrium melts, with similar trace element abundances for wehrlitic and websteritic orthopyroxene. It has positive Nb-Ta and Ti anomalies and a smoth decrease from LREE to HREE. Websteritic orthopyroxene has equilibrium melts with a slight negative Zr-Hf anomaly, while the wehrlitic orthopyroxene equilibrium melt has a slight positive Zr-Hf anomaly.

Table 11: Average mineral/melt partition coefficients used for calculating hypothetical melts in equilibrium with clinopyroxene, orthopyroxene and garnet. Corresponding references and their equilibration conditions are displayed in the lower part of the table.

	$D_{cpx/melt}$	$D_{grt/melt}$	$D_{opx/melt}$
Nb	0.00595	0.02	0.00132
Ta	0.019	0.076	0.0025
La	0.341	0.0059	0.0008
Ce	0.361	0.0244	0.00268
Pr	-	0.0072	0.0032
Sr	0.336	0.00552	0.0012
Nd	0.469	0.15	0.01308
Zr	0.162	0.736	0.0236
Hf	0.226	0.527	0.04756
Sm	0.581	0.618	0.0222
Eu	0.554	1.01	0.03
Ti	0.386	0.779	0.109
Gd	0.738	0.855	0.034
Tb	-	1.465	0.054
Dy	0.749	2.96	0.077
Ho	-	5.2	0.100
Y	0.533	3.745	0.0938
Er	0.762	4.64	0.0974
Yb	0.699	7.58	0.1502
Lu	0.684	12.895	0.1712

	reference	**rock-type**	**pressure**
$D_{cpx/melt}$	Green 2000	hydrous basalt	20 kbar
	Shimizu 1980	high-Al basalt and alkali olivine basalt	20-30 kbar
	Jenner et al. 1993	basalt	25 kbar
	Hauri et al. 1994	high-Al basalt	25 kbar
	Johnson 1998	basalt	20-30 kbar
	Hart and Dunn 1993	alkali basalt	30 kbar
$D_{grt/melt}$	Zack et al. 1997	garnet pyroxenite	
	Green et al. 2000	hydrous basalt	30 kbar
	Hauri et al. 1994	high-Al basalt	25 kbar
	Jenner et al. 1994	basalt	25 kbar
	Shimizu 1980	high-Al basalt and alkali olivine basalt	30 kbar
$D_{opx/melt}$	Matsui et al. 1977	basalt	
	Salters and Longhi 1999	basalt	24-28 kbar
	Green 2000	hydrous tholeiite	20kbar

We have compared these equilibrium melts with possible metasomatising melts such as highly silicate melt, produced by partial melting of eclogite at high pressure (Rapp et al., 1999), which is similar to TTG melts (tonalite-trondjemite-granodiorite; Clemens et al., 2006), with Group I and Group II kimberlites (Le Roex et al., 2003) and carbonatite melts (Bizimis et al., 2003). The trace element compositions of wehrlitic clinopyroxene, garnet and orthopyroxene equilibrium melts agree best with high pressure eclogite partial melt (Fig. 18), which has a smooth trace element pattern, with a positive Zr-Hf anomaly indicating subalkaline melt compositions (Zinngrebe and Foley, 1995). In contrast, the negative HFSE

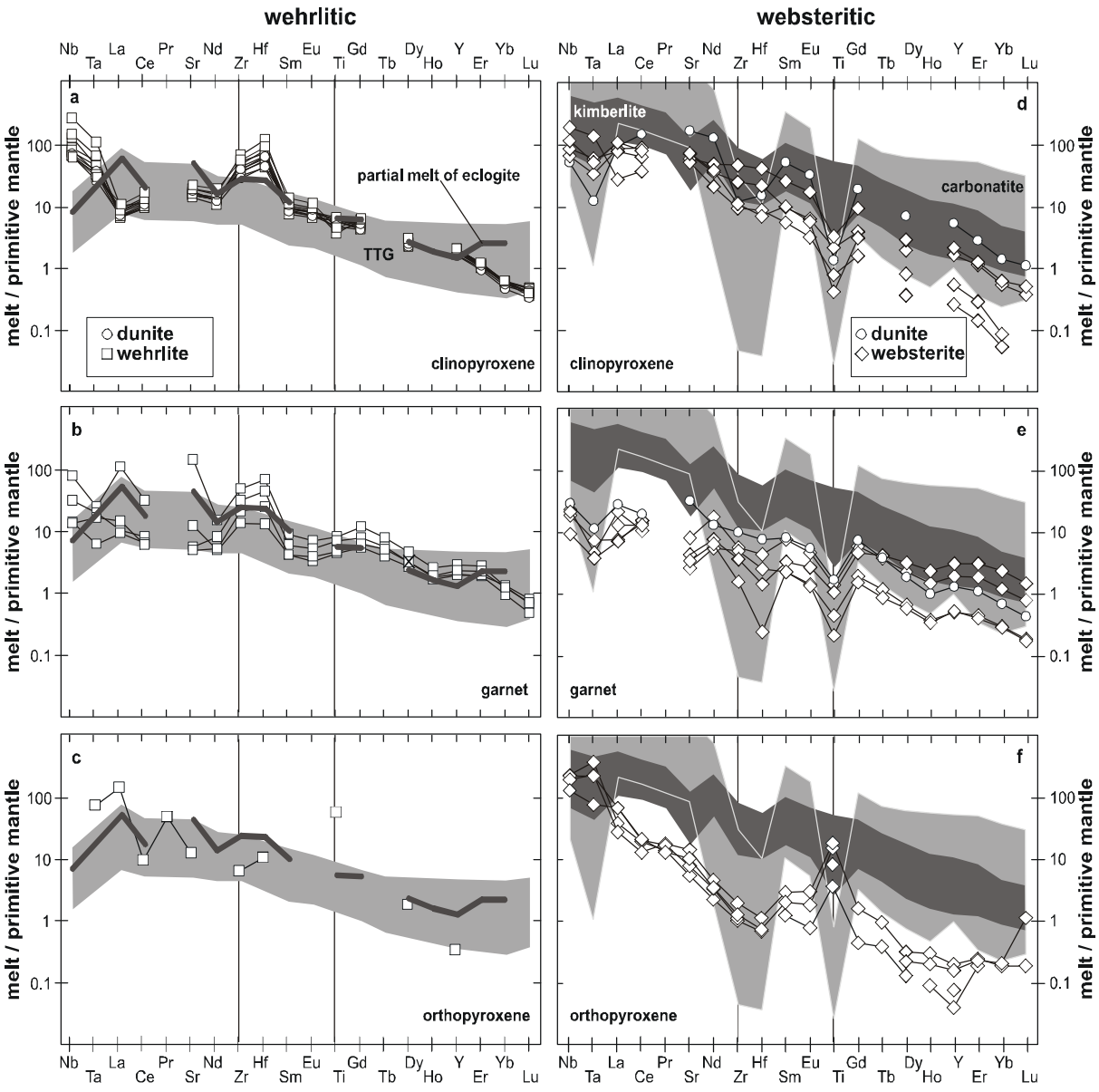

Fig. 18: Trace element composition of recalculated parental melt in equilibrium with clinopyroxene (a) and (d), garnet (b) and (e) and orthopyroxene (c) and (f) of dunite, wehrlite and websterite xenoliths: (a-c) wehrlitic patterns, (d-f) websteritic patterns. Equilibrium melt is calculated using average basaltic mineral/melt partition coefficients (Table 11). The equilibrium melts are compared in (a), (b) and (c) with eclogite partial melt (dark grey; Rapp and Shimizu, 2003) and TTG melt (light grey field; Clemens et al., 2006), and in (d), (e) and (f) with carbonatite (light grey field; Bizimis et al., 2003) and Group I and Group II kimberlites (dark grey field; LeRoex et al., 2003; Becker and Le Roex, 2006).

anomalies of websteritic garnet and clinopyroxene equilibrium melts is rather similar to trace element compositions of carbonatite, kimberlite and ultramafic lamprophyre melts (e.g. Bizimis et al., 2003; Le Roex et al., 2003; Tappe et al., 2003; Becker and Le Roex, 2006). But the overall trace element abundance of these alkaline melts is higher than the websteritic garnet and clinopyroxene equilibrium melts. Hence, websterite xenoliths have experienced a cryptic metasomatic overprint changing the trace element composition of the pre-existing silicate minerals partly. It did not affect dunite and wehrlite xenoliths.

6.3. Different styles of metasomatism in the Kaapvaal Craton

A metasomatic overprint of wehrlite and websterite xenoliths is indisputable due to clear metasomatic textures (Fig. 1 c-h) and geochemical modification of the previously strongly depleted dunitic to harzburgitic protoliths. Amoeboid interstitial minerals such as clinopyroxene, garnet, orthopyroxene and oxide minerals in the studied samples are produced by small amounts of mantle derived melt that infiltrate the peridotitic upper mantle, which leads to crystallization of secondary minerals producing a three dimensional network along grain margins (as described by Harte et al., 1993). Such minerals are often described from Kaapvaal craton mantle peridotites and interpreted to be of secondary origin (e.g. Erlank et al., 1987; Grégoire et al., 2003). The slightly lighter oxygen isotope composition of most clinopyroxene and garnet in dunite, wehrlite and websterite xenoliths compared to mantle peridotites clearly reflects metasomatism by melt from altered oceanic crust (Fig. 6; Perkins et al., 2006).

The limited range in equilibration pressure and temperature of websterite xenoliths, lying within the field of Kaapvaal peridotites (Fig. 16) and similar major and trace element compositions manifests a close relationship of websterites and fertile peridotites. In contrast, wehrlite xenoliths have a larger range in equilibration temperature and pressure and different major and trace element compositions, displaying rather remote lithologies within the subcratonic upper mantle. The larger range in wehrlite equilibration temperatures (especially in wehrlite DJ0256) can be explained by local heating within the upper mantle. While websterites have up to 67-100 Vol. % secondary minerals, wehrlites have 1-35 Vol. % secondary minerals. Websterites represent assemblages that were in direct contact with metasomatising agents such as subducted oceanic crust or veins of melt percolation. Fertile peridotites, wehrlites and dunites represent upper mantle assemblages that are systematically further away from the direct influence of the metasomatising agent. The metasomatic overprint decreases from websterite to fertile peridotite to wehrlite and dunite, with refractory peridotite representing the metasomatically unaffected strongly depleted mantle (e.g. Viljoen et al., 1992; Schulze, 1995).

6.3.1. Orthopyroxene enrichment

Chemical disequilibrium between orthopyroxene and garnet-clinopyroxene, indicated by mineral mineral partition coefficients (Fig. 12) and a lack of complementary Ti and Zr anomalies between orthopyroxenen and clinopyroxene (Fig. 10; Rampone et al., 1991), has point to a different petrogenetic history for orthopyroxene in wehrlite and websterite xenoliths. Orthopyroxene enrichment has often been described from fertile mantle peridotites in the Kaapvaal Craton (e.g. Menzies et al., 1987; Boyd, 1989a; Pearson et al., 1995a; Zhang et al., 2001; Simon et al., 2007) and interpreted to have effected large parts of the whole Kaapvaal mantle. Dunite and wehrlite xenoliths do not have such high orthopyroxene contents (Table 1), indicating that orthopyroxene enrichment did not take place all over the Kaapvaal craton sublithospheric mantle.

Orthoyproxene differs between dunite, wehrlite and webtserite xenoliths not only in the abundance within the xenoliths, but also in composition of major and trace elements. Orthoyproxene in dunite and wehrlite xenoliths have higher Mg# than orthopyroxene in websterite xenoliths (0.91-0.93 versus 0.88-0.90, respectively), which points to a primary origin after melt depletion. Orthopyroxene in websterite xenoliths has higher modal abundances and lower TiO_2, Cr_2O_3, CaO, Na_2O, Cu, Ga, Rb, Y and Ba contents compared to orthopyroxene in dunites DJ0273 and DJ0274 and wehrlite xenoliths (Table 3). This may indicate, that orthopyroxene in websteritic xenoliths are reaction products between a silica-rich melt and the surrounding peridotite mantle, similar to orthopyroxenite veins found in ophiolites (Kelemen et al., 1998; McInnes et al., 2001; Tamura and Arai, 2006). By this process orthopyroxene replaces olivine in the near vein assemblages, inheriting the low TiO_2, Cr_2O_3, CaO and Na_2O content from olivine and enriching the whole- rock in SiO_2. Refractory harzburgitic to dunitic mantle is transformed into orthopyroxenite at direct contact with the melt and fertile harzburgite further away (Fig. 19 a). Such Si-rich melts can be produced at high pressure by low-degree partial eclogite melting, resulting in a dacitic melt composition (>63 wt. % SiO_2; Yaxley and Green, 1998a). This implies the presence of subducted oceanic crust in the mantle, which may be related to the amalgamation of micro continents and cratonisation of the Kaapvaal craton in the Archaean (<2.9 Ga; de Wit et al., 1992). The proof for the presence of subducted oceanic crust underneath Kimberley is the occurrence of eclogite xenoliths (e.g. Boyd and Nixon, 1978; Jagoutz et al., 1984; MacGregor and Manton, 1986; Neal et al., 1990; Jacob et al., 2005) and eclogitic mineral inclusions in diamonds in the Kimberley kimberlites (e.g. Richardson et al., 2001; Shirey et al., 2003; Appleyard et al., 2004) and a larger range of $\delta^{18}O$ in orthopyroxene in websterite xenoliths compared to orthopyroxene in mantle peridotites (Fig. 6; Mattey et al., 1994) being caused by low pressure, low temperature processes (Clayton et al., 1975).

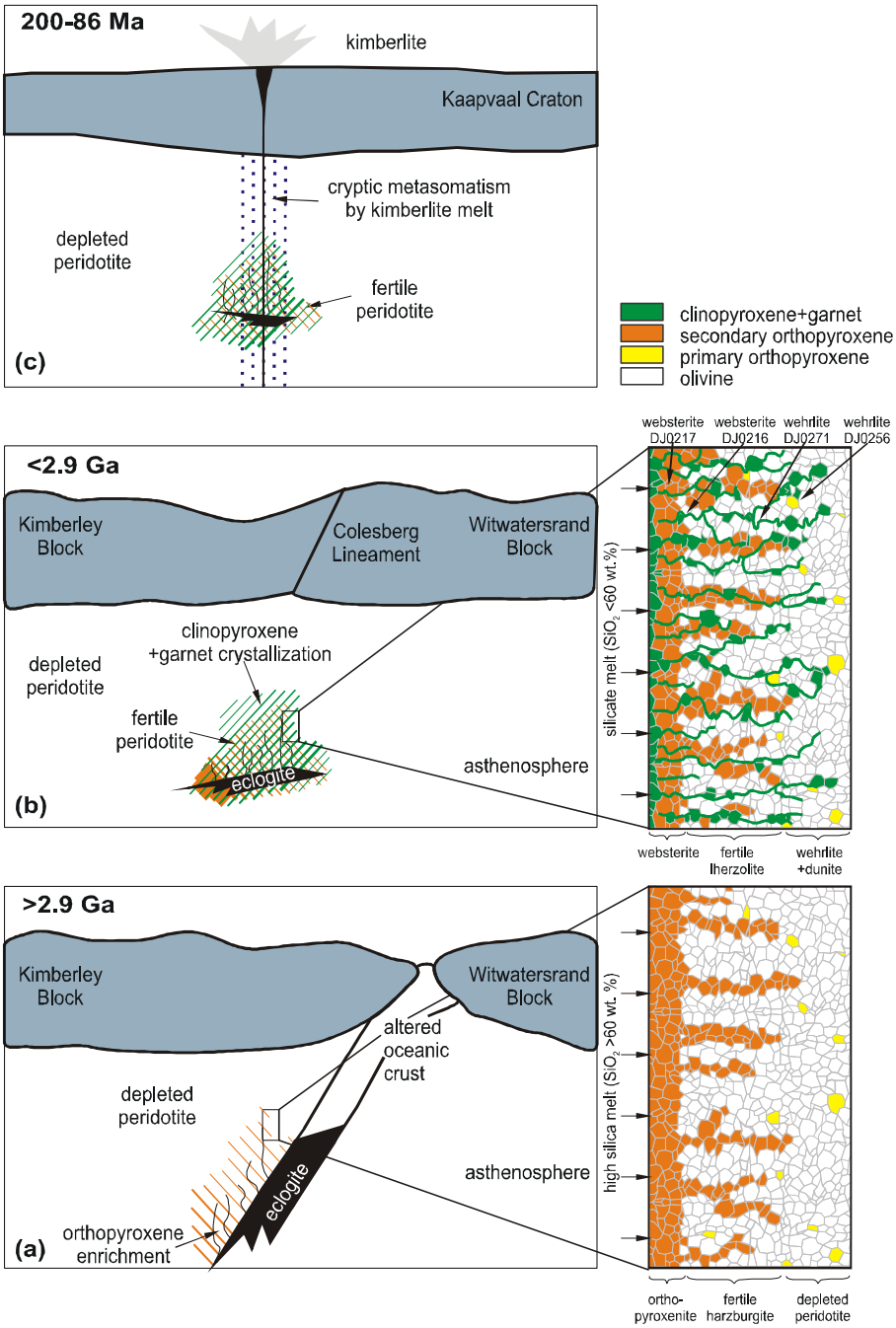

Fig. 19: Petrogenetic model for dunite, wehrlite and websterite xenoliths: a) previously strongly depleted sublithospheric upper mantle gets enriched in orthopyroxene due to reaction of mantle peridotite with silica-rich melt with >60 wt. % SiO_2 (Yaxley and Green, 1998b) produced at the contact with subducted and eclogitized oceanic crust, b) at ~2.9 Ga at higher temperature partial melting of eclogite produces basaltic melts with lower SiO_2 content, which percolates larger areas of the upper mantle (e.g. Yaxley and Green, 1998b; Rapp and Shimizu, 2003) with clinopyroxene and garnet crystallization along grain margins and c) at <200 Ma silica-carbonatite hybrid melts (kimberlite) percolate and erupt through the upper mantle and crust, metasomatising the upper mantle cryptically and transporting the mantle xenoliths to the Earth's surface.

Wehrlitic and websteritic orthopyroxene has similar low trace element compositions (Fig. 10) typical for orthopyroxene in depleted peridotite. Both have positive Ti anomalies, in addition orthopyroxene in websterites has a positive Nb-Ta anomaly. The trace element composition is not solely related to the Archaean melt depletion event or the subduction related high Si melt reacting with surrounding mantle peridotite. The slight anomalies have been rather imprinted upon the orthopyroxene during a later re-enrichment process.

6.3.2. Origin of garnet

Garnet in mantle peridotite xenoliths of the Kaapvaal craton has been interpreted in many different ways, i) as primary mantle garnets that were cryptically overprinted (e.g. Stachel et al., 1998), ii) as exsolution garnets from orthopyroxene (e.g. Saltzer et al., 2001; Simon et al., 2003; Dawson, 2004) or iv) as crystallization products of percolating melts (e.g. e.g. Zhang et al., 2001; Burgess and Harte, 2004; Simon et al., 2007). Garnet exsolution from clinopyroxene has only been described from eclogite xenoliths, in which it was exsolved from clinopyroxene with high tschermakite component (Harte and Gurney, 1975; Jerde et al., 1993). Two different types of garnets occur in the studied samples, high Mg# titanian-pyrope to titanian uvarovite-pyrope garnet in wehrlites (G11 garnets after Dawson and Stephens, 1975) and low Mg# chrome pyrope garnet in websterites (G9).

Websteritic garnet has two distinct textures. One fine-grained, necklace texture, where garnet has crystallized along orthopyroxene and clinopyroxene grain margins (websterites DJ0215 and DJ0218) and another coarse-grained texture, where garnet occurs as inclusion in orthopyroxene and has clinopyroxene along its margins (websterite DJ0217 and DJ0218; Fig. 1 g and h). On the one hand the necklace textured garnet can be interpreted to reflect exsolution from orthopyroxene, with clinopyroxene crystallizing later predominantly along garnet chains, sometimes totally surrounding garnet (Fig. 1 g), while the coarse-grained textured garnet may represent replacement of orthopyroxene by garnet or a pooling of exsolved garnet along orthopyroxene grain margins (Harte and Gurney, 1975). Exsolution of garnet from orthopyroxene is supported by low LREE contents of websteritic garnet (Fig. 10; Simon et al., 2003). On the other hand low Mg#, TiO_2, Cr_2O_3, CaO and higher Al_2O_3 and MnO contents (Fig. 5) and the G9 composition of websteritic garnets rather speaks for a cumulatic origin from percolating basaltic melt (e.g. Burgess and Harte, 2004). Hence percolating melt may have initiated garnet exsolution along orthopyroxene grain margins, while clinopyroxene crystallizes alongside the garnet grains. The simultaneity of this exsolution and crystallization process has led to chemical equilibrium between garnet and clinopyroxene (Fig. 12 a).

Wehrlitic garnet also displays two different textures. In wehrlites DJ0271 and AJE401 garnet occurs as amoeboid minerals together with clinopyroxene in schlieren along olivine

grain margins and is similar strong depleted in LREE as websteritic garnets (Fig. 1 e, Fig. 10 e). In wehrlite DJ0256 garnet occurs as small euhedral grains in schlieren together with primary orthopyroxene and is slightly enriched in LREE (Fig. 1 f, Fig. 10 e). In contrast to websteritic garnet wehrlitic garnet has lower Al_2O_3, MnO, higher Cr_2O_3, CaO, Na_2O and TiO_2 contents and higher Mg#. Garnet Cr_2O_3 contents > 5 wt. % indicate crystallization from highly depleted precursory rocks that experienced partial melting in the spinel stability field which results in high Cr/Al ratios (Fig. 5; Stachel et al., 1998). Additionally, the high TiO_2 contents, positive HFSE anomalies, high LREE contents in garnet of wehrlite DJ0256 and an amoeboid texture of garnet in wehrlites DJ0271 and AJE401 point to secondary crystallization of garnet in conjunction with clinopyroxene crystallization. The trace element pattern of melt in equilibrium with wehrlitic garnet is similar to high pressure eclogite melt (Fig. 18; Rapp et al., 1999). Hence a multiphase origin of wehrlitic garnet must have been at work: i) crystallization in a highly depleted precursory rock and ii) metasomatic overprint and co-crystallization of clinopyroxene from partial melt of eclogite.

6.3.3. Clinopyroxene and garnet crystallization

Clinopyroxene and garnet in wehrlitic xenoliths and clinopyroxene in websteritic xenoliths have a clear infiltration texture, crystallizing as amoeboid crystals along olivine and orthopyroxene grain boundaries (Fig. 1). They are also subduction related (Fig. 19 b) due to their slightly lower $\delta^{18}O$ contents, similar to clinopyroxene and garnet in Kaapvaal craton mantle peridotites and diamonds (Lowry et al., 1999; Zhang et al., 2000) and subduction related mantle xenoliths of the Colorado Plateau (Perkins et al., 2006). Recalcluated whole-rock major element compositions of dunite, wehrlite and websterite xenoliths indicate a slight Fe and Ti enrichment, which may be due to basaltic melt (e.g. Gurney and Harte, 1980; Ehrenberg, 1982; Harte, 1983; Menzies et al., 1987), as seen more intensely by mantle xenoliths of the Premier kimberlite pipe, which have experienced basalt metasomatism related to the Bushveld intrusion (Hoal, 2003; Grégoire et al., 2005). Since this subduction related melt did not produce orthopyroxene, but clinopyroxene and garnet plus probably an Fe-Ti enrichment, it has lower Si contents, but higher Ca, Al, Ti and Fe than the Si-rich melt that lead to the formation of orthopyroxene. High temperature (>1300°C) partial melting of eclogite results in more basaltic melts than the one from which orthopyroxene crystallized, having lower SiO_2 contents and higher FeO and TiO_2 (Yaxley and Green, 1998b). The trace element composition of wehrlitic clinopyroxene and garnet equilibrium melts with positive Zr-Hf and ± positive Nb-Ta anomalies is similar to high pressure partial melts of eclogite (Fig. 18b and c; Rapp and Shimizu, 2003). The positive Zr-Hf anomalies of clinopyroxene and garnet equilibrium melts (Fig. 18) is a feature of subalkaline melt composition, which reduces the solubility of Zr in the melt (Zinngrebe and Foley, 1995; Glaser et al., 1999). This may

initiate local crystallization of Cr-rich rutile together with clinopyroxene as seen in wehrlites DJ0214 and DJ0271 (Fig. 1 c and e). Additionally, the subchondritic Nb/Ta ratios of rutile in these wehrlites reflects a subduction-related origin of the metasomatising melt (Rudnick et al., 2000).

In the Kimberley area basaltic melts occure at the Earth's surface during the Ventersdorp (2.7 Ga; Crow and Condie, 1988) and Karoo magmatic events (~200 Ma; Duncan et al., 1997). Both have produced large quantities of basaltic rocks. On the one hand, large quantities of basaltic melt metasomatising large parts of the upper mantle must have been produced in order to infiltrate not only the near vein assemblage, but also distal to the vein lithologies, since such clinopyroxene and garnet occure in websterites, fertile lherzolites, wehrlites and dunites. On the other hand, this basaltic melt only may have metasomatised the Kaapvaal upper mantle, never reaching the Earth's surface.

Replacement of clinopyroxene by orthopyroxene as seen only in one wehrlite sample (DJ0214; Fig. 5 c) may be a later local reaction with silicate melt similar to the silicate melt replacing olivine. Orthopyroxene replacing clinopyroxene has the highest Cr_2O_3 and CaO contents (1.2 wt. % and 1.0 wt. %, respectively) compared to primary orthopyroxene in wehrlite DJ0256 (0.7 wt. % and 0.8 wt. %, respectively) and secondary orthopyroxene replacing olivine in websterite and fertile lherzolite xenoliths (0.1-0.8 wt. % and 0.1-0.8 wt. %;Table 3; e.g. Carswell et al., 1979; Simon, 2004). Such a process occurred after clinopyroxene crystallization and has been shown to produce fertile harzburgites xenoliths (Griffin et al., 1999b; Zhang et al., 2001).

How melt penetrats into and through the upper mantle is highly speculative and can not clearly be determined upon the studied mantle xenoliths. It may creep along grain boundaries, consuming neighbouring peridotitic minerals and thereby changing its melt composition or pressing a path along mineral margins pushing primary minerals aside. Another possibility is percolation of melts predominantly using pre-existing veins.

6.3.4. Kimberlite infiltration

Clinopyroxene, orthopyroxene and garnet in websterite xenoliths and dunite DJ0259 have trace element patterns indicating partial change in trace element composition of the pre-existing clinopyroxene, orthopyroxene and garnet minerals due to highly alkaline melt (e.g. kimberlite). This is mainly shown in clinopyroxene by a strong depletion in HFSE and an enrichment in LREE, resulting in low Ti/Eu and high $(La/Yb)_N$ ratios (Fig. 17; Coltorti et al., 1999). Metasomatism due to carbonatite and kimberlite melt has often been supposed to have affected sublithospheric upper mantle (e.g. Yaxley et al., 1991; Rudnick et al., 1993; Gorring and Kay, 2000; van Achterbergh et al., 2004). MARID xenoliths are interpreted to represent cumulatic veins of kimberlite in the mantle crystallized 200 Ma ago (e.g. Waters et

al., 1989; Konzett et al., 1998). But this metasomatism can only have changed the trace element composition of clinopyroxene, orthopyroxene and garnet. The high silica major and high orthopyroxene modal composition of the websterite xenoltihs cannot be attributed to carbonatite or kimberlite melts (Fig. 7). Additionally, the similarity of trace element patterns between carbonatitic or kimberlitic melts and websteritic equilibrium melts decreases from clinopyroxene to garnet to orthopyroxene, indicating a decrease in cryptic trace element equilibration with the high alkaline melt. In orthopyroxene, only a negative Zr-Hf anomaly shows equilibration with kimberlitic melt (Fig. 18). The kimberlitic metasomatism did only affect near vein assemblages, not remote mantle lithologies, since these trace element features of negative Ti, Zr-Hf and high LREE are missing in wehrlitic orthopyroxene, clinopyroxene and garnet (Fig. 10).

Porphyroclastic textures as seen in some dunite and wehrlite samples and often described in fertile peridotites may occur due to deformation by the thermal aureaole of the host kimberlite (Mercier, 1979; Moore and Belousova, 2005). Similarly, the olivine zonation as observed in samples DJ0259 and DJ0275 reflects quenched re-equilibration with the host kimberlite (increase in FeO, MnO, transition metals, Al, Ca, Ti, Zr and decrease in SiO_2, MgO, NiO; Table 2). Incorporation into the kimberlite magma and fast ascent to the Earth's surface results in contamination with the kimberlite melt along grain boundaries and in cracks and leads to kelyphitisation of garnet due to temperature decrease (Hunter and Taylor, 1982) and rutile breakdown to chromite and ilmenite due to pressure decrease. Future Re-depletion model ages and high Re contents reflect local enrichment in Re because of kimberlite infiltration in dunite samples DJ02100 and DJ0297 and probably also websterite DJ0216.

7. Conclusions

The Kimberley kimberlites in South Africa have carried large quantities of mantle peridotites of uniquely variable lithologies, displaying a complex history of melt depletion and multiple re-enrichment of the sublithospheric upper mantle of the Kaapvaal craton. Dunite, wehrlite and websterite xenoliths represent two end-members of metasomatic re-enrichment, while fertile peridotites are intermediate to these end-members; refractory dunites and harzburgites are the starting point after extensive melt depletion.

3.2 and 2.9 Ga: high degree of partial melting in an oceanic rift setting or in a mantle wedge during subduction resets the Re-Os system and produces refractory mantle peridotites that are depleted in magmaphile elements.

>2.9 Ga: Subduction-related high silica melt (>60 wt. %), produced by low temperature partial melting of altered oceanic crust, reacts with the surrounding mantle peridotites, transforming olivine into orthopyroxene and

enriching the mantle in SiO_2. This re-enrichment is related to the amalgamation of continental crust and cratonisation of the Kaapvaal Craton. The youngest cratonisation event within the Kaapvaal Craton was the collision of the Kimberely Block with the Witwatersrand Block 2.9 Ga ago.

~2.9 Ga: A second metasomatic overprint by subalkaline melt with lower SiO_2 content, but higher CaO, Al_2O_3, FeO and HFSE produced clinopyroxene and in some samples garnet, which crystallizes along olivine and orthopyroxene grain boundaries. It has low $\delta^{18}O$ contents and triggers Fe-Ti enrichment in large parts of the mantle. In some areas the subalkaline nature of the melt induces clinopyroxene and rutile crystallization.

<200 Ma Protokimberlitic or kimberlitic melts are produced in the upper mantle, overprinting websteritic and lherzolitic assemblages cryptically and enriching the metasomatised mantle in Re. To a decreasing extend clinopyroxene, orthopyroxene and garnet get depleted in HFSE and enriched in LREE and Sr.

Ascent within the host kimberlite to the Earth's surface leads to decomposition of high-pressure phases such as garnet and rutile due to decrease in temperature and pressure. A high reactivity of kimberlite leads to reaction with the mantle xenoliths it has picked up, enriching them in cracks or along grain boundaries in compatible elements like Ca, Ti, Ba, Sr, LREE and Re.

Hence we can spatially distinguish two end-members of metasomatism within the mantle peridotites of the Kimberley kimberlites. On the one side, the websterite-lherzolite suite occurs, closely associated with subducted oceanic crust and intensely metasomatised. It has experienced several metasomatising events: orthopyroxene-enrichment, clinopyroxene and garnet crystallization in percolation veins and cryptic metasomatism due to kimberlite infiltration. On the other side dunite and wehrlite xenoliths represent mantle peridotite pieces from distal mantle lithologies, which have experienced only one metasomatic overprint by peralkaline melt produced by high temperature partial melting of subducted oceanic crust. Clinopyroxene and in some samples garnet and rutile crystallized from this melt along olivine, orthopyroxene or garnet grain boundaries. In contrast to the often referred carbonatite metasomatism, being able to metasomatise the sublithospheric cratonic mantle intensely, rather silicate melt overprinted and changed large areas of the Kaapvaal mantle, and is detectable in websterite, lherzolite, wehrlite and dunite xenoliths.

REFERENCES

Allsopp H. L. and Barrett D. R. (1975) Rb-Sr age determinations on South African kimberlite pipes. *Phys. Chem. Earth* **9**, 605-617.

Alt J. C., Anderson T. F., Bonnell L. and Muehlenbachs K. (1989) Mineralogy, chemistry, and stable isotopic composition of hydrothermally altered sheeted dikes: ODP hole 504B, Leg 111. *Proc. ODP Sci. Res.* **111**, 27-40.

Appleyard C. M., Viljoen K. S. and Dobbe R. (2004) A study of eclogitic diamonds and their inclusions from the Finsch kimberlite pipe, South Africa. *Lithos* **77**, 317-332.

Arai S. (1994) Characterization of spinel peridotites by olivine-spinel compositional relationships: Review and interpretation. *Chem. Geol.* **113**, 191-204.

Armstrong A. (1995) CITZAF - A package of correction programs for the quantitative electron microbeam X-ray-analysis of thick polished materials, thin-films, and partickles. *Microbeam Analy.* **4**, 177-200.

Aulbach S., Stachel T., Viljoen K. S., Brey G. P. and Harris J. W. (2002) Eclogitic and websteritic diamond sources beneath the Limpopo Belt - is slab-melting the link? *Contrib. Mineral. Petrol.* **143**, 56-70.

Barth M. G., Rudnick R. L., Carlson R. W., Horn I. and McDonough W. F. (2002a) Re-Os and U-Pb geochronological constraints on the eclogite-tonalite connection in the Archean Man Shield, West Africa. *Precambrian Res.* **118**, 267-283.

Barth M. G., Rudnick R. L., Horn I., McDonough W. F., Spicuzza M. J., Valley J. W. and Haggerty S. E. (2001) Geochemistry of xenolithic eclogites from West Africa, Part I: A link between low MgO eclogites and Archean crust formation. *Geochim. Cosmochim. Acta* **65**, 1499-1527.

Barth M. G., Rudnick R. L., Horn I., McDonough W. F., Spicuzza M. J., Valley J. W. and Haggerty S. E. (2002b) Geochemistry of xenolithic eclogites from West Africa, Part II: Origins of the high MgO eclogites. *Geochim. Cosmochim. Acta* **66**, 4325-4345.

Becker M. and Le Roex A. P. (2006) Geochemistry of South African on- and off-craton, Group I and Group II kimberlites: Petrogenesis and source region evolution. *J. Petrol.* **47**, 673-703.

Bédard J. H. (2006) A catalytic delamination-driven model for coupled genesis of Archaean crust and sub-continental lithospheric mantle. *Geochim. Cosmochim. Acta* **70**, 1188-1214.

Bickle M. J., Nisbet E. G. and Martin A. (1994) Archean greenstone belts are not oceanic crust. *J. Geol.* **102**, 121-138.

Bizimis M., Salters V. J. M. and Dawson J. B. (2003) The brevity of carbonatite sources in the mantle: evidence from Hf isotopes. *Contrib. Mineral. Petrol.* **145**, 281-300.

Boyd F. (1989a) Compositional distinction between oceanic and cratonic lithosphere. *Earth Planet. Sci. Lett.* **96**, 15-26.

Boyd F. R. (1974) Ultramafic nodules from the Frank Smith kimberlite pipe, South Africa. *Carnegie I. Wash.* **Year Book 73**, 285-294.

Boyd F. R. (1989b) Compositional distinction between oceanic and cratonic lithosphere. *Earth Planet. Sci. Lett.* **96**, 15-26.

Boyd F. R. and Nixon P. H. (1978) Ultramafic nodules from the Kimberley pipes, South Africa. *Geochim. Cosmochim. Acta* **42**, 1367-1382.

Boyd F. R. and Mertzman S. A. (1987) Composition and structure of the Kaapvaal lithosphere, southern Africa. In *Magmatic processes: physicochemical principles*, Vol. 1 (ed. B. O. Mysen). The Geochemical Society. pp. 13-24.

Boyd F. R., Pokhilenko N. P., Pearson D. G., Mertzman S. A., Sobolev N. V. and Finger L. W. (1997) Composition of the Siberian cratonic mantle: evidence from Udachnaya peridotite xenoliths. *Contrib. Mineral. Petrol.* **128**, 228-246.

Brey G. P. and Köhler T. (1990) Geothermobarometry in four-phase lherzolites, Part II: New thermobarometers and practical assessment of existing thermobarometers. *J. Petrol.* **31**, 1353-1378.

Burgess S. R. and Harte B. (2004) Tracing lithsphere evolution through the analysis of heterogeneous G9-G10 garnets in peridotite xenoliths, II: REE Chemistry. *J. Petrol.* **45**, 609-634.

Carlson R. W. and Moore R. O. (2004) Age of the Eastern Kaapvaal mantle: Re-Os isotope data for peridotite xenoliths from the Monastery kimberlite. *S. Afr. J. Geol.* **107**, 81-90.

Carlson R. W., Pearson D. G., Boyd F. R., Shirey S. B., Irvine G., Menzies A. H. and Gurney J. J. (1999) Re-Os systematics of lithospheric peridotites: Implications for lithosphere formation and preservation. *Proceedings of the 7th International Kimberlite Conference*. Cape Town. 99-108.

Carswell D. A. (1975) Primary and secondary phlogopites and clinopyroxenes in garnet lherzolite xenoliths. *Phys. Chem. Earth* **9**, 417-429.

Carswell D. A. and Dawson J. B. (1970) Garnet peridotite xenoliths in South African kimberlite pipes and their petrogenesis. *Contrib. Mineral. Petrol.* **25**, 163-184.

Carswell D. A., Clarke D. B. and Mitchell R. H. (1979) The petrology and geochemistry of ultramafic nodules from pipe 200, northern Lesotho. In *Kimberlites, diatremes and diamonds: Their geology, petrology and geochemistry*, Vol. 2 (eds. F. R. Boyd and H. O. A. Meyer). American Geophysical Union, Washington. pp. 127-144.

Clague D. A. (1988) Petrology of ultramafic xenoliths from Loihi Seamount, Hawaii. *J. Petrol.* **29**, 1161-1186.

Clayton R. N., Goldsmith J. R., Karel V. J., Mayeda T. K. and Newton R. C. (1975) Limits on the effect of pressure on isotopic fractionation. *Geochim. Cosmochim. Acta* **39**, 1197-1201.

Clemens J. D., Yearron L. M. and Stevens G. (2006) Barberton (South Africa) TTG magmas: Geochemical and experimental constraints on source-rock petrology, pressure of formation and tectonic setting. *Precambrian Res.* **151**, 53-78.

Coleman R. G., Lee D. E., Beatty L. B. and Brannock W. W. (1965) Eclogites and eclogites: their differences and similarities. *Bull. Geol. Soc. Am.* **76**, 483-508.

Coltorti M., Bonadiman C., Hinton R. W., Siena F. and Upton B. G. J. (1999) Carbonatite metasomatism of the oceanic upper mantle: evidence from clinopyroxenes and glasses in ultramafic xenoliths of Grande Comore, Indian Ocean. *J. Petrol.* **40**, 133-165.

Crow C. and Condie K. C. (1987) Geochemistry and origin of late Archean volcanic rocks from the Rhenosterhoeck Formation, Dominion Group, South Africa. *Precambrian Res.* **37**, 217-229.

Crow C. and Condie K. C. (1988) Geochemistry and origin of Late Archean volcanics from the Ventersdorp Supergroup, South Africa. *Precambrian Res.* **42**, 19-37.

Dalton J. and Wood B. (1993) The composition of primary carbonate melts and their evolution through wall-rock reaction in the mantle. *Earth Planet. Sci. Lett.* **119**, 511-525.

Davis D. L. (1977) The ages and uranium contents of zircons from kimberlites and associated rocks. *Carnegie I. Wash.* **76**, 631-653.

Dawson J. B. (1984) Contrasting types of upper-mantle metasomatism. In *Kimberlites II: The mantle and crust-mantle relationships* (ed. J. Kornprobst). Elsevier, Amsterdam. pp. 289-294.

Dawson J. B. (1987a) The MARID suite of xenoliths in Kimberlites: relationship to veined and metasomatised peridotite xenoliths. In *Mantle Xenoliths* (ed. P. H. Nixon). John Wiley, Chichester. pp. 465-474.

Dawson J. B. (1987b) Metasomatized harzburgites in kimberlite and alkaline magmas: enriched restites and "flushed" lherzolites. In *Mentle metasomatism* (eds. M. A. Menzies and C. J. Hawkesworth). Academic Press, London. pp. 125-144.

Dawson J. B. (2004) A fertile harzburgite-garnet lherzolite transition: Possible inferences for the roles of strain and metasomatism in upper mantle peridotites. *Lithos* **77**, 553-569.

Dawson J. B. and Stephens W. E. (1975) Statistical classification of garnets from kimberlite and associated xenoliths. *J. Geol.* **83**, 589-607.

Dawson J. B. and Smith C. B. (1977) The MARID (mica-amphibole-rutile-ilmenite-diopside) suite of xenoliths in kimberlite. *Geochim. Cosmochim. Acta* **41**, 309-323.

Dawson J. B., Hervig R. L. and Smith J. V. (1981) Fertile iron-rich dunite xenoliths from the Bultfontein kimberlite, South Africa. *Fortschr. Mineral.* **59**, 303-324.

de Wit M. J., Roering C., Hart R. J., Armstrong A., de Ronde C. E. J., Green R. W. E., Tredoux M., Peberdy E. and Hart R. A. (1992) Formation of an Archaean continent. *Nature* **357**, 553-562.

Delaney J., Smith J., Carswell D. and Dawson J. (1980) Chemistry of micas from kimberlites and xenoliths - II. Primary- and secondary-textured micas from peridotite xenoliths. *Geochim. Cosmochim. Acta* **44**, 857-872.

Droop G. T. R. (1987) A general equation for estimating Fe^{3+} concentrations in ferromagnesian silicates and oxides from microprobe analyses, using stoichiometric criteria. *Mineral. Mag.* **51**, 431-435.

Drummond M. S. and Defant M. J. (1990) A model for trondhjemite-tonalite-dacite genesis and crustal growth via slab melting; Archean to modern comparisons. *Journal of Geophysical Research, B, Solid Earth and Planets* **95**, 21,503-21,521.

Duncan R. A., Hooper P. R., Rehacek J., Marsh J. S. and Duncan A. R. (1997) The timing and duration of the Karoo igneous event, southern Gondwana. *J. Geophys. Res.* **102**, 18127-18138.

Ehrenberg S. N. (1982) Petrogenesis of garnet lherzolite and megacrystalline nodules from the Thumb, Navajo Volcanic Field. *J. Petrol.* **23**, 507-547.

Ellam R. M. and Cox K. G. (1989) A Proterozoic lithospheric source for Karoo magmatism: evidence from the Nuanetsi picrites. *Earth Planet. Sci. Lett.* **92**, 207-218.

Erlank A., Allsopp H., Duncan A. and Bristow J. (1980) Mantle heterogeneity beneath southern Africa: evidence from the volcanic record. *Phil. Trans. R. Soc. Lond.* **297**, 295-307.

Erlank A. J., Waters F. G., Hawkesworth C. J., Haggerty S. E., Allsopp H. L., Rickard R. S. and Menzies M. (1987) Evidence for mantle metasomatism in peridotite nodules from the Kimberley pipes, South Africa. In *Mantle metasomatism* (eds. M. A. Menzies and C. J. Hawkesworth). Academic Press, London. pp. 221-311.

Foley S. F., Buhre S. and Jacob D. E. (2003a) Evolution of the Archean crust by delamination and shallow subduction. *Nature* **421**, 249-252.

Foley S. F., Buhre S., Jacob D. and Rehfeldt T. (2003b) Pyroxenite and dunite xenoliths as metamorphosed cumulates from the Archean lower ocean crust. *Extended Abtracts of the 8th International Kimberlite Conference*. Victoria. 1-3.

Foley S. F., Andronikov A. V., Jacob D. E. and Melzer S. (2006) Evidence from Antarctic mantle peridotite xenoliths for changes in mineralogy, geochemistry and geothermal gradients beneath a developing rift. *Geochim. Cosmochim. Acta* **70**, 3096-3120.

Frey F. A., Green D. H. and Roy S. D. (1978) Integrated models of basalt petrogenesis: A study of quartz tholeiites to olivine melilitites from south eastern Australia utilizing geochemical and experimental petrological data. *J. Petrol.* **19**, 463-513.

Frezzotti M. L., Andersen T., Neumann E.-R. and Simonsen S. L. (2002) Carbonatite melt-CO_2 fluid inclusions in mantle xenoliths from Tenerife, Canary Islands: a story of trapping, immiscibility and fluid-rock interaction in the upper mantle. *Lithos* **64**, 77-96.

Glaser S. M., Foley S. F. and Günther D. (1999) Trace element compositions of minerals in garnet and spinel peridotite xenoliths from the Vitim volcanic field, Transbaikalia, eastern Siberia. *Lithos* **48**, 263-285.

Glebovitsky V. A., Nikitina L. P., Khiltova V. Y. and Ovchinnikov N. O. (2004) The thermal regimes of the upper mantle beneath Precambrian and Phanerozoic structures up to the thermobarometry data of mantle xenoliths. *Lithos* **74**, 1-20.

Gorring M. L. and Kay S. M. (2000) Carbonatite metasomatized peridotite xenoliths from southern Patagonia: implications for lithospheric processes and Neogene plateau magmatism. *Contrib. Mineral. Petrol.* **140**, 55-72.

Green D. H. (2000) Magmatism Originating in the Upper Mantle. *Crust - Mantle Interactions: Proceedings of the International School Earth and Planetary Sciences*. Sienna. 77-95.

Green D. H. and Falloon T. J. (1998) Pyrolite: A Ringwood concept and its current expression. In *The Earth's mantle: composition, structure and evolution* (ed. I. Jackson). University Press, Cambridge. pp. 311-380.

Green T. and Pearson N. (1987) An experimental study of Nb and Ta partitioning between Ti-rich minerals and silicate liquids at high pressure and temperature. *Geochim. Cosmochim. Acta* **51**, 55-62.

Green T. H., Blundy J. D., Adam J. and Yaxley G. M. (2000) SIMS determination of trace element partition coefficients between garnet, clinopyroxene and hydrous basaltic liquids at 2-7.5 GPa and 1080-1200°C. *Lithos* **53**, 165-187.

Grégoire M., McInnes B. I. A. and O'Reilly S. Y. (2001) Hydrous metasomatism of oceanic sub-arc mantle, Lihir, Papua New Guinea Part 2 . Trace element characteristics of slab-derived fluids. *Lithos* **59**, 91-108.

Grégoire M., Bell D. R. and Le Roex A. P. (2002) Trace element geochemistry of phlogopite-rich mafic mantle xenoliths: Their classification and their relationship to phlogopite-bearing peridtotites and kimberlites revisited. *Contrib. Mineral. Petrol.* **142**, 603-625.

Grégoire M., Bell D. R. and Le Roex A. P. (2003) Garnet lherzolites from the Kaapvaal Craton (South Africa): Trace element evidence for a metasomatic history. *J. Petrol.* **44**, 629-657.

Grégoire M., Tinguely C., Bell D. R. and Le Roex A. P. (2005) Spinel lherzolite xenoliths from the Premier kimberlite (Kaapvaal craton, South Africa): Nature and evolution of the shallow upper mantle beneath the Bushveld complex. *Lithos* **84**, 185-205.

Grégoire M., Moine B. N., O'Reilly S. Y., Cottin J.-Y. and Giret A. (2000) Trace element residence and partitioning in mantle xenoliths metasomatized by highly alkaline, silicate- and carbonate-rich melts (Kerguelen Islands, Indian Ocean). *J. Petrol.* **41**, 477-509.

Gregory R. T. and Taylor J., H.P. (1981) An oxygen isotope profile in a section of cretaceous oceanic crust, Samail Ophiolite, Oman: evidence for $\delta^{18}O$ buffering of the oceans by deep (>5 km) seawater-hydrothermal circulation at mid-ocean ridges. *J. Geophys. Res.* **86**, 2737-2755.

Griffin W. L., O'Reilly S. Y. and Ryan C. G. (1999a) The composition and origin of sub-continental lithospheric mantle. In *Mantle petrology: field observations and high-pressure experimentation: A tribute to Francis R. (Joe) Boyd*, Vol. 6 (eds. Y. Fei, C. M. Bertka and B. O. Mysen). The Geochemical Society, Special Publications, Houston. pp. 13-46.

Griffin W. L., O'Reilly S. Y., Natapov L. M. and Ryan C. G. (2003a) The evolution of lithospheric mantle beneath the Kalahari Craton and its margins. *Lithos* **71**, 215-241.

Griffin W. L., Graham S., O'Reilly S. Y. and Pearson N. J. (2004) Lithosphere evoution beneath the Kaapvaal Craton: Re-Os systematics of sulfides in mantle-derived peridotites. *Chem. Geol.* **208**, 89-118.

Griffin W. L., Shee S. R., Ryan C. G., Win T. T. and Wyatt B. A. (1999b) Harzburgite to lherzolite and back again: metasomatic processes in ultramafic xenoliths form the Wesselton kimberlite, Kimberley, South Africa. *Contrib. Mineral. Petrol.* **134**, 232-250.

Griffin W. L., Natapov L. M., O'Reilly S. Y., van Achterbergh E., Cherenkova A. F. and Cherenkov V. G. (2005) The Kharamai kimberlite filed, Siberia: Modification of the lithospheric mantle by the Siberian Trap event. *Lithos* **81**, 167-187.

Griffin W. L., O'Reilly S. Y., Abe N., Aulbach S., Davies R. M., Pearson N. J., Doyle B. J. and Kivi K. (2003b) The origin and evolution of Archean lithospheric mantle. *Precambrian Res.* **127**, 19-41.

Gurney J. J. and Harte B. (1980) Chemical variations in upper mantle nodules from southern Africa kimberlites. *Philosophical Transactions of the Royal Society of London* **A297**, 273-293.

Gurney J. J., Jacob W. R. O. and Dawson J. B. (1979) Megacrysts from the Monastery kimberlite pipe, South Africa. In *Kimberlites, diatremes and diamonds: their geology, petrology and geochemistry* (eds. F. R. Boyd and H. O. A. Meyer). American Geophysical Union, Washington. pp. 222-243.

Gurney J. J., Moore R. B., Otter M. L., Kirkley M. B., Hops J. J. and McCandless T. E. (1991) Southern African kimberlites and their xenoliths. In *Magmatism in extensional structural settings* (eds. A. B. Kampunzu and R. T. Lubala). Springer, Heidelberg. pp. 495-536.

Haggerty S. E. and Tompkins L. A. (1983) Redox state of Earth's upper mantle from kimberlitic ilmenites. *Nature* **303**, 295-300.

Harley S. L. (1984) An experimental study of the partitioning of iron and magnesium between garnet and orthopyroxene. *Contrib. Mineral. Petrol.* **86**, 359-373.

Hart S. R., Blusztajn J., Dick H. J. B., Meyer P. S. and Muehlenbachs K. (1999) The fingerprint of seawater circulation in a 500-meter section of ocean crust gabbros. *Geochim. Cosmochim. Acta* **63**, 4059-4080.

Harte B. (1983) Mantle peridotites and processes - the Kimberlite sample. In *Continental Basalts and Mantle Xenoliths* (eds. C. J. Hawkesworth and M. J. Norry). Shiva, Cheshire. pp. 46-91.

Harte B. and Gurney J. J. (1975) Evolution of clinopyroxene and garnet in an eclogite nodule form the Roberts Victor kimberlite pipe, South Africa. *Phys. Chem. Earth* **9**, 367-387.

Harte B., Winterburn P. A. and Gurney J. J. (1987) Metasomatic and enrichment phenomena in garnet peridotite facies mantle xenoliths from the Matsoku kimberlite pipe, Lesotho. In *Mantle metasomatism* (eds. M. A. Menzies and C. J. Hawkesworth). Academic Press, London. pp. 145-220.

Harte B., Hunter R. H. and Kinny P. D. (1993) Melt geometry, movement and crystallizsation, in relation to mantle dykes, veins and metasomatism. *Phil. Trans. R. Soc. Lond.* **342**, 1-21.

Hawkesworth C. J., Erlank A. J., Kempton P. D. and Waters F. G. (1990) Mantle metasomatism: Isotope and trace-element trends in xenoliths from Kimberley, South Africa. *Chem. Geol.* **85**, 19-34.

Hellebrand E., Snow J. E. and Mühe R. (2002) Mantle melting beneath Gakkel Ridge (Arctic Ocean): abyssal peridotite spinel compositions. *Chem. Geol.* **182**, 227-235.

Hervig R., Smith J. and Dawson J. (1986) Lherzolite xenoliths in kimberlites and basalts: petrogenetic and crystallochemical significance of some minor and trace elements in olivine, pyroxenes, garnet and spinel. *Trans. Roy. Soc. Edinburgh, Earth Sci.* **77**, 181-201.

Hoal K. O. (2003) Samples of Proterozoic iron-enriched mantle from the Premier kimberlite. *Lithos* **71**, 259-272.

Hops J. J., Gurney J. J., Harte B. and Winterburn P. A. (1986) Megacrysts and high temperature nodules from the Jagersfontain kimberlite pipe. *4th International Kimberlite Conference*. Perth. 759-770.

Hunter R. H. and Taylor L. A. (1982) Instability of garnet from the mantle; glass as evidence of metasomatic melting. *Geology* **10**, 617-620.

Ionov D. (2004) Chemical variations in peridotite xenoliths from Vitim, Siberia: inferences for REE and Hf behaviour in the garnet-facies upper mantle. *J. Petrol.* **45**, 343-367.

Irvine G. J., Pearson D. G. and Carlson R. W. (2001) Lithospheric mantle evolution of the Kaapvaal Craton: A Re-Os isotope study of peridotite xenoliths from Lesotho kimberlites. *Geophys. Res. Let.* **28**, 2505-2508.

Jacob D. E. (2004) Nature and origin of eclogite xenoliths from kimberlites. *Lithos* **77**, 295-316.

Jacob D. E. and Foley S. F. (1999) Evidence for Archean ocean crust with low high field strength element signature from diamondiferous eclogite xenoliths. *Lithos* **48**, 317-336.

Jacob D. E., Bizimis M. and Salters V. J. M. (2005) Lu-Hf and geochemical systematics of recycled ancient oceanic crust: evidence from Roberts Victor eclogites. *Contrib. Mineral. Petrol.* **148**, 707-720.

Jacob D. E., Jagoutz E., Lowry D., Mattey D. and Kudrjavtseva G. (1994) Trace elements in diamondiferous eclogites from Siberia: Remnants of Archean oceanic crust. *Geochim. Cosmochim. Acta* **58**, 5191-5207.

Jagoutz E., Dawson J., Hoernes S., Spettel B. and Wänke H. (1984) Anorthositic oceanic crust in Archean Earth. *15th Lunar and Planetary Science Conference*. Houston. 395-396.

James D. E., Niu F. and Rokosky J. (2003) Crustal structure of the Kaapvaal craton and its significance for early crustal evolution. *Lithos* **71**, 413-429.

Jerde E. A., Taylor L. A., Crozaz G. and Sobolev N. V. (1993) Exsolution of garnet within clinopyroxene of mantle eclogites; major- and trace-element chemistry. *Contrib. Mineral. Petrol.* **114**, 148-159.

Jochum K. P., Dingwell D. B., Rocholl A., Stoll B., Hofmann A. W., Becker S., Besmehn A., Bessette D., Dietze H. J., Dulski P., Erzinger J., Hellebrand E., Hoppe P., Horn I., Janssens K., Jenner G. A., Klein M., McDonough W. F., Maetz M., Mezger K., Munker C., Nikogosian I. K., Pickhardt C., Raczek I., Rhede D., Seufert H. M., Simakin S. G., Sobolev A. V., Spettel B., Straub S., Vincze L., Wallianos A., Weckwerth G., Weyer S., Wolf D. and Zimmer M. (2000) The preparation and preliminary characterisation of eight geological MPI-DING reference glasses for in-site microanalysis. *Geostandards Newsletter* **24**, 87-133.

Kelemen P., Hart S. R. and Bernstein S. (1998) Silica enrichment in the continental upper mantle via melt/rock reaction. *Earth Planet. Sci. Lett.* **164**, 387-406.

Kelemen P. B., Dick H. J. B. and Quick J. E. (1992) Formation of harzburgite by pervasive melt/rock reaction in the upper mantle. *Nature* **358**, 635-641.

Klein-BenDavid O., Izraeli E. S., Hauri E. and Navon O. (2004) Mantle fluid-evolution - a tale of one diamond. *Lithos* **77**, 243-253.

Klein-BenDavid O., Izraeli E. S., Hauri E. and Navon O. (2007) Fluid inclusions in diamonds from the Diavik mine, Canada and the evolution of diamond-forming fluids. *Geochim. Cosmochim. Acta* **71**, 723-744.

Koga K. T., Kelemen P. B. and Shimizu N. (2001) Petrogenesis of the crust-mantle transition zone and the origin of lower crustal wehrlite in the Oman ophiolite. *Geochem. Geophys. Geosys.* **2**, 2000GC000132.

Kogiso T. and Hirschmann M. M. (2006) Partial melting experiments of bimineralic eclogite and the role of recycled mafic oceanic crust in the genesis of ocean island basalts. *Earth Planet. Sci. Lett.* **249**, 188-199.

Köhler T. and Brey G. P. (1990) Calcium exchange between olivine and clinopyroxene calibrated as a geothermobarometer for natural peridotites from 2 to 60 kb with application. *Geochim. Cosmochim. Acta* **54**, 2375-2388.

Konzett J., Armstrong R. A. and Günther D. (2000) Modal metasomatism in the Kaapvaal craton lithosphere: Constraints on timing and genesis from U-Pb zircon dating of metasomatized peridotites and MARID-type xenoliths. *Contrib. Mineral. Petrol.* **139**, 704-719.

Konzett J., Armstrong R. A., Sweeney R. J. and Compston W. (1998) The timing of MARID metasomatism in the Kaapvaal mantle: an ion probe study of zircons from MARID xenoliths. *Earth Planet. Sci. Lett.* **160**, 133-145.

Krogh E. J. (1988) The garnet-clinopyroxene Fe-Mg geothermometer - a reinterpretation of existing experimental data. *Contrib. Mineral. Petrol.* **99**, 44-48.

Kröner A. (1985) Evolution of the Archean continental crust. *Ann. Rev. Earth Planet. Sci.* **13**, 49-74.

Le Roex A. P., Bell D. R. and Davis P. (2003) Petrogenesis of group I kimberlites from Kimberley, South Africa: Evidence from bulk rock geochemistry. *J. Petrol.* **44**, 2261-2286.

LeRoex A. P., Bell D. R. and Davis P. (2003) Petrogenesis of group I kimberlites from Kimberley, South Africa: evidence from bulk-rock geochemistry. *J. Petrol.* **44**, 2261-2286.

Lowry D., Mattey D. and Harris J. W. (1999) Oxygen isotope composition of syngenetic inclusions in diamond from the Finsch Mine, RSA. *Geochim. Cosmochim. Acta* **63**, 1825-1836.

Lowry D., Appel P. W. U. and Rollinson H. R. (2003) Oxygen isotopes of an early Archaean layered ultramafic body, southern West Greenland: Implications for magma source and post-intrusion history. *Precambrian Res.* **126**, 273-288.

MacGregor I. D. (1975) Petrologic and thermal structure of the upper mantle beneath South Africa in the Cretaceous. *Phys. Chem. Earth* **9**, 455-466.

MacGregor I. D. and Manton W. I. (1986) Roberts Victor eclogites: Ancient oceanic crust. *J. Geophys. Res.* **91**, 14063-14079.

Marsh J. S., Hooper P. R., Rehacek J., Duncan R. A. and Duncan A. R. (1997) Stratigraphy and age of Karoo basalts of Lesotho and implications for correlations within the Karoo igneous province. In *Large igneous Provinces: continental, oceanic, and planetary flood volcanism* (eds. J. J. Mahoney and M. F. Coffin). American Geohysical Union, Washington. pp. 247-272.

Mattey D. (1997) LaserPrep: An automatic laser-fluorination system for Micromass 'Optima' or 'Prism' mass spectrometers. *Micromass Appl. Note* **107**, 1-7.

Mattey D. and Macpherson C. (1993) High-precision oxygen isotope microanalysis of ferromagnesian minerals by laser-fluorination. *Chem. Geol.* **105**, 305-318.

Mattey D., Lowry D. and Macpherson C. (1994) Oxygen isotope composition of mantle peridotite. *Earth Planet. Sci. Lett.* **128**, 231-241.

McCandless T. E. and Gurney J. J. (1986) Sodium in garnet and potassium in clinopyroxene: criteria for classifying mantle eclogites. *Fourth International Kimberlite Conference*. Perth. 827-832.

McDonough W. F. and Sun S.-S. (1995) The composition of the Earth. *Chem. Geol.* **120**, 223-253.

McInnes B. I. A., Gregoire M., Binns R. A., Herzig P. M. and Hannington M. D. (2001) Hydrous metasomatism of oceanic sub-arc mantle, Lihir, Papua New Guinea: petrology and geochemistry of fluid-metasomatised mantle wedge xenoliths. *Earth Planet. Sci. Lett.* **188**, 169-183.

Meisel T., Walker R. J., Irving A. J. and Lorand J.-P. (2001) Osmium isotopic composition of mantle xenoliths: A global perspective. *Geochim. Cosmochim. Acta* **65**, 1311-1323.

Menzies A. H., Carlson R. W., Shirey S. B. and Gurney J. J. (1999) Re-Os systematics of Newlands peridotite xenoliths: Implications for diamond and lithosphere formation. In *7th International Kimberlite Conference*, Vol. 2 (eds. J. J. Gurney, J. L. Gurney, M. D. Pascoe and S. H. Richardson). Red Roof, Cape Town. pp. 566-573.

Menzies M., Rogers N., Tindle A. and Hawkesworth C. J. (1987) Metasomatic and enrichment processes in lithospheric peridotites, an effect of asthenosphere-lithosphere interaction. In *Mantle metasomatism* (eds. M. Menzies and C. J. Hawkesworth). Academic Press, London. pp. 313-361.

Mercier J.-C. C. (1979) Peridotite xenoliths and the dymanics of kimberlite intrusion. In *The mantle sample* (eds. F. R. Boyd and H. A. O. Meyer). American Geophysical Union, Washington. pp. 197-212.

Mitchell R. H. (1973) Magnesian ilmenite and its role in kimbelite petrogenesis. *J. Geol.* **81**, 301-311.

Mitchell R. H. (1987) Megacrysts in kimberlites from the Gibeon field, Namibia. *N. Jb. Miner. Abh.* **157**, 267-283.

Moine B. N., Grégoire M., O'Reilly S. Y., Sheppard S. M. F. and Cottin J.-Y. (2001) High field strength element fractionation in the upper mantle: evidence from amphibole-rich composite mantle xenoliths from the Kerguelen Islands (Indian Ocean). *J. Petrol.* **42**, 2145-2167.

Moore A. and Belousova E. (2005) Crystallization of Cr-poor and Cr-rich megacryst suites from the host kimberlite magma: implications for mantle structure and the generation of kimberlite magmas. *Contrib. Mineral. Petrol.* **149**, 462-481.

Moore A. E. (1987) A model for the origin of ilmenite in kimberlite and diamond: implications for the genesis of the discrete nodule (megacryst) suite. *Contrib. Mineral. Petrol.* **95**, 245-253.

Neal C. R., Taylor L. A., Davidson J. P., Holden P., Halliday A. N., Nixon P. H., Paces J. B., Clayton R. N. and Mayeda T. K. (1990) Eclogites with oceanic crustal and mantle

signatures from the Bellsbank kimberlite, South Africa, part 2: Sr, Nd, and O isotope geochemistry. *Earth Planet. Sci. Lett.* **99**, 362-379.

Nickel K. G. and Green D. H. (1985) Empirical geothermobarometry for garnet peridotites and implications for the nature of the lithosphere, kimberlites and diamonds. *Earth Planet. Sci. Lett.* **73**, 158-170.

Nimis P. and Taylor W. R. (2000) Single clinopyroxene thermobarometry for garnet peridotites. Part I. Calibration and testing of the Cr-in-Cpx barometer and an enstatite-in-Cpx thermometer. *Contrib. Mineral. Petrol.* **139**, 541-554.

Nixon P. H. and Boyd F. R. (1973) Petrogenesis of the granular and sheared ultrabasic nodule suite in kimberlites. In *Lesotho Kimberlites* (ed. P. H. Nixon). Lesotho National Development Corporation. pp. 48-56.

Nixon P. H., Rogers N. W., Gibson I. L. and Grey A. (1981) Depleted and fertile mantle xenoliths from southern African kimberlites. *Ann. Rev. Earth Planet. Sci.* **9**, 285-309.

Nutman A. P., Friend C. R. L., Kinny P. D. and Mcgregor V. R. (1993) Anatomy of an Early Archean gneiss complex: 3900 to 3600 My crustal evolution in southern West Greenland. *Geology* **21**, 415-418.

O'Neill H. S. C. and Wood B. J. (1979) An experimental study of Fe-Mg partitioning between garnet and olivine and its calibration as a geothermometer. *Contrib. Mineral. Petrol.* **70**, 59-70.

Pearce N. J. G., Perkins W. T., Westgate J. A., Gorton M. P., Jackson S. E., Neal C. R. and Chenery S. P. (1997) A compilation of new and published major and trace element data for NIST SRM 610 and NIST SRM 612 glass reference materials. *Geostandards Newsletter* **21**, 115-144.

Pearson D. G., Carlson R. W., Shirey S. B., Boyd F. R. and Nixon P. H. (1995a) Stabilisation of Archaean lithospheric mantle: A Re-Os isotope study of peridotite xenoliths from the Kaapvaal craton. *Earth Planet. Sci. Lett.* **134**, 341-357.

Pearson D. G., Rogers N. W., Irving A. J., Smith C. B. and Hawkesworth C. J. (1995b) Source region of kimberlites and lamproites: Constraints from Re-Os isotopes. *6th International Kimberlite Conference*. Novosibirsk. 430-432.

Pearson D. G., Shirey S. B., Carlson R. W., Boyd F. R., Pokhilenko N. P. and Shimizu B. (1995c) Re-Os, Sm-Nd, and Rb-Sr isotope evidence for thick Archaean lithospheric mantle beneath the Siberian craton modified by multistage metasomatism. *Geochim. Cosmochim. Acta* **59**, 959-977.

Perkins G. B., Sharp Z. D. and Selverstone J. (2006) Oxygen isotope evidence for subduction and rift-related mantle metasomatism beneath the Colorado Plateau-Rio Grande rift transition. *Contrib. Mineral. Petrol.* **151**, 633-650.

Priestley K., McKenzie D. and Debayle E. (2006) The state of the upper mantle beneath southern Africa. *Tectonophysics* **416**, 101-112.

Rampone E., Bottazzi P. and Ottolini L. (1991) Complementary Ti and Zr anomalies in orthopyroxene and clinopyroxene from mantle peridotites. *Nature* **354**, 518-520.

Rapp R. P. and Shimizu N. (2003) On the origin of eclogite and websterite parageneses in the cratonic mantle, and their relationship to TTG granitoid magmatism. *8th International Kimberlite Conference*. Vancouver. 2.2.

Rapp R. P., Shimizu N., Norman M. D. and Applegate G. S. (1999) Reaction between slap-derived melts and peridotite in the mantle wedge: experimental constraints at 3.8 GPa. *Chem. Geol.* **160**, 335-356.

Rehfeldt T., Jacob D. E., Carlson R. W. and Foley S. F. (2007) Fe-rich dunite xenoliths from South African kimberlites: cumulates from Karoo flood basalts. *J. Petrol.* **48**, 1387-1409.

Richardson S. H., Shirey S. B. and Harris J. W. (2004) Episodic diamond genesis at Jwaneng, Botswana, and implications for Kaapvaal craton evolution. *Lithos* **77**, 143-154.

Richardson S. H., Shirey S. B., Harris J. W. and Carlson R. W. (2001) Archean subduction recorded by Re-Os isotopes in eclogitic sulfide inclusions in Kimberley diamonds. *Earth Planet. Sci. Lett.* **191**, 257-266.

Rudnick R. L. and Nyblade A. A. (1999) The thickness and heat production of Archean lithosphere: constraints from xenolith thermobarometry and surface heat flow. In *Mantle petrology: Field observation and high pressure experimentation: A tribute to Francis R. (Joe) Boyd*, Vol. 6 (eds. Y. Fei, C. M. Bertka and B. O. Mysen). The Geochemical Society, Special Publications, Washington. pp. 3-12.

Rudnick R. L., McDonough W. F. and Chappel B. W. (1993) Carbonatite metasomatism in the northern Tanzania mantle: Petrographic and geochemical characteristics. *Earth Planet. Sci. Lett.* **114**, 463-475.

Rudnick R. L., Barth M. G., Horn I. and McDonough W. F. (2000) Rutile-bearing refractory eclogites: missing link between continents and depleted mantle. *Science* **287**, 278-281.

Saltzer R. L., Chatterjee N. and Grove T. L. (2001) The spatial distribution of garnets and pyroxenes in mantle peridotites: pressure-temperature history of peridotites from the Kaapvaal Craton. *J. Petrol.* **42**, 2215-2229.

Schiano P. and Clocchiatti R. (1994) Worldwide occurrence of silica-rich melts in sub-continental and sub-oceanic mantle minerals. *Nature* **368**, 621-624.

Schmickler B., Jacob D. E. and Foley S. F. (2004) Eclogite xenoliths from the Kuruman kimberlites, South Africa: Geochemical fingerprinting of deep subduction and cumulate processes. *Lithos* **75**, 173-207.

Schmitz M. D., Bowring S. A., de Wit M. J. and Gartz V. (2004) Subduction and terrane collision stabilize the western Kaapvaal craton tectosphere 2.9 billion years ago. *Earth Planet. Sci. Lett.* **222**, 363-376.

Schulze D. J. (1987) Megacrysts from alkalic volcanic rocks. In *Mantle xenoliths* (ed. P. H. Nixon). John Wiley, Chichester. pp. 433-451.

Schulze D. J. (1995) Low-Ca garnet harzburgites from Kimberley, South Africa: Abundance and bearing on the structure and evolution of the lithosphere. *J. Geophys. Res.* **100**, 12.513-12.526.

Schulze D. J., Valley J. W., Viljoen K. S. and Spicuzza M. J. (2003) Oxygen isotope composition of mantle eclogites. *8th International Kimberlite Conference*. Vancouver. 2.P11.

Shirey S. B., Harris J. W., Richardson S. H., Fouch M., James D. E., Cartigny P., Deines P. and Viljoen F. (2003) Regional patterns in the paragenesis and age of inclusions in diamond, dianomd composition, and the lithosphereic seismic structure of Southern Africa. *Lithos* **71**, 243-258.

Simon N. S. C. (2004) The formation and modification of cratonic lithospheric roots - A petrological and geochemical study of xenoliths from the Kaapvaal Craton. PhD, Vrije Universiteit.

Simon N. S. C., Pearson D. G., Carlson R. W. and Davies G. R. (2002) Origin of garnet and clinopyroxene in Kaapvaal low-T peridotite xenoliths: Implications from secondary ionisation mass spectrometry (SIMS) data. *Geochim. Cosmochim. Acta* **66**, A717-A717.

Simon N. S. C., Carlson R. W., Pearson D. G. and Davies G. R. (2007) The origin and evolution of the Kaapvaal cratonic lithospheric mantle. *J. Petrol.* **48**, 589-625.

Simon N. S. C., Irvine G. J., Davies G. R., Pearson D. G. and Carlson R. W. (2003) The origin of garnet and clinopyroxene in "depleted" Kaapvaal peridotites. *Lithos* **71**, 289-322.

Skinner E. M. W. (1989) Contrasting Group I and Group II kimberlite petrology: towards a genetic model for kimberlites. In *Kimberlites and related rocks*, Vol. 14 (ed. J. Ross). Geological Society of Australia, Special Publications, Victoria. pp. 417-435.

Smith C. B. (1983) Pb, Sr and Nd isotopic evidence for sources of southern African Cretaceous kimberlites. *NATURE* **304**, 51-54.

Stachel T. and Harris J. W. (1997) Diamond precipitation and mantle metasomatism - evidence from the trace element chemistry of silicate inclusions in diamonds from Akwatia, Ghana. *Contrib. Mineral. Petrol.* **129**, 143-154.

Stachel T., Viljoen K. S., Brey G. P. and Harris J. W. (1998) Metasomatic processes in lherzolitic and harzburgitic domains of diamondiferous lithospheric mantle: REE in garnets from xenoliths and inclusions in diamonds. *Earth Planet. Sci. Lett.* **159**, 1-12.

Stiefenhofer J., Viljoen K. S. and Marsh J. S. (1997) Petrology and geochemistry of peridotite xenoliths from the Letlhakane kimberlites, Botswana. *Contrib. Mineral. Petrol.* **127**, 147-158.

Suhr G. (1999) Melt migration under oceanic ridges: Inferences from reactive transport modelling of upper mantle hosted dunites. *J. Petrol.* **40**, 575-599.

Sweeney R. J., Duncan A. R. and Erlank A. J. (1994) Geochemistry and petrogenesis of Central Lebombo basalts of the Karoo igneous province. *J. Petrol.* **35**, 95-125.

Sweeney R. J., Prozesky V. and Przybylowicz W. (1995) Selected trace and minor element partitioning between peridotite minerals and carbonatite melts at 18-46 kb pressure. *Geochim. Cosmochim. Acta* **59**, 3671-3683.

Tamura A. and Arai S. (2006) Harzburgite-dunite-orthopyroxenite suite as a record of supra-subduction zone setting for the Oman ophiolite mantle. *Lithos* **90**, 43-56.

Tankard A. J., Jackson M. P. A., Eriksson K. A., Hobday D. K., Hunter D. R. and Minter W. E. L. (1982) *Crustal evolution of southern Africa: 3.8 billion years of Earth history*. Springer, New York.

Tappe S., Foley S. F., Jenner G. A., Ryan B., Besserer D. and Kjarsgaard B. A. (2003) Ultramafic lamprophyre dyke swarm, Torngat Mountains, Quebec and Labrador: Mineralogy and geochemistry. *8th Interantional Kimberlite Conference*. Vancouver. 7.2.

Tegtmeyer A. R. and Kröner A. (1987) U-Pb zircon ages bearing on the nature of early Archaean greenstone belt evolution, Barberton Mountainland, Southern Africa. *Precambrian Res.* **36**, 1-20.

van Achterbergh E. (2004) Geochemical fingerprints of mantle metasomatism. PhD, Macquarie University.

van Achterbergh E., Griffin W. L. and Stiefenhofer J. (2001) Metasomatism in mantle xenoliths from the Letlhakane kimberlites: estimation of element fluxes. *Contrib. Mineral. Petrol.* **141**, 397-414.

van Achterbergh E., Griffin W. L., Ryan C. G., O'Reilly S. Y., Pearson N. J., Kivi K. and Doyle B. J. (2004) Melt inclusions from the deep Slave lithosphere: implications for the origin and evolution of mantle-derived carbonatite and kimberlite. *Lithos* **76**, 461-474.

Van Orman J. A., Grove T. L. and Shimizu N. (2001) Rare earth element diffusion in diopside: influence of temperature, pressure, and ionic radius, and an elastic model for diffusion in silicates. *Contrib. Mineral. Petrol.* **141**, 687-703.

van Thienen P., van den Berg A. P. and Vlaar N. J. (2004) Production and recycling of oceanic crust in the early Earth. *Tectonophysics* **386**, 41-65.

Verwoerd W. J. (1992) A review of South Africa research on volcanic rocks and mantle processes, 1987-1991. *S. Afr. J. Sci.* **88**, 315-324.

Viljoen K. S., Swash P. M., Otter M. L., Schulze D. J. and Lawless P. J. (1992) Diamondiferous garnet harzburgites from the Finsch kimberlite Northern Cape, South Africa. *Contrib. Mineral. Petrol.* **110**, 133-138.

Walker R. J., Carlson R. W., Shirey S. B. and Boyd F. R. (1989) Os, Sr, Nd and Pb isotope systematics of southern African peridotite xenoliths: Implications for the chemical evolution of subcontinental mantle. *Geochim. Cosmochim. Acta* **53**, 1583-1595.

Walter M. J. (2005) Melt extraction and compositional variability in mantle lithosphere. In *Treatise on Geochemistry: The mantle and core*, Vol. 2 (ed. R. W. Carlson). Elsevier, Amsterdam. pp. 363-394.

Waters F. G., Erlank A. J. and Daniels L. R. M. (1989) Contact relationships between MARID rock and metasomatised peritotite in a kimberlite xenolith. *Geochem. J.* **23**, 11-17.

Windley B. F. (1998) Tectonic models for the geological evolution of crust, cratons and continents in the Archaean. *Rev. Brasil. Geocien.* **28**, 183-188.

Winterburn P. A., Harte B. and Gurney J. J. (1990) Peridotite xenoliths from the Jagersfontein kimberlite pipe: I. Primary and primary-metasomatic mineralogy. *Geochim. Cosmochim. Acta* **54**, 329-341.

Wyatt B. A., Baumgartner M., Ancker E. and Grutter H. (2004) Compositional classification of "kimberlitic" and "non-kimberlitic" ilmenite. *Lithos* **77**, 819-840.

Xu X., O'Reilly S. Y., Griffin W. L., Zhou X. and Huang X. (1998) The nature of the Cenozoic lithosphere at Nushan, estern China. In *Mantle dynamics and plate interactions in east Asia* (eds. M. Flower, S. L. Chung, C. H. Lo and T. Y. Lee). American Geophysical Union, Washington. pp. 167-196.

Yaxley G. and Green D. (1998a) Reactions between eclogite and peridotite: mantle refertilisation by subduction of oceanic crust. *Schweiz Min Petr Mitt* **78**, 243-255.

Yaxley G. M. and Green D. H. (1998b) Reactions between eclogite and peridotite: mantle refertilisation by subduction of oceanic crust. *Schweiz. Mineral. Petrogr. Mitt.* **78**, 243-255.

Yaxley G. M., Crawford A. J. and Green D. H. (1991) Evidence for carbonatite metasomatism in spinel peridotite xenoliths from western Victoria, Australia. *Earth Planet. Sci. Lett.* **107**, 305-317.

Zack T. and Brumm R. (1998) Ilmenite/liquid partition coefficients of 26 trace elements determined through ilmenite/clinopyroxene partitioning in garnet pyroxenite. *Proc. 7th Int. Kimb. Conf.*, 986-988.

Zack T., Foley S. F. and Jenner G. A. (1997) A consistent partition coefficient set for clinopyroxene, amphibole and garnet from laser ablation microprobe analysis of garnet pyroxenites from Kakanui, New Zealand. *N. Jb. Miner. Abh.* **172**, 23-41.

Zegers T. E. and van Keken P. E. (2001) Middle Archean continent formation by crustal delamination. *Geology* **29**, 1083-1086.

Zhang H., Menzies M. A., Gurney J. J. and Zhou X. (2001) Cratonic peridotites and silica-rich melts: Diopside-enstatite relationships in polymict xenoliths, Kaapvaal, South Africa. *Geochim. Cosmochim. Acta* **65**, 3365-3377.

Zhang H.-F., Menzies M. A. and Mattey D. (2003) Mixed mantle provenance: diverse garnet composition in polymict peridotites, Kaapvaal craton, South Africa. *Earth Planet. Sci. Lett.* **216**, 329-346.

Zhang H.-F., Mattey D., Grassineau N., Lowry D., Brownless M., Gurney J. J. and Menzies M. A. (2000) Recent fluid processes in the Kaapvaal Craton, South Africa: Coupled Oxygen isotope and trace element disequilibrium in polymict peridotites. *Earth Planet. Sci. Lett.* **176**, 57-72.

Zheng J. P., Zhang R. Y., Griffin W. L., Liou J. G. and O'Reilly S. Y. (2005) Heterogeneous and metasomatized mantle recorded by trace elements in minerals of the Donghai garnet peridotite, Sulu UHP terrane, China. *Chem. Geol.* **221**, 243-259.

Zinngrebe E. and Foley S. F. (1995) Metasomatism in mantle xenoliths form Gees, West Eifel, Germany: evidence for the genesis of calc-alkaline glasses and metasomatic Ca-enrichment. *Contrib. Mineral. Petrol.* **122**, 79-96.

FE-RICH DUNITE XENOLITHS FROM SOUTH AFRICAN KIMBERLITES: CUMULATES FROM KAROO FLOOD BASALTS

Tatjana Rehfeldt, Dorrit E. Jacob, Richard W. Carlson, Stephen F. Foley

Journal of Petrology 2007, doi: 10.1093/petrology/egm023

ABSTRACT

Fe-rich dunite xenoliths from the Kimberley kimberlites comprise olivine neoblasts with minor elongated, parallel-oriented ilmenite, and rarely olivine porphyroclasts and spinel. Compared to typical mantle peridotites, olivines in Fe-rich dunites have lower forsterite (Fo87-89) and NiO contents (1300-2800 ppm), which precludes a restitic origin for the dunites. Chrome-rich spinels are remnants of a metasomatic reaction which produced ilmenite and phlogopite. Trace element compositions differ between porphyroclastic and neoblastic olivine, the latter having higher Ti, V, Cr and Ni and lower Zn, Zr and Nb contents, documenting their different origins. The dunites have high $^{187}Os/^{188}Os$ ratios (0.11-0.15) that result in young model ages for most samples, whereas three samples show isotopic mixtures between Phanerozoic neoblasts and ancient porphyroclastic material. Most Fe-rich dunite xenoliths are interpreted to be recrystallized cumulates related to fractional crystallisation of Jurassic Karoo flood basalt magmatism, whereas the porphyroclasts are interpreted to be remnants from a much earlier (probably Archaean Ventersdorp) magmatic episode. The calculated parental magma for the most primitive olivine neoblasts in the Fe-rich dunites is similar to low-Ti Karoo basalts. Modelling the crystal fractionation of the inferred parental magma with pMELTS yields element fractionation trends that mirror the element variation of primitive low-Ti Karoo basalts.

KEYWORDS

Dunite xenoliths; Fractional crystallization; Karoo; Large igneous province; pMELTS; Re-Os; trace elements

1. INTRODUCTION

Kimberlites of the Kaapvaal craton in southern Africa contain large quantities of mafic and ultramafic xenoliths that have been intensively studied over the last 40 years (Carswell & Dawson, 1970; Nixon & Boyd, 1973; Gurney & Harte, 1980; Boyd, 1989; Gurney et al., 1991; Pearson et al., 2003). Eclogite and peridotite xenoliths in particular have been targeted for investigation in order to study the lithospheric mantle of the Archaean Kaapvaal craton (e.g. MacGregor & Carter, 1970; Gurney & Harte, 1980; Erlank et al., 1987; Taylor, 1993; Shirey et al., 2001; Jacob et al., 2003; Schmickler et al., 2004; Dawson, 2004). With a few exceptions, these studies have neglected dunite xenoliths, whose depth of origin and temperature of equilibration are difficult to constrain because of their simple mineralogy.

Dunite xenoliths are found in numerous localities worldwide (e.g. Boyd & Nixon, 1975; Rudnick et al., 1993; Neumann et al., 1995; Kubo, 2002; Rehfeldt et al., 2006). Gurney & Harte (1980) classified dunites into two sub-groups, a high forsterite group (IIIa) with olivines of Fo_{93-95}, which are the most refractory rocks found in kimberlites, and a low forsterite group (IIIb) with olivines of Fo_{88-90}, that are interpreted as magnesian cumulates. Some group IIIa dunites have experienced a metasomatic overprint that introduced Fe, Ti, Al, Ca, K, Na and Cr (Boyd et al., 1983; Harte et al. 1975, Rudnick et al., 1993). Group IIIb dunites with low forsterite contents of Fo_{87-89} and a sheared texture have been described from northern Lesotho and the Frank Smith kimberlite near Kimberley, RSA (Boyd & Nixon, 1975) and interpreted to be of cumulate origin due to their Fe-rich nature. Abundant dunite xenoliths have also been described from western Greenland (Scott, 1981; Scott Smith, 1987), where they were interpreted as metasomatically overprinted cumulates. An origin for Fe-rich dunite xenoliths of the Kaapvaal Craton as cumulates of Karoo basalts was first suggested by Dawson et al. (1981).

Here, we report major and trace element, and oxygen isotope compositions of constituent minerals and Re/Os isotope systematics of olivine separates and whole-rocks from Fe-rich dunite xenoliths from Kimberley to assess a possible cumulate origin and the age of formation. Integrating these data with calculations of the magma in equilibrium with olivine neoblasts of the dunite xenoliths, we test the hypothesis that the origin of these dunites is linked to Karoo basalt magmatism.

2. SAMPLE LOCALITY

The dunite samples are part of a new collection from the Boshof Road dump, Northern Cape Province, South Africa. Sample AJE410 was provided by the University of Cape Town (RSA) and is part of the A. J. Erlank collection. The samples are by-products of diamond mining at the DuToitspan, Bultfontein and Kimberley kimberlite pipes. The Kimberley group of

kimberlites is found close to the town of Kimberley, RSA, within the southern low-Ti part of the Jurassic Karoo basalt province (183 ± 1 Ma; Cox et al., 1967; Duncan et al., 1997; Fig. 20) and adjacent to the Archaean Ventersdorp volcanics (~ 2.7 Ga; Crow & Condie, 1988). The kimberlites were emplaced during the Cretaceous at 86 ± 3 Ma (Allsopp & Barrett, 1975; Davis, 1977). All kimberlites of the Kimberley cluster are Group I kimberlites and originate from an undifferentiated to slightly depleted mantle (Smith, 1983; Le Roex et al., 2003). These kimberlites contain xenoliths of both dunite types (Gurney & Harte 1980): Group IIIa and Group IIIb. The former Group IIIa dunites contain highly forsteritic olivines, are coarse-grained granular rocks and similar in appearance to peridotite xenoliths. The second type,

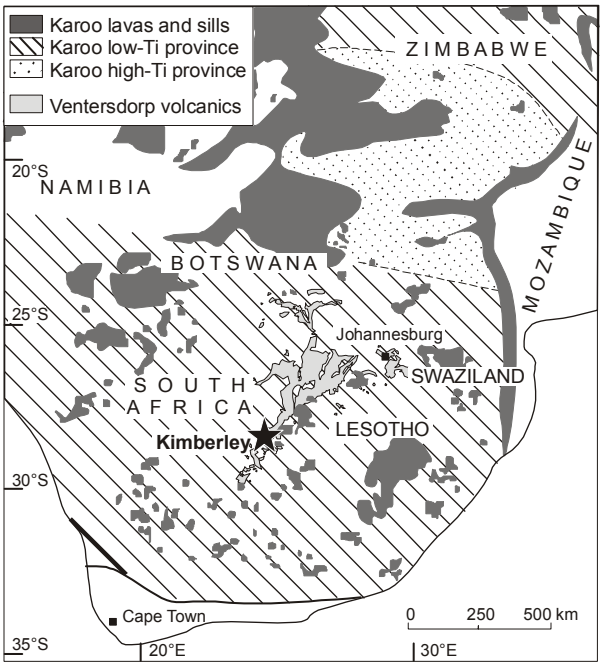

Fig. 20: Map of Archaean Ventersdorp Supergroup and Jurassic Karoo flood basalt province in southern Africa with Karoo low-Ti and high-Ti basalt sub-provinces (modified after Ellam & Cox, 1991, Eglington & Armstrong, 2004 and Jourdan et al., 2004). The Fe-rich dunite xenolith locality is Kimberley, indicated with a black star.

Group IIIb dunites contain olivine with lower forsterite contents and are fine-grained, recrystallised, granular to porphyroclastic dunites. This paper concentrates on the Group IIIb dunites (Table 12).

Table 12: Modal compositions of Fe-rich dunite xenoliths determined graphically with the ScionImage program. Abbreviations: spl = spinel; ilm = ilmenite; nb = neoblasts; ol = olivine; pc = porphyroclasts; phl = phlogopite.

sample	ol-pc	ol-nb	phl	spl	ilm	other
fine-grained texture						
AJE410	-	98	-	1	1	-
DJ0267	-	98	1	-	1	-
DJ0268	-	99	-	-	1	-
DJ0269	-	99	-	-	1	-
porphyroclastic texture						
DJ0270	1	98	-	-	1	-
KP0403	1	76	1	5	17	-
GB0402	55	42	2	0.5	0.5	clinopyroxene

3. ANALYTICAL METHODS

Major element compositions of olivine, spinel, ilmenite and phlogopite in the dunite xenoliths were analysed with a JEOL JXA 8900 RL electron microprobe at the Department of Geosciences, Johannes Gutenberg-University of Mainz, Germany, using wavelength dispersive analysis and a range of natural and synthetic standards (Table 13). The data were corrected using the CITZAF procedure (Armstrong, 1995), and detection limits were between 0.01 and 0.07 wt. %. Fluorine in phlogopite had detection limits of 0.17 wt. %.

Trace elements were analysed in situ by Laser Ablation - Inductively Coupled Plasma Mass Spectrometry (LA-ICP-MS) in the same department using an Agilent 7500ce quadrupole ICP-MS coupled to a New Wave Research UP-213 laser ablation system. Measurements were carried out with laser energy densities of ~6.5 J/cm^2 and helium was used as carrier gas. All measurements were performed on polished thin sections of 100 µm thickness. In olivine, spot sizes were mostly 100 µm in diameter, whereas spots as small as 30 µm were used for the smaller ilmenite grains. Electron microprobe measurements of Si for silicate minerals, Ti for ilmenite and Cr for spinel were used as internal standards to calculate concentrations from LA-ICP-MS data; external standards were NIST SRM 612 glass for silicate minerals and NIST SRM 610 glass for oxide minerals (Pearce et al., 1997). USGS reference glass BCR-2G was measured as an unknown after every seventh sample spot and is in agreement with literature data (Table 14). Data reduction was carried out with GLITTER version 4. Average detection limits in olivine, ilmenite and spinel are summarized in Table 14. Detection limits were generally higher in ilmenite and spinel than in olivine.

Optically clean mineral separates of olivine neoblasts and porphyroclasts were prepared for oxygen isotope measurements by handpicking under a binocular microscope. The grains were rinsed in water and ethanol, and analysed by laser-assisted fluorination mass-spectrometry at the Department of Geology, Royal Holloway University of London following the method of Mattey & Macpherson (1993) and Mattey (1997). All values are reported as $\delta^{18}O$ relative to Vienna – Standard Mean Ocean Water (Table 13). San Carlos Olivine (SC OL) and Gore Mountain Garnet (GMG II) were measured as standards and were reproducible within ± 0.08 ‰ (1σ, n=21). Replicate measurements on one sample of this study yielded an external precision of 0.12 ‰.

Table 13: Average major and trace element compositions (and 1σ standard deviation) of the constituent minerals in Fe-rich dunite xenoliths.

sample	**AJE410**						**DJ0267**						
mineral	ol		ilm		spl		ol		ilm		ilm	phl	
comment	neoblasts		Type II				neoblasts		Type I		Type II	metasomatic	
major elements [wt. %]													
	n=6	1σ	n=4	1σ	n=3	1σ	n=9	1σ	n=6	1σ	n=1	n=4	1σ
Na_2O	<dl		0.08	±0.03	<dl		<dl		<dl		<dl	0.22	±0.05
SiO_2	39.69	±0.17	<dl		<dl		39.72	±0.27	<dl		<dl	40.62	±0.84
K_2O	<dl		<dl		<dl		<dl		<dl		<dl	10.52	±0.39
TiO_2	<dl		52.52	±0.78	7.03	±0.36	<dl		49.55	±0.43	50.20	2.66	±0.58
FeO_t	13.13	±0.18	29.68	±0.47	33.09	±0.88	12.92	±0.52	29.69	±0.29	31.03	5.09	±0.04
Al_2O_3	<dl		0.16	±0.03	5.82	±1.59	<dl		0.16	±0.04	0.12	11.38	±0.91
MgO	46.28	±0.17	12.79	±0.43	10.38	±0.43	46.83	±0.41	11.91	±0.42	12.91	23.10	±1.06
CaO	<dl		0.06	±0.02	<dl		0.05	±0.02	0.05	±0.02	0.15	<dl	
Cr_2O_3	<dl		3.80	±0.41	41.39	±0.57	<dl		6.92	±0.32	3.20	0.81	±0.54
MnO	0.13	±0.03	0.23	±0.03	0.22	±0.04	<dl		0.24	±0.03	0.29	0.04	±0.01
NiO	0.31	±0.02	0.25	±0.03	0.26	±0.04	0.29	±0.05	0.22	±0.04	0.15	0.19	±0.03
Cl												0.02	±0.01
F												0.77	±0.56
Total	99.54		99.57		98.19		99.92		98.74		98.05	95.42	
Mg#	0.87		0.42		0.45		0.88		0.42		0.43	0.89	
$\delta^{18}O$ [‰]	nd		nd		nd		5.22		nd		nd	nd	
trace elements [ppm]													
	n=6	1σ	n=4	1σ	n=2	1σ	n=8	1σ	n=4	1σ			
Sc	3.190	±0.520	29.8	±0.4	4.51		3.45	±0.62	35.8	±2.3			
Cr	196	±9	29600	+3700	IST		156	±18	46800	±2200			
Co	138	±1	315	±8	395	±27	135	±4	224	±19			
Ni	nd		2790	±90	3060	±10	2260	±80	1980	±220			
Cu	2.47	±0.69	61.5	±7.0	104	±11	4.81	±2.22	33.6	±9.2			
Zn	nd		472	±1	2240	±70	79.5	±5.2	253	±49			
Y	<dl		0.615	±0.099	2.55		<dl		0.301	±0.336			
Ti	125	±14	IST		35400	±200	110	±22	IST				
V	3.43	±0.21	1060	±60	1510	±100	3.25	±0.84	1180	±50			
Zr	0.284	±0.094	858	±9	15.0	±5.5	0.533	±0.216	601	±79			
Nb	<dl		552	±23	2.96	±1.64	<dl		796	±25			
Hf	<dl		25.6	±1.6	1.62		<dl		22.7	±3.2			
Ta	<dl		77.0	7.9	<dl		<dl		116	±8			
Ca	407	±78	1100	±250	<dl		nd		nd				
Li	4.03	±0.42	5.03	±1.07	<dl		3.72	±0.52	3.60	±0.85			
B	<dl		nd		nd		<dl		nd				
Rb	nd		nd		nd		nd		nd				
Sr	<dl		nd		nd		<dl		nd				
Ba	<dl		40.8		<dl		<dl		<dl				
Ga	<dl		8.05	±2.62	78.9	±2.6	<dl		7.46	±1.19			
Ge	nd		<dl		<dl		nd		<dl				
Sn	nd		5.95		5.67	±1.56	nd		7.96	±1.25			
Sb	nd		<dl		<dl		nd		<dl				
Pb	nd		1.26		<dl		nd		4.41	±1.77			
U	nd		0.164	±0.019	<dl		nd		<dl				

Abbreviations as in Table 12 plus dl = detection limit; FeO_t = total iron as ferrous iron; IST = internal standard; Mg# = $Mg/(Mg+Fe^{2+})$; n = number of measurements; nd = not determined.

Table 13: continued.

sample	**DJ0268**				**DJ0269**				**DJ0270**			
mineral	ol		ilm		ol		ilm		ol		ol	
comment	neoblasts		Type I		neoblasts		Type I		porphyroclasts		neoblasts	
major elements [wt. %]												
	n=6	1σ	n=6	1σ	n=6	1σ	n=3	1σ	n=2	1σ	n=5	1σ
Na_2O	<dl		nd		<dl		nd		<dl		<dl	
SiO_2	40.81	±0.28	<dl		39.82	±0.14	<dl		40.04	±0.01	39.64	±0.11
K_2O	<dl		nd		<dl		nd		<dl		<dl	
TiO_2	<dl		48.86	±0.11	<dl		48.01	±0.16	nd		nd	
FeO_t	11.59	±0.12	30.32	±0.80	11.81	±0.31	30.84	±0.20	10.46	±0.12	11.98	±0.14
Al_2O_3	<dl		0.60	±0.09	0.03	±0.01	0.58	±0.09	<dl		<dl	
MgO	47.48	±0.19	11.96	±0.30	47.71	±0.34	11.73	±0.14	49.21	±0.04	47.63	±0.21
CaO	<dl		0.03	±0.01	<dl		nd		<dl		<dl	
Cr_2O_3	<dl		7.23	±0.59	<dl		6.73	±0.26	<dl		<dl	
MnO	0.14	±0.02	0.20	±0.02	0.12	±0.02	0.20	±0.01	0.14	±0.04	0.13	±0.02
NiO	0.33	±0.07	0.25	±0.03	0.32	±0.07	0.23	±0.03	0.22	±0.01	0.35	±0.04
Cl	nd		nd		nd		nd		nd		nd	
F	nd		nd		nd		nd		nd		nd	
Total	100.35		99.45		99.81		98.32		100.07		99.73	
Mg#	0.88		0.41		0.89		0.40		0.91		0.89	
$\delta^{18}O$ [‰]	nd		nd		nd		nd		5.14		nd	
trace elements [ppm]												
	n=6	1σ	n=5	1σ	n=6	1σ	n=3	1σ	n=4	1σ	n=6	1σ
Sc	5.79	±0.86	26.6	±4.0	5.13	±0.09	34.2	±6.7	2.36	±0.21	2.75	±0.15
Cr	236	±4	47000	±6300	258	±5	51000	2900	66.0	±7.5	234	±16
Co	145	±2	223	±19	163	±3	212	±6	116	±8	130	±6
Ni	2340	±90	2420	±360	2790	±100	2200	±70	nd		nd	
Cu	3.17	±0.21	41.4	±8.1	3.55	±0.15	26.9	±1.1	1.10	±0.33	2.87	±0.22
Zn	78.3	±2.7	273	±63	131	±3	191	±9	67.8	±7.1	73.8	±4.3
Y	0.024	±0.007	0.171	±0.106	nd		0.294	±0.235	<dl		0.023	±0.010
Ti	304	±6	IST		296	±11	IST		151	±9	246	±23
V	5.29	±0.03	1160	±90	5.47	±0.10	1380	±110	4.43	±0.36	4.79	±0.49
Zr	0.230	±0.038	389	±56	0.224	±0.016	597	±192	0.302	±0.050	0.160	±0.031
Nb	0.024	±0.007	244	±10	0.029	±0.009	312	±55	0.101	±0.015	0.041	±0.007
Hf	<dl		12.3	±0.6	0.013	±0.002	17.8	±4.3	0.020	±0.007	<dl	
Ta	0.004	±0.013	42.0	±5.1	0.004	±0.002	52.4	±2.2	0.008	±0.001	<dl	
Ca	367	±27	nd		320	±13	<dl		192	±13	351	±35
Li	2.66	±0.07	2.85	±0.19	nd		1.68	±0.45	2.02	±0.14	2.49	±0.08
B	0.920	±0.069	nd		nd		nd		0.738	±0.171	0.556	±0.107
Rb	nd		nd		<dl		nd		nd		nd	
Sr	<dl		nd		0.007	±0.001	nd		0.045	±0.035	<dl	
Ba	<dl		<dl		<dl		0.750	±0.608	<dl		<dl	
Ga	0.154	±0.021	15.4	±2.6	nd		16.0	±1.5	0.097	±0.023	0.136	±0.020
Ge	nd		<dl		nd		2.06	±1.79	nd		nd	
Sn	nd		5.51	±3.36	nd		8.28	±1.65	nd		nd	
Sb	nd		<dl		nd		0.611	±0.433	nd		nd	
Pb	nd		3.01	±1.40	nd		75.8	±50.5	nd		nd	
U	nd		0.036	±0.028	nd		0.088	±0.069	nd		nd	

Table 13: continued.

sample	DJ0270		GB0402										
mineral	ilm		ol		ol	ol		ilm		spl	spl	phl	
comment	Type I		porphyroclasts		pc rim	neoblasts		Type II					
major elements [wt. %]													
	n=3	1σ	n=4	1σ	n=1	n=3	1σ	n=7	1σ	n=1	n=1	n=2	1σ
Na_2O	nd		<dl		<dl	<dl		<dl		nd	nd	0.40	±0.00
SiO_2	<dl		40.17	±0.22	40.46	40.53	±0.16	<dl		0.07	0.08	39.45	±0.04
K_2O	nd		<dl		<dl	<dl		<dl		nd	nd	9.95	±0.01
TiO_2	47.74	±0.77	<dl		<dl	nd		52.89	±0.31	16.08	4.00	3.37	±0.08
FeO_t	30.51	±0.30	12.95	±0.84	11.77	12.61	±0.27	30.85	±0.52	47.10	29.39	5.57	±0.57
Al_2O_3	0.66	±0.08	<dl		<dl	<dl		0.12	±0.02	1.91	1.05	12.43	±0.12
MgO	11.64	±0.31	46.83	±0.60	47.54	46.98	±0.16	12.51	±0.49	9.58	8.77	23.97	±0.15
CaO	nd		<dl		<dl	0.08	±0.02	0.10	±0.02	<dl	<dl	<dl	
Cr_2O_3	7.15	±0.77	<dl		<dl	<dl		2.04	±0.40	22.63	54.81	0.54	±0.14
MnO	0.20	±0.05	0.20	±0.03	0.17	0.14	±0.01	0.32	±0.05	0.27	0.20	<dl	
NiO	0.23	±0.02	0.17	±0.08	0.28	0.30	±0.11	0.15	±0.04	0.36	0.16	nd	
Cl	nd		nd		nd	nd		nd		nd	nd	<dl	
F	nd		nd		nd	nd		nd		nd	nd	0.76	±0.07
Total	98.13		100.32		100.22	100.64		98.98		98.00	98.46	96.44	
Mg#	0.40		0.87		0.88	0.87		0.38		0.35	0.42	0.89	
$\delta^{18}O$ [‰]	nd		4.83* 4.59*		nd	4.95		nd		nd	nd	nd	
trace elements [ppm]													
	n=8	1σ	n=4	1σ	n=1	n=5	1σ						
Sc	26.4	±2.4	5.60	±0.28	5.44	5.24	±0.19						
Cr	48200	±4200	34.7	±3.8	217	249	±20						
Co	233	±14	158	±3	173	176	±2						
Ni	nd		1280	±10	2610	2820	±140						
Cu	41.4	±1.8	<dl		nd	5.41	±5.31						
Zn	270	±54	154	±6	142	140	±6						
Y	<dl		nd		nd	nd							
Ti	IST		115	±3	269	217	±12						
V	1210	±60	2.74	±0.76	4.72	3.81	±0.27						
Zr	440	±80	0.592	±0.062	0.291	0.232	±0.036						
Nb	265	±20	0.779	±0.079	0.062	0.034	±0.017						
Hf	13.2	±2.2	0.021	±0.001	0.012	0.023	±0.014						
Ta	46.6	±4.4	0.058	±0.023	0.003	<dl							
Ca	469	±99	110	±8	392	353	±16						
Li	2.94	±0.93	nd		nd	nd							
B	nd		nd		nd	nd							
Rb	nd		<dl		<dl	<dl							
Sr	nd		<dl		0.039	0.029	±0.009						
Ba	<dl		0.198	±0.021	<dl	0.142	±0.082						
Ga	15.3	±1.8	nd		nd	nd							
Ge	<dl		nd		nd	nd							
Sn	6.19	±1.06	nd		nd	nd							
Sb	<dl		nd		nd	nd							
Pb	1.21	±0.18	nd		nd	nd							
U	<dl		nd		nd	nd							

* oxygen isotope replicate measurements with 1σ reproducibility of ±0.12 ‰

Table 13: continued.

sample	**KP0403**									
mineral	ol		ol		ilm		spl		phl	
comment	porphyroclasts		neoblasts		Type I					
major elements [wt. %]										
	n=2	1σ	n=4	1σ	n=8	1σ	n=6	1σ	n=6	1σ
Na_2O	<dl		<dl		<dl		<dl		0.43	±0.03
SiO_2	40.76	±0.28	40.64	±0.06	<dl		<dl		39.53	±0.19
K_2O	<dl		<dl		<dl		<dl		9.90	±0.12
TiO_2	<dl		<dl		46.83	±0.3	6.87	±1.39	2.98	±0.15
FeO_t	11.78	±0.02	11.92	±0.27	31.14	±0.3	31.55	±2.42	4.95	±0.13
Al_2O_3	<dl		<dl		1.10	±0.0	10.81	±2.22	13.97	±0.25
MgO	47.79	±0.08	47.41	±0.48	11.02	±0.3	11.61	±0.10	23.29	±0.26
CaO	<dl		<dl		<dl		<dl		<dl	
Cr_2O_3	<dl		<dl		9.16	±0.2	38.32	±2.15	1.43	±0.10
MnO	0.16	±0.02	0.14	±0.01	0.15	±0.0	0.17	±0.03	<dl	
NiO	0.16	±0.004	0.31	±0.13	0.23	±0.0	0.27	±0.02	nd	
Cl	nd		nd		nd		nd		0.03	±0.003
F	nd		nd		nd		nd		0.44	±0.06
Total	100.65		100.42		99.63		99.60		96.95	
Mg#	0.88		0.88		0.39		0.49		0.89	
$\delta^{18}O$ [‰]	nd		nd		nd		nd		nd	
trace elements [ppm]										
	n=3	1σ	n=3	1σ	n=7	1σ	n=6	1σ	n=5	1σ
Sc	5.00	±0.23	5.58	±0.05	30.2	±1.2	<dl		3.28	±0.29
Cr	34.6	±2.5	285	±26	65600	±24	IST		nd	
Co	130	±6	175	±6	211	±6	338	±56	nd	
Ni	1270	±70	2850	±50	nd		nd		1290	±150
Cu	nd		3.72	±0.35	29.3	±2.6	63.0	±3.6	nd	
Zn	98.5	±4.6	112	±8	149	±14	1780	±300	nd	
Y	nd		nd		0.097	±0.0	<dl		<dl	
La	nd		nd		nd		nd		0.198	±0.088
Ce	nd		nd		nd		nd		0.404	±0.261
Nd	nd		nd		nd		nd		0.678	±0.306
Ti	98.3	±4.5	180	±64	IST		34500	±7200	nd	
V	3.03	±0.06	6.20	±2.58	1560	±40	1420	±110	128	±5
Zr	0.550	±0.023	0.532	±0.309	515	±24	8.81	±4.57	7.18	±1.11
Nb	0.333	±0.055	0.148	±0.066	430	±21	1.53	±0.69	11.1	±2.8
Hf	0.018	±0.008	<dl		18.3	±0.5	<dl		0.607	±0.231
Ta	0.029	±0.009	0.025	±0.012	72.6	±8.8	1.18	±0.21	1.66	±0.94
Ca	192	±50	395	±74	<dl		<dl		279	±47
Li	nd		nd		1.83	±0.1	2.60	±1.63	2.04	±0.78
B	nd		nd		nd		nd		nd	
Rb	<dl		<dl		nd		nd		576	±66
Sr	<dl		0.218	±0.060	nd		nd		26.0	±3.2
Ba	<dl		<dl		<dl		<dl		476	±42
Ga	nd		nd		19.8	±1.0	115	±6	nd	
Ge	nd		nd		0.817	±0.2	<dl		nd	
Sn	nd		nd		6.72	±0.5	<dl		nd	
Sb	nd		nd		0.120	±0.0	<dl		nd	
Pb	nd		nd		14.2	±3.3	21.5	±5.6	6.54	±2.07
U	nd		nd		0.039	±0.0	<dl		<dl	

Table 14: Average LA-ICP-MS detection limits [ppm] in olivine, ilmenite, spinel, phlogopite and clinopyroxene and trace element composition of BCR-2G measured as unknown, ± 1σ standard deviation of n measurements (literature data: 1 = Neumann et al., 2002; 2 = Barth et al., 2001; 3 = Halter et al., 2002; 4 = Zack et al., 2002.

	detection limits				**BCR-2G**				
	olivine	ilmenite	spinel	phlogopite	this study	1σ	n	literature	
Sc	0.523	1.49	4.68	1.51	34.1	±2.8	57	32.2	1
Cr	2.91	7.57	nd	nd	20.4	±10.1	57	17	2
Co	0.115	0.610	3.81	nd	38.6	±3.6	43	35.8	1
Ni	0.547	1.78	5.97	1.72	13.3	±2.0	57	11.23	1
Cu	1.05	3.34	11.2	nd	19.2	±2.8	43	18.74	3
Zn	1.53	3.97	11.7	nd	167	±25	43	163	2
Y	0.061	0.262	0.365	0.122	30.4	±2.8	49	34.3	1
La	nd	nd	nd	0.103	24.3	±1.3	14	25.2	1
Ce	nd	nd	nd	0.138	50.7	±2.1	30	53.0	1
Nd	nd	nd	nd	0.378	27.7	±1.3	14	29.8	1
Ti	2.48	nd	16.0	nd	14300	±1700	57	14090	1
V	0.184	0.756	1.56	0.542	436	±31	49	419	1
Zr	0.101	0.488	0.718	0.295	164	±16	57	190	1
Nb	0.062	0.290	0.768	0.160	12.2	±1.0	57	13.32	1
Hf	0.080	0.368	0.628	0.208	4.41	±0.49	57	5.06	1
Ta	0.033	0.153	0.256	0.105	0.758	±0.137	57	0.82	1
Ca	100	244	660	267	51200	±3500	57	48600	3
Li	0.197	0.652	2.08	0.453	10.4	±1.0	41	9.67	1
B	3.35	nd	nd	nd					
Rb	0.025	nd	nd	0.400	45.2	±4.1	22	49.6	1
Sr	0.076	nd	nd	0.199	321	±18	30	346	1
Ba	0.311	1.14	nd	1.91	660	±44	57	684	1
Ga	0.157	0.587	1.55	nd	39.2	±4.9	39	22.2	1
Ge	nd	3.81	13.7	nd	2.26	±0.21	27	1.49	4
Sn	nd	1.34	4.55	nd	2.29	±0.25	27	4.3	2
Sb	nd	0.681	2.03	nd	0.446	±0.122	27	0.303	4
Pb	nd	0.433	nd	0.420	11.6	±1.4	41	11.3	1
U	nd	0.189	0.762	0.112	1.86	±0.20	41	1.93	1

Whole-rock powders for Re/Os isotope analyses were prepared with a corundum ring mill from representative sample fractions that were free of vein and rim material. Olivine separates were prepared from two samples (GB0402 and AJE410) and analysed for Re-Os isotopes for comparison with whole-rock powder analyses. Olivine separates were obtained by a four step procedure including magnetic separation, heavy liquid separation from the 300-500 µm grain fraction using methylene iodide (3.3 g/cm^3), and hand-picking to remove remaining oxide grains under a binocular microscope, followed by rinsing with water and ethanol. The olivine separates were a mixture of neoblasts and porphyroclasts, since after crushing the porphyroclasts broke into smaller pieces and could not be distinguished optically from smaller neoblasts.

Re and Os analyses were carried out at the Department of Terrestrial Magnetism, Carnegie Institution of Washington, USA. The analyses were performed on 2 g of whole-rock powder or 1 g of olivine separate, following the procedure of Carlson et al. (1999). The whole-rock powder was dissolved in 3 ml concentrated HCl and 6 ml concentrated HNO_3. These large quantities of acids are necessary to avoid sample loss in the Carius tube due to the high viscosity of the Si-gel produced by olivine dissolution. Dissolution of whole-rock

powders contained no visible grains, whereas dissolution of olivine separates produced residual grains that were intensely altered by the dissolution procedure. Because both sulphide and chromite are soluble in the acids used, it is likely that these residual grains were spinel or ilmenite formerly included in the olivines. After extracting Re by column chemistry and Os by extraction with CCl_4 followed by microdistillation (Carlson et al., 1999), the samples were analysed by negative thermal ionization mass spectrometry using a 15 inch single collector mass spectrometer for Re and a Finnigan Triton multicollector mass spectrometer for Os. Laboratory blanks of 2 pg Os and 1 pg Re were obtained during the course of the project.

4. RESULTS

4.1. Petrography and mineral chemistry

Most xenoliths studied here are fine-grained foliated rocks (samples AJE410, DJ0267, DJ0268, DJ0269; Fig. 21a-b): three samples (DJ0270, KP0403, GB0402) contain porphyroclasts but only sample (GB0402) is porphyroclast-rich (55 %; Table 12). The fine-grained samples comprise olivine neoblasts (30-720 µm), with minor amounts of acicular ilmenites (5-280 µm) oriented parallel to the foliation, in some samples intergrown with spinel (Fig. 22). Phlogopite occurs in three samples as small, single crystals (750-140 µm) within the neoblast groundmass, in cracks within porphyroclasts (Fig. 21b) or together with ilmenite overgrowing spinel (Fig. 21d and Fig. 22b). These textural features indicate that spinel is a pre-metasomatic phase, so that the original mineralogy comprised spinel-bearing dunite. The olivine porphyroclasts are 3.5-1.1 mm in size with irregular margins that merge into the fine-grained olivine neoblast groundmass (Fig. 21c-d) and are oriented parallel to the foliation. Porphyroclasts are intensely cracked and turbid due to minute inclusions of oxide minerals and glass. Porphyroclasts and neoblasts have comparable major element compositions with forsterite contents ranging from 87 to 91. NiO contents are low (0.2-0.3 wt. %) compared to olivines in typical mantle peridotites, with porphyroclastic dunites having olivine with more variable and lower NiO contents than olivine in fine-grained dunites. As a result, olivines plot away from the mantle olivine array (MOA) defined by Takahashi (1986; Fig. 23).

Both fine-grained and porphyroclastic samples contain elongated ilmenites (average 20 µm width and 3 mm to 1.5 cm long) within the olivine neoblast groundmass. They often surround olivine and show reaction boundaries with it. Ilmenites have an anhedral, amoeboid appearance and are oriented parallel to the foliation (Fig. 21a, d). KP0403 is unique in having a very high modal ilmenite content (17 vol. %), that is accompanied by layers of fine grained phlogopite oriented parallel to the ilmenite grains. In all samples, ilmenite can be divided into

two types on the basis of chemical composition (Fig. 24). Both have similar MgO contents (10.5-12.9 wt. %) higher than is typical for mantle-derived ilmenite (4.5 – 8.7 wt. %; Hills & Haggerty, 1989; Zack & Brumm, 1989). Type I ilmenites have higher Al_2O_3 (0.5-1.2 vs. 0.1-0.3 wt. %), Cr_2O_3 (6.3-9.5 vs. 1.7-7.2 wt. %) and lower TiO_2 contents (46.5-49.0 vs. 49.2-53.4 wt. %) than Type II ilmenites. Type II ilmenites plot in the field defined by ilmenites from Group I kimberlites (Wyatt et al., 2004), supporting a secondary origin by kimberlite infiltration into the xenoliths. Both ilmenite types are distinct from ilmenites described from dunite cumulates in Hawaiian basalts (Fig. 24), which have much lower Cr#. Textural evidence suggests that Type I ilmenite grew at the expense of spinel (Fig. 22), explaining the elevated Al_2O_3 and Cr_2O_3.

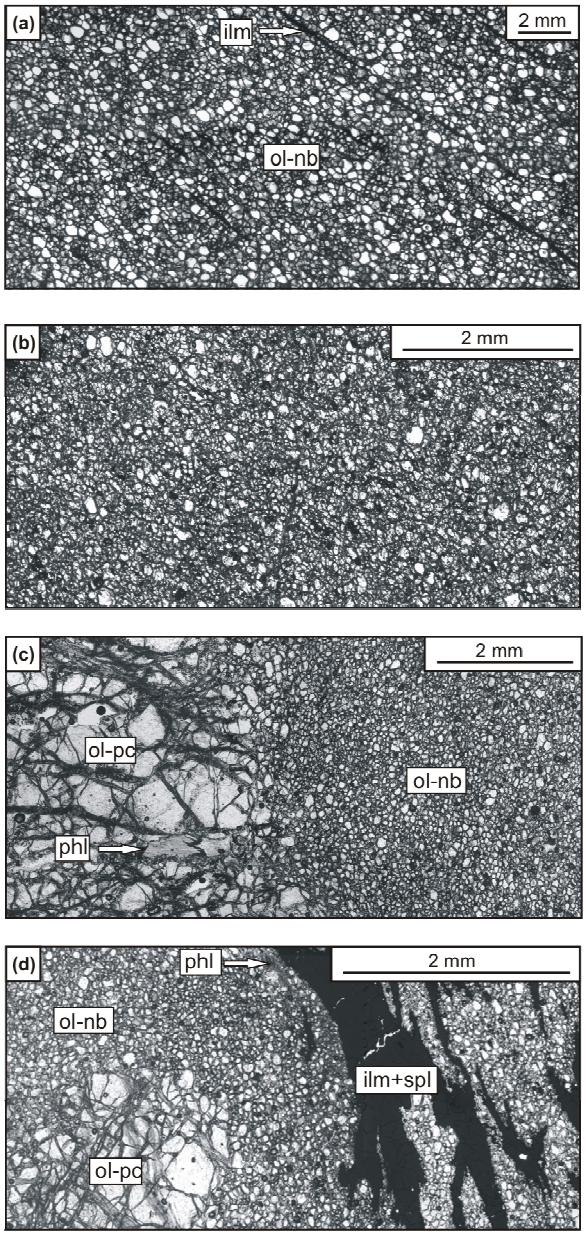

Fig. 21: Photomicrographs of representative Fe-rich dunite xenoliths: (a) granular, fine-grained olivine with parallel oriented ilmenite (DJ0269); (b) granular, fine-grained olivine (AJE410); (c) heterogranular dunite with fine-grained olivine neoblasts and coarse olivine porphyroclasts (GB0402); (d) porphyroclastic dunite with fine-grained olivine neoblasts, coarse olivine porphyroclasts, as well as ilmenite and spinel schlieren (KP0403). Abbreviations as in Table 1.

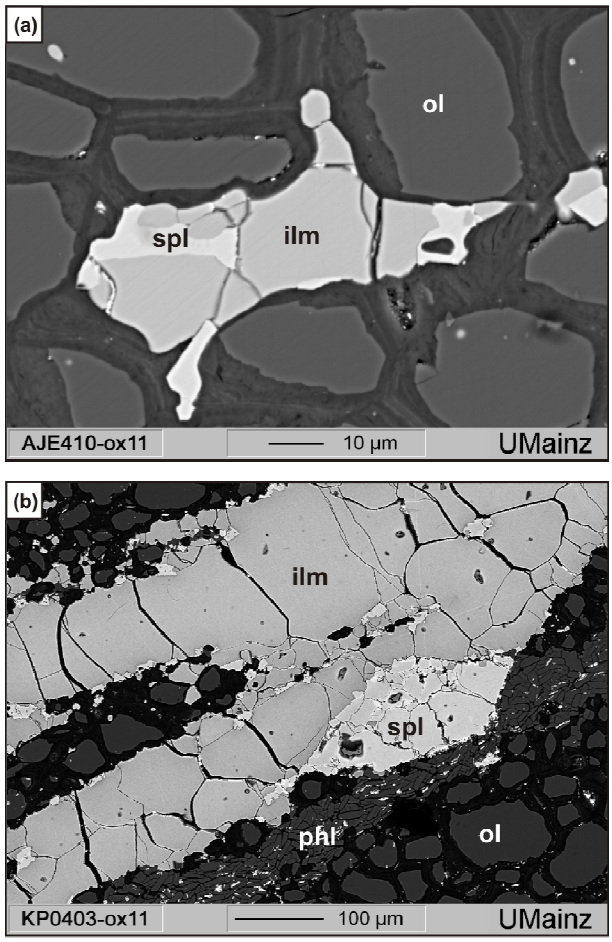

Fig. 22: Back scattered electron images of oxide phases in Fe-rich dunite xenoliths: (a) ilmenite intergrown with chromian spinel (AJE410), (b) chromian spinel (light grey) surrounded by ilmenite (grey), that is formed in association with fine-grained phlogopite (KP0403). Abbreviations as in Table 1.

Spinels are remnant primary phases commonly showing reaction coronas of ilmenite and occasionally also phlogopite. They also occur as inclusions in ilmenite. Chemically, they have low Mg# ($Mg/(Mg+Fe^{2+})$) of 0.36-0.50, high Cr# ($Cr/(Cr+Al)$) of 0.67-0.97 and high TiO_2 contents (4-16 wt. %), compared to spinel in mantle spinel peridotites of the Kaapvaal craton (Mg# 0.48-0.78, Cr# 0.27-0.88, TiO_2 <3 wt. %; Carswell et al., 1979; Fig. 23). Their compositions overlap with the high-Cr# end of the Kaapvaal peridotite array, whereas olivines lie conspicuously to lower Fo, showing no overlap (Fig. 25). However, the reaction rims around spinels indicate that spinel compositions may not reflect their original chemistry. Ilmenite and phlogopite crystallize at the expense of spinel during metasomatism, but not all Cr of the spinel can be incorporated into ilmenite or phlogopite, so that the remaining spinel is enriched in Cr. The Type I ilmenites are very rich in Cr_2O_3 (6.3-9.5 wt. %) with high Cr#, so that the Cr# of spinels may have increased during the metasomatic reaction, but probably only by a few percent Cr# (max. 8-10 %). There is no systematic compositional difference between spinels from fine-grained or porphyroclastic dunite xenoliths.

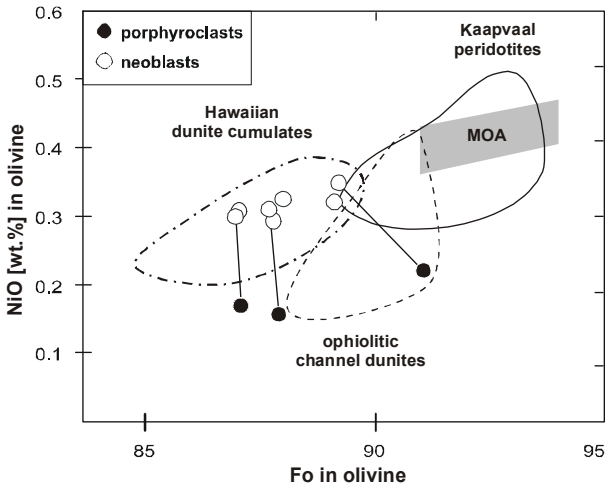

Fig. 23: NiO versus forsterite content in Fe-rich dunite olivines compared to olivine in mantle peridotites, ophiolitic channel dunites and Hawaiian dunite cumulates (Kaapvaal peridotite: Carswell et al., 1979; Simon, 2004; ophiolitic channel dunite: Suhr, 1999; Koga et al., 2001; Hawaii: Clague, 1988); grey shaded field = MOA: mantle olivine array of continental peridotites after Takahashi (1986).

Phlogopite occurring with ilmenite in the Fe-rich dunite xenoliths has slightly lower Mg# (0.88-0.90) and higher TiO_2 contents (1.8-3.4 wt. %) compared to phlogopite in mantle peridotites (Mg# = 0.90-0.95 and TiO_2 = 0.1-1.9 wt. %; Erlank et al., 1987).

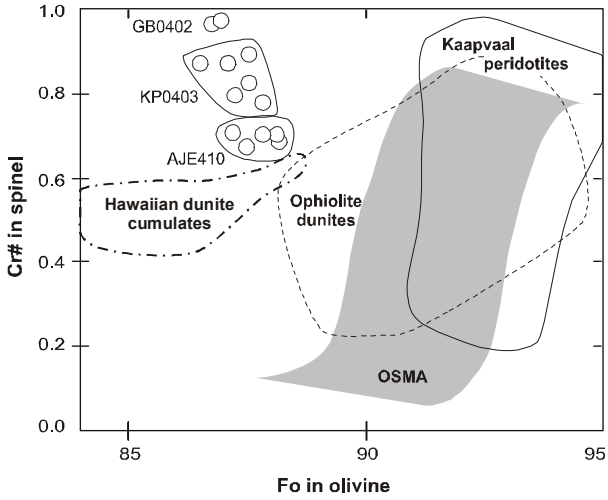

Fig. 24: Spinel Cr# versus forsterite content of coexisting olivine in Fe-rich dunite xenoliths with compositional fields of mantle peridotites, ophiolitic and Hawaiian dunites as in Fig. 4. OSMA = olivine-spinel mantle array of Arai (1994).

All dunites are slightly serpentinized along grain margins and in cracks of olivine porphyroclasts. Serpentine occurs with small magnetite and sulphide minerals. Only the porphyroclastic sample GB0402 contains clinopyroxene (<< 1 %) and secondary phases such as apatite, perovskite and calcite, which are probably introduced by the kimberlite host, as they occur together with serpentine along olivine grain margins. Overall, the mineralogy of the Fe-rich dunite xenoliths is typical for dunite xenoliths from the Kaapvaal Craton (e.g. Boyd & Nixon, 1975) that are often described to contain ilmenite and other metasomatic minerals. In contrast to dunites of the Tanzania Craton (Lee & Rudnick, 1999), Fe-rich dunite xenoliths of this study are generally poor in chromian spinel, and chrome diopside has not been found in any thin sections.

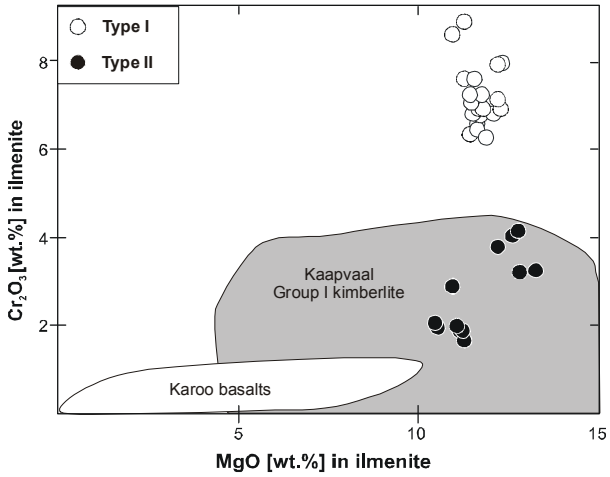

Fig. 25: Cr_2O_3 versus MgO in ilmenites of Fe-rich dunite xenoliths, compared to ilmenite composition in Karoo basalts and group I kimberlites (Wyatt et al., 2004).

4.2. Oxygen isotope compositions

Oxygen isotope ratios were analyzed in order to check the possibility that dunite xenoliths may originate as ultramafic cumulates in the lower reaches of ocean crust or oceanic plateaux (Foley et al., 2003 a, b). This would mean that dunites and pyroxenites would be related to the eclogite suite, which commonly show oxygen isotope values differing from mantle values (Jacob, 2004). It has recently been shown that fluids may circulate through cracks to very deep levels in oceanic lithosphere and that oxygen isotopes may be influenced at much deeper levels than expected (Hart et al., 1999). Olivines from the dunite xenoliths define a small range of $\delta^{18}O$ values (5.14-5.22 ‰; Table 13) that overlaps with the $\delta^{18}O$ range of mantle peridotite olivine (5.18 ± 0.14 ‰; Mattey et al., 1994). These data provide no evidence for exchange with seawater, but do not discount an origin as mantle samples or as cumulates from mantle-derived melts, either continental or oceanic. Sample GB0402 has a slightly lower $\delta^{18}O$ value than the average for peridotitic olivine (4.83) and duplication yielded a higher value outside the analytical uncertainty (Table 13). This is most probably the effect of minute chromite inclusions that are visible in the olivine porphyroclasts. Chromite has lower oxygen isotope values than olivine (average spinel $\delta^{18}O$ <2.5 ‰; Lowry et al., 2003) decreasing the $\delta^{18}O$ value of the olivine.

4.3. Trace elements

Although they have Mg# different to mantle peridotites, olivines in the dunite xenoliths exhibit similar trace element compositions (Fig. 26). The compositional range of dunite xenoliths fully overlaps for V, Nb, Zr and Cr, whereas Ti contents extend to higher values than found in olivines from mantle peridotites. Ni contents in olivine porphyroclasts are lower than in mantle peridotites, whereas those of the neoblasts overlap with the peridotite field. Some trace element compositions differ between porphyroclasts and neoblasts: neoblasts are enriched in Sr, Co, Ni and Ti as well as in Ca, but depleted in Mn, Zr, Ta and Nb compared to

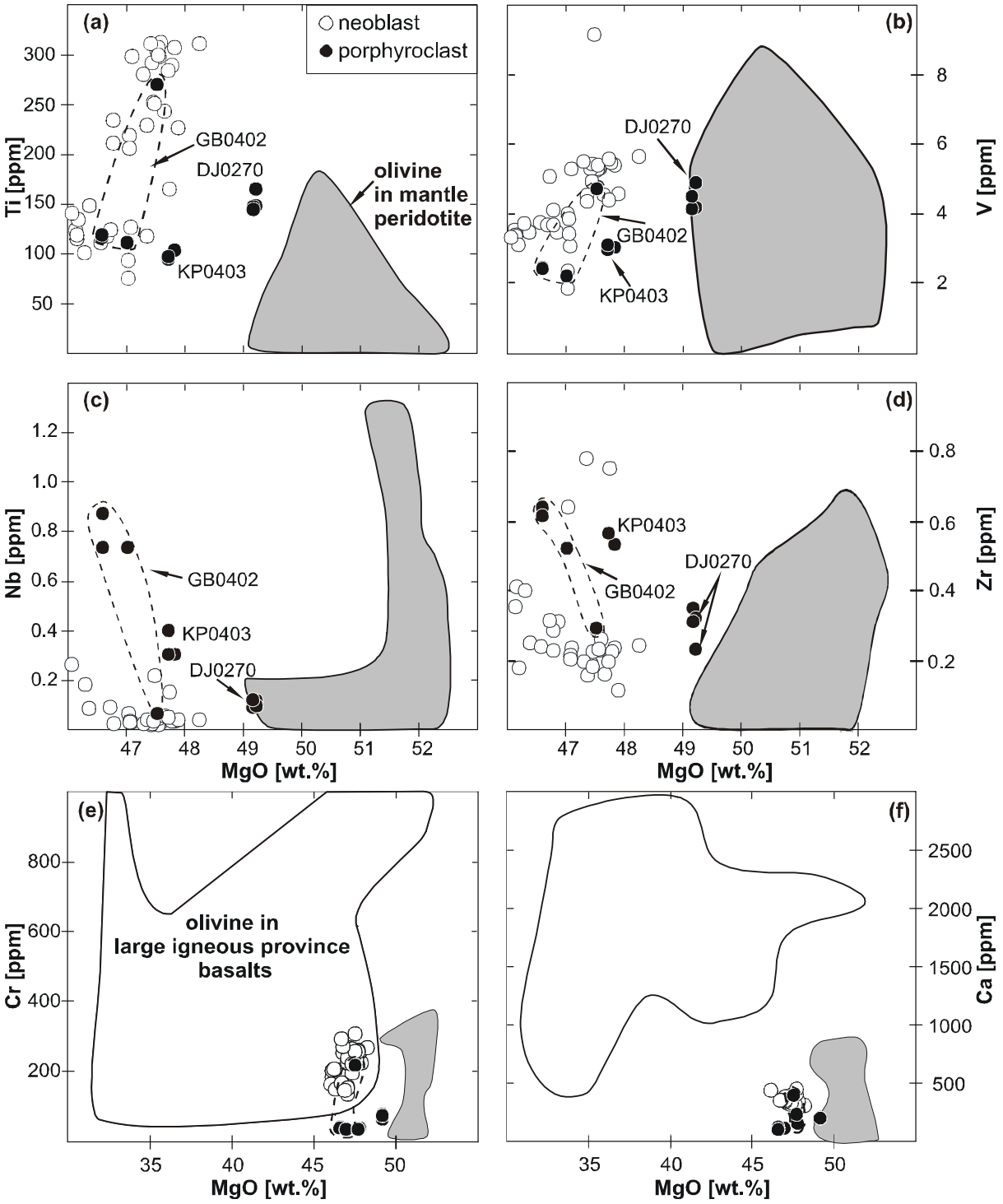

Fig. 26: Trace element composition (a) Ti, (b) V, (c) Nb, (d) Zr, (e) Cr and (f) Ca versus MgO of olivine neoblasts and porphyroclasts in comparison to olivine from mantle peridotites (grey field; Grégoire et al., 2000; 2001; van Achterbergh, 2004) and olivine from large igneous province basalts (white field in e and f; Etendeka: Gibson et al., 2000; Thompson et al., 2001) Note different scales in e) and f). Dashed line represents compositional variation in porphyroclast rims in GB0402.

porphyroclasts (Table 13; Fig. 26). Olivine porphyroclasts in sample GB0402 have rims which are closer in composition to neoblast compositions than the cores (Fig. 26). Olivine neoblasts have Cr and Ni contents within the compositional range of olivine in large igneous province basalts (Fe-rich dunite olivine neoblasts Cr 290-160 ppm and Ni 2850-2070 ppm vs. e.g. Etendeka olivine Cr 1200-70 ppm and Ni 4870-630; Gibson et al., 2000; Thompson et al., 2001), whereas porphyroclasts plot to lower values (Cr 66-35 ppm and Ni 1300 ppm; Fig. 26e).

Trace element patterns of ilmenites are compared to ilmenite megacrysts from kimberlites (grey field) and mantle derived ilmenites (black field) in Fig. 27a. Ilmenite incorporates predominantly HFSE and Sc (Zack & Brumm, 1998). Compared to mantle derived ilmenites, both types of ilmenite in the dunite xenoliths are strongly enriched in Cr. Type I ilmenites are more enriched in Cr and Ga, consistent with their growth at the expense of chromian spinel. Additionally, they are enriched in Sc and V, but depleted in Y, Cu and Zn. Both Type I and II ilmenites are characterised by higher Ni at comparable Cr than megacrystic ilmenites that are interpreted to be the cumulates of kimberlitic melts (e.g. Nowell et al., 2004). Spinels (Fig. 27b) have lower HFSE and higher Zn, Cr and Ga contents than ilmenite. Their HFSE concentrations are higher than in spinels in abyssal peridotite xenoliths (Grégoire et al., 2000; Moine et al., 2001; Grégoire et al., 2001), while the Cr contents are similar. The former may indicate overprint by the HFSE-enriched melt or fluid from which ilmenite crystallized.

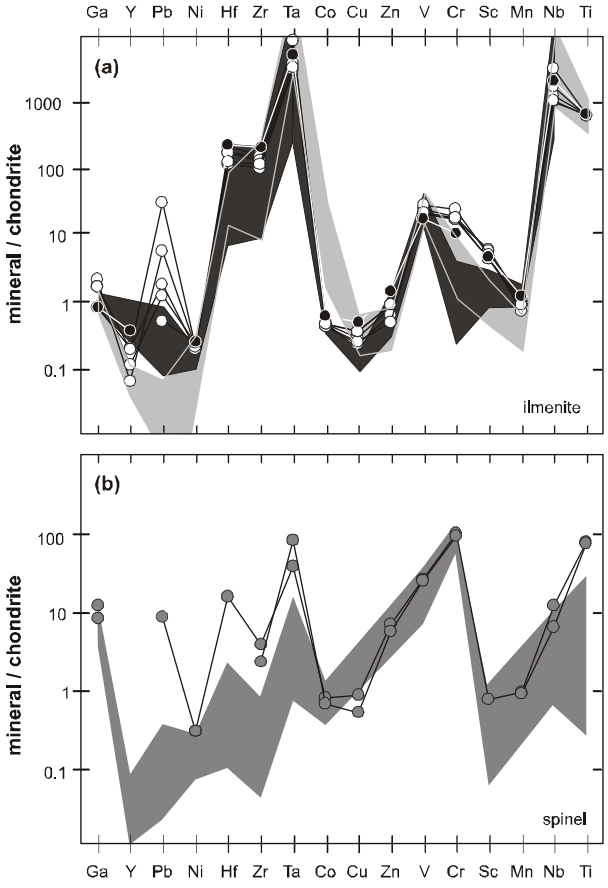

Fig. 27: Chondrite normalized (McDonough & Sun, 1995) trace element pattern of average oxide compositions in Fe-rich dunite xenoliths: (a) ilmenites: white circles = Type I ilmenite and black circles = Type II ilmenite are plotted together with mantle derived ilmenites in eclogites and garnet pyroxenites (black field; Barth et al., 2002; Zack & Brumm, 1989) and megacryst ilmenite from South African kimberlites and the Grib kimberlite (grey field; Kostrovitsky et al., 2004 and references therein); (b) spinel in paragenesis with ilmenite is compared with spinel from abyssal peridotites (Grégoire et al., 2000; Moine et al., 2001; Grégoire et al., 2001).

Phlogopites have trace element compositions typical of metasomatic phlogopite in mantle peridotites (Grégoire et al., 2002; van Achterbergh, 2004) with high Ba, Rb, Nb, Ta and Ti and low Ni, V, Zr, Hf, Sr, Pb and Th contents (Table 13).

4.4. Re-Os isotope systematics

The Os concentrations and isotope compositions of most dunite xenoliths are readily distinguished from those of mantle peridotites (Fig. 28). Whole-rocks have similar Re contents to Kaapvaal mantle peridotites (mostly <0.4 ppb, Fig. 28; Table 15), but on average lower Os contents (mostly <1 ppb in Fe-rich dunites, ~4 ppb in mantle peridotites). The one exception is sample GB0402 that has the high Os concentration typical of cratonic peridotites. South African kimberlites have a wider range in Re content (0.02-0.7 ppb with a mean 0.3±0.2 ppb; Pearson et al., 1995a) than the Fe-rich dunites and a similar range in Os content (0.7-3.1 ppb with a mean 1.3±0.8 ppb). The $^{187}Os/^{188}Os$ ratios of most Fe-rich dunites calculated back to the age of kimberlite eruption at 86 Ma (Table 15) have a wide range and are more radiogenic than in Kaapvaal mantle peridotites (γOs from -12 to 14 in dunite xenoliths vs. -18 to 3 with most below -12 in mantle peridotites; Fig. 28e; Pearson et al., 1995b; Walker et al., 1989; Carlson et al., 1999; Menzies et al., 1999; Irvine et al., 2001; Meisel et al., 2001; Carlson & Moore, 2004; Simon, 2004). Again, sample GB0402 is exceptional, showing the lowest $^{187}Os/^{188}Os$ of the dunites. In contrast, kimberlite has γOs of -10 to 7 (Pearson et al., 1995a), which is higher than Kaapvaal mantle peridotites, but not as high as the most extreme values for Fe-rich dunites. The olivine separate analyzed from

Table 15: Re and Os isotope composition of Fe-rich dunite whole-rock samples and olivine separates (*italic*). Re-depletion ages (T_{RD}), model ages (T_{MA}) and γOs were calculated according to Walker *et al.*, (1989) using present day bulk silicate earth (BSE) values of $^{187}Os/^{188}Os_{BSE}$=0.1296 and $^{187}Re/^{188}Os_{BSE}$=0.4353 (Meisel *et al.*, 2001). The $^{187}Os/^{188}Os$(t) and γOs(t) ratios are age-corrected to a mean Kimberley kimberlite eruption age of 86±3 Ma and a Karoo eruption age of 183±1 Ma.

sample	**AJE410**		**DJ0267**	**DJ0268**	**DJ0269**	**DJ0270**	**GB0402**		**KP0403**
comment	whole-rock	*olivine*	whole-rock	whole-rock	whole-rock	whole-rock	whole-rock	*olivine*	whole-rock ilm-rich
Re [ppb]	0.01720	*0.00760*	0.16840	0.10420	0.22240	0.10590	0.01110	*0.00800*	0.31540
Os [ppb]	0.12410	*0.06770*	0.91330	0.06400	0.04450	0.09560	3.38050	*4.32910*	0.68210
$^{187}Re/^{188}Os$	0.67180	*0.53870*	0.88890	7.83750	24.10740	5.33450	0.01590	*0.00890*	2.23330
2 σ error	0.01980	*0.07850*	0.00320	0.07190	0.27620	0.03760	0.00070	*0.00120*	0.00420
$^{187}Os/^{188}Os$	0.14790	*0.13470*	0.12590	0.13370	0.15160	0.12660	0.11440	*0.11340*	0.14380
2σ error	0.00011	*0.00067*	0.00003	0.00032	0.00027	0.00026	0.00001	*0.00002*	0.00002
$^{187}Os/^{188}Os$ (86)	0.14694	*0.13393*	0.12463	0.12246	0.11704	0.11895	0.11438	*0.11339*	0.14060
γOs (86)	13.93	*3.84*	-3.37	-5.05	-9.26	-7.77	-11.32	*-12.09*	9.01
$^{187}Os/^{188}Os$	0.14585	*0.13306*	0.12319	0.10977	0.07789	0.11031	0.11435	*0.11337*	0.13698
γOs (183)	13.70	*3.73*	-3.96	-14.42	-39.20	-14.00	-10.85	*-11.61*	6.79
T_{RD} [Ga]	-2.44	*-0.60*	0.68	0.98	1.71	1.45	2.06	*2.19*	-1.54
2 σ error	0.21	*0.24*	0.11	0.14	0.12	0.12	0.07	*0.07*	0.17
T_{MA} [Ga]	4.47	*2.89*	-0.49	0.03	0.05	-0.04	2.14	*2.24*	0.47
2 σ error	0.33	*1.25*	-0.13	-0.004	0.001	-0.01	0.07	*0.06*	-0.02

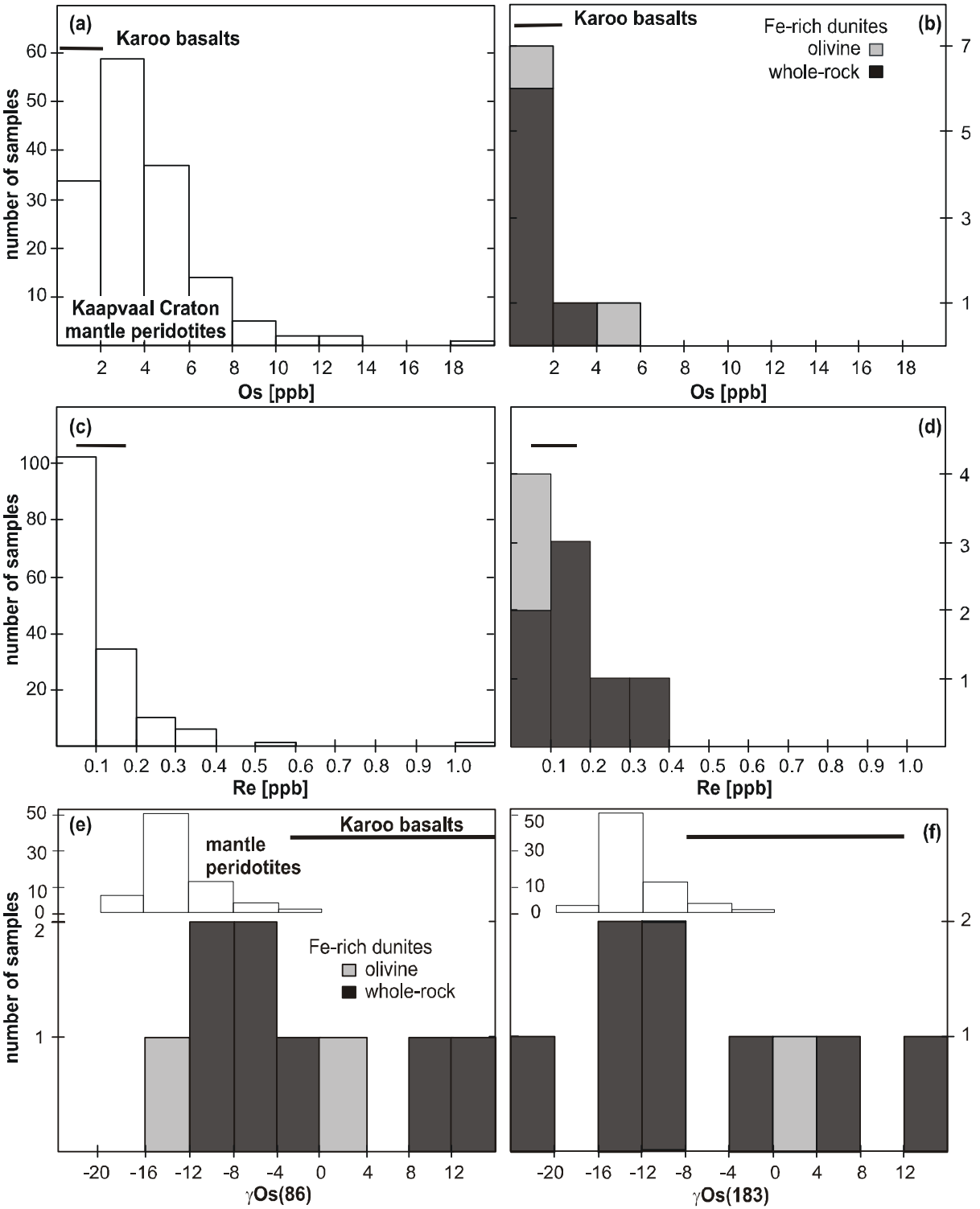

Fig. 28: Re-Os systematics of whole-rock and olivine separates of Fe-rich dunites (b, d, e and f), Karoo basalts (horizontal lines; Ellam et al., 1992) and Kaapvaal mantle peridotites (a, c, e and f; Walker et al., 1989; Pearson et al., 1995b; Carlson et al., 1999; Menzies et al., 1999; Irvine et al., 2001; Meisel et al., 2001; Carlson & Moore, 2004; Simon, 2004): (a) and (b) histogram of Os content, (c) and (d) histogram of Re content and (e) histogram of γOs at the time of kimberlite eruption (86 Ma) and (f) at the time of Karoo basalt magmatism (183 Ma).

GB0402 is distinguished from the whole-rock by lower Re, but higher Os concentrations (30 %) with a slightly lower $^{187}Os/^{188}Os$ ratio (0.1134 versus 0.1144, respectively). In contrast, the olivine from sample AJE410 has dramatically lower Re and Os concentrations and $^{187}Os/^{188}Os$ ratio compared to the whole-rock. The tie-line connecting the Re/Os and Os isotope ratios of the olivine and whole-rock analysis from AJE410 (not shown) corresponds to an apparent "age" in excess of 8 Ga. This must reflect the presence of an extraneous component introduced into the whole-rock that did not reach chemical and isotopic equilibrium with the constituent minerals. Along with AJE410, the ilmenite-rich sample KP0403 is the only other dunite to have an age-corrected $^{187}Os/^{188}Os$ ratio higher than the model primitive mantle. Overall, the samples show little or no correlation between Re/Os and Os isotope composition.

Fig. 29: $^{187}Os/^{188}Os$ versus time evolution diagram of whole-rocks and olivine separates of Fe-rich dunite xenoliths.

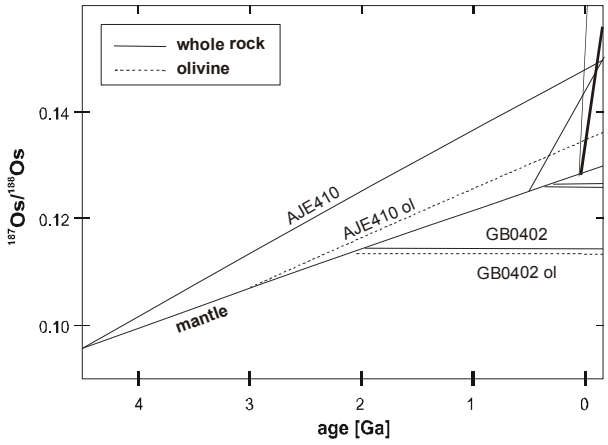

5. DISCUSSION

5.1. Metasomatic overprint

A fundamental problem frequently discussed for mantle peridotites from the Kaapvaal craton is the degree of metasomatic overprinting (Grégoire et al., 2003; Konzett et al., 2000). Kimberley is a particularly well-studied locality for mantle metasomatism (Erlank et al., 1987; Simon et al., 2007): mantle peridotite xenoliths retrieved from kimberlites of the Kimberley cluster are strongly metasomatised, resulting in enrichment of the rocks in Ti, Fe, K, LREE and other large ion lithophile (LIL) elements (Menzies et al., 1987). This metasomatic overprint can change the chemical composition of the primary minerals (cryptic metasomatism; Dawson, 1984) and, at higher degrees of metasomatism, change the modal composition of a rock (modal metasomatism; Harte, 1983) by adding phlogopite and amphibole (e.g. Carswell, 1975; Winterburn et al., 1990), ilmenite and rutile (Mitchell, 1973; Harte et al., 1987), and/or pyroxene and garnet (e.g. Hawkesworth et al., 1990; Simon et al., 2002; 2003; Grégoire et al., 2003) that grow at the expense of the primary minerals.

The exact composition of these metasomatising agents is highly debated, as is their nature (melt or fluid) and the timing of metasomatism (Erlank et al., 1987). Often a combination of metasomatic fluids and melts of different compositions are proposed, resulting from fractionation of the original metasomatising agent (Dawson & Smith, 1977; Stachel et al., 1998; Moine et al., 2001) or from different episodes of metasomatism (Dawson, 1984; Carlson et al., 1999; Griffin et al., 2003). In the case of the Kimberley kimberlite cluster, a range of metasomatising processes related to late Achaean subduction (Griffin et al., 1999; Simon et al., 2003; Schmitz et al., 2004; van Achterbergh, 2004; Simon et al., 2007), Mesozoic Karoo basalt magmatism (Erlank et al., 1980; Hawkesworth et al., 1990; Griffin et al., 2003), and later Cretaceous kimberlite events (Dawson, 1987; Konzett et al., 2000; Grégoire et al., 2003; Simon et al., 2003; 2007) have been suggested.

Kimberlite infiltration leads to enrichment in incompatible trace elements and MgO in the whole-rock. Additionally, post-emplacement weathering and reaction with percolating groundwater results in serpentinitization of olivine rims (average 10 vol. % serpentine in the Fe-rich dunite xenoliths). The analysis of unmetasomatised primary minerals for major and trace elements often helps to see through the metasomatic overprint and the effect of kimberlite infiltration (Barth et al., 2001). In the Fe-rich dunite xenoliths, secondary minerals that are not related to near-surface alteration, such as ilmenite and phlogopite make up only 1 - 2.5 % of the whole-rock (Table 12), which is much less than typical for metasomatised peridotite xenoliths from the same area (Erlank et al., 1987), so that thorough modification of all trace elements in the remaining 98 % of the rock is unlikely.

Metasomatic phases are ilmenite, which occurs in all samples and replaces chromite, and phlogopite, which has been found in three samples. In contrast, serpentine is related to weathering of the kimberlite. The elevated TiO_2 contents in chromite and phlogopite and the metasomatic nature of ilmenite and phlogopite in the Fe-rich dunites documents both a modal as well as cryptic metasomatic overprint. If all ilmenites replace spinel, most dunite xenoliths would have had ~ 1 % primary spinel, probably with slightly lower Cr# than analyzed. The high modal content of olivine argues that its uniform Mg# is unlikely to result from metasomatic alteration from an originally higher Mg#. The high Ti contents in olivine, however, might indicate cryptic metasomatism by equilibration with a Ti-rich percolating melt (not the host kimberlite, since it is low in TiO_2; Le Roex et al., 2003).

The timing of the metasomatism is difficult to constrain, but must have taken place before kimberlite entrainment. Type I ilmenites probably crystallised from a Ti- and Fe-rich melt as commonly proposed to cause Fe-Ti-rich metasomatism in peridotites of the Kaapvaal Craton. Their Cr-rich composition and distinction in trace elements from megacrystic ilmenites (Fig. 27a) may be due to the involvement of spinel in their formation. In contrast,

the lower Cr, V and Sc contents of Type II ilmenites may be explained by a similar origin from Fe-Ti-rich melts, but lacking reaction with pre-existing spinel. Konzett et al. (2000) demonstrated that zircons in MARID xenoliths from this area crystallized immediately before kimberlite eruption. Despite their contrasting mineralogy, MARID xenoliths may be related to the metasomatic reactions in peridotite described by Erlank et al. (1987), as these also produce K-richterite as end-products. The metasomatism experienced by the dunite xenoliths is possibly related to this event. The deformation documented by foliation along which olivine porphyroclasts and ilmenites are aligned, and which led to recrystallization of the olivines as neoblasts, is temporally related to the metasomatism. This is indicated by zonation of the porphyroclasts towards compositions of neoblasts, which are themselves recrystallized during the deformation.

5.2. Origin of the dunite xenoliths – residual mantle, cumulates, or reaction channels

Possible origins for the dunite xenoliths include: (i) residua of peridotite melting in the mantle after removal of a high melt fraction and elimination of clinopyroxene and othropyroxene; (ii) reaction products produced by removal of pyroxenes during reaction with percolating melts, as has been described from ophiolites (Kelemen et al., 1992); (iii) liquidus cumulates from picritic melts that crystallized in the upper mantle or crust, probably along the walls of cracks through which the melt moved. We restrict ourselves in this discussion to the chemical features that pre-date metasomatism. The texture of the dunite xenoliths is associated with the metasomatic event, probably immediately before eruption of the kimberlite and consequently provides little information as to the processes responsible for initial dunite formation.

2.1. Are dunite xenoliths residual after high degrees of melting of peridotite?

Several geochemical features of the dunite xenolith samples contradict an origin as metasomatized mantle peridotites that had previously experienced extensive melt removal. These are: (i) olivine neoblasts that have lower forsterite contents (Fo_{87-89}) than would be expected for a restitic dunite (Fo_{93-95}; Gurney & Harte, 1980). Advocating later lowering of the Mg# by Fe-Ti metasomatism is unreasonable, as this process would need to homogenise 98 % of the rock and none of the original Os isotope signal would survive. (ii) low Ni contents compared to typical mantle peridotites (Fig. 23 and Fig. 26f), which could be expected to be even higher after substantial melt loss due to the high D_{Ni} for olivine/melt pairs (Hart & Davis, 1978). (iii) the range in γOs (86 Ma) of -12 to 14 is large compared to mantle xenoliths from the Kaapvaal craton, which have γOs (86 Ma) mostly below -12 (Fig. 28e). The main carrier phases of Os in the mantle are sulphides and alloys, which break down during mantle

melting. Hence, although these signatures could be interpreted to reflect melt extraction exceeding the point of sulphide/alloy breakdown, the Re/Os ratios of all dunites except GB0402 are higher than primitive mantle, which implies interaction with a high Re/Os ratio melt, such as basalt or kimberlite. The Re-Os data thus provide a strong argument that the majority of the Fe-rich dunites are not simply residua of extensive melt extraction in the Archaean, the explanation commonly applied to the origin of Kaapvaal harzburgites and lherzolites. The high Cr# of spinels could be taken to be evidence for a restitic origin (Kurat et al., 1980), but these compositions may not be a true reflection of the original composition of the spinels due to metasomatic interaction. Furthermore, on account of their high TiO_2, these spinels are not similar to Cr-Al spinels typical of peridotites.

There are few trace element analyses of olivine in peridotites available for a systematic comparison to the trace element data reported here, so that the field for "mantle peridotites" in Fig. 26 should be treated with some caution until more analyses are available. Some pointers can nevertheless be found: if the dunites originate as residua after high degrees of melt loss from peridotite, then the major and trace element compositions of their olivines must correspond to clinopyroxene-undersaturated conditions. Foley et al. (2006) studied trace elements in olivines from Antarctica and described differences between rocks saturated in clinoyproxene (lherzolite) and those which were not. Apart from the expected low Ca contents, olivines from the harzburgitic population have lower Ti (<35, mostly <10 ppm), V (<2 ppm), Cr (<60 ppm) and Zn (average 20 ppm) concentrations than those from the lherzolitic population. Olivines in the dunite xenoliths from Kimberley have concentrations of these elements that are much higher than in the Antarctic harzburgites and correspond more closely to the lherzolitic population. There is thus no indication that the olivines originated as components of strongly depleted members of the peridotite suite.

2.2. Do dunite xenoliths correspond to reaction products between peridotite and percolating melts?

Many descriptions of dunites in the mantle sections of ophiolites attribute their formation to a reaction process resulting in removal of orthopyroxene by reaction with percolating melts (Kelemen et al., 1992; Suhr et al., 1998). Several points can be used to argue against such an origin for the dunite xenoliths at Kimberley.

(1) Olivine in ophiolitic dunite channels have Mg# and Mg-Ni characteristics within the mantle array, similar to Kaapvaal mantle peridotites (Fig. 23).

(2) The Re-Os signal should reflect the in-situ budget of peridotitic material diluted by the signal from the percolating melt. In the mantle sections of ophiolite complexes, harzburgite has higher Os, but lower Re contents than dunite channels and the initial Os isotope ratio of

harzburgite is more unradiogenic than that of the dunites (Büchl et al., 2002; Hanghøj et al., 2004). The Kaapvaal dunite xenoliths have similar to slightly less radiogenic initial Os isotope composition compared to ophiolitic dunites (0.1144-0.1469 vs. 0.1245-0.1477, respectively), whereas the Re and Os contents of the dunite xenoliths are lower than in ophiolitic channel dunites (0.1±0.1 ppb Re and mostly <1 ppb Os). Becker et al. (2006) calculated that melt/rock ratios up to 400 were required to remove 50-70 % of the osmium from a peridotite by this process. Reduction of Os contents from the 3.5 - 5.5 ppb Os typical of peridotite (Becker et al., 2006) to <1 ppb in Kimberley dunite olivines requires unrealistically high melt/rock ratios (Becker et al., 2001, Hanghøj et al., 2004).

(3) The reaction channel mechanism is documented for low pressure oceanic lithosphere settings in which low SiO_2 melts react with peridotite due to the pressure contrast between the depth of origin of the melt and the reaction location. In the case of the dunite xenoliths from Kimberley, formation of dunite in reaction channels would occur within the thick continental lithosphere where this pressure contrast is unlikely to be so great.

(4) Dunite xenoliths from ocean island basalts (e.g. Hawaii, Kerguelen) have olivine with lower forsterite contents and similar major element and transitional metal element compositions to olivine neoblasts in the dunite xenoliths from Kimberley (Grégoire et al., 2000, Moine et al., 2001). These xenoliths have been ascribed to either crystallization in conduits of the ascending basaltic magma (Kerguelen; Grégoire et al., 2000) or to accumulation in magma chambers (Hawaiian dunites; Clague, 1988; Clague and Bohrson, 1991; Gaffney, 2002). However, trace element analyses of these dunite xenoliths are not available, so that a thorough assessment of similarities and differences to the Kimberley dunites cannot be made.

2.3. Are dunite xenoliths liquidus cumulates of Karoo picrite-basalt?

An origin of Kimberley dunite xenoliths as cumulates is compatible with the similarity of the olivine compositions to olivine megacrysts in Karoo picrites (Fo_{82-92}) and in kimberlites (Fo_{80-88}), both of which are believed to be of cumulate origin (Cox & Jamieson, 1974; Boyd, 1974; Dawson et al., 1981; Schulze, 1987; Nowell et al., 2004). Chromites with Cr# up to 0.74, at the lower end of the range for spinel in the dunite xenoliths (0.67-0.97), are known from Karoo basalts and are interpreted as cumulate minerals (Eales, 1979). Furthermore, they have high TiO_2 contents of 0.4-9.2 wt. %, offering an explanation for the high TiO_2 content of spinel in the Fe-rich dunites. The Re and Os isotope compositions of the most Fe-rich dunite xenoliths have similar Os evolution trends to the Karoo basalts (Fig. 29; Ellam et al., 1992), yielding Re/Os ages of 30 Ma to 1.5 Ga (Table 15), which overlaps with Re/Os ages obtained for Karoo basalts (Duncan et al., 1997). Although apparently at odds with an origin

as cumulates, sheared textures have been described for megacrysts from kimberlites that are also interpreted as cumulates. This kind of deformation in kimberlite megacrysts has been attributed to deformation by the thermal aureole of the host kimberlite (Moore & Belousova, 2005).

Several lines of evidence suggest that the olivine porphyroclasts may be remnants of much earlier (probably Archaean) cumulate wall rocks, which were incorporated into, or strongly interacted with, the melt from which the olivine neoblasts crystallized. Compared to olivine neoblasts, the porphyroclasts have slightly higher forsterite contents (Fo_{87-91}) and different trace element compositions (Fig. 26). The observation of slight chemical variation towards neoblast composition from porphyroclast core to rim in sample GB0402 (Table 13, Fig. 26) indicates progressive equilibration between the magma and the incorporated wall rock. Sample DJ0270 has olivine porphyroclasts with V and Nb concentrations that plot within the compositional field of olivine in mantle peridotites. However, the low Ni content of olivine porphyroclasts (1300 ppm) precludes an origin for the porphyroclasts as peridotitic olivines. The porphyroclasts with low Ni contents are best explained as liquidus crystallization from a slightly fractionated Mg-rich melt, and thus also as cumulates from a magmatic event. However, the Re-Os isotope data require that this "porphyroclast event" occurred much earlier, possibly during Archaean times. Such an Archaean event might correspond to the Ventersdorp magmatism, whose surface expression comprises basaltic komatiites, basalts, basaltic andesites, andesites and felsic volcanics (Crow & Condie, 1988). The lower Ca content of olivine porphyroclasts compared to olivine neoblasts indicates that olivine porphyroclasts crystallized at slightly higher pressures (Köhler & Brey, 1990). This may indicate incorporation of the older porphyroclast cumulate component from lower levels during ascent of the Karoo magma and crystallization of olivine neoblasts at higher levels.

The Os isotope compositions place some constraints on the origin of the high Re/Os ratio of the majority of the Fe-rich dunites. Using the measured Re/Os ratios of the samples and correcting back to the eruption age of the host kimberlite (86 Ma), the Os isotope composition of the dunites ranges from significantly higher than estimates for primitive mantle (i.e. samples AJE410 and KP0403 with γOs (86 Ma) between +4 and +14) through values slightly lower than primitive mantle (samples DJ0267, DJ0268, DJ0269 and DJ0270 with γOs (86 Ma) = -3 to -9), to sample GB0402 with an Os isotope composition approaching that typical for Kaapvaal peridotites (-12.5±0.2; Fig. 28e). If corrected back to the ~183 Ma eruption age of the Karoo basalts (Duncan et al., 1997), however, samples DJ0268 and DJ0270 would have Os isotope compositions within the range of most Kaapvaal peridotites, whereas sample DJ0269, with the highest Re/Os of the dataset, would have unrealistically low $^{187}Os/^{188}Os$ ratio, below that of the initial $^{187}Os/^{188}Os$ of the Earth (Fig. 28f). Clearly, for samples DJ0268, DJ0269 and DJ0270, the high Re/Os ratio must be a fairly recent (i.e.

Phanerozoic) phenomenon. If the dunites formed during the Karoo event and their Re/Os ratios were not significantly perturbed by infiltration by the host kimberlite, then the low $^{187}Os/^{188}Os$ at 183 Ma of samples DJ0268, DJ0270 and GB0402, are compatible with the suggestion that the dunites formed from interaction between Karoo melts and pre-existing ancient lithosphere. Sample GB0402 has the lowest Re/Os and $^{187}Os/^{188}Os$ of all Fe-rich dunites, suggesting the bulk of the Os is derived from an Archaean source consistent with the high modal abundance of porphyroclastic olivine. Hence, while most samples seem to have originated from Phanerozoic (Karoo) magmas, the preserved porphyroclasts and the Re-Os isotope systematics of samples DJ0268, DJ0270 and GB0402 show evidence for incorporation of Archaean (possibly Ventersdorp) cumulate material, which may indicate reactivation of old melt channels.

The unrealistically low $^{187}Os/^{188}Os$ calculated for sample DJ0269 at 183 Ma, however, indicates modification of the Re-Os system more recently than Karoo volcanism, and the likely candidate here is infiltration of the xenoliths by their host kimberlite. The significant difference in Os isotope composition between the olivine separate and whole-rock for sample AJE410, and the presence of ilmenite in KP0403 with similar Os isotope characteristics to AJE410, provide additional evidence that interaction with the host kimberlite indeed played a role in modifying the composition of these three dunites.

5.3. Picrite fractionation and dunite crystallization conditions

From the above discussion, an origin of most dunite xenoliths as metasomatically modified and deformed liquidus cumulates from picrite-basalt melts of the Karoo period appears most likely. To further evaluate this hypothesis, we calculated the parental magma compositions for olivines in the dunites and compared them with primitive basalt compositions from the southern low-Ti Karoo basalt province (Fig. 20) from which the dunites may have crystallized. This hypothetical parental magma is calculated from the olivine composition, using published crystal-melt partition $\left(D_{liq}^{ol} = \frac{X_{element}^{ol}}{X_{element}^{liq}} \right)$ and distribution coefficients $\left(K_D = \frac{X_{oxide1}^{ol} / X_{oxide2}^{ol}}{X_{oxide1}^{liq} / X_{oxide2}^{liq}} \right)$.

The olivine compositions were assumed to represent pre-metasomatic chemistry (i.e. Mg# was not lowered during metasomatism): the Mg# calculated for coexisting melts are thus minimum values. The olivine neoblasts have FeO/MgO ratios of 0.22-0.27, corresponding to a coexisting melt composition with FeO/MgO of 0.69-0.89 using a K_D of 0.30 (Roeder & Emslie, 1970), and lie within the lower part of the FeO/MgO range of primitive low-Ti Karoo basalt (0.39-2.38; Cox 1983; Cox et al., 1967; Marsh et al., 1997). Olivine porphyroclasts have FeO/MgO ratios of 0.18-0.27, corresponding to FeO/MgO ratio of the coexisting melt of 0.58-0.88. The parental melts calculated for olivine porphyroclasts have lower FeO/MgO

ratios than for the coexisting olivine neoblasts, indicating a higher MgO content (Table 16), which is consistent with the basal section of the Ventersdorp Klipriviersberg Group comprising high-Mg and komatiitic rocks progressing to later tholeiitic basalts (e.g. Crow & Condie, 1988; Eriksson et al., 2002). This is consistent with the interpretation that the olivine porphyroclasts are remnants of an initially more magnesian, but slightly fractionated melt, explaining their lower Ni contents. Following the procedure of Eales & Marsh (1979), and using a total iron content (as Fe_2O_3*) of 11.6 wt. % (average low-Ti Karoo basalt) and a Fe_2O_3/FeO ratio of 0.20 (Brooks, 1976) we recalculated the iron and magnesium content of the parental melt of the olivine neoblasts and porphyroclasts (Table 16). The most primitive olivine neoblasts have a parental melt compositions with Fe_2O_3 = 2.1 wt. %, FeO = 10.5 wt. % and MgO = 15.3 wt. %. Additionally, it is possible to calculate concentrations of SiO_2, CaO, NiO, MnO, Cr_2O_3, Al_2O_3 and TiO_2 in the parental melt using experimental and naturally determined olivine / basalt melt partition coefficients. The predicted TiO_2 content of the parental magmas is 0.7-2.4 wt. % and lies within the TiO_2 range of primitive low-Ti Karoo basalts (0.4-2.4 wt. %). The calculated parental magma composition lies within the range of primitive low-Ti Karoo basalt composition for all major elements (Table 16). This observation together with the high MgO content of the parental magma, supports the interpretation that the Fe-rich dunites are cumulates from low-Ti Karoo picrites that erupted in the same area in Jurassic times (Fig. 20).

Table 16: Parental magma composition [wt. %] calculated from olivine trace element compositions in Table 13 and literature partition coefficients Dol/liq and compared with primitive low-Ti Karoo basalts (Cox et al., 1967; Eales & Marsh, 1979; Cox, 1983; 1988). Abbreviations as in Table 12 and Table 13; references of partition coefficients 1 = Roeder & Emslie (1970); 2 = Beattie et al. (1991); 3 = Bédard (2005); 4 = Colson *et al.* (1988); 5 = Higuchi & Nagasawa (1969); 6 = Ohtani *et al.* (1989); 7 = Dunn (1987); 8 = Hart & Davis (1978).

sample	**AJE410**	**DJ0267**	**DJ0268**	**DJ0269**	**DJ0270**		**GB0402**		**KP0403**		**Karoo**	$D_{ol/liq}$
	nb	nb	nb	nb	pc	nb	pc	nb	pc	nb	range	ref.
FeO/MgO	0.89	0.83	0.83	0.69	0.58	0.72	0.88	0.89	0.82	0.84	0.46-2.40	1
MgO	11.84	12.67	12.90	14.43	18.00	14.68	11.92	11.75	12.78	12.53	4.70-31.49	1
SiO_2	43.62	43.81	44.85	43.75	44.00	43.56	44.57	44.49	44.25	44.39	42.46-53.80	2
TiO_2	0.89	0.80	2.22	2.36	1.32	1.88	0.82	1.48	0.72	1.30	0.41-2.40	3
Al_2O_3	3.73	1.58	7.73	-	2.08	7.00	-	-	-	-	5.97-16.49	4
CaO	6.06	-	7.39	7.63	3.69	6.37	4.86	8.42	17.38	10.80	4.36-12.60	5
Cr_2O_3	0.11	0.09	0.13	0.14	0.04	0.13	0.03	0.14	0.02	0.16	-	6
MnO	0.07	0.07	0.09	0.12	0.07	0.07	0.18	0.13	0.11	0.09	0.15-0.25	7
NiO	0.03	0.04	0.04	0.06	0.04	0.04	0.02	0.05	0.02	0.05	-	8

In order to test this hypothesis and to reproduce the Fe-rich dunite olivine composition, we modelled the fractional crystallization of the calculated parental picrite melt of the most primitive olivine neoblast with pMELTS (Ghiorso & Hirschmann, 1998), which uses the same olivine/melt FeO/MgO distribution coefficient of 0.30 used in calculating the parental magma composition (Ghiorso & Sack, 1995). Fractional crystallization was modelled isobarically (10 kbar) in temperature intervals of 1 °C, beginning at the liquidus calculated by

pMELTS (~1400 °C). Since Karoo basalts are hydrous with water contents of 0.5 to 2.6 wt. % (Eales & Marsh, 1979) olivine fractionation was modelled under hydrous conditions (2 % water). This yielded 15 % olivine fractionation and led towards more tholeiitic melt compositions. Subsequently, spinel and clinopyroxene crystallize from the melt. The modelled fractional crystallization shows similar oxide variation to that seen in the primitive basalts of low-Ti Karoo basalts (Table 16) and other large igneous provinces worldwide. At similar forsterite contents, olivine fractionating from parental melt of the most primitive olivine porphyroclasts has lower NiO (0.1-0.2 wt. %), MnO (0.2 wt. %) and CaO (0.3 wt. %) contents than olivine from the neoblast parental melt, which agrees well with the composition of olivine porphyroclasts. The NiO content of the modelled olivine overlaps with the composition of olivine the Fe-rich dunite xneoliths (NiO = 0.3-0.8 wt. %), whereas MnO and CaO are slightly overestimated (0.5 and 0.3-0.4 wt. %, respectively). The calculated parental melt of the most primitive olivine porphyroclasts has lower Al_2O_3, TiO_2, CaO and higher SiO_2 fractionation trends (modelled hydrous, at 10 kbar with pMELTS). This is similar to Ventersdorp volcanics that also have higher SiO_2 and lower Al_2O_3, TiO_2 and CaO contents than low-Ti Karoo basalts (Crow & Condie, 1988; Marsh et al., 1989).

6. CONCLUSIONS

Fine-grained Fe-rich dunite xenoliths from South African kimberlites have minerals with major and trace element compositions differing from those in mantle peridotites. Their low forsterite and NiO contents as well as low Os content and high Re/Os and $^{187}Os/^{188}Os$ ratios contradict an origin as restite after melting of peridotite, but are strong evidence for an origin as recrystallized magmatic cumulates. Modelling of fractional crystallization from estimated parental magma composition with pMELTS yields up to 15 % olivine fractionation followed by spinel and clinopyroxene crystallization, which drives the melt compositions towards tholeiitic compositions. The composition of the fractionating olivine is similar to olivine in the Fe-rich dunites. Modelled element fractionation trends successfully reproduce the compositional variation of large igneous province basalts. In contrast, olivine porphyroclasts have higher Fo and lower NiO contents than olivine neoblasts, showing that these are remnants of cumulates from different, much earlier magmatic episodes. Re-Os isotope systematics indicates an Archaean age for these porphyroclasts. The petrogenetic history of the Fe-rich dunites can be summarized as follows:

i) Ca. 2.7 Ga: fractional crystallization and accumulation of olivine from an Archaean (probably Ventersdorp) komatiite-picrite melt, indicated by low $^{187}Os/^{188}Os$ at 183 Ma, and now present as olivine porphyroclasts.

ii) 183 Ma: Karoo magmatism results in formation of olivine cumulates carrying the Re-Os signature of low-Os melts at this time. Abundant olivine crystallization, now represented by the neoblast population, is accompanied by minor spinel crystallization (1-2 %). The rare porphyroclasts in the dunites are incorporated from event (i) torn out by reactivation of Archaean veins.

iii) Ca. 90-86 Ma: Metasomatic overprinting of the dunites, resulting in reaction of spinel to form Type I ilmenite ± phlogopite, and readjustment of the Re-Os system. Deformation occurred at about the same time, resulting in growth of neoblasts and elimination of earlier textures. Only the largest porphyroclasts remain intact from earlier episodes. This event corresponds to the zircon ages in MARID xenoliths from the same area (Konzett et al., 2000).

iv) 86 Ma: Incorporation into the kimberlite melt.

ACKNOWLEDGEMENTS

Samples were collected by DEJ and provided to us by the University of Cape Town (A.J. Erlank collection) and by G.P. Brey (J.W. Goethe University, Frankfurt). J. Robey (DeBeers, Kimberley) provided expert assistance in collecting xenoliths. The help of the laboratory managers B. Schulz-Dobrick and M.G. Barth (Mainz University), D. Lowry (Royal Holloway University of London), M. Horan and T.D. Mock (Carnegie Institution of Washington) is gratefully acknowledged. The manuscript was improved by helpful comments of the two reviewers Hilary Downes and Nina Simon. This project was financially supported by the Deutsche Forschungsgemeinschaft (Fo181/17-1).

REFERENCES

Allsopp, H. L. & Barrett, D. R. (1975). Rb-Sr age determinations on South African kimberlite pipes. Physics and Chemistry of the Earth 9, 605-617.

Arai, S. (1994). Characterization of spinel peridotites by olivine-spinel compositional relationships: Review and interpretation. Chemical Geology 113, 191-204.

Armstrong, A. (1995). CITZAF - A package of correction programs for the quantitative electron microbeam X-ray-analysis of thick polished materials, thin-films, and particles. Microbeam Analysis 4, 177-200.

Barth, M. G., Rudnick, R. L., Horn, I., McDonough, W. F., Spicuzza, M. J., Valley, J. W. & Haggerty, S. E. (2001). Geochemistry of xenolithic eclogites from West Africa, Part I: A link between low MgO eclogites and Archean crust formation. Geochimica et Cosmochimica Acta 65, 1499-1527.

Barth, M. G., Rudnick, R. L., Horn, I., McDonough, W. F., Spicuzza, M. J., Valley, J. W. & Haggerty, S. E. (2002). Geochemistry of xenolithic eclogites from West Africa, part 2: Origins of the high MgO eclogites. Geochimica et Cosmochimica Acta 66, 4325-4345.

Beattie, P., Ford, C. & Russell, D. (1991). Partition coefficients for olivine-melt and orthopyroxene-melt systems. Contributions to Mineralogy and Petrology 109, 212-224.

Becker, H., Shirey, S. B. & Carlson, R. W. (2001). Effects of melt percolation on the Re-Os systematics of peridotites from a Paleozoic convergent plate margin. Earth and Planetary Science Letters 188, 107-121.

Becker, H., Horan, M.F., Walker, R.J., Gao, S., Lorand, J.-P., & Rudnick, R.L. (2006) Highly siderophile element composition of the Earth's primitive upper mantle: constraints from new data on peridotite massifs and xenoliths. Geochimica et Cosmochimica Acta 70, 4528-4550.

Bédard, J. H. (2005). Partitioning coefficients between olivine and silicate melts. Lithos 83, 394-419.

Boyd, F. R. (1974). Olivine megacrysts from the kimberlite of the Monastery and Frank Smith kimberlite pipe, South Africa. Carnegie Institution of Washington Year Book 73, 282-285.

Boyd, F. R. & Nixon, P. H. (1975). Origins of the ultramafic nodules from some kimberlites of northern Lesotho and the Monastery mine, South Africa. Physics and Chemistry of the Earth 9, 431-454.

Boyd, F. R., Jones, A. P. & Nixon, G. T. (1983). Mantle metasomatism: the Kimberley dunites. Carnegie Institution of Washington Yearbook 83, 330-337.

Boyd, F. R. (1989). Compositional distinction between oceanic and cratonic lithosphere. Earth and Planetary Science Letters 96, 15-26.

Brooks, C. K. (1976). The Fe2O3/FeO ratio of basalt analyses: An appeal for a standardized procedure. Bulletin of the Geological Society of Denmark 25, 117-120.

Büchl, A., Brügmann, G., Batanova, V. G., Münker, C. & Hofmann, A. W. (2002). Melt percolation monitored by Os isotopes and HSE abundances: a case study from the mantle section of the Troodos Ophiolite. Earth and Planetary Science Letters 204, 385-402.

Carlson, R. W., Pearson, D. G., Boyd, F. R., Shirey, S. B., Irvine, G., Menzies, A. H. & Gurney, J. J. (1999). Re-Os systematics of lithospheric peridotites: Implications for lithosphere formation and preservation. In: Gurney, J. J., Gurney, J. L., Pascoe, M. D. & Richardson, S. H. (eds.). Proceedings of the 7th International Kimberlite Conference. Cape Town: Red Roof, 1, 99-108.

Carlson, R. W. & Moore, R. O. (2004). Age of the Eastern Kaapvaal mantle: Re-Os isotope data for peridotite xenoliths from the Monastery kimberlite. South African Journal of Geology 107, 81-90.

Carswell, D. A. & Dawson, J. B. (1970). Garnet peridotite xenoliths in South African kimberlite pipes and their petrogenesis. Contributions to Mineralogy and Petrology 25, 163-184.

Carswell, D. A. (1975). Primary and secondary phlogopites and clinopyroxenes in garnet lherzolite xenoliths. Physics and Chemistry of the Earth 9, 417-429.

Carswell, D. A., Clarke, D. B. & Mitchell, R. H. (1979). The petrology and geochemistry of ultramafic nodules from pipe 200, northern Lesotho. In: Boyd, F. R. & Meyer, H. O. A. (eds.). Kimberlites, diatremes and diamonds: Their geology, petrology and geochemistry. Washington: American Geophysical Union, 2, 127-144.

Clague, D. A. (1988). Petrology of ultramafic xenoliths from Loihi Seamount, Hawaii. Journal of Petrology 29, 1161-1186.

Clague, D. A. & Bohrson, W. A. (1991). Origin of xenoliths in the trachyte at Puu Waawaa, Hualalai Volcano, Hawaii. Contributions to Mineralogy and Petrology 108, 439-452.

Colson, R. O., McKay, G. A. & Taylor, L. A. (1988). Temperature and composition dependencies of trace element partitioning: Olivine/melt and low-Ca pyroxene/melt. Geochimica et Cosmochimica Acta 52, 539-553.

Cox, K. G., Macdonald, R. & Hornung, G. (1967). Geochemical and petrographic provinces in the Karroo basalts of southern Africa. American Mineralogist 52, 1451-1474.

Cox, K. G. & Jamieson, B. G. (1974). The olivine-rich lavas of Nuanetsi: A study of polybaric magmatic evolution. Journal of Petrology 15, 269-301.

Cox, K. G. (1983). The Karoo province of southern Africa: Origin of trace element enrichment patterns. In: Hawkesworth, C. J. & Norry, M. J. (eds.). Continental Basalts and Mantle Xenoliths. Leicester: Shiva, 139-157.

Cox, K. G. (1988). The Karoo province. In: Macdougall, J. D. (ed.) Continental flood basalts. Dordrecht: Kluwer, 239-271.

Crow, C. & Condie, K. C. (1988). Geochemistry and origin of Late Archean volcanics from the Ventersdorp Supergroup, South Africa. Precambrian Research 42, 19-37.

Davis, D. L. (1977). The ages and uranium contents of zircons from kimberlites and associated rocks. Carnegie Institution of Washington 76, 631-653.

Dawson, J. B. & Smith, C. B. (1977). The MARID (mica-amphibole-rutile-ilmenite-diopside) suite of xenoliths in kimberlite. Geochimica et Cosmochimica Acta 41, 309-323.

Dawson, J. B., Hervig, R. L. & Smith, J. V. (1981). Fertile iron-rich dunite xenoliths from the Bultfontein kimberlite, South Africa. Fortschritte der Mineralogie 59, 303-324.

Dawson, J. B. (1984). Contrasting types of upper-mantle metasomatism. In: Kornprobst, J. (ed.) Kimberlites II: The mantle and crust-mantle relationships. Amsterdam: Elsevier, 289-294.

Dawson, J. B. (1987). The MARID suite of xenoliths in Kimberlites: relationship to veined and metasomatised peridotite xenoliths. In: Nixon, P. H. (ed.) Mantle Xenoliths. Chichester: John Wiley, 465-474.

Dawson, J. B. (2004). A fertile harzburgite-garnet lherzolite transition: Possible inferences for the roles of strain and metasomatism in upper mantle peridotites. Lithos 77, 553-569.

Duncan, R. A., Hooper, P. R., Rehacek, J., Marsh, J. S. & Duncan, A. R. (1997). The timing and duration of the Karoo igneous event, southern Gondwana. Journal of Geophysical Research 102, 18127-18138.

Dunn, T. (1987). Partitioning of Hf, Lu, Ti, and Mn between olivine, clinopyroxene and basaltic liquid. Contributions to Mineralogy and Petrology 96, 476-484.

Eales, H. V. (1979). Anomalous Karroo spinels along the chromite-titanomagnetite join. South African Journal of Science 75, 24-29.

Eales, H. V. & Marsh, J. S. (1979). High-Mg tholeiitic rocks and their significance in the Karroo Central Province. South African Journal of Science 75, 400-404.

Eglington, B. M. & Armstrong, R. A. (2004). The Kaapvaal Craton and adjacent orogens, southern Africa: a geochronological database and overview of the geological development of the craton. South African Journal of Geology 107, 13-32.

Ellam, R. M. & Cox, K. G. (1991). An interpretation of Karoo picrite basalts in terms of interaction between asthenospheric magmas and the mantle lithosphere. Earth and Planetary Science Letters 105, 303-342.

Ellam, R., Carlson, R. & Shirey, S. (1992). Evidence from Re-Os isotopes for plume-lithosphere mixing in Karoo flood basalt genesis. Nature 359, 718-721.

Eriksson, P. G., Condie, K. C., van der Westhuizen, W., van der Merwe, R., de Bruiyn, H., Nelson, D. R., Altermann, W., Catuneanu, O., Bumby, A. J., Lindsay, J. & Cunningham, M. J. (2002). Late Archaean superplume events: a Kaapvaal-Pilbara perspective. Journal of Geodynamics 34, 207-247.

Erlank, A., Allsopp, H., Duncan, A. & Bristow, J. (1980). Mantle heterogeneity beneath southern Africa: evidence from the volcanic record. Philosophical Transactions of the Royal Society of London 297, 295-307.

Erlank, A. J., Waters, F. G., Hawkesworth, C. J., Haggerty, S. E., Allsopp, H. L., Rickard, R. S. & Menzies, M. (1987). Evidence for mantle metasomatism in peridotite nodules from the Kimberley pipes, South Africa. In: Menzies, M. A. & Hawkesworth, C. J. (eds.). Mantle metasomatism. London: Academic Press, 221-311.

Foley, S. F., Buhre, S., Jacob, D. & Rehfeldt, T. (2003a). Pyroxenite and dunite xenoliths as metamorphosed cumulates from the Archean lower ocean crust. 8th International Kimberlite Conference. Vancouver, 2.P12.

Foley, S.F., Buhre, S. & Jacob, D.E. (2003b) Evolution of the Archaean crust by delamination and shallow subduction. Nature 421, 249-252.

Foley, S. F., Andronikov, A. V., Jacob, D. E. & Melzer, S. (2006). Evidence from Antarctic mantle peridotite xenoliths for changes in mineralogy, geochemistry and geothermal gradients beneath a developing rift. Geochimica et Cosmochimica Acta 70, 3096-3120.

Gaffney, A. M. (2002). Environments of crystallization and compositional diversity of Mauna Loa xenoliths. Journal of Petrology 43, 963-980.

Ghiorso, M. S. & Sack, R. O. (1995). Chemical mass transfer in magmatic processes IV. A revised and internally consistent thermodynamic model for the interpolation and extrapolation of liquid-solid equilibria in magmatic systems at elevated temperatures and pressures. Contributions to Mineralogy and Petrology 119, 197-212.

Ghiorso, M. S. & Hirschmann, M. M. (1998). pMELTS: A revised calibration of MELTS for modeling peridotite melting at high pressure. EOS 79, F1005.

Gibson, S. A., Thompson, R. N. & Dickin, A. P. (2000). Ferropicrites: geochemical evidence for Fe-rich streaks in upwelling mantle plumes. Earth and Planetary Science Letters 174, 355-374.

Grégoire, M., Moine, B. N., O'Reilly, S. Y., Cottin, J.-Y. & Giret, A. (2000). Trace element residence and partitioning in mantle xenoliths metasomatized by highly alkaline, silicate- and carbonate-rich melts (Kerguelen Islands, Indian Ocean). Journal of Petrology 41, 477-509.

Grégoire, M., McInnes, B. I. A. & O'Reilly, S. Y. (2001). Hydrous metasomatism of oceanic sub-arc mantle, Lihir, Papua New Guinea Part 2 . Trace element characteristics of slab-derived fluids. Lithos 59, 91-108.

Grégoire, M., Bell, D. R. & Le Roex, A. P. (2002). Trace element geochemistry of phlogopite-rich mafic mantle xenoliths: Their classification and their relationship to phlogopite-bearing peridotites and kimberlites revisited. Contributions to Mineralogy and Petrology 142, 603-625.

Grégoire, M., Bell, D. R. & Le Roex, A. P. (2003). Garnet lherzolites from the Kaapvaal Craton (South Africa): Trace element evidence for a metasomatic history. Journal of Petrology 44, 629-657.

Griffin, W. L., Shee, S. R., Ryan, C. G., Win, T. T. & Wyatt, B. A. (1999). Harzburgite to lherzolite and back again: metasomatic processes in ultramafic xenoliths form the Wesselton kimberlite, Kimberley, South Africa. Contributions to Mineralogy and Petrology 134, 232-250.

Griffin, W. L., O'Reilly, S. Y., Natapov, L. M. & Ryan, C. G. (2003). The evolution of lithospheric mantle beneath the Kalahari Craton and its margins. Lithos 71, 215-241.

Gurney, J. J. & Harte, B. (1980). Chemical variations in upper mantle nodules from southern Africa kimberlites. Philosophical Transactions of the Royal Society of London A297, 273-293.

Gurney, J. J., Moore, R. B., Otter, M. L., Kirkley, M. B., Hops, J. J. & McCandless, T. E. (1991). Southern African kimberlites and their xenoliths. In: Kampunzu, A. B. & Lubala, R. T. (eds.). Magmatism in extensional structural settings. Heidelberg: Springer, 495-536.

Halter, W. E., Pettke, T., Heinrich, C. A. & Rothen-Rutishauser, B. (2002). Major to trace element analysis of melt inclusions by laser-ablation ICP-MS: Methods of quantification. Chemical Geology 183, 63-86.

Hanghøj, K., Hassler, D. & Kelemen, P. B. (2004). Re-Os isotope and PGE systematics of peridotites from the Oman Ophiolite. Geochimica et Cosmochimica Acta 68, A703.

Hart, S. R. & Davis, K. E. (1978). Nickel partitioning between olivine and silicate melt. Earth and Planetary Science Letters 40, 203-219.

Hart, S.R, Blusztajn, J., Dick, H.J.B., Meyer, P.S. & Muehlenbachs, K. (1999) The fingerprint of seawater circulation in a 500-meter section of ocean crust gabbros. Geochimica et Cosmochimica Acta 63, 4059-4080.

Harte, B., Cox, K. G. & Gurney, J. J. (1975). Petrography and geological history of upper mantle xenoliths from the Matsoku kimberlite pipe. Physics and Chemistry of the Earth 9, 477-506.

Harte, B. (1983). Mantle peridotites and processes - the Kimberlite sample. In: Hawkesworth, C. J. & Norry, M. J. (eds.). Continental Basalts and Mantle Xenoliths. Cheshire: Shiva, 46-91.

Harte, B., Winterburn, P. A. & Gurney, J. J. (1987). Metasomatic and enrichment phenomena in garnet peridotite facies mantle xenoliths from the Matsoku kimberlite pipe, Lesotho. In: Menzies, M. A. & Hawkesworth, C. J. (eds.). Mantle metasomatism. London: Academic Press, 145-220.

Hawkesworth, C. J., Erlank, A. J., Kempton, P. D. & Waters, F. G. (1990). Mantle metasomatism: Isotope and trace-element trends in xenoliths from Kimberley, South Africa. Chemical Geology 85, 19-34.

Higuchi, H. & Nagasawa, H. (1969). Partition of trace elements between rock-forming minerals and the host volcanic rocks. Earth and Planetary Science Letters 7, 281-287.

Hills, D. V. & Haggerty, S. E. (1989). Petrochemistry of eclogites from the Koidu Kimberlite Complex, Sierra Leone. Contributions to Mineralogy and Petrology 103, 397-422.

Irvine, G. J., Pearson, D. G. & Carlson, R. W. (2001). Lithospheric mantle evolution of the Kaapvaal Craton: A Re-Os isotope study of peridotite xenoliths from Lesotho kimberlites. Geophysical Research Letters 28, 2505-2508.

Jacob, D. E., Schmickler, B. & Schulze, D. J. (2003). Trace element geochemistry of coesite-bearing eclogites from the Roberts Victor kimbelite, Kaapvaal craton. Lithos 71, 337-351.

Jacob, D. E. (2004). Nature and origin of eclogite xenoliths from kimberlites. Lithos 77, 295-316.

Jourdan, F., Féraud, G., Bertrand, H., Kampunzu, A. B., Tshoso, G., Le Gall, B., Tiercelin, J. J. & Capize, P. (2004). The Karoo triple junction questioned: Evidence from Jurassic and Proterozoic 40Ar/39Ar ages and geochemistry of the giant Okavango dyke swarm (Botswana). Earth and Planetary Science Letters 222, 989-1006.

Koga, K. T., Kelemen, P. B. & Shimizu, N. (2001). Petrogenesis of the crust-mantle transition zone and the origin of lower crustal wehrlite in the Oman ophiolite. Geochemistry, Geophysics, Geosystems 2, Paper number 2000GC000132.

Kelemen, P.B., Dick, H.J.B. & Quick, J.E. (1992) Formation of harzburgite by pervasive melt/rock reaction in the upper mantle. Nature 358, 635-641.

Konzett, J., Armstrong, R. A. & Günther, D. (2000). Modal metasomatism in the Kaapvaal craton lithosphere: Constraints on timing and genesis from U-Pb zircon dating of metasomatized peridotites and MARID-type xenoliths. Contributions to Mineralogy and Petrology 139, 704-719.

Köhler, T. & Brey, G. P. (1990). Calcium exchange between olivine and clinopyroxene calibrated as a geothermobarometer for natural peridotites from 2 to 60 kb with application. Geochimica et Cosmochimica Acta 54, 2375-2388.

Kostrovitsky, S. I., Malkovets, V. G., Verichev, E. M., Garanin, V. K. & Suvorova, L. V. (2004). Megacrysts from the Grib kimberlite pipe (Arkhangelsk Province, Russia). Lithos 77, 511-523.

Kubo, K. (2002). Dunite formation processes in highly depleted peridotite: case study of the Icanaidake peridotite, Hokkaido, Japan. Journal of Petrology 43, 423-448.

Kurat, G., Palme, H., Spettel, B., Baddenhausen, H., Hofmeister, H., Palme, C. & Wänke, H. (1980). Geochemistry of ultramafic xenoliths from Kapfenstein, Austria: evidence for a variety of upper mantle processes. Geochimica et Cosmochimica Acta 44, 45-60.

Lee, C.-T. & Rudnick, R. L. (1999). Compositional stratified cratonic lithosphere: Petrology and geochemistry of peridotite xenoliths from the Labait Volcano, Tanzania. In: Gurney, J. J., Gurney, J. L., Pascoe, M. D. & Richardson, S. H. (eds.). Proceedings of the 7th International Kimberlite Conference. Nixon volume, 503-521.

Le Roex, A. P., Bell, D. R. & Davis, P. (2003). Petrogenesis of group I kimberlites from Kimberley, South Africa: Evidence from bulk rock geochemistry. Journal of Petrology 44, 2261-2286.

Lowry, D., Appel, P. W. U. & Rollinson, H. R. (2003). Oxygen isotopes of an early Archaean layered ultramafic body, southern West Greenland: Implications for magma source and post-intrusion history. Precambrian Research 126, 273-288.

MacGregor, I. D. & Carter, J. L. (1970). The chemistry of clinopyroxenes and garnets of eclogite and peridotite xenoliths from the Roberts Victor mine, South Africa. Physics of the Earth and Planetary Interoirs 3, 391-397.

Marsh, J. S., Bowen, M. P., Rogers, N. W. & Bowen, T. B. (1989). Volcanic rocks of the Witwatersrand Triad, South Africa. II: Petrogenesis of mafic and felsic rocks of the Dominion Group. Precambrian Research 44, 39-65.

Marsh, J. S., Hooper, P. R., Rehacek, J., Duncan, R. A. & Duncan, A. R. (1997). Stratigraphy and age of Karoo basalts of Lesotho and implications for correlations within the Karoo igneous province. In: Mahoney, J. J. & Coffin, M. F. (eds.). Large igneous Provinces: continental, oceanic, and planetary flood volcanism. Washington: American Geohysical Union 100, 247-272.

Mattey, D. & Macpherson, C. (1993). High-precision oxygen isotope microanalysis of ferromagnesian minerals by laser-fluorination. Chemical Geology 105, 305-318.

Mattey, D., Lowry, D. & Macpherson, C. (1994). Oxygen isotope composition of mantle peridotite. Earth and Planetary Science Letters 128, 231-241.

Mattey, D. (1997). LaserPrep: An automatic laser-fluorination system for Micromass 'Optima' or 'Prism' mass spectrometers. Micromass Application Note 107, 1-7.

McDonough, W. F. & Sun, S.-S. (1995). The composition of the Earth. Chemical Geology 120, 223-253.

Meisel, T., Walker, R. J., Irving, A. J. & Lorand, J.-P. (2001). Osmium isotopic composition of mantle xenoliths: A global perspective. Geochimica et Cosmochimica Acta 65, 1311-1323.

Menzies, M., Rogers, N., Tindle, A. & Hawkesworth, C. J. (1987). Metasomatic and enrichment processes in lithospheric peridotites, an effect of asthenosphere-lithosphere interaction. In: Menzies, M. & Hawkesworth, C. J. (eds.). Mantle metasomatism. London: Academic Press, 313-361.

Menzies, A. H., Carlson, R. W., Shirey, S. B. & Gurney, J. J. (1999). Re-Os systematics of Newlands peridotite xenoliths: Implications for diamond and lithosphere formation. In: Gurney, J. J., Gurney, J. L., Pascoe, M. D. & Richardson, S. H. (eds.). 7th International Kimberlite Conference. Cape Town: Red Roof, 2, 566-573.

Mitchell, R. H. (1973). Magnesian ilmenite and its role in kimbelite petrogenesis. Journal of Geology 81, 301-311.

Moine, B. N., Grégoire, M., O'Reilly, S. Y., Sheppard, S. M. F. & Cottin, J.-Y. (2001). High field strength element fractionation in the upper mantle: evidence from amphibole-rich composite mantle xenoliths from the Kerguelen Islands (Indian Ocean). Journal of Petrology 42, 2145-2167.

Moore, A. & Belousova, E. (2005). Crystallization of Cr-poor and Cr-rich megacryst suites from the host kimberlite magma: implications for mantle structure and the generation of kimberlite magmas. Contributions to Mineralogy and Petrology 149, 462-481.

Neumann, E.-R., Wulff-Pedersen, E., Johnsen, K., Andersen, T. & Krogh, E. (1995). Petrogenesis of spinel harzburgite and dunite suite xenoliths from Lanzarote, eastern Canary Islands: Implications for the upper mantle. Lithos 35, 83-107.

Neumann, E.-R., Wulff-Pedersen, E., Pearson, N. J. & Spencer, E. A. (2002). Mantle xenoliths from Tenerife (Canary Islands): Evidence for reactions between mantle peridotite and silicic carbonatite melts inducing Ca metasomatism. Journal of Petrology 43, 825-857.

Nixon, P. H. & Boyd, F. R. (1973). Petrogenesis of the granular and sheared ultrabasic nodule suite in kimberlites. In: Nixon, P. H. (ed.) Lesotho Kimberlites. Lesotho National Development Corporation, 48-56.

Nowell, G. M., Pearson, D. G., Bell, D. R., Carlson, R. W., Smith, C. B., Kempton, P. D. & Noble, S. R. (2004). Hf isotope systematics of kimberlites and their megacrysts: New constraints on their source regions. Journal of Petrology 45, 1583-1612.

Ohtani, E., Kawabe, I., Moriyama, J. & Nagata, Y. (1989). Partitioning of elements between majorite garnet and melt and implications for petrogenesis of komatiite. Contributions to Mineralogy and Petrology 103, 263-269.

Pearce, N. J. G., Perkins, W. T., Westgate, J. A., Gorton, M. P., Jackson, S. E., Neal, C. R. & Chenery, S. P. (1997). A compilation of new and published major and trace element data for

NIST SRM 610 and NIST SRM 612 glass reference materials. Geostandards Newsletter 21, 115-144.

Pearson, D. G., Rogers, N. W., Irving, A. J., Smith, C. B. & Hawkesworth, C. J. (1995a). Source region of kimberlites and lamproites: Constraints from Re-Os isotopes. Extended Abstracts of the 6th International Kimberlite Conference. Novosibirsk, 430-432.

Pearson, D. G., Carlson, R. W., Shirey, S. B., Boyd, F. R. & Nixon, P. H. (1995b). Stabilisation of Archaean lithospheric mantle: A Re-Os isotope study of peridotite xenoliths from the Kaapvaal Craton. Earth and Planetary Science Letters 134, 341-357.

Pearson, D. G., Canil, D. & Shirey, S. B. (2003). Mantle samples included in volcanic rocks: xenoliths and diamonds. In: Carlson, R. W. (ed.) Treatise on Geochemistry: The mantle and core. Elsevier, 2, 171-275.

Rehfeldt, T., Obst, K. & Johansson, L. (2006). Petrogenesis of ultramafic and mafic xenoliths from Mesozoic basanites in southern Sweden: constraints from mineral chemistry. International Journal of Earth Sciences DOI 10.1007/s00531-006-0116-4.

Roeder, P. L. & Emslie, R. F. (1970). Olivine-liquid equilibrium. Contributions to Mineralogy and Petrology 29, 275-289.

Rudnick, R. L., McDonough, W. F. & Chappel, B. W. (1993). Carbonatite metasomatism in the northern Tanzania mantle: Petrographic and geochemical characteristics. Earth and Planetary Science Letters 114, 463-475.

Schmickler, B., Jacob, D. E. & Foley, S. F. (2004). Eclogite xenoliths from the Kuruman kimberlites, South Africa: Geochemical fingerprinting of deep subduction and cumulate processes. Lithos 75, 173-207.

Schmitz, M. D., Bowring, S. A., de Wit, M. J. & Gartz, V. (2004). Subduction and terrane collision stabilize the western Kaapvaal craton tectosphere 2.9 billion years ago. Earth and Planetary Science Letters 222, 363-376.

Schulze, D. J. (1987). Megacrysts from alkalic volcanic rocks. In: Nixon, P. H. (ed.) Mantle xenoliths. Chichester: John Wiley, 433-451.

Scott, B. H. (1981). Kimberlite and lamproite dykes from Holsteinsborg, West Greenland. Meddelelser om Grønland Geoscience, 3-24.

Scott Smith, B. H. (1987). Greenland. In: Nixon, P. H. (ed.) Mantle Xenoliths. Chichester: John Wiley, 23-32.

Shirey, S. B., Carlson, R. W., Richardson, S. H., Menzies, A., Gurney, J. J., Pearson, D. G., Harris, J. W. & Wiechert, U. (2001). Archean emplacement of eclogitic components into the lithospheric mantle during formation of the Kaapvaal craton. Geophysical Research Letters 28, 2509-2512.

Simon, N. S. C., Pearson, D. G., Carlson, R. W. & Davies, G. R. (2002). Origin of garnet and clinopyroxene in Kaapvaal low-T peridotite xenoliths: Implications from secondary ionisation mass spectrometry (SIMS) data. Geochimica et Cosmochimica Acta 66, A717-A717.

Simon, N. S. C., Irvine, G. J., Davies, G. R., Pearson, D. G. & Carlson, R. W. (2003). The origin of garnet and clinopyroxene in "depleted" Kaapvaal peridotites. Lithos 71, 289-322.

Simon, N. S. C. (2004). The formation and modification of cratonic lithospheric roots - A petrological and geochemical study of xenoliths from the Kaapvaal Craton. PhD thesis, Amsterdam: Vrije Universiteit, pp. 251.

Simon, N. S. C., Carlson, R. W., Pearson, D. G., Davies, G. R. (2007) The origin and evolution of the Kaapvaal Craton lithospheric mantle. Journal of Petrology, in press.

Smith, C. B. (1983). Pb, Sr and Nd isotopic evidence for sources of southern African Cretaceous kimberlites. Nature 304, 51-54.

Stachel, T., Viljoen, K. S., Brey, G. P. & Harris, J. W. (1998). Metasomatic processes in lherzolitic and harzburgitic domains of diamondiferous lithospheric mantle: REE in garnets from xenoliths and inclusions in diamonds. Earth and Planetary Science Letters 159, 1-12.

Suhr, G., Seck, H. A., Shimizu, N., Günther, D. & Jenner, G. A. (1998). Infiltration of refractory melts into the lowermost oceanic crust: evidence from dunite- and gabbro-hosted clinopyroxenes in the Bay of Islands Ophiolite. Contributions to Mineralogy and Petrology 131, 136-154.

Suhr, G. (1999). Melt migration under oceanic ridges: Inferences from reactive transport modelling of upper mantle hosted dunites. Journal of Petrology 40, 575-599.

Takahashi, E. (1986). Melting of dry peridotite KLB-1 up to 14 GPa: Implications on the origin of peridotitic upper mantle. Journal of Geophysical Research 91, 9367-9382.

Taylor, L. A. (1993). Evolution of the subcontinental mantle beneath the Kaapvaal Craton: A review of evidence for crustal subduction for Bellsbank eclogites. Geologija i geofizika : naucnyj zurnal 34, 25-47.

Thompson, R. N., Gibson, S. A., Dickin, A. P. & Smith, P. M. (2001). Early Cretaceous basalt and picrite dykes of the Southern Etendeka Region; NW Namibia: Windows into the role of the Tristan Mantle Plume in Paraná-Etendeka magmatism. Journal of Petrology 42, 2049-2081.

van Achterbergh, E. (2004). Geochemical fingerprints of mantle metasomatism. PhD thesis, Sydney: Macquarie University, pp. 223.

Walker, R. J., Carlson, R. W., Shirey, S. B. & Boyd, F. R. (1989). Os, Sr, Nd and Pb isotope systematics of southern African peridotite xenoliths: Implications for the chemical evolution of subcontinental mantle. Geochimica et Cosmochimica Acta 53, 1583-1595.

Winterburn, P. A., Harte, B. & Gurney, J. J. (1990). Peridotite xenoliths from the Jagersfontein kimberlite pipe: I. Primary and primary-metasomatic mineralogy. Geochimica et Cosmochimica Acta 54, 329-341.

Wyatt, B. A., Baumgartner, M., Ancker, E. & Grutter, H. (2004). Compositional classification of "kimberlitic" and "non-kimberlitic" ilmenite. Lithos 77, 819-840.

Zack, T. & Brumm, R. (1998). Ilmenite/liquid partition coefficients of 26 trace elements determined through ilmenite/clinopyroxene partitioning in garnet pyroxenite. Extended Abstracts of the 7th International Kimberlite Conference. Cape Town, 986-988.

Zack, T., Kronz, A., Foley, S. F. & Rivers, T. (2002). Trace element abundances in rutiles from eclogites and associated garnet mica schists. Chemical Geology 184, 97-122.

APPENDIX: REPRESENTATIVE MAJOR AND TRACE ELEMENT COMPOSITIONS OF DUNITE, WEHRLITE AND WEBSTERITE XENOLITHS

Abbreviations

cpx = clinopyroxene
cr = chromite
Cr# = Cr/(Cr+Al)
cr-spl = chromian spinel
dl = detection limit
gk = geikielite = $2xMg/(Ti\text{-}Fe^{2+}+Fe^{3+}+Mg)$
grt = garnet
ilm = ilmenite = $2xFe^{2+}/(Ti\text{-}Fe^{2+}+Fe^{3+}+Mg)$
ilm-gk = ilmenite-geikielite
IST = internal standard
Mg# = Mg/(Mg+Fe)
n = number of measurements
nb = neoblasts
nd = not determined
ol = olivine
opx = orthopyroxene
pc = porphyroclasts
repl. = replacing
RSA = Republic of South Africa
sec. = secondary
serp = serpentine
spl = spinel

AJE362: wehrlite xenolith, Kimberley, RSA

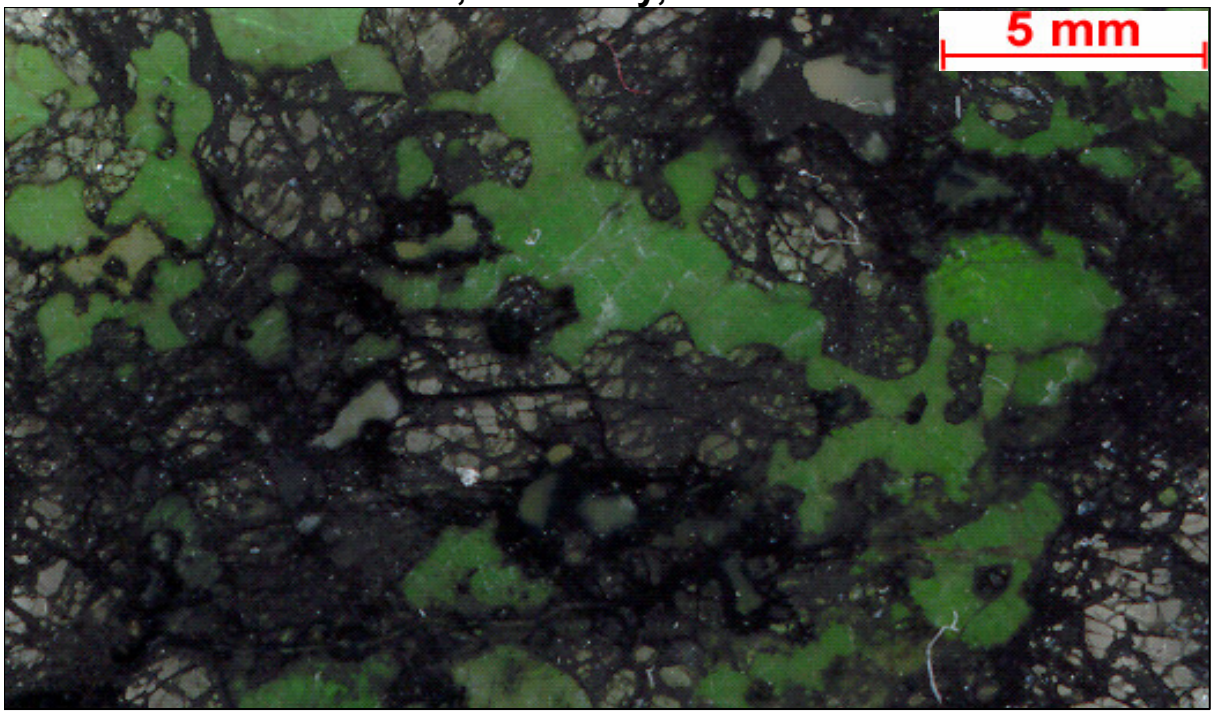

Granular, coarse-grained with 65 % intensely cracked olivine (9.2-1.2 mm) with serpentine along grain boundaries and in cracks and 32 % amoeboidal clinopyroxene (5.7 mm-450 µm) crystallized along olivine margins enclosing and replacing olivine, 1.5 % phlogopite (560-40 µm), 1.5 % ilmenite and chromite (185-5 µm).

Representative mineral major element composition [wt. %]

	ol			**cpx**			**cr-spl**
SiO_2	40.49	40.66	40.64	54.41	54.62	54.43	0.09
TiO_2	<dl	<dl	0.08	0.41	0.40	0.41	1.57
Al_2O_3	<dl	<dl	<dl	2.61	2.25	2.52	13.06
Cr_2O_3	<dl	<dl	0.06	2.12	2.16	2.30	52.03
V_2O_3	nd	nd	nd	nd	nd	nd	0.33
BaO	nd	nd	nd	nd	nd	nd	nd
CaO	0.04	0.04	0.05	18.35	19.04	18.32	nd
FeO	8.38	8.58	8.53	2.72	2.59	2.70	16.48
MgO	50.18	50.13	50.19	16.08	16.02	15.83	nd
MnO	0.12	0.08	0.11	0.10	0.07	0.10	14.67
NiO	0.29	0.34	0.29	<dl	<dl	<dl	0.25
SrO	nd	nd	nd	nd	nd	nd	0.09
Na_2O	<dl	<dl	<dl	2.61	2.47	2.63	nd
K_2O	<dl	<dl	<dl	<dl	0.03	<dl	nd
Cl	nd	nd	nd	nd	nd	nd	nd
F	nd	nd	nd	nd	nd	nd	nd
total	99.50	99.84	99.94	99.41	99.65	99.24	98.57
Mg/(Mg+Fe)	0.92	0.92	0.92	0.91	0.92	0.91	0.68
Cr/(Cr+Al)	-	-	-	-	-	-	0.73
Ilm	-	-	-	-	-	-	-
Gk	-	-	-	-	-	-	-
Hem	-	-	-	-	-	-	-

Representative mineral trace element composition [ppm]

	ol			**cpx**		
Cr	177	176	181	11576	14486	8738
Mn	903	908	908	nd	nd	nd
Co	124	132	124	nd	nd	nd
Ni	2272	2563	2275	240	240	246
Cu	1.81	1.74	1.70	nd	nd	nd
Zn	65.8	69.8	65.8	nd	nd	nd
Ga	0.115	0.104	0.101	nd	nd	nd
Ti	208	196	206	2832	2784	2524
V	4.44	4.35	4.76	274	270	267
Zr	0.282	0.233	0.265	78.3	71.6	63.9
Nb	0.0918	0.0696	0.0821	0.408	0.548	0.345
Hf	0.0086	<0.0219	0.0089	4.70	3.88	3.27
Ta	0.0072	0.0076	0.0029	0.0356	0.0449	0.0302
La	nd	nd	nd	1.78	1.69	1.64
Ce	0.0047	<0.0074	0.0034	7.00	6.27	6.32
Pr	nd	nd	nd	1.40	1.24	1.25
Nd	nd	nd	nd	7.92	7.21	7.27
Sm	nd	nd	nd	2.25	1.99	2.08
Eu	nd	nd	nd	0.723	0.611	0.653
Gd	nd	nd	nd	2.21	1.94	1.99
Tb	nd	nd	nd	0.270	0.240	0.232
Dy	nd	nd	nd	1.44	1.24	1.29
Ho	nd	nd	nd	0.208	0.173	0.171
Er	nd	nd	nd	0.419	0.372	0.361
Tm	nd	nd	nd	0.0399	0.0360	0.0368
Yb	nd	nd	nd	0.179	0.193	0.188
Lu	nd	nd	nd	0.0204	0.0207	0.0180
Sc	3.25	2.84	2.99	35.7	36.5	37.4
Rb	nd	nd	nd	0.0294	nd	0.0400
Sr	0.0112	<0.0101	0.0064	103	97.05	98.88
Y	0.0025	0.0103	0.0031	4.72	4.22	4.17
Ba	<0.0140	<0.063	0.0045	0.906	nd	1.04
Th	nd	nd	nd	0.0328	nd	0.0301
U	nd	nd	nd	0.0094	0.0096	0.0079
Li	2.56	2.42	2.47	nd	nd	nd
B	0.595	0.580	0.760	nd	nd	nd
Al	45.8	43.4	47.5	nd	nd	nd
Ca	162	160	158	IST	IST	IST

AJE400: wehrlite xenolith, Kimberely, RSA

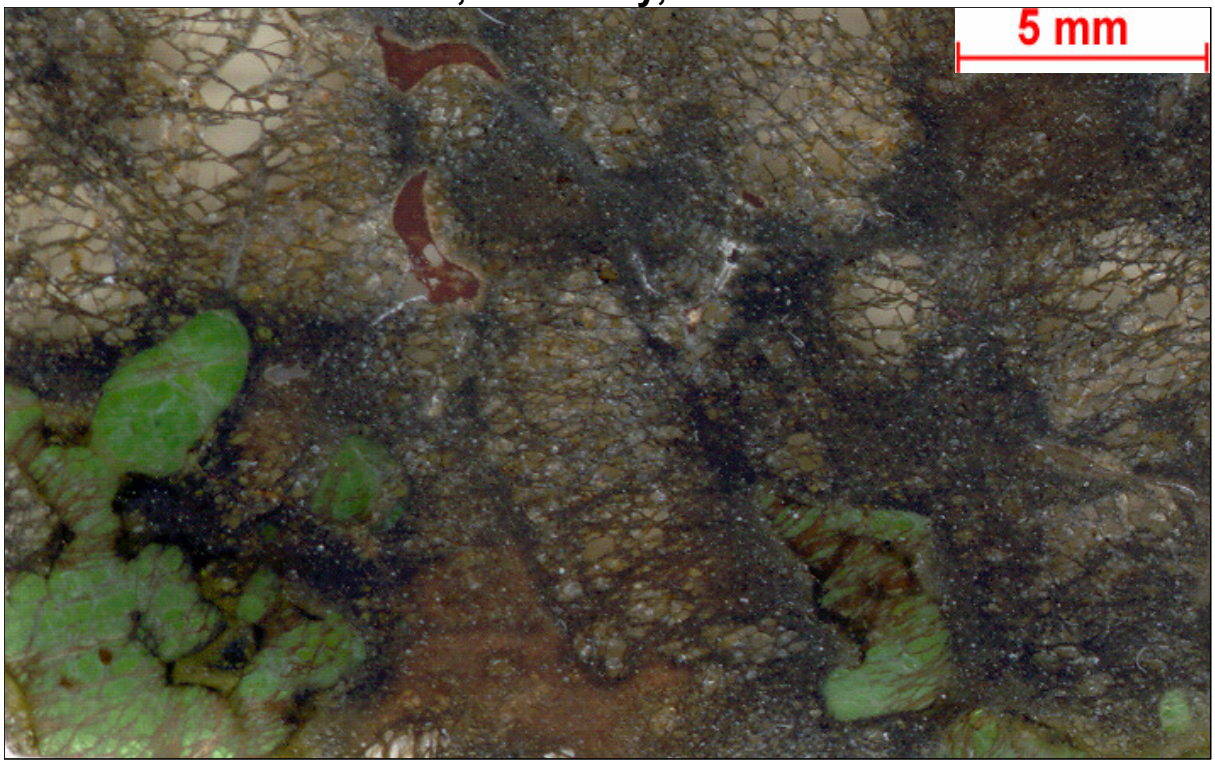

Porphyroclastic wehrlite with 70% coarse grained olivine porphyroclasts (18-3 mm) surrounded by 10% fine-grained olivine neoblasts (460-5 µm), 16% clinopyroxene (12-1 µm), 3% phlogopoite (450-400 µm) and 2% spinel (1 mm-5 µm).

Representative mineral major element composition [wt. %]

	ol-pc			**ol-nb**			**cpx**			**phl**			**cr-spl**	
SiO_2	40.53	40.60	40.39	40.42	40.56	40.39	54.39	54.57	54.35	40.92	40.86	41.31	<dl	<dl
TiO_2	<dl	<dl	<dl	<dl	<dl	<dl	0.36	0.38	0.42	1.94	1.93	1.91	3.07	3.40
Al_2O_3	<dl	<dl	<dl	<dl	<dl	<dl	1.98	2.05	2.43	12.74	12.91	12.69	11.61	5.18
Cr_2O_3	<dl	0.04	<dl	0.04	<dl	<dl	2.17	2.19	2.22	0.68	0.84	0.80	48.42	55.80
V_2O_3	nd	nd	nd	nd	nd	nd	nd	nd	nd	nd	nd	nd	0.27	0.18
BaO	nd	nd	nd	nd	nd	nd	nd	nd	nd	<dl	<dl	<dl	nd	nd
CaO	<dl	<dl	<dl	<dl	0.05	<dl	18.77	18.56	18.01	0.05	<dl	<dl	nd	nd
FeO	9.30	9.22	9.30	9.15	9.30	9.21	2.90	3.00	2.95	3.64	3.62	3.33	21.40	22.45
MgO	50.04	49.42	50.19	49.86	49.67	50.04	16.34	16.50	16.47	23.74	24.74	24.61	12.87	11.69
MnO	0.13	0.15	0.13	0.09	0.09	0.08	0.08	0.07	0.08	<dl	<dl	<dl	0.28	0.23
NiO	0.40	0.33	0.34	0.33	0.35	0.36	0.10	<dl	<dl	0.21	nd	nd	0.19	0.18
K_2O	<dl	<dl	<dl	<dl	<dl	<dl	<dl	<dl	<dl	10.16	9.75	10.16	nd	nd
Na_2O	<dl	0.03	0.03	<dl	<dl	<dl	2.41	2.44	2.57	0.40	0.48	0.22	nd	nd
Cl	nd	nd	nd	nd	nd	nd	nd	nd	nd	0.04	0.04	0.05	nd	nd
F	nd	nd	nd	nd	nd	nd	nd	nd	nd	0.42	0.45	0.44	nd	nd
total	100.40	99.79	100.38	99.90	100.03	100.09	99.50	99.76	99.50	94.95	95.61	95.53	98.10	99.11
Mg#	0.92	0.91	0.92	0.92	0.91	0.92	0.91	0.91	0.91	-	-	-	0.59	0.54
Cr#	-	-	-	-	-	-	-	-	-	-	-	-	0.74	0.88

Representative mineral trace element composition [ppm]

	ol-pc			ol-nb			cpx		
Cr	197	192	196	197	194	198	10597	10736	9761
Mn	821	807	813	837	817	823	nd	nd	nd
Co	137	138	136	145	147	155	nd	nd	nd
Ni	2730	2770	2709	3069	3125	3292	265	267	265
Cu	1.79	1.87	1.78	1.98	2.14	1.96	nd	nd	nd
Zn	72.1	76.7	74.2	81.6	81.6	79.5	nd	nd	nd
Ga	0.161	0.159	0.143	0.160	0.167	0.150	nd	nd	nd
Ti	205	198	211	208	214	185	2957	2794	2405
V	5.67	5.64	5.82	5.68	5.61	5.92	290	254	204
Zr	0.252	0.239	0.263	0.264	0.254	0.290	75.2	66.9	53.2
Nb	0.0846	0.078	0.0868	0.0762	0.0880	0.0910	0.261	0.253	0.229
Hf	0.0050	<0.0066	<0.0066	0.0116	<0.036	<0.105	5.03	4.24	2.6
Ta	0.0065	0.0038	0.0054	0.0056	<0.0138	<0.036	0.0181	0.0293	0.0237
La	nd	nd	nd	nd	nd	nd	1.45	1.49	1.47
Ce	0.0017	<0.0029	0.0026	<0.0050	<0.0152	<0.040	5.61	5.71	5.44
Pr	nd	nd	nd	nd	nd	nd	1.18	1.28	1.17
Nd	nd	nd	nd	nd	nd	nd	7.63	7.55	6.97
Sm	nd	nd	nd	nd	nd	nd	2.15	2.14	2.01
Eu	nd	nd	nd	nd	nd	nd	0.624	0.664	0.589
Gd	nd	nd	nd	nd	nd	nd	2.08	2.04	1.72
Tb	nd	nd	nd	nd	nd	nd	0.273	0.262	0.218
Dy	nd	nd	nd	nd	nd	nd	1.37	1.37	1.13
Ho	nd	nd	nd	nd	nd	nd	0.197	0.203	0.158
Er	nd	nd	nd	nd	nd	nd	0.386	0.391	0.318
Tm	nd	nd	nd	nd	nd	nd	0.0241	0.0375	0.0306
Yb	nd	nd	nd	nd	nd	nd	0.200	0.230	0.151
Lu	nd	nd	nd	nd	nd	nd	0.0155	0.0193	0.0181
Sc	3.12	2.87	2.384	2.82	2.95	2.38	31.9	28.7	26.4
Rb	nd	nd	nd	nd	nd	nd	<0.0216	<0.0069	<0.0093
Sr	0.0029	<0.0041	0.0036	<0.0073	<0.0183	<0.056	92.4	95.0	99.6
Y	0.0042	0.0046	0.0070	<0.0061	<0.0203	<0.051	4.88	4.43	3.74
Ba	<0.0149	<0.0227	<0.0235	<0.035	0.138	<0.31	0.0622	0.0500	0.0440
Th	nd	nd	nd	nd	nd	nd	<0.0100	0.0213	0.0185
U	nd	nd	nd	nd	nd	nd	<0.0065	0.0061	0.0033
Li	2.43	2.38	2.44	2.42	2.33	2.27	nd	nd	nd
B	0.530	0.620	0.800	0.760	1.250	<1.95	nd	nd	nd
Al	56.5	56.0	56.1	61.3	59.8	61.3	nd	nd	nd
Ca	158	136	159	156	158	<181	IST	IST	IST

AJE401: grt-wehrlite xenolith, Kimberley, RSA

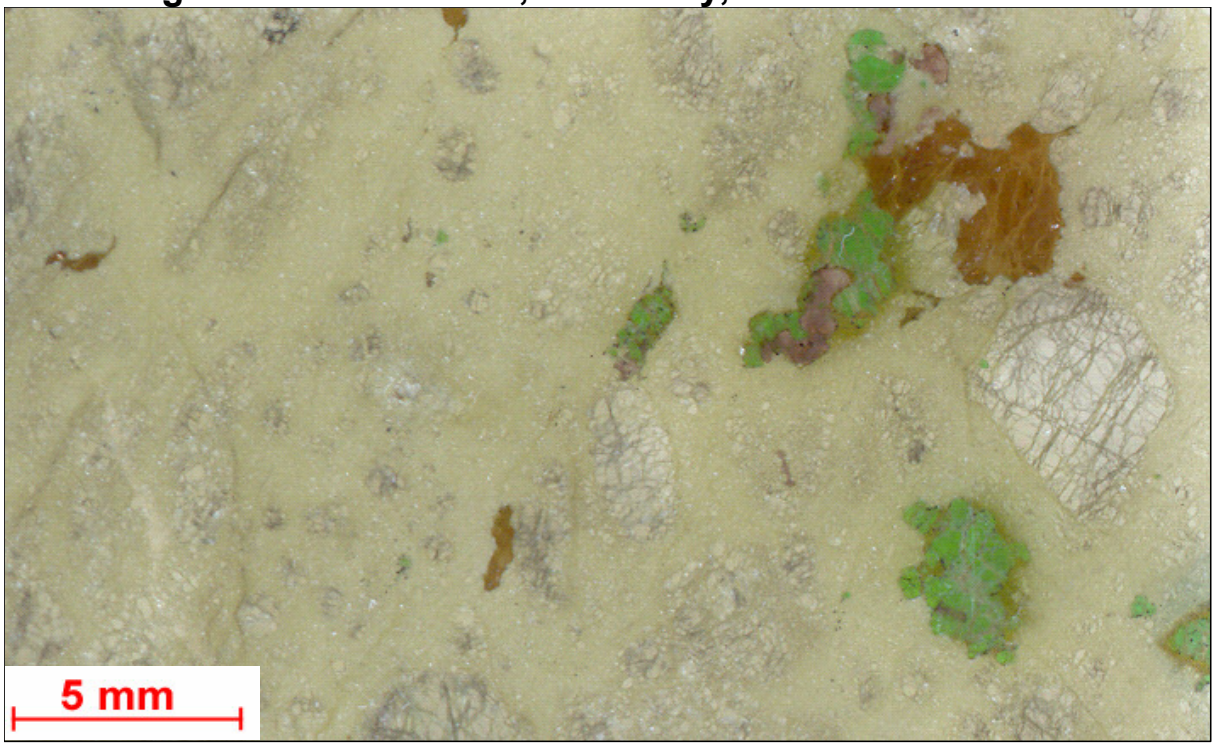

Porphyroclastic wehrlite with 22% olivine porphyroclasts (10 mm-100 µm) and patches of clinopyroxene (3%, 4 mm-90 µm), garnet (1%, 2 mm-50 µm), phlogopite (2%, 5 mm-10 µm) surounded by olivine neoblasts (72%, 300-5 µm) and intergrown with spinel (<1%, 170-5 µm).

Representative mineral major element composition [wt. %]

	ol-pc			**ol-nb**			**cpx**			**grt**		
SiO_2	40.80	41.10	40.87	40.99	40.83	41.11	54.33	54.35	54.29	41.22	40.69	40.96
TiO_2	<dl	<dl	<dl	<dl	<dl	<dl	0.44	0.45	0.39	1.06	1.44	0.70
Al_2O_3	0.03	<dl	<dl	<dl	0.03	<dl	2.58	2.68	2.55	18.63	16.86	17.65
Cr_2O_3	0.04	0.05	0.06	0.04	0.06	0.04	3.61	3.76	3.59	4.89	5.91	6.24
V_2O_3	nd	nd	nd	nd	nd	nd	nd	nd	nd	nd	nd	nd
BaO	nd	nd	nd	nd	nd	nd	nd	nd	nd	nd	nd	nd
CaO	<dl	<dl	0.03	0.04	0.04	0.04	17.87	17.72	17.87	6.56	7.95	6.23
FeO	7.70	7.56	7.45	7.48	7.53	7.29	2.29	2.27	2.30	6.29	6.57	6.87
MgO	51.03	50.87	51.19	50.81	50.78	50.91	15.32	15.15	15.34	20.33	18.72	19.85
MnO	0.14	0.14	0.10	0.08	0.09	0.09	0.10	0.05	0.07	0.28	0.41	0.38
NiO	0.36	0.39	0.36	0.33	0.34	0.36	0.06	<dl	0.05	<dl	<dl	<dl
ZnO	nd	nd	nd	nd	nd	nd	nd	nd	nd	nd	nd	nd
K_2O	<dl	<dl	<dl	<dl	<dl	<dl	<dl	0.03	<dl	<dl	<dl	<dl
Na_2O	<dl	<dl	<dl	<dl	<dl	<dl	2.94	3.14	2.97	0.08	0.14	0.05
Cl	nd	nd	nd	nd	nd	nd	nd	nd	nd	nd	nd	nd
F	nd	nd	nd	nd	nd	nd	nd	nd	nd	nd	nd	nd
total	100.10	100.11	100.07	99.77	99.69	99.84	99.54	99.60	99.41	99.34	98.69	98.92
Mg/(Mg+Fe)	0.93	0.93	0.94	0.93	0.93	0.93	0.92	0.92	0.92	0.85	0.85	0.84
Cr/(Cr+Al)	-	-	-	-	-	-	-	-	-	-	-	-

Representative mineral major element composition [wt. %]

	phl			**cr**		
SiO_2	38.87	40.60	38.83	<dl	<dl	<dl
TiO_2	2.61	1.58	2.66	2.35	2.79	2.74
Al_2O_3	13.64	12.66	15.00	11.54	11.81	13.91
Cr_2O_3	2.19	1.24	1.95	53.32	51.77	49.14
V_2O_3	nd	nd	nd	0.24	0.26	0.25
BaO	0.03	0.02	0.27	nd	nd	nd
CaO	0.03	0.06	0.11	nd	nd	nd
FeO	2.96	2.78	2.98	17.26	17.42	17.80
MgO	23.11	24.13	23.22	14.28	14.75	15.17
MnO	0.05	0.05	0.00	0.20	0.22	0.22
NiO	0.16	0.17	nd	0.13	0.18	0.16
ZnO	nd	nd	nd	nd	nd	nd
K_2O	10.19	10.47	8.89	nd	nd	nd
Na_2O	0.36	0.16	0.87	nd	nd	nd
Cl	0.03	0.06	0.01	nd	nd	nd
F	0.31	0.36	0.23	nd	nd	nd
total	94.54	94.34	95.02	99.32	99.20	99.39
Mg/(Mg+Fe)	0.93	0.94	0.93	0.65	0.66	0.67
Cr/(Cr+Al)	-	-	-	0.76	0.75	0.70

Representative mineral trace element composition [ppm]

	ol-pc core			**ol-pc rim**			**ol-nb**			**cpx**		
Cr	313	314	298	299	304	284	285	270	283	18534	18337	16673
Mn	848	857	841	797	815	784	807	745	754	nd	nd	nd
Co	125	124	126	126	129	131	125	131	131	nd	nd	nd
Ni	2685	2628	2784	2731	2842	2898	2705	2823	2878	237	241	234
Cu	1.58	1.62	1.56	1.13	1.53	2.01	1.94	1.70	1.52	nd	nd	nd
Zn	51.5	51.7	54.7	47.8	53.2	54.4	51.3	48.8	48.8	nd	nd	nd
Ga	0.105	0.0810	0.0960	0.127	0.125	0.110	0.145	0.143	<dl	nd	nd	nd
Ti	228	232	215	218	223	172	188	160	163	2518	2623	2454
V	4.97	4.70	4.45	4.61	4.60	5.88	5.56	4.80	5.48	266	263	263
Zr	0.280	0.279	0.339	0.431	0.240	0.202	0.241	0.274	0.221	54.2	64.8	58.8
Nb	0.0934	0.0777	0.106	0.117	0.0710	0.0390	0.0804	0.0630	0.0290	0.665	<dl	0.330
Hf	<0.0076	0.0070	0.0142	<0.095	<0.046	<0.046	0.0023	<dl	0.0030	3.28	3.39	3.07
Ta	0.0028	0.0033	<0.004	<0.036	<0.014	<0.017	0.0114	<dl	<dl	0.0417	<dl	0.0187
La	nd	nd	nd	nd	nd	nd	nd	nd	nd	1.53	<dl	1.48
Ce	0.0028	0.0036	<0.005	<0.040	<0.015	<0.017	0.0039	<dl	<dl	5.46	<dl	5.83
Pr	nd	nd	nd	nd	nd	nd	nd	nd	nd	1.09	<dl	1.17
Nd	nd	nd	nd	nd	nd	nd	nd	nd	nd	6.12	8.46	6.58
Sm	nd	nd	nd	nd	nd	nd	nd	nd	nd	1.70	2.27	1.86
Eu	nd	nd	nd	nd	nd	nd	nd	nd	nd	0.531	0.645	0.586
Gd	nd	nd	nd	nd	nd	nd	nd	nd	nd	1.60	1.81	1.72
Tb	nd	nd	nd	nd	nd	nd	nd	nd	nd	0.200	0.243	0.226
Dy	nd	nd	nd	nd	nd	nd	nd	nd	nd	1.01	1.24	1.08
Ho	nd	nd	nd	nd	nd	nd	nd	nd	nd	0.143	0.153	0.148
Er	nd	nd	nd	nd	nd	nd	nd	nd	nd	0.294	0.315	0.331
Tm	nd	nd	nd	nd	nd	nd	nd	nd	nd	0.0370	0.0279	0.0232
Yb	nd	nd	nd	nd	nd	nd	nd	nd	nd	0.128	0.177	0.149
Lu	nd	nd	nd	nd	nd	nd	nd	nd	nd	0.0188	0.0153	0.0228
Sc	2.20	2.22	2.05	<dl	2.24	2.58	3.62	3.49	3.18	31.9	31.7	33.1
Rb	nd	nd	nd	nd	nd	nd	nd	nd	nd	0.206		0.0810
Sr	0.0054	<0.003	0.0106	<0.050	<dl	<dl	0.0076	<dl	0.0060	85.6	110	100
Y	0.0082	0.0064	0.0067	<0.041	<0.017	<0.020	0.0032	<dl	<dl	3.38	3.86	3.60
Ba	<0.023	<0.018	<0.045	<0.300	<0.134	<0.148	<dl	<dl	<dl	3.79	<dl	1.14
Th	nd	nd	nd	nd	nd	nd	nd	nd	nd	0.0590	<dl	0.0312
U	nd	nd	nd	nd	nd	nd	nd	nd	nd	0.0146	<dl	0.0089
Li	2.06	2.18	2.00	2.17	2.24	1.91	2.00	1.86	1.65	nd	nd	nd
B	1.00	1.14	1.32	<dl	1.27	<0.99	3.17	<dl	2.70	nd	nd	nd
Al	68.3	61.7	57.4	81.1	61.5	<dl	90.9	90.4	85.6	nd	nd	nd
Ca	166	179	152	265	181	235	205	181	<dl	IST	IST	IST

Representative mineral trace element composition [ppm]

	grt			phl		
Cr	69906	46783	25546	6504	6593	6073
Mn	4388	2799	nd	nd	nd	nd
Co	69.7	42.7	nd	nd	nd	nd
Ni	115	95.9	51.5	1017	1012	957
Cu	nd	nd	nd	nd	nd	nd
Zn	34.8	18.7	nd	nd	nd	nd
Ga						
Ti	8388	6996	6686	10924	11184	9941
V	564	365	299	82.4	87.7	76.1
Zr	320	338	254	3.89	5.25	4.69
Nb	0.92	0.54	0.349	5.09	5.02	4.94
Hf	7.65	9.53	6.83	0.132	0.174	0.164
Ta	<0.080	<0.14	0.0588	0.295	0.348	0.317
La	0.280	0.390	0.0376	<0.0089	0.0278	0.0980
Ce	1.03	0.360	0.322	0.542	0.0382	0.158
Pr	0.289	0.0970	0.150	0.0092	0.0157	0.0175
Nd	1.88	1.95	1.52	<0.037	0.0260	0.0560
Sm	1.38	1.11	1.53	0.019	<0.029	<0.00
Eu	1.09	0.980	0.849	<0.0150	0.0193	0.0106
Gd	4.26	6.98	3.55	<0.024	0.0050	0.0270
Tb	0.830	1.16	0.791	<0.0076	<0.002	<0.0017
Dy	8.05	9.13	6.10	<0.0179	<0.018	<0.00
Ho	1.95	1.72	1.33	<0.0128	<0.004	<0.00118
Er	6.19	6.01	3.75	<0.0090	<0.007	<0.0034
Tm	1.07	0.84	0.465	<0.0058	<0.004	<0.00156
Yb	6.28	6.58	2.83	<0.0129	<0.015	0.0057
Lu	0.710	0.930	0.370	<0.0071	<0.002	<0.00103
Sc	195	172	106	3.76	3.68	4.03
Rb	nd	nd	0.089	539	553	525
Sr	1.60	<0.60	0.571	8.75	7.55	6.82
Y	51.0	50.5	31.9	<0.0217	0.0125	0.0157
Ba	<1.04	0.740	0.0430	194	194	179
Th	<0.096	<0.090	0.0091	<dl	0.0076	0.0102
U	0.0584	<0.062	0.0238	<dl	0.0008	0.0076
Li	0.79	<0.63	nd	nd	nd	nd
B	nd	nd	nd	nd	nd	nd
Al	nd	nd	nd	nd	nd	nd
Ca	IST	IST	IST	<139.33	199	228

AJE410: Fe-rich dunite xenolith, Kimberley, RSA

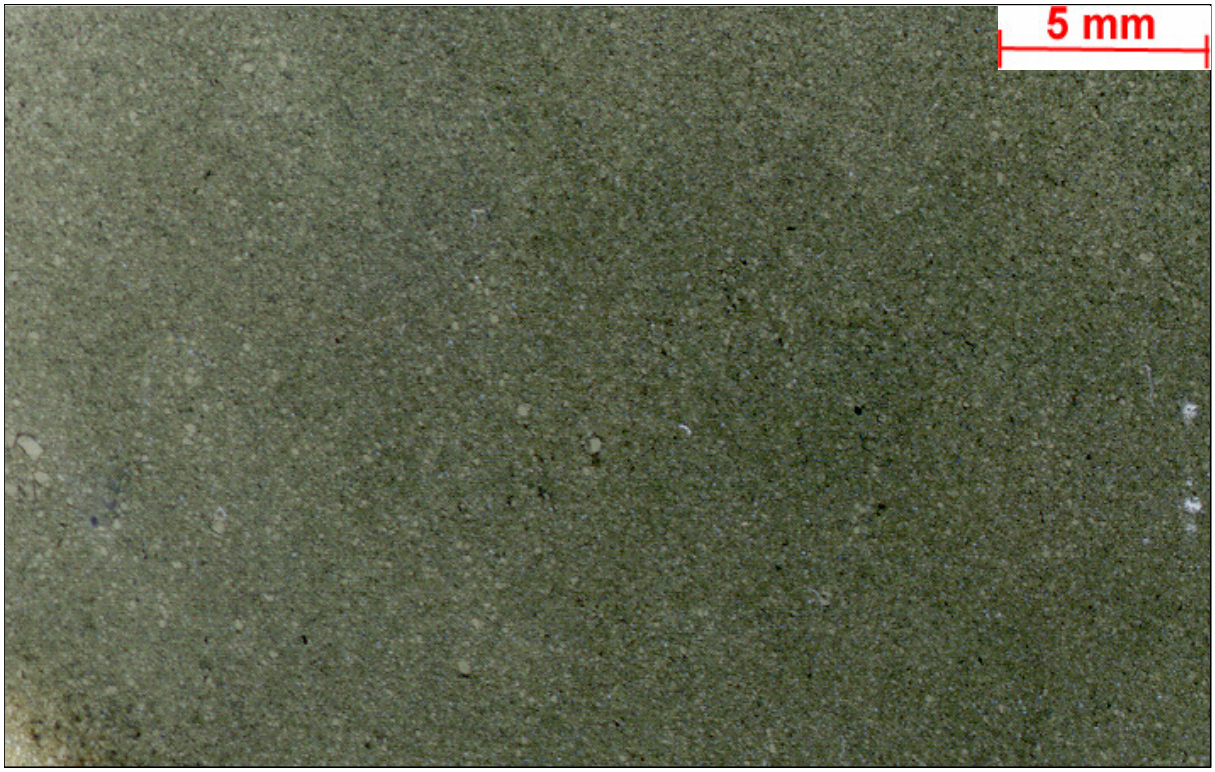

Fine-grained, granular dunite xenolith with 98% olivine (330-5 µm), ilmenite and spinel (300-5 µm).

Representative mineral major element composition [wt. %]

	ol			**ilm**			**spl**		
SiO_2	39.67	39.42	39.61	<dl	<dl	0.05	<dl	<dl	<dl
TiO_2	<dl	<dl	<dl	52.87	53.44	52.01	7.42	6.73	6.93
Al_2O_3	<dl	<dl	<dl	0.20	0.17	0.14	4.09	7.21	6.16
Cr_2O_3	0.04	0.03	0.05	3.79	3.23	4.04	41.20	40.93	42.03
V_2O_3	nd	nd	nd	0.02	0.08	<dl	0.26	0.18	0.27
CaO	0.06	0.06	0.06	nd	0.04	0.06	nd	nd	<dl
CoO	nd	nd	nd	nd	0.06	0.04	nd	nd	0.03
FeO	13.22	13.16	12.84	29.67	29.01	29.95	34.10	32.47	32.70
MgO	46.39	46.14	46.58	12.30	13.33	12.68	10.03	10.25	10.86
MnO	0.12	0.13	0.12	0.22	0.24	0.20	0.25	0.18	0.23
NiO	0.28	0.31	0.32	0.21	0.25	0.27	0.30	0.25	0.23
ZnO	nd	nd	nd	nd	0.04	0.00	nd	nd	0.09
K_2O	<dl	<dl	<dl	nd	0.00	0.00	nd	nd	<dl
Na_2O	<dl	<dl	<dl	nd	<dl	0.11	nd	nd	<dl
total	99.78	99.26	99.57	99.27	99.89	99.55	97.66	98.20	99.53
Mg/(Mg+Fe)	0.87	0.87	0.88	-	-	-	0.44	0.44	0.47
Cr/(Cr+Al)	-	-	-	-	-	-	0.87	0.79	0.82
Ilm	-	-	-	0.51	0.46	0.46	-	-	-
Gk	-	-	-	0.44	0.47	0.46	-	-	-

Representative mineral trace element composition [ppm]

	ol			**ilm**			**spl**	
Cr	202	203	187	27639	28330	32868	283140	283140
Mn	741	742	743	2404	2466	2325	1843	1764
Co	139	139	138	319	319	307	414	376
Ni	2082	2120	1973	2759	2723	2885	3069	3057
Cu	1.73	1.80	2.62	71.4	55.5	61.5	96.3	112
Zn	65.7	64.9	59.3	508	363	510	2291	2189
Ga	<0.139	<0.169	<0.206	9.79	8.27	6.08	80.7	77.0
Sn	nd	nd	nd	9.85	2.38	<5.63	6.78	4.57
W	nd	nd	nd	1.74	<2.26	<2.27	<1.11	<0.93
Ti	148	124	112	IST	IST	IST	35214	35510
V	3.46	3.52	3.74	1016	958	1100	1434	1580
Zr	0.247	0.351	0.236	832	851	819	11.2	18.9
Nb	0.0800	<0.066	<0.094	559	539	526	1.80	4.12
Hf	<0.095	<0.105	<0.129	27.8	21.3	25.6	1.62	<0.50
Ta	<0.029	<0.036	<0.028	82.1	76.8	70.9	0.430	0.660
La	nd	nd	nd	nd	nd	nd	nd	nd
Ce	<0.040	<0.042	<0.042	nd	nd	nd	nd	nd
Pr	nd	nd	nd	nd	nd	nd	nd	nd
Nd	nd	nd	nd	nd	nd	nd	nd	nd
Sm	nd	nd	nd	nd	nd	nd	nd	nd
Eu	nd	nd	nd	nd	nd	nd	nd	nd
Gd	nd	nd	nd	nd	nd	nd	nd	nd
Tb	nd	nd	nd	nd	nd	nd	nd	nd
Dy	nd	nd	nd	nd	nd	nd	nd	nd
Ho	nd	nd	nd	nd	nd	nd	nd	nd
Er	nd	nd	nd	nd	nd	nd	nd	nd
Tm	nd	nd	nd	nd	nd	nd	nd	nd
Yb	<0.154	<0.165	<0.147	nd	nd	nd	nd	nd
Lu	nd	nd	nd	nd	nd	nd	nd	nd
Sc	2.65	3.73	3.88	27.9	30.3	27.3	4.51	<3.65
Rb	nd	nd	nd	nd	nd	nd	nd	nd
Sr	<0.078	<0.080	<0.070	nd	nd	nd	nd	nd
Y	<0.059	<0.055	<0.083	0.610	0.440	0.750	2.55	<0.42
Ba	<0.53	0.0073	<0.43	<2.64	<0.71	<6.50	<2.04	<1.98
Th	nd	nd	nd	<0.18	<0.091	<0.28	<0.18	<0.23
U	nd	nd	nd	0.173	<0.052	0.200	<0.149	<0.118
Li	3.78	3.46	4.35	4.43	2.87	5.95	<3.85	<1.32
B	<5.70	<5.22	<5.55	nd	nd	nd	nd	nd
Al	65.7	59.4	59.6	1324	1460	1469	57090	47608
Ca	<456.97	<427.71	<465.06	682	1040	<1139.2	1321	<608.36

DJ0214: wehrlite xenolith, Kimberley, RSA

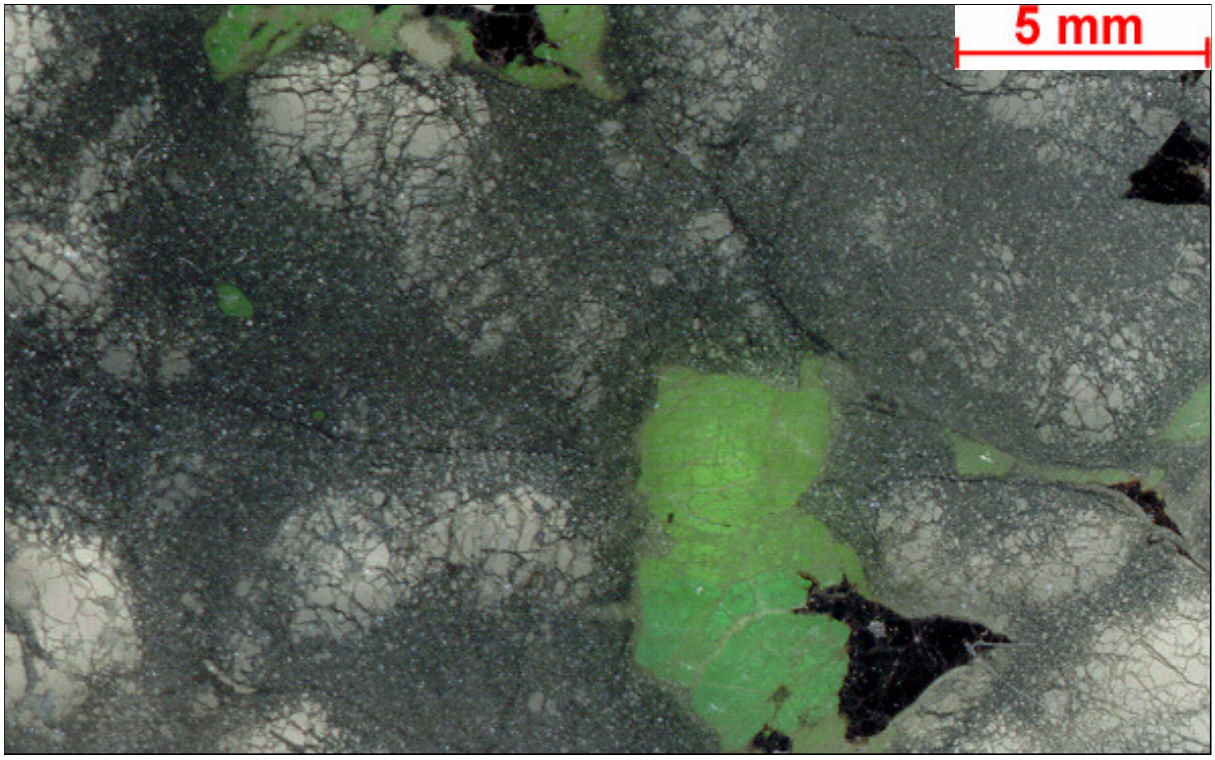

Porphyroclastic wehrlite xenolith with 29% olivine porphyroclasts (2 mm-300 µm) surrounded by olivine neoblasts (65%, 240-5 µm). Clinopyroxene crystallized along grain boundaries and in cracks (5 mm-600 µm) together with rutile and chromite (5 mm-100 µm).

Representative mineral major element composition [wt. %]

	ol-pc			**ol-nb**			**sec. opx around cpx**			**cpx**		
SiO_2	40.78	40.78	40.47	40.59	40.50	40.96	57.38	55.84	56.19	54.57	54.11	54.43
TiO_2	<dl	<dl	<dl	<dl	<dl	<dl	0.19	0.27	0.22	0.35	0.38	0.37
Al_2O_3	<dl	<dl	<dl	<dl	<dl	<dl	0.68	0.85	0.94	2.36	2.35	2.34
Cr_2O_3	0.05	<dl	0.06	0.05	0.05	0.04	0.59	1.07	1.34	3.49	3.55	3.62
V_2O_3	nd	nd	nd	nd	nd	nd	nd	nd	nd	nd	nd	nd
BaO	nd	nd	nd	nd	nd	nd	nd	nd	nd	nd	nd	nd
CaO	<dl	<dl	0.04	<dl	0.04	<dl	0.78	1.13	0.99	18.34	18.24	18.32
FeO	8.04	7.89	7.98	8.08	7.99	7.91	4.88	4.99	5.05	2.29	2.28	2.38
MgO	50.56	50.45	50.47	50.78	50.70	50.80	35.74	34.57	34.84	15.46	15.44	15.44
MnO	0.14	0.12	0.13	0.11	0.10	0.07	0.12	0.13	0.13	0.05	0.08	0.07
NiO	0.37	0.33	0.35	0.31	0.31	0.34	0.09	0.18	0.15	0.04	0.03	0.02
ZnO	nd	nd	nd	nd	nd	nd	nd	nd	nd	nd	nd	nd
K2O	<dl	<dl	<dl	<dl	<dl	<dl	<dl	<dl	<dl	0.03	0.01	0.02
Na_2O	<dl	<dl	<dl	<dl	<dl	<dl	0.13	0.19	0.25	2.84	3.01	2.82
Cl	nd	nd	nd	nd	nd	nd	nd	nd	nd	nd	nd	nd
F	nd	nd	nd	nd	nd	nd	nd	nd	nd	nd	nd	nd
total	99.93	99.58	99.50	99.92	99.70	100.11	100.58	99.21	100.09	99.81	99.48	99.83
Mg/(Mg+Fe)	0.93	0.93	0.93	0.93	0.93	0.93	0.93	0.93	0.92	0.92	0.92	0.92
Cr/(Cr+Al)	-	-	-	-	-	-	-	-	-	-	-	-
Ilm	-	-	-	-	-	-	-	-	-	-	-	-
Gk	-	-	-	-	-	-	-	-	-	-	-	-

Representative mineral major element composition [wt. %]

	sec. cpx			**spl**	**rutile**			**ilm**		**phl**		
SiO_2	53.00	53.09	53.33	<dl	<dl	<dl	<dl	<dl	0.04	41.51	40.34	40.37
TiO_2	0.44	0.42	0.37	3.32	90.56	92.37	91.58	48.23	50.77	2.58	3.09	2.95
Al_2O_3	2.46	2.62	2.70	7.08	0.18	<dl	0.07	0.22	0.53	12.19	12.77	12.31
Cr_2O_3	3.28	3.19	3.30	54.72	6.38	5.25	5.43	11.57	11.14	1.76	1.50	1.53
V_2O_3	nd	nd	nd	0.18	<dl	0.05	0.04	0.03	0.05	nd	nd	nd
BaO	nd	nd	nd	nd	nd	nd	nd	nd	nd	0.03	0.00	0.00
CaO	17.35	17.45	17.40	nd	<dl	<dl	nd	<dl	<dl	0.06	0.00	0.01
FeO	2.55	2.53	2.53	20.89	0.44	0.06	0.22	25.62	22.73	3.09	3.03	3.10
MgO	15.94	16.56	16.16	12.71	<dl	<dl	<dl	13.51	14.81	24.37	24.02	23.54
MnO	0.10	0.05	0.08	0.25	<dl	<dl	0.02	0.14	0.15	0.00	0.00	0.03
NiO	0.03	0.11	0.08	0.12	<dl	<dl	<dl	0.32	0.29	nd	nd	0.16
ZnO	nd	nd	nd	nd	0.42	0.27	nd	0.37	0.34	nd	nd	nd
K2O	0.05	0.20	0.02	nd	<dl	<dl	nd	<dl	<dl	9.61	9.84	10.30
Na_2O	2.71	2.60	2.73	nd	<dl	<dl	nd	0.07	0.04	0.54	0.47	0.47
Cl	nd	nd	nd	nd	nd	nd	nd	nd	nd	0.31	0.01	0.00
F	nd	nd	nd	nd	nd	nd	nd	nd	nd	0.60	0.50	0.42
total	97.90	98.82	98.70	99.28	97.98	97.99	97.36	100.07	100.88	96.65	95.57	95.19
Mg/(Mg+Fe)	0.92	0.92	0.92	0.58	-	-	-	-	-	-	-	-
Cr/(Cr+Al)	-	-	-	0.84	-	-	-	-	-	-	-	-
Ilm	-	-	-	-	-	-	-	0.37	0.37	-	-	-
Gk	-	-	-	-	-	-	-	0.52	0.56	-	-	-

Representative mineral trace element composition [ppm]

	ol-pc core			**ol-pc rim**			**ol-nb**			**cpx**		
Cr	272	279	279	268	289	252	254	268	246	17692	19171	20632
Mn	815	815	819	811	761	745	755	820	746	nd	nd	nd
Co	122	122	122	131	129	125	123	125	123	nd	nd	nd
Ni	2605	2380	2393	2847	2815	2696	2634	2679	2656	214	216	218
Cu	1.45	1.48	1.48	1.81	1.62	1.13	1.74	1.49	1.77	nd	nd	nd
Zn	61.0	58.0	58.4	63.8	61.0	59.2	51.7	59.1	51.9	nd	nd	nd
Ga	0.0891	0.106	0.104	0.109	<0.116	<0.098	<0.116	0.132	<0.131	nd	nd	nd
Ge	nd	nd	nd	nd	nd	nd	nd	nd	nd	nd	nd	nd
Mo	nd	nd	nd	nd	nd	nd	nd	nd	nd	nd	nd	nd
Sn	nd	nd	nd	nd	nd	nd	nd	nd	nd	nd	nd	nd
Sb	nd	nd	nd	nd	nd	nd	nd	nd	nd	nd	nd	nd
W	nd	nd	nd	nd	nd	nd	nd	nd	nd	nd	nd	nd
Ti	202	206	210	189	180	175	200	210	187	2761	2711	3010
V	4.36	4.44	4.46	4.25	4.52	4.57	4.18	4.39	3.90	277	252	266
Zr	0.295	0.302	0.322	0.232	0.275	0.215	0.372	0.294	0.255	89.6	78.2	94.3
Nb	0.0916	0.0917	0.0919	0.0590	0.149	0.0590	0.164	0.142	0.083	0.373	0.348	1.04
Hf	<0.0096	0.0091	0.0068	<0.044	<0.080	<0.084	<0.086	<0.033	<0.108	4.96	3.91	5.31
Ta	0.0055	0.0059	0.0075	<0.0125	<0.030	<0.030	<0.032	0.0224	<0.031	0.0298	0.0224	0.0714
La	nd	nd	nd	nd	nd	nd	nd	nd	nd	1.33	1.42	1.49
Ce	<0.0033	<0.002	0.0090	<0.0148	<0.028	<0.029	<0.04	0.0031	<0.034	5.38	5.71	5.61
Pr	nd	nd	nd	nd	nd	nd	nd	nd	nd	1.16	1.20	1.27
Nd	nd	nd	nd	nd	nd	nd	nd	nd	nd	6.77	7.21	7.56
Sm	nd	nd	nd	nd	nd	nd	nd	nd	nd	2.03	2.06	2.26
Eu	nd	nd	nd	nd	nd	nd	nd	nd	nd	0.636	0.604	0.669
Gd	nd	nd	nd	nd	nd	nd	nd	nd	nd	1.93	1.95	2.00
Tb	nd	nd	nd	nd	nd	nd	nd	nd	nd	0.259	0.247	0.252
Dy	nd	nd	nd	nd	nd	nd	nd	nd	nd	1.30	1.12	1.40
Ho	nd	nd	nd	nd	nd	nd	nd	nd	nd	0.200	0.187	0.195
Er	nd	nd	nd	nd	nd	nd	nd	nd	nd	0.401	0.368	0.401
Tm	nd	nd	nd	nd	nd	nd	nd	nd	nd	0.0462	0.0378	0.0349
Yb	nd	nd	nd	nd	nd	nd	nd	nd	nd	0.175	0.212	0.180
Lu	nd	nd	nd	nd	nd	nd	nd	nd	nd	0.0171	0.0229	0.0225
Sc	2.82	2.89	2.91	2.57	2.58	2.33	2.00	3.11	2.73	35.9	37.5	36.3
Rb	nd	nd	nd	nd	nd	nd	nd	nd	nd	<0.0135	<0.008	0.449
Sr	<0.0052	0.0030	0.0417	<0.0206	<0.051	<0.039	0.0500	<0.021	<0.053	96.4	108	99.2
Y	<0.0047	0.0045	0.0064	<0.0195	<0.040	<0.045	<0.049	0.0200	<0.048	4.56	4.18	4.76
Ba	<0.034	<0.017	0.0390	<0.118	<0.31	<0.23	<0.32	<0.117	<0.30	0.135	0.115	3.86
Th	nd	nd	nd	nd	nd	nd	nd	nd	nd	0.0102	0.0187	0.0289
U	nd	nd	nd	nd	nd	nd	nd	nd	nd	0.0063	0.0054	0.0057
Li	2.25	2.30	2.33	2.20	2.08	2.36	1.85	2.27	1.69	nd	nd	nd
B	0.970	0.620	0.800	1.20	<1.79	<1.52	<1.78	2.45	2.11	nd	nd	nd
Al	52.0	53.3	54.7	50.1	54.0	54.6	50.8	58.5	52.5	nd	nd	nd
Ca	168	162	170	70.2	<160.7	150	<163.11	148	232	IST	IST	IST

Representative mineral trace element composition [ppm]

	rutile			**spl**	
Cr	49695	49733	53190	374327	374327
Mn	7.97	4.88	17.16	2147	2131
Co	2.75	2.20	2.33	295	298
Ni	42.1	34.3	32.1	1485	1539
Cu	7.30	9.12	8.80	28.9	29.4
Zn	11.8	15.4	15.5	948	871
Ga	2.97	2.22	2.59	85.3	85.1
Ge	0.554	0.435	0.429	0.97	1.03
Mo	13.6	13.8	13.8	0.127	0.164
Sn	32.2	34.2	35.3	1.47	1.81
Sb	0.284	0.262	0.322	0.477	0.990
W	12.3	12.0	12.1	0.016	0.0170
Ti	IST	IST	IST	21617	21081
V	1375	1398	1418	1556	1611
Zr	3619	3435	3654	4.83	5.93
Nb	12416	12439	12982	1.20	3.19
Hf	127	121	127	0.247	0.233
Ta	1729	1678	1759	0.0730	0.334
La	nd	nd	nd	nd	nd
Ce	nd	nd	nd	nd	nd
Pr	nd	nd	nd	nd	nd
Nd	nd	nd	nd	nd	nd
Sm	nd	nd	nd	nd	nd
Eu	nd	nd	nd	nd	nd
Gd	nd	nd	nd	nd	nd
Tb	nd	nd	nd	nd	nd
Dy	nd	nd	nd	nd	nd
Ho	nd	nd	nd	nd	nd
Er	nd	nd	nd	nd	nd
Tm	nd	nd	nd	nd	nd
Yb	nd	nd	nd	nd	nd
Lu	nd	nd	nd	nd	nd
Sc	9.35	8.80	9.76	2.26	2.77
Rb	nd	nd	nd	nd	nd
Sr	nd	nd	nd	nd	nd
Y	0.0631	0.0580	0.0560	0.0210	0.0570
Ba	<0.0069	<0.009	0.0220	<0.040	1.85
Th	0.0022	<0.002	0.0019	0.0070	0.0085
U	3.02	2.98	3.09	0.0051	0.0033
Li	0.465	0.471	0.372	1.14	1.31
B	nd	nd	nd	nd	nd
Al	2009	1347	1903	IST	IST
Ca	18.8	16.2	8.01	81.5	136

DJ0215: grt-websterite xenolith, Kimberley, RSA

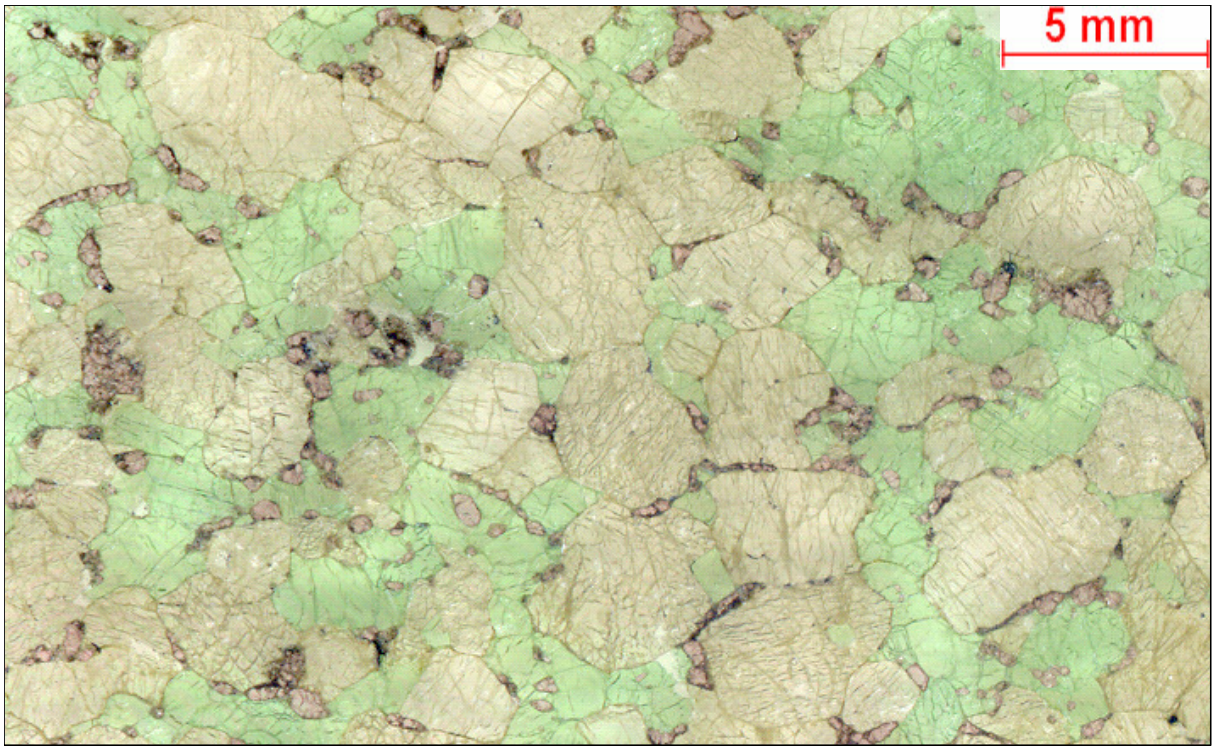

Granular websterite comprising 60% orthopyroxene (7 mm-200 µm), 32% clinopyroxene (5 mm-550 µm) and 8% garnet (2 mm-90 µm), which crystallized along pyroxene grain boundaries and within clinopyroxene.

Representative mineral major element composition [wt. %]

	opx			**cpx**			**grt**		
SiO_2	57.01	56.83	56.78	54.36	54.43	53.67	40.98	41.02	41.00
TiO_2	<dl	<dl	<dl	<dl	0.10	0.06	<dl	<dl	0.08
Al_2O_3	0.68	0.64	0.71	1.40	1.55	1.56	20.83	20.88	21.28
Cr_2O_3	0.16	0.15	0.23	0.85	0.81	0.86	2.63	2.86	2.50
BaO	nd	nd	nd	nd	nd	nd	nd	nd	nd
CaO	0.30	0.33	0.34	22.50	22.22	21.88	5.65	5.60	5.39
FeO	6.67	6.76	6.75	2.82	2.80	2.65	10.51	10.41	10.23
MgO	34.61	34.61	35.62	16.74	16.65	17.34	18.31	18.08	18.57
MnO	0.15	0.11	0.17	0.14	<dl	0.08	0.63	0.54	0.60
NiO	0.11	0.11	0.08	0.09	0.06	0.11	<dl	<dl	<dl
K_2O	<dl	<dl	<dl	<dl	<dl	<dl	<dl	<dl	<dl
Na_2O	<dl	0.05	0.06	1.19	1.16	1.25	0.03	<dl	0.04
Cl	nd	nd	nd	nd	nd	nd	nd	nd	nd
F	nd	nd	nd	nd	nd	nd	nd	nd	nd
total	99.69	99.59	100.75	100.08	99.78	99.46	99.57	99.39	99.69
Mg/(Mg+Fe)	0.90	0.90	0.90	0.91	0.91	0.92	0.76	0.76	0.76

Representative mineral trace element composition [ppm]

	opx			**cpx**			**grt**		
Cr	995	1015	989	5029	4424	4440	13811	13584	14424
Mn	nd	nd	nd	nd	nd	nd	nd	nd	nd
Co	nd	nd	nd	nd	nd	nd	nd	nd	nd
Ni	754	767	741	337	326	331	26.22	25.24	26.43
Cu	nd	nd	nd	nd	nd	nd	nd	nd	nd
Zn	nd	nd	nd	nd	nd	nd	nd	nd	nd
Ga	nd	nd	nd	nd	nd	nd	nd	nd	nd
Ti	229	229	233	375	351	353	397	415	437
V	40.9	42.2	40.2	248	229	236	162	165	175
Zr	0.258	0.253	0.237	17.9	14.6	15.4	25.9	40.9	40.6
Nb	0.194	0.180	0.218	0.390	0.308	0.288	0.195	0.321	0.269
Hf	<0.007	0.0093	0.0085	0.567	0.535	0.535	0.213	0.425	0.443
Ta	0.0277	0.0405	0.0340	0.0406	0.0459	0.0374	0.0115	0.0144	0.0131
La	0.0121	0.0254	0.0221	15.4	17.2	16.2	0.0498	0.102	0.095
Ce	0.0723	0.0850	0.0935	38.4	35.3	36.5	0.397	0.470	0.442
Pr	<d.l.	0.0109	0.0106	4.34	3.51	3.87	0.116	0.146	0.136
Nd	0.0344	0.0326	0.0393	14.4	10.7	12.5	0.812	1.09	1.01
Sm	<0.013	<0.0065	0.0220	1.57	1.11	1.33	0.466	0.611	0.701
Eu	<0.005	<0.0030	0.0034	0.335	0.231	0.280	0.177	0.252	0.236
Gd	<0.015	<0.0091	<0.0131	0.777	0.534	0.617	0.613	0.938	0.870
Tb	<0.004	0.0013	<0.00167	0.0628	0.0456	0.0378	0.139	0.170	0.179
Dy	<0.010	<0.0057	<0.0060	0.231	0.150	0.184	1.04	1.37	1.49
Ho	<0.005	0.0017	0.0010	0.0283	0.0179	0.0210	0.228	0.307	0.338
Er	<0.010	0.0083	0.0074	0.0562	0.0374	0.0508	0.732	0.950	0.949
Tm	<0.004	<0.00142	<0.00069	0.0036	0.0050	0.0052	0.132	0.128	0.142
Yb	<0.009	<0.0047	<0.0075	0.0146	<0.010	0.0208	0.890	1.01	0.973
Lu	<0.005	0.00104	<0.00155	0.0022	0.0046	0.0041	0.141	0.164	0.166
Sc	6.03	6.13	6.40	30.0	27.3	27.2	130	127	129
Rb	<0.014	<0.0094	<0.0162	<0.017	0.0780	<0.018	<0.0185	<0.025	0.0210
Sr	0.129	0.171	0.130	357	308	328	0.185	0.365	0.311
Y	<0.008	0.0084	0.0227	0.728	0.535	0.585	6.89	8.37	8.62
Ba	<0.019	0.112	<0.0095	0.059	0.106	0.184	<dl	0.139	<0.035
Th	<0.003	0.0083	0.0075	0.493	0.565	0.485	0.0156	<dl	0.0282
U	0.0024	0.0016	0.0023	0.0244	0.0254	0.0269	0.0315	0.0327	0.0321
Li	nd	nd	nd	nd	nd	nd	nd	nd	nd
B	nd	nd	nd	nd	nd	nd	nd	nd	nd
Al	nd	nd	nd	nd	nd	nd	nd	nd	nd
Ca	2172	2354	2357	IST	IST	IST	IST	IST	IST

DJ0216: grt-websterite, Kimberley, RSA

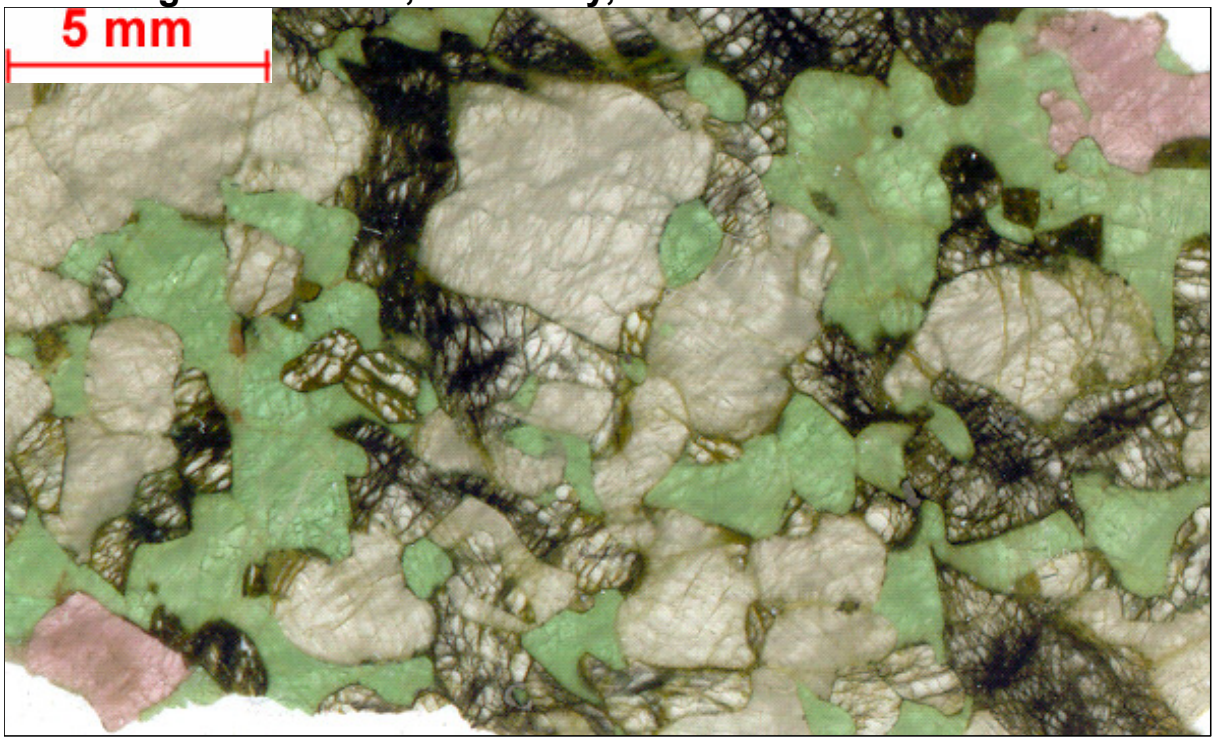

Granular websterite comprising 33% strongly serpentinised olivine (6-1 mm) that is surrounded and replaced by 40% orthopyroxene (6-2 mm), 23% clinopyroxene (6 mm-35 µm), 4% coarse garnet (6-3 mm), additionally phlogopite (900-350 µm) and serpentine.

Representative mineral major element composition [wt. %]

	ol			opx			cpx			grt		
SiO_2	40.05	40.09	40.26	56.96	56.81	56.91	54.18	54.58	54.22	41.07	41.19	41.16
TiO_2	<dl	<dl	0.05	0.08	0.14	0.08	0.19	0.18	0.16	0.11	0.11	0.12
Al_2O_3	<dl	<dl	<dl	0.71	0.63	0.64	2.39	2.47	2.56	20.93	21.56	21.04
Cr_2O_3	<dl	<dl	<dl	0.15	0.12	0.12	0.96	0.98	1.38	2.41	1.94	2.51
BaO	nd	nd	nd	nd	nd	nd	nd	nd	nd	nd	nd	nd
CaO	<dl	0.05	<dl	0.28	0.25	0.28	20.51	20.58	20.19	4.91	4.63	4.85
FeO	11.12	10.97	11.06	6.85	6.94	6.78	3.30	3.34	3.26	10.81	10.73	10.81
MgO	48.31	48.45	48.40	34.52	34.58	34.49	15.76	15.42	15.38	18.62	18.87	18.60
MnO	0.12	0.11	0.13	0.15	0.15	0.16	0.06	0.10	0.08	0.56	0.56	0.60
NiO	0.38	0.38	0.44	0.08	0.07	0.07	0.05	<dl	0.06	<dl	<dl	<dl
K_2O	<dl	<dl	<dl	<dl	<dl	<dl	<dl	<dl	<dl	<dl	<dl	<dl
Na_2O	<dl	<dl	<dl	0.11	0.07	0.08	2.04	2.15	2.23	<dl	<dl	<dl
Cl	nd	nd	nd	nd	nd	nd	nd	nd	nd	nd	nd	nd
F	nd	nd	nd	nd	nd	nd	nd	nd	nd	nd	nd	nd
total	99.98	100.05	100.34	99.89	99.76	99.60	99.44	99.80	99.53	99.42	99.58	99.69
Mg/(Mg+Fe)	0.90	0.90	0.90	0.90	0.90	0.90	0.89	0.89	0.89	0.75	0.76	0.75

major elements [wt. %]

	phl	
SiO_2	40.44	40.46
TiO_2	0.62	0.60
Al_2O_3	12.98	13.14
Cr_2O_3	0.43	0.42
BaO	0.52	0.47
CaO	0.15	<dl
FeO	3.95	3.79
MgO	24.50	24.52
MnO	<dl	<dl
NiO	0.21	0.22
K_2O	9.09	9.63
Na_2O	0.71	0.74
Cl	0.08	0.06
F	0.17	0.30
total	93.85	94.36
Mg/(Mg+Fe)	0.92	0.92

Representative mineral trace element composition [ppm]

	ol			**opx**			**cpx**			**grt**		
Cr	38.0	38.0	37.5	840	698	763	5687	5856	5329	13690	12108	26274
Mn	977	976	961	957	nd	nd	nd	nd	nd	nd	nd	nd
Co	168	168	167	62.8	nd	nd	nd	nd	nd	nd	nd	nd
Ni	3059	2983	3001	721	577	588	240	242	244	21.4	22.7	43.5
Cu	0.146	0.145	0.142	0.260	nd	nd	nd	nd	nd	nd	nd	nd
Zn	68.2	66.0	66.4	36.4	nd	nd	nd	nd	nd	nd	nd	nd
Ga	0.0233	0.0341	0.0311	2.22	nd	nd	nd	nd	nd	nd	nd	nd
Ti	127	121	136.43	419	403	387	1127	1134	1059	747	734	1688
V	2.70	2.82	2.75	29.1	27.2	29.2	303	302	296	112	119	251
Zr	0.237	0.191	0.233	0.283	0.205	0.271	49.6	46.8	40.9	18.5	26.1	48.3
Nb	0.57	0.52	0.59	0.0560	0.0640	0.0620		0.308	0.294	0.0930	0.0900	0.184
Hf	<dl	0.0007	0.0048	<dl	<0.0071	0.0109	1.63	1.65	1.33	0.122	0.211	0.366
Ta	0.0052	0.0175	0.0182	nd	<0.0069	0.0044	0.0267	0.0298	0.0222	0.0088	0.0065	0.0169
La	nd	nd	nd	nd	<0.0116	0.04	20.7	21.7	21.4	0.0273	0.145	0.0960
Ce	<dl	<dl	0.00	0.0860	0.0796	0.1250	58.9	59.8	57.0	0.397	0.503	0.842
Pr	nd	nd	Nd	nd	0.0083	0.0134	7.19	7.17	6.63	0.135	0.151	0.302
Nd	Nd	nd	nd	nd	0.0510	0.0560	24.1	23.6	21.6	0.959	0.939	2.360
Sm	nd	nd	nd	nd	<0.0229	0.0226	2.61	2.55	2.61	0.577	0.605	1.46
Eu	nd	nd	nd	nd	<0.0075	0.0066	0.594	0.598	0.561	0.286	0.335	0.741
Gd	nd	nd	nd	nd	<0.0178	<0.0200	1.78	1.71	1.69	1.61	1.51	3.84
Tb	nd	nd	nd	nd	<0.0085	<0.0028	0.230	0.221	0.207	0.431	0.466	1.06
Dy	nd	nd	nd	nd	<0.0149	0.0120	1.18	1.08	1.03	4.57	4.59	11.7
Ho	nd	nd	nd	nd	<0.0108	<0.0025	0.168	0.182	0.166	1.26	1.31	3.29
Er	nd	nd	nd	nd	<0.0099	<0.0073	0.395	0.381	0.340	4.40	4.73	11.5
Tm	nd	nd	nd	nd	<0.0052	<0.0025	0.0402	0.0370	0.0293	0.733	0.769	2.01
Yb	<dl	<dl	<dl	<dl	<0.0105	0.0142	0.219	0.163	0.185	5.58	6.09	15.06
Lu	nd	nd	nd	nd	<0.0065	<0.0024	0.0192	0.0196	0.0196	0.916	0.991	2.42
Sc	2.36	2.28	2.48	4.70	6.90	7.12	55.6	55.1	50.6	155	147	369
Rb	nd	nd	nd	<dl	<0.0174	<0.0199	<0.0199	<0.0238	<0.0218	<0.024	<0.019	<0.050
Sr	<dl	0.0040	0.0055	0.169	0.167	0.435	511	535	504	0.324	0.482	0.613
Y	<dl	<dl	0.0069	<dl	<0.026	0.0760	4.31	4.28	4.02	35.8	35.7	88.5
Ba	<dl	0.0030	0.0253	<dl	<0.041	0.232	0.0480	0.238	0.0540	0.0590	0.0934	0.0890
Th	nd	nd	nd	nd	<0.0059	0.0061	0.298	0.424	0.354	0.0079	0.0153	0.0128
U	nd	nd	nd	nd	<0.0035	0.0039	<dl	0.0322	0.0190	0.0116	0.0205	0.0316
Li	1.91	1.94	2.02	0.850	nd	nd	nd	nd	nd	nd	nd	nd
B	1.36	0.919	1.28	2.39	nd	nd	nd	nd	nd	nd	nd	nd
Al	16.0	17.9	20.7	4275	nd	nd	nd	nd	nd	nd	nd	nd
Ca	56.1	67.5	74.6	1545	1810	1845	IST	IST	IST	IST	IST	IST

DJ0217: grt-websterite, Kimberley, RSA

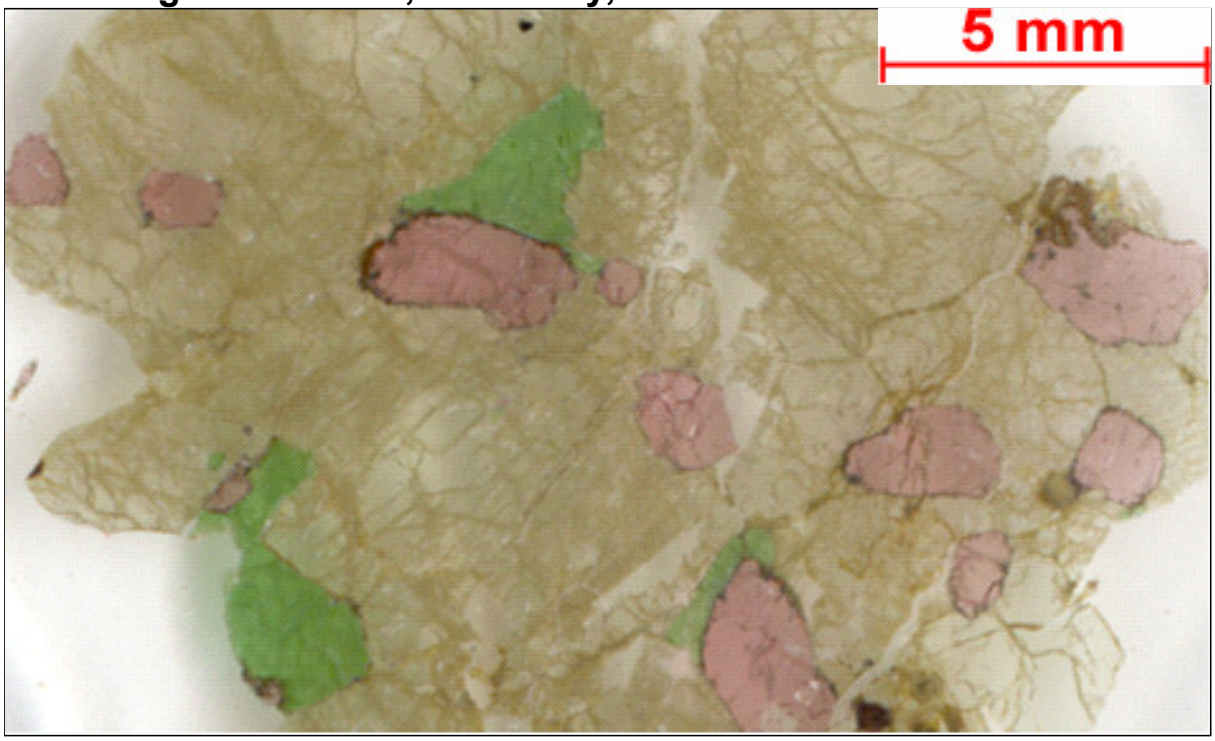

Coarse granular websterite comprising 85 % orthopyroxene (15 mm-350 µm), 5 % clinopyroxene (5 mm-250 µm) and 10 % garnet (3 mm-250 µm) and additionally phlogopite (2 mm-200 µm), spinel and ilmenite (250-50 µm).

Representative mineral major element composition [wt. %]

	opx			**cpx**			**grt**			**phl replacing grt**	
SiO_2	56.42	56.87	56.58	54.32	54.17	54.42	40.37	40.72	40.67	37.65	38.86
TiO_2	0.09	0.08	0.08	0.21	0.25	0.19	0.19	0.17	0.20	2.20	1.52
Al_2O_3	0.61	0.66	0.63	2.52	2.72	2.69	19.77	19.82	20.25	14.56	11.31
Cr_2O_3	0.23	0.23	0.21	1.54	1.71	1.68	3.48	3.59	3.47	1.19	1.28
V_2O_3	nd	nd	nd	nd	nd	nd	nd	nd	nd	nd	nd
BaO	nd	nd	nd	nd	nd	nd	nd	nd	nd	0.27	0.17
CaO	0.37	0.34	0.37	19.58	19.13	19.01	5.27	5.31	5.30	0.23	0.26
CoO	-	-									
FeO	7.99	7.80	7.83	3.89	3.85	3.79	11.91	11.94	11.99	5.34	4.82
MgO	33.26	33.56	33.34	15.30	14.99	15.11	17.65	17.39	17.51	21.65	25.26
MnO	0.14	0.13	0.19	0.09	0.11	0.11	0.49	0.44	0.42	0.05	0.03
NiO	0.12	0.09	0.15	0.06	<dl	0.09	<dl	<dl	<dl	0.24	0.13
ZnO	nd	nd	nd	nd	nd	nd	nd	nd	nd	nd	nd
K_2O	<dl	<dl	<dl	<dl	<dl	<dl	<dl	<dl	<dl	7.88	6.69
Na_2O	0.10	0.10	0.09	2.45	2.69	2.42	0.04	0.08	0.07	1.12	0.65
Cl	nd	nd	nd	nd	nd	nd	nd	nd	nd	0.05	0.02
F	nd	nd	nd	nd	nd	nd	nd	nd	nd	0.32	0.21
total	99.33	99.85	99.47	99.95	99.62	99.51	99.16	99.46	99.88	92.74	91.21
Mg/(Mg+Fe)	0.88	0.88	0.88	0.88	0.87	0.88	0.73	0.72	0.72	0.88	0.90
Cr/(Cr+Al)	-	-	-	-	-	-	-	-	-	-	-

Representative mineral major element composition [wt. %]

	ilm	**spl**		
SiO_2	0.02	0.09	0.07	0.05
TiO_2	46.78	1.33	2.10	1.52
Al_2O_3	0.49	23.76	16.72	27.08
Cr_2O_3	5.78	37.15	43.39	33.53
V_2O_3	0.38	0.08	0.05	0.06
BaO	nd	nd	nd	nd
CaO	0.01	0.08	0.08	0.02
CoO		0.12	0.10	0.09
FeO	35.16	23.94	25.54	23.66
MgO	9.97	12.53	11.31	13.23
MnO	0.23	0.27	0.34	0.25
NiO	0.26	0.27	0.18	0.26
ZnO	0.07	0.25	0.25	0.17
K_2O	0.00	<dl	<dl	<dl
Na_2O	0.04	<dl	<dl	<dl
Cl	nd	nd	nd	nd
F	nd	nd	nd	nd
total	99.19	99.86	100.13	99.91
Mg/(Mg+Fe)	-	0.58	0.53	0.59
Cr/(Cr+Al)	-	0.51	0.64	0.45
Ilm	0.49	-	-	-
Gk	0.37	-	-	-

Representative mineral trace element composition [ppm]

	opx			**cpx**			**grt**			**phl**		
Cr	1293	1403	1257	8105	8683	7479	20331	20328	20245	4326	10412	10650
Mn	nd	nd	nd	nd	nd	nd	nd	nd	nd	nd	nd	nd
Co	nd	nd	nd	nd	nd	nd	nd	nd	nd	nd	nd	nd
Ni	775	793	783	280	305	284	29.9	29.0	30.7	1424	1070	1491
Cu	nd	nd	nd	nd	nd	nd	nd	nd	nd	nd	nd	nd
Zn	nd	nd	nd	nd	nd	nd	nd	nd	nd	nd	nd	nd
Ga	nd	nd	nd	nd	nd	nd	nd	nd	nd	nd	nd	nd
Ti	493	515	502	1542	1535	1495	1256	1285	1289	6645	15372	12288
V	36.3	36.8	37.3	313	323	310	188	178	180	109	224	229
Zr	0.416	0.444	0.534	79.7	81.7	76.4	38.1	43.9	51.0	9.69	19.7	18.53
Nb	0.162	0.193	0.143	0.780	0.765	0.638	0.283	0.218	0.231	12.6	26.9	34.0
Hf	0.0151	0.0172	0.0153	2.64	2.76	2.57	0.607	0.594	0.690	0.334	0.697	0.619
Ta	0.0170	0.0191	0.0246	0.0895	0.100	0.0907	0.0236	0.0175	0.0182	1.18	2.62	2.44
La	0.0212	0.0133	0.0083	5.67	5.87	5.75	0.0330	0.0305	0.0308	0.328	0.300	0.479
Ce	0.0728	0.0562	0.0410	21.6	22.2	21.3	0.594	0.548	0.579	0.313	0.463	1.49
Pr	0.0159	0.0144	0.0126	4.75	4.99	4.48	0.332	0.269	0.313	0.0930	0.0985	0.161
Nd	0.0860	0.0880	0.0460	27.4	28.1	25.6	3.04	3.52	3.38	0.130	0.204	0.631
Sm	0.0390	0.0270	0.0250	6.09	6.14	5.50	1.71	1.93	2.09	0.0190	0.0430	0.137
Eu	0.0102	0.0200	0.0136	1.45	1.50	1.44	0.633	0.685	0.869	0.05	0.239	0.166
Gd	0.0380	0.0246	0.0290	3.64	3.83	3.67	2.38	2.76	3.12	<0.019	<0.030	0.0940
Tb	0.0046	0.0042	0.0053	0.364	0.343	0.324	0.500	0.566	0.549	<0.0053	<0.0048	<0.0097
Dy	0.0108	0.0176	0.0237	1.44	1.55	1.43	4.47	4.59	4.91	<0.0172	<0.0160	0.0350
Ho	<0.0025	0.0038	0.0049	0.196	0.211	0.215	1.02	1.18	1.19	<0.0024	0.0053	0.0041
Er	0.0127	<0.0106	0.0074	0.403	0.419	0.446	3.50	3.91	3.93	<0.0094	<0.0161	0.0340
Tm	0.0022	0.0036	0.0013	0.0433	0.0476	0.0366	0.539	0.608	0.626	<0.0034	<0.0026	0.0061
Yb	<0.0118	0.0144	0.0144	0.188	0.190	0.194	3.56	4.21	4.14	<0.0142	0.0194	0.0165
Lu	<0.0025	0.0028	0.0014	0.0231	0.0258	0.0238	0.622	0.738	0.691	0.0060	<0.0064	0.0191
Sc	7.52	7.55	7.10	61.0	60.6	59.8	151	161	153	8.51	15.3	12.7
Rb	0.00	<d.l.	<0.0086	<0.0085	<0.0066	<0.0072	0.0307	<0.0140	0.0200	103	221	194
Sr	0.396	0.342	0.279	375	375	403	0.658	0.544	1.485	89.7	112	103
Y	0.0810	0.0640	0.0870	4.81	4.86	4.84	28.3	32.1	31.8	0.0750	0.0440	0.1990
Ba	0.175	0.0377	<0.022	0.158	0.605	0.981	<0.0175	<0.0207	0.0280	1114	2409	2162
Th	0.0036	0.0017	0.0036	0.0660	0.0781	0.0831	0.0211	0.0173	0.0141	0.0083	0.118	0.0180
U	0.0049	0.0036	0.0058	0.0145	0.0142	0.0185	0.0340	0.0375	0.0190	<0.0064	0.0203	0.0210
Li	nd	nd	nd	nd	nd	nd	nd	nd	nd	nd	nd	nd
B	nd	nd	nd	nd	nd	nd	nd	nd	nd	nd	nd	nd
Al	nd	nd	nd	nd	nd	nd	nd	nd	nd	nd	nd	nd
Ca	IST	IST	IST	IST	IST	IST	IST	IST	IST	6527	482	730

DJ0218: grt-wehrlite, Kimberley, RSA

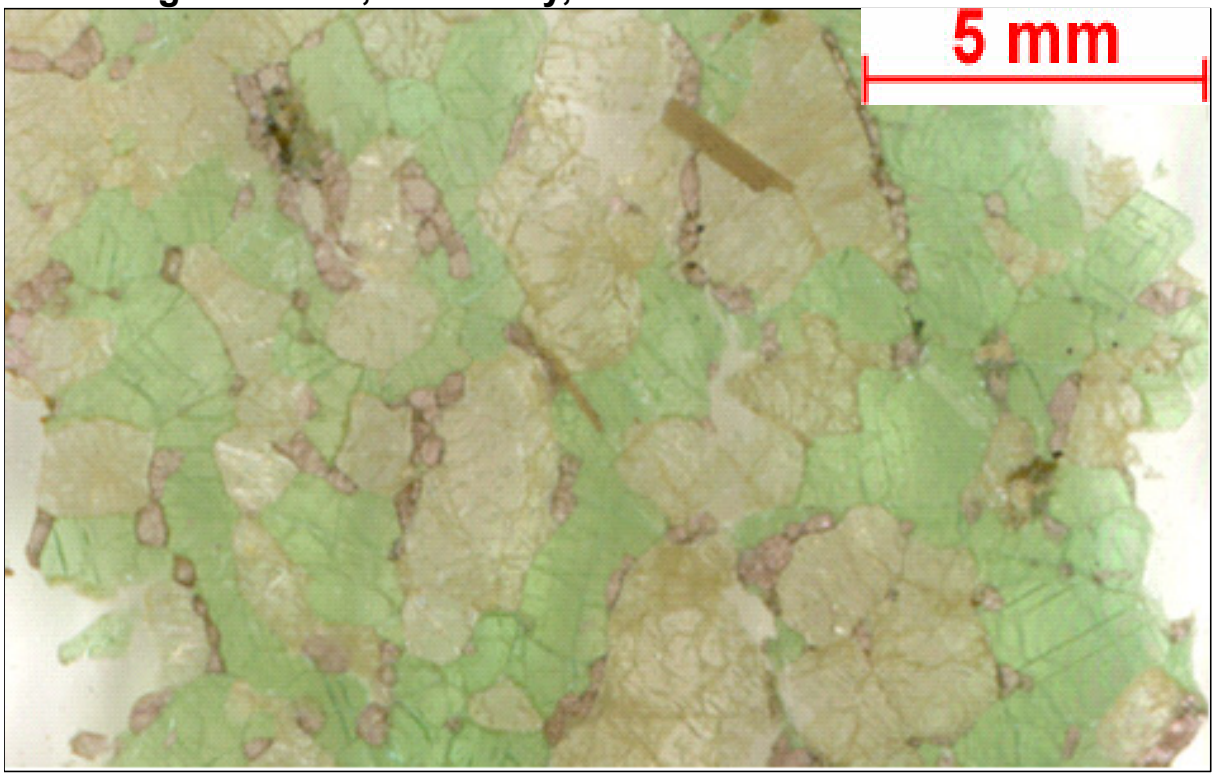

Coarse granular websterite comprising 49 % orthopyroxene (6 mm-150 µm), 42 % clinopyroxene (4 mm-150 µm) and 9 % garnet (1 mm-70 µm), slightly disintegrating to kelyphite with phlogopite (1 mm-80 µm) and spinel (250-5 µm).

Representative mineral major element composition [wt. %]

	opx			**cpx**			**grt**			**primary phl**	
SiO_2	56.73	57.04	57.58	54.69	54.69	54.77	41.32	41.58	41.12	40.65	40.75
TiO_2	<dl	0.07	0.11	0.04	<dl	0.04	<dl	<dl	<dl	0.20	0.12
Al_2O_3	0.67	0.65	0.70	1.60	1.62	1.65	21.47	21.58	21.25	12.86	13.10
Cr_2O_3	0.17	0.17	0.19	0.97	0.89	0.97	2.18	2.12	2.30	0.57	0.61
V2O3	nd	nd	nd	nd	nd	nd	nd	nd	nd	nd	nd
BaO	nd	nd	nd	nd	nd	nd	nd	nd	nd	0.33	0.28
CaO	0.32	0.30	0.30	22.09	21.99	21.70	5.06	5.05	5.05	<dl	<dl
CoO	nd	nd	nd	nd	nd	nd	nd	nd	nd	nd	nd
FeO	6.46	6.38	6.24	2.64	2.69	2.62	10.02	10.28	10.19	3.65	3.53
MgO	34.63	34.89	35.45	16.56	16.87	17.15	19.07	19.07	19.06	25.34	25.00
MnO	nd	nd	nd	0.07	0.07	0.08	0.56	0.55	0.45	<dl	<dl
NiO	0.16	0.12	0.19	0.06	0.09	0.09	<dl	<dl	<dl	0.27	0.27
ZnO	0.12	0.09	0.09	nd	nd	nd	nd	nd	nd	nd	nd
K_2O	<dl	<dl	<dl	<dl	<dl	<dl	<dl	<dl	<dl	10.27	10.29
Na_2O	<dl	0.06	<dl	1.45	1.36	1.34	<dl	<dl	<dl	0.42	0.42
Cl	nd	nd	nd	nd	nd	nd	nd	nd	nd	0.09	0.10
F	nd	nd	nd	nd	nd	nd	nd	nd	nd	<dl	<dl
total	99.27	99.77	100.84	100.18	100.26	100.42	99.68	100.23	99.42	94.64	94.46
Mg/(Mg+Fe)	0.91	0.91	0.91	0.92	0.92	0.92	0.77	0.77	0.77	0.93	0.93

Representative mineral trace element composition [ppm]

	opx			**cpx**			**grt**			**phl**		
Cr	951	987	938	4493	4828	5044	13751	13903	13870	3305	3455	3163
Mn	nd	nd	nd	nd	nd	nd	nd	nd	nd	nd	nd	nd
Co	nd	nd	nd	nd	nd	nd	nd	nd	nd	nd	nd	nd
Ni	785	827	765	336	356	328	27.5	28.9	25.1	1672	1783	1594
Cu	nd	nd	nd	nd	nd	nd	nd	nd	nd	nd	nd	nd
Zn	nd	nd	nd	nd	nd	nd	nd	nd	nd	nd	nd	nd
Ga	nd	nd	nd	nd	nd	nd	nd	nd	nd	nd	nd	nd
Ti	107	100	105	187	182	202	213	211	194	1044	851	1057
V	29.8	30.2	29.7	199	200	198	120	118	104	84.6	86.5	86.6
Zr	<dl	0.225	0.32	17.8	12.8	23.1	18.7	13.6	8.12	1.55	1.30	1.64
Nb	0.162	0.204	0.199	0.432	0.406	0.489	0.308	0.236	0.293	34.6	27.1	34.2
Hf	<0.0081	0.0042	0.0063	0.431	0.242	0.580	0.0360	0.0456	0.0283	0.0836	0.0630	0.0820
Ta	0.0151	0.0212	0.0239	0.0351	0.0303	0.0436	<0.0165	0.0123	0.0133	1.79	1.20	1.74
La	<dl	0.0324	0.0366	22.7	24.4	23.7	0.0673	0.0309	<dl	0.0097	0.0092	0.0199
Ce	<dl	0.100	0.0833	47.6	40.5	52.2	0.593	0.437	0.569	0.0106	0.0311	0.0137
Pr	<dl	0.0109	0.0159	6.12	4.57	7.00	0.146	0.136	0.143	<0.00102	0.0014	<0.0052
Nd	<dl	0.0541	0.0517	22.4	16.1	26.3	1.35	1.28	0.973	<0.0162	<0.0074	0.0038
Sm	<0.0141	0.0124	0.0092	2.49	1.59	2.81	0.755	0.582	0.484	0.0056	<0.0083	<0.0191
Eu	<0.0122	0.0033	0.0038	0.486	0.306	0.616	0.261	0.244	0.159	0.1140	0.1060	0.0920
Gd	<0.0232	0.0085	0.0078	1.30	0.766	1.44	0.932	0.801	0.532	0.0122	0.0210	0.0340
Tb	<0.0073	0.0017	0.0023	0.0969	0.0721	0.123	0.135	0.149	0.108	<0.00083	0.0033	0.0130
Dy	<0.0151	<0.0057	0.0067	0.365	0.251	0.517	1.45	1.21	0.925	<0.00	<0.0044	<0.00
Ho	<0.0062	<0.00179	0.0012	0.0482	0.0325	0.0648	0.302	0.292	0.220	<0.00165	<0.00107	0.0011
Er	<0.0112	0.0036	<0.0026	0.0880	0.0683	0.1100	0.953	0.837	0.744	<0.00240	<0.00	<0.0071
Tm	<0.0059	<0.00224	0.0017	<0.00238	0.0049	0.0097	0.119	0.125	0.112	<0.00077	<0.00199	<0.00228
Yb	<0.0139	<0.0040	<0.0026	0.0295	0.0115	0.0374	1.03	0.942	0.942	<0.0048	<0.0044	0.0200
Lu	<0.0053	<0.00120	<0.0032	0.0027	0.0027	0.0062	0.135	0.153	0.176	<0.00071	<0.00130	0.0005
Sc	5.21	5.14	5.20	25.1	25.3	26.3	119	115	121	3.63	3.55	3.52
Rb	<0.0198	0.0101	0.0331	<0.0075	<0.0062	<0.0049	<0.027	0.0132	<0.0151	202	227	195
Sr	<dl	0.169	0.205	486	375	535	0.778	0.122	0.216	96.6	71.5	100.6
Y	0.0286	0.0266	0.0363	1.12	0.798	1.67	10.7	8.50	7.13	0.0171	0.0350	0.0193
Ba	0.057	0.157	<dl	0.0920	0.0780	0.0560	0.160	0.0320	0.181	2644	2035	2582
Th	0.0142	0.0150	0.0104	0.784	0.794	0.702	<0.0142	0.0188	0.0266	5.96	3.96	6.09
U	<0.0039	0.0028	0.0034	0.0459	0.0485	0.0495	0.0326	0.0433	0.0562	0.261	0.257	0.253
Li	nd	nd	nd	nd	nd	nd	nd	nd	nd	nd	nd	nd
B	nd	nd	nd	nd	nd	nd	nd	nd	nd	nd	nd	nd
Al	nd	nd	nd	nd	nd	nd	nd	nd	nd	nd	nd	nd
Ca	<dl	2093	2218	IST	IST	IST	IST	IST	IST	353	752	728

DJ0223: dunite xenolith, Kimberley, RSA

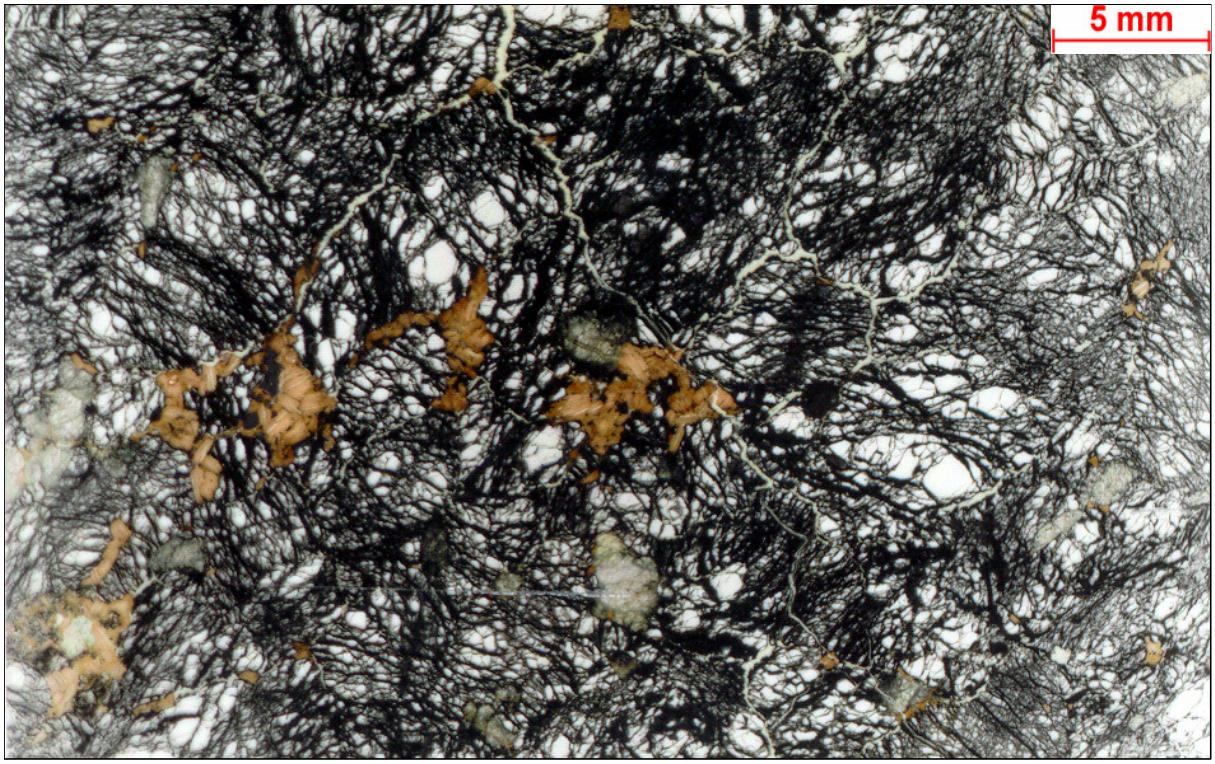

Granular, coarse grained dunite xenolith with 92% olivine (10-1 mm), 3% orthopyroxene (4 mm - 220 µm), 3% phlogopite (3 mm - 50 µm) and 2% rutile.

Representative mineral major element composition [wt. %]

	ol			**opx**			**sec. phl**		**pri. phl**	**rut**
SiO_2	41.52	41.55	41.43	57.96	57.71	57.70	40.16	41.83	43.27	0.02
TiO_2	<dl	<dl	<dl	0.06	0.08	0.08	3.88	1.23	0.73	96.70
Al_2O_3	<dl	<dl	<dl	0.03	0.02	0.03	12.86	11.84	10.62	nd
Cr_2O_3	0.03	0.04	0.06	0.10	0.17	0.14	1.41	0.64	0.53	3.30
V_2O_3	<dl	<dl	<dl	<dl	<dl	<dl	nd	nd	nd	nd
BaO	nd	nd	nd	nd	nd	nd	<dl	<dl	0.09	nd
CaO	0.02	0.02	<dl	0.26	0.27	0.26	<dl	0.04	<dl	0.05
CoO	0.05	0.03	<dl	0.02	0.02	0.05	nd	nd	nd	<dl
FeO	7.52	7.55	7.70	4.62	4.51	4.65	4.21	3.66	3.26	0.47
MgO	50.41	50.44	50.88	36.04	36.04	36.09	22.93	25.42	26.69	0.16
MnO	0.11	0.16	0.14	0.15	0.12	0.15	<dl	0.04	0.06	nd
NiO	0.32	0.33	0.32	0.07	0.11	0.06	nd	nd	nd	nd
ZnO	<dl	<dl	<dl	<dl	<dl	<dl	nd	nd	nd	nd
K_2O	<dl	<dl	<dl	<dl	<dl	<dl	10.23	10.16	10.67	nd
Na_2O	<dl	<dl	<dl	0.06	0.05	<dl	0.35	0.41	0.09	nd
Cl	nd	nd	nd	nd	nd	nd	0.02	0.02	0.04	nd
F	nd	nd	nd	nd	nd	nd	0.47	0.51	0.74	nd
total	99.99	100.11	100.53	99.37	99.09	99.22	96.51	95.80	96.79	100.69
Mg/(Mg+Fe)	0.92	0.92	0.92	0.93	0.93	0.93	0.91	0.93	0.94	-

Representative mineral trace element composition [ppm]

	ol			**opx**		
Cr	90.6	87.1	84.7	709	729	706
Mn	842	840	834	992	1011	993
Co	130	130	127	52.5	48.8	50.7
Ni	2618	2731	2534	669	630	659
Cu	0.385	0.243	0.276	<0.57	<0.78	<0.80
Zn	58.1	59.0	56.0	39.7	35.2	36.9
Ga	0.0208	<0.0145	<0.0105	nd	nd	nd
Ti	150	146	151	499	526	513
V	3.29	3.14	3.16	13.0	13.9	13.0
Zr	0.295	0.275	0.265	0.192	0.182	<0.123
Nb	0.123	0.114	0.117	<0.054	<0.086	<0.064
Hf	<0.0103	<0.0151	<0.0097	<0.116	<0.130	<0.149
Ta	<0.0034	<0.0042	0.0047	<0.039	<0.062	<0.058
La	nd	nd	nd	<0.041	<0.065	<0.059
Ce	<0.0032	<0.0043	<0.0033	<0.037	0.061	<0.059
Pr	nd	nd	nd	<0.033	<0.053	<0.050
Nd	nd	nd	nd	0.260	<0.35	<0.29
Sm	nd	nd	nd	<0.26	<0.29	<0.39
Eu	nd	nd	nd	<0.074	<0.093	<0.089
Gd	nd	nd	nd	0.260	<0.32	<0.35
Tb	nd	nd	nd	nd	nd	nd
Dy	nd	nd	nd	<0.159	<0.25	<0.252
Ho	nd	nd	nd	nd	nd	nd
Er	nd	nd	nd	<0.110	<0.114	<0.145
Tm	nd	nd	nd	nd	nd	nd
Yb	nd	nd	nd	0.170	<0.27	<0.23
Lu	nd	nd	nd	<0.033	<0.051	<0.044
Sc	2.38	2.30	2.35	3.37	3.18	3.65
Rb	nd	nd	nd	0.0992	<0.163	<0.148
Sr	<0.0044	<0.0070	<0.0041	0.216	0.222	0.209
Y	0.0078	0.0057	0.0058	nd	nd	nd
Ba	<0.029	0.0460	<0.031	0.810	<0.50	<0.45
Pb	nd	nd	nd	nd	nd	nd
Th	nd	nd	nd	nd	nd	nd
U	nd	nd	nd	nd	nd	nd
Li	2.10	1.98	1.96	0.870	<0.78	<0.77
B	0.608	0.780	0.470	nd	nd	nd
Al	2.90	1.97	2.00	nd	nd	nd
Ca	82.4	64.7	89.3	1889	1837	1727

DJ0256: grt-wehrlite xenolith, Kimberley, RSA

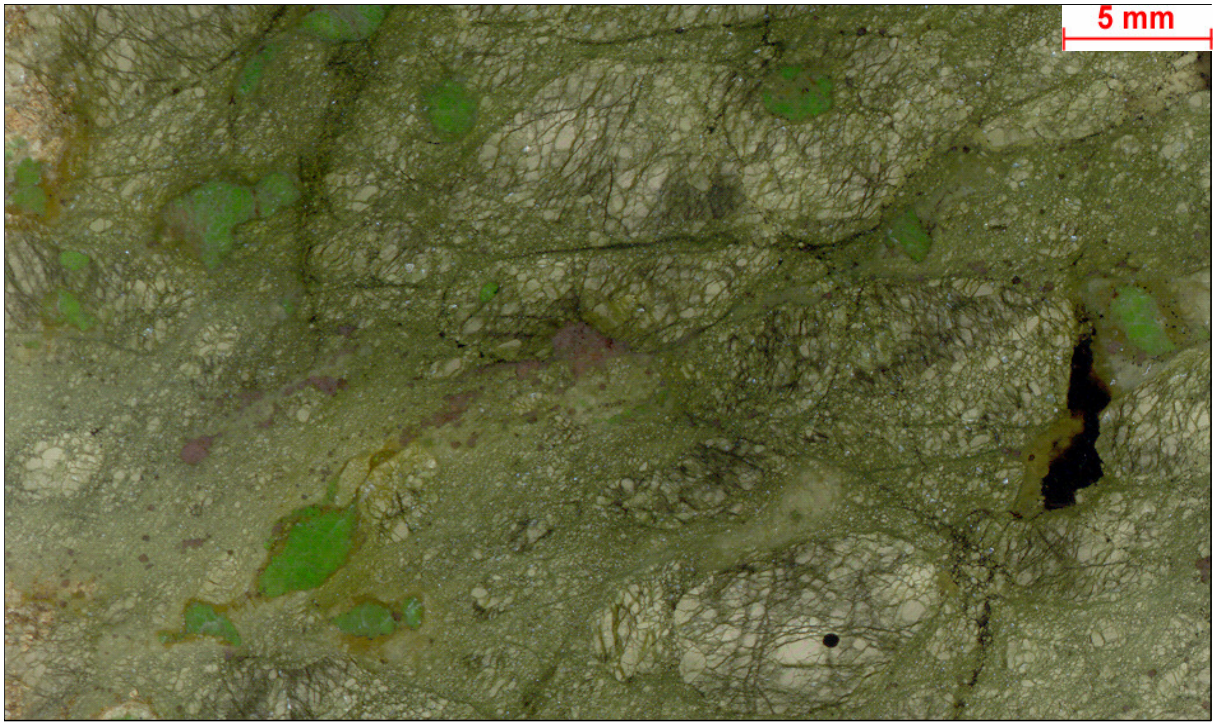

Porphyroclastic wehrlite with 55% olivine porphyroclasts (20-1 mm) surrounded by olivine neoblasts (30%, 1 mm - 20 µm), 6% anhedral clinopyroxene (10mm - 750µm) that crystallized together with garnet (1%, 1,5mm - 70µm), orthopyroxene (2%, 1mm - 70µm) and oxide minerals (1%, spinel, ilmenite, rutile, 200 - 5 µm). Garnet is euhedral and keliphytised dissolving into phlogopite and spinel.

Representative mineral major element composition [wt. %]

	ol			**opx**			**cpx**			**grt**		
SiO_2	40.64	40.72	40.42	57.37	56.58	56.91	54.66	54.76	54.63	41.79	41.30	40.45
TiO_2	<dl	<dl	0.04	0.19	0.20	0.26	0.39	0.38	0.39	1.21	1.10	1.17
Al_2O_3	0.03	<dl	<dl	1.16	1.62	1.46	2.45	2.59	2.49	19.99	18.44	17.45
Cr_2O_3	0.06	<dl	<dl	0.66	0.87	0.73	3.13	2.91	2.87	3.06	5.19	6.04
V_2O_3	nd	nd	nd	nd	nd	nd	nd	nd	nd	nd	nd	nd
BaO	nd	nd	nd	nd	nd	nd	nd	nd	nd	nd	nd	nd
CaO	0.04	<dl	0.05	0.79	0.86	0.64	18.42	17.97	17.98	5.96	6.42	7.10
CoO	nd	nd	nd	nd	nd	nd	nd	nd	nd	nd	nd	nd
FeO	8.87	8.43	9.48	5.25	5.24	5.14	2.41	2.51	2.60	7.39	7.35	7.33
MgO	49.94	50.34	49.53	34.89	34.62	35.44	15.89	16.00	16.10	20.49	20.16	19.26
MnO	0.11	0.07	0.09	0.09	0.11	0.07	0.09	0.08	0.06	0.34	0.34	0.26
NiO	0.36	0.36	0.32	0.08	0.15	0.11	0.04	<dl	0.04	<dl	<dl	<dl
ZnO	nd	nd	nd	nd	nd	nd	nd	nd	nd	nd	nd	nd
K_2O	<dl	<dl	<dl	<dl	<dl	<dl	<dl	<dl	<dl	<dl	<dl	<dl
Na_2O	<dl	<dl	<dl	0.17	0.25	0.15	2.75	2.74	2.70	0.1158	0.1241	0.07
Cl	nd	nd	nd	nd	nd	nd	nd	nd	nd	nd	nd	nd
F	nd	nd	nd	nd	nd	nd	nd	nd	nd	nd	nd	nd
total	100.04	99.92	99.92	100.66	100.51	100.92	100.24	99.94	99.86	100.35	100.42	99.13
Mg/(Mg+Fe)	0.92	0.92	0.91	0.92	0.92	0.92	0.92	0.92	0.92	0.83	0.83	0.82
Cr/(Cr+Al)	-	-	-	-	-	-	-	-	-	-	-	-

Representative mineral major element composition [wt. %]

	phl replacing grt			phl replacing cpx			rt			spl		
SiO_2	39.05	37.65	39.03	39.79	39.51	39.32	0.09	0.05	0.06	0.01	0.03	0.04
TiO_2	3.21	3.02	3.05	3.95	3.73	3.70	83.87	92.35	92.45	2.28	3.09	3.55
Al_2O_3	14.21	15.14	14.65	13.01	12.71	13.08	2.25	<dl	<dl	21.25	13.84	11.25
Cr_2O_3	3.16	2.78	2.44	1.82	1.71	1.81	7.27	4.11	4.47	41.63	47.81	48.81
V_2O_3	nd	nd	nd	nd	nd	nd	<dl	0.19	0.09	0.29	0.30	0.28
BaO	0.12	<dl	<dl	0.07	<dl	0.01	nd	nd	nd	nd	nd	nd
CaO	<dl	0.16	<dl	0.04	<dl	0.03	0.14	nd	nd	nd	nd	nd
CoO	nd	nd	nd	nd	nd	nd	0.03	nd	nd	nd	nd	nd
FeO	3.66	4.39	3.33	3.42	3.30	3.25	2.54	0.24	0.27	17.46	18.98	19.86
MgO	21.82	22.70	22.57	22.35	22.94	22.27	1.77	0.03	0.05	15.36	14.16	13.84
MnO	<dl	0.10	<dl	0.02	0.03	0.04	0.07	0.03	<dl	0.16	0.23	0.21
NiO	nd	nd	nd	0.17	0.17	0.21	<dl	<dl	<dl	0.17	0.19	0.18
ZnO	nd	nd	nd	nd	nd	nd	<dl	nd	nd	nd	nd	nd
K_2O	10.07	8.14	9.63	9.97	10.30	10.36	nd	nd	nd	nd	nd	nd
Na_2O	0.35	0.71	0.50	0.39	0.37	0.46	nd	nd	nd	nd	nd	nd
Cl	0.02	0.03	0.02	0.02	0.03	0.02	nd	nd	nd	nd	nd	nd
F	0.50	0.23	0.36	0.38	0.42	0.33	nd	nd	nd	nd	nd	nd
total	96.18	95.05	95.57	95.39	95.21	94.89	98.01	97.00	97.39	98.62	98.64	98.02
Mg/(Mg+Fe)	0.91	0.90	0.92	0.92	0.93	0.92	-	-	-	0.67	0.63	0.62
Cr/(Cr+Al)	-	-	-	-	-	-	-	-	-	0.57	0.70	0.74

Representative mineral trace element composition [ppm]

	ol			opx			cpx			grt		
Cr	288	357	256	7110	8016	5536	16880	18265	15862	28765	40488	24857
Mn	884	849	766	904	1007	841	nd	nd	nd	nd	nd	nd
Co	156	129	140	63.5	63.5	63.5	nd	nd	nd	nd	nd	nd
Ni	3382	2652	3014	958	968	971	225	230	220	89.6	82.9	62.6
Cu	2.36	2.29	2.85	2.29	2.12	1.72	nd	nd	nd	nd	nd	nd
Zn	85.1	62.9	68.2	47.2	48.0	46.3	nd	nd	nd	nd	nd	nd
Ga	0.289	0.208	0.256	8.74	10.5	9.41	nd	nd	nd	nd	nd	nd
Ti	197	196	153	1724	1937	1530	2878	2831	2582	<dl	6455	9273
V	8.08	8.40	7.07	104	132	104	276	276	256	471	464	443
Zr	0.277	0.229	0.127	1.71	2.05	1.47	76.5	71.5	65.8	603	271	518
Nb	<0.024	0.0249	<0.053	<0.053	0.0363	<0.049	<dl	1.09	0.85	1.57	0.792	0.446
Hf	<0.049	0.0073	<0.104	0.12	0.147	<0.128	4.26	4.62	3.70	15.5	7.42	14.78
Ta	<0.0151	<0.0025	<0.033	<0.029	0.0067	<0.040	0.0910	0.0842	0.0557	0.110	0.0521	0.0740
La	nd	nd	nd	0.0540	0.0120	0.158	<dl	2.32	2.08	0.865	0.411	0.0840
Ce	<0.0153	<0.0029	<0.039	0.0480	0.0374	<0.043	<dl	6.91	6.47	2.05	1.35	0.479
Pr	nd	nd	nd	<0.026	<0.0096	0.054	1.44	1.41	1.29	0.409	0.251	0.993
Nd	nd	nd	nd	<0.147	<0.059	<0.17	7.95	7.79	7.78	3.66	2.27	2.21
Sm	nd	nd	nd	<0.163	<0.066	<0.20	2.18	2.13	2.08	2.50	1.99	2.55
Eu	nd	nd	nd	<0.044	0.0183	<0.054	0.692	0.659	0.631	1.36	0.958	1.24
Gd	nd	nd	nd	<0.157	<0.064	<0.21	1.98	2.05	2.01	6.79	4.57	6.35
Tb	nd	nd	nd	nd	nd	nd	0.261	0.279	0.246	1.49	0.993	1.22
Dy	nd	nd	nd	0.119	0.0700	<0.124	1.24	1.27	1.27	11.38	8.38	10.53
Ho	nd	nd	nd	nd	nd	nd	0.204	0.176	0.170	2.33	1.86	2.43
Er	nd	nd	nd	<0.087	<0.032	<0.105	0.354	0.387	0.332	6.62	5.48	6.33
Tm	nd	nd	nd	nd	nd	nd	0.0377	0.0386	0.0349	0.831	0.728	0.806
Yb	nd	nd	nd	<0.106	<0.052	<0.17	0.208	0.178	0.157	4.78	4.12	5.52
Lu	nd	nd	nd	<0.028	<0.0100	<0.029	0.0167	0.0235	0.0107	0.675	0.590	0.711
Sc	2.25	3.43	2.18	5.93	7.08	5.60	36.0	34.8	36.0	145	136	140
Rb	nd	nd	nd	0.099	<0.027	0.186	<dl	0.482	0.579	2.49	2.14	0.09
Sr	<0.024	<0.0033	<0.055	0.284	0.307	0.260	108	104	105	11.1	4.90	0.930
Y	<0.0205	0.0072	<0.044	0.169	0.160	0.112	4.34	4.40	4.09	55.9	42.9	52.5
Ba	<0.138	<0.0191	<0.36	0.690	<0.030	0.330	<dl	6.64	6.30	16.6	5.15	0.940
Th	nd	nd	nd	nd	nd	nd	<dl	0.141	0.126	0.177	0.101	0.0480
U	nd	nd	nd	nd	nd	nd	<dl	0.0187	0.0253	0.0821	0.0533	0.0540
Li	2.11	2.56	1.21	1.39	1.77	1.35	nd	nd	nd	nd	nd	nd
B	1.45	0.877	<2.13	<1.74	0.620	<1.90	nd	nd	nd	nd	nd	nd
Al	108	112	76.6	10212	12471	9176	nd	nd	nd	nd	nd	nd
Ca	208	343	193	5830	6771	4855	IST	IST	IST	IST	IST	IST

DJ0258A: wehrlite xenolith, Kimberley, RSA

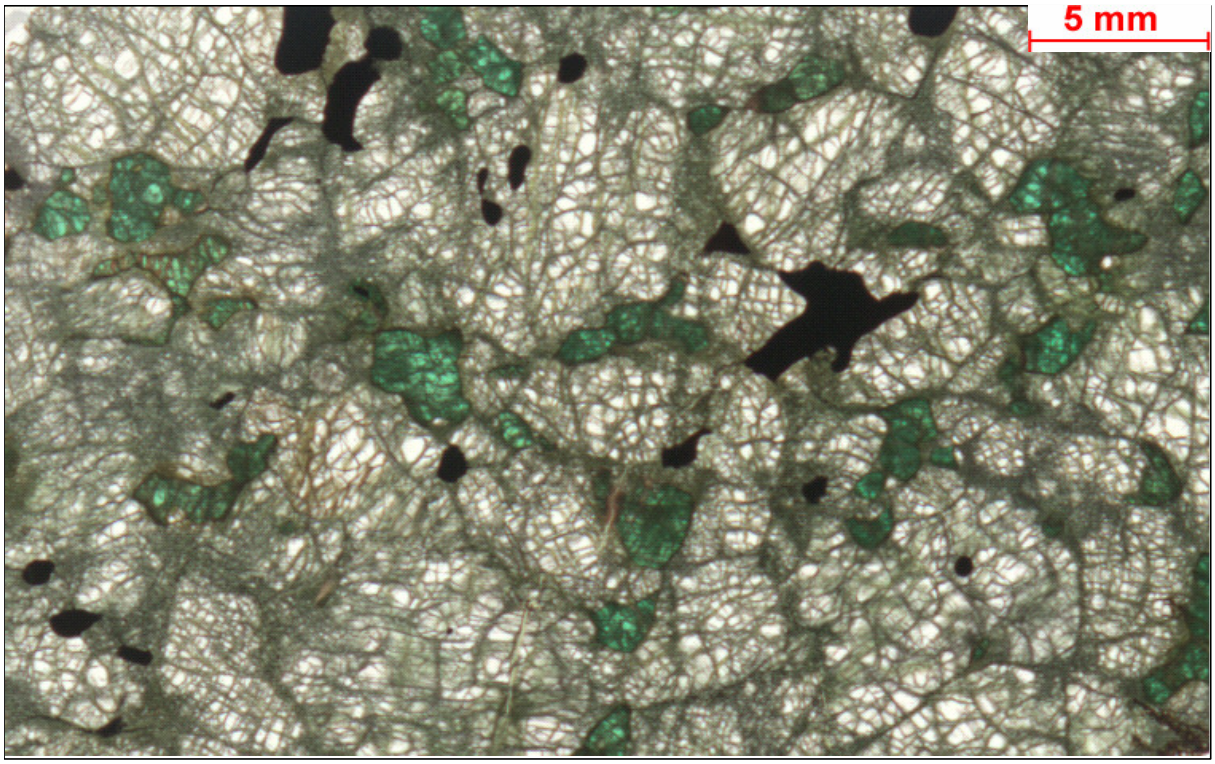

Granular, coarse grained wehrlite xenolith with 87% olivine (8 – 2 mm), 10% rounded, vermicular clinopyroxene (4 mm - 150 µm), large serpentine patches, chromite (3%, 50 - 5 µm) and traces of garnet.

Representative mineral major element composition [wt. %]

	ol			**cpx**			**grt**			**cr**
SiO_2	41.40	41.21	40.82	53.58	55.77	55.90	42.47	43.33	42.53	0.10
TiO_2	0.06	0.04	0.04	0.40	0.44	0.44	0.68	0.59	0.61	2.27
Al_2O_3	<dl	<dl	<dl	2.82	2.69	2.80	16.79	19.02	19.30	15.44
Cr_2O_3	0.06	0.02	0.07	2.52	3.25	2.68	8.01	5.22	5.16	49.35
V_2O_3	<dl	<dl	<dl	nd	0.06	0.05	0.03	<dl	0.04	0.05
CaO	0.04	0.03	0.04	17.41	17.20	17.35	5.90	5.01	5.02	0.05
CoO	0.05	0.04	0.02	nd	<dl	0.04	0.04	<dl	<dl	0.07
FeO	7.52	7.60	7.46	2.57	2.20	2.32	6.30	6.63	6.65	17.03
MgO	51.05	50.85	50.95	16.52	15.53	15.96	19.70	20.69	20.84	15.35
MnO	0.10	0.10	0.11	0.15	0.14	0.08	0.31	0.37	0.32	0.18
NiO	0.37	0.35	0.33	<dl	<dl	<dl	<dl	<dl	<dl	0.19
ZnO	<dl	<dl	<dl	nd	<dl	<dl	<dl	<dl	<dl	0.30
K_2O	<dl	<dl	<dl	<dl	<dl	<dl	<dl	<dl	<dl	<dl
Na_2O	<dl	<dl	<dl	2.82	3.10	2.90	0.15	<dl	0.09	0.06
Cl	nd	nd	nd	nd	nd	nd	nd	nd	nd	nd
F	nd	nd	nd	nd	nd	nd	nd	nd	nd	nd
total	100.65	100.22	99.83	98.78	100.38	100.52	100.38	100.86	100.56	100.45
Mg/(Mg+Fe)	0.92	0.92	0.93	0.92	0.93	0.92	0.85	0.85	0.85	0.70
Cr/(Cr+Al)	-	-	-	-	-	-	-	-	-	0.68

Representative mineral trace element composition [ppm]

	ol			**cpx**			**grt**		
Cr	242	251	250	19313	18554	12397	36782	37414	38389
Mn	795	795	795	727	720	nd	3068	2989	3134
Co	129	126	126	23.6	22.2	nd	40.1	38.9	46.7
Ni	2828	2356	2318	375	368	301	54.3	50.1	60.8
Cu	2.810	2.700	2.730	nd	nd	nd	nd	nd	nd
Zn	61.4	64.5	66.5	14.7	11.0	nd	14.9	11.7	15.0
Ga	0.142	nd	nd	nd	nd	nd	nd	nd	nd
Ti	237	184	195	3275	3130	2660	4541	4599	4629
V	5.85	5.67	5.82	331	325	<dl	201	211	224
Zr	0.331	0.265	0.357	66.9	64.6	55.0	131	120	114
Nb	0.110	0.06	0.07	0.430	0.488	0.255	0.149	0.174	0.227
Hf	<0.0132	0.0063	0.0142	3.34	4.13	2.92	2.88	2.46	2.25
Ta	0.0073	0.0061	0.0054	0.0190	0.0370	0.0235	0.0174	0.0139	0.0330
La	nd	nd	nd	1.77	1.78	1.53	0.0177	<dl	0.0090
Ce	<0.0051	<0.0039	<0.00075	6.42	6.48	6.43	0.136	<dl	0.135
Pr	nd	nd	nd	1.28	1.23	1.24	0.0600	0.0784	0.0550
Nd	nd	nd	nd	7.53	7.61	6.83	0.889	0.973	0.870
Sm	nd	nd	nd	2.18	1.46	1.92	0.972	1.07	0.820
Eu	nd	nd	nd	0.727	0.696	0.609	0.561	0.516	0.467
Gd	nd	nd	nd	1.87	2.08	1.81	2.95	2.65	2.76
Tb	nd	nd	nd	0.257	0.324	nd	0.721	0.678	0.576
Dy	nd	nd	nd	1.56	1.55	1.20	6.15	5.95	5.72
Ho	nd	nd	nd	0.175	0.195	nd	1.55	1.40	1.43
Er	nd	nd	nd	0.482	0.458	0.356	4.85	4.78	4.75
Tm	nd	nd	nd	0.0330	0.0490	nd	0.778	0.701	0.739
Yb	nd	<0.0086	<0.0017	<dl	0.173	0.211	5.27	4.90	4.65
Lu	nd	nd	nd	0.0100	0.0360	0.0248	0.780	0.785	0.789
Sc	1.66	4.64	4.80	32.4	30.0	26.3	104	102	106
Rb	<dl	<0.0071	0.0109	0.118	<dl	0.01	0.0329	<dl	0.0260
Sr	<0.0085	<0.0064	0.0029	92.1	92.0	92.4	0.237	0.262	0.232
Y	0.0072	nd	nd	5.07	4.95	4.17	38.1	35.1	35.9
Ba	<0.046	<0.0117	<0.0035	0.380	<dl	0.05	0.227	<dl	0.0500
Th	nd	nd	nd	0.0412	0.0380	0.0237	0.0020	0.0047	<dl
U	nd	nd	nd	0.0100	0.0121	0.0060	0.0080	<dl	<dl
Li	2.56	nd	nd	0.767	0.939	nd	0.221	<dl	0.272
B	0.550	nd	nd	nd	nd	nd	nd	nd	nd
Al	65.7	nd	nd	nd	nd	nd	nd	nd	nd
Ca	180	145	154	IST	IST	IST	IST	IST	IST

DJ0259: dunite xenolith, Kimberley, RSA

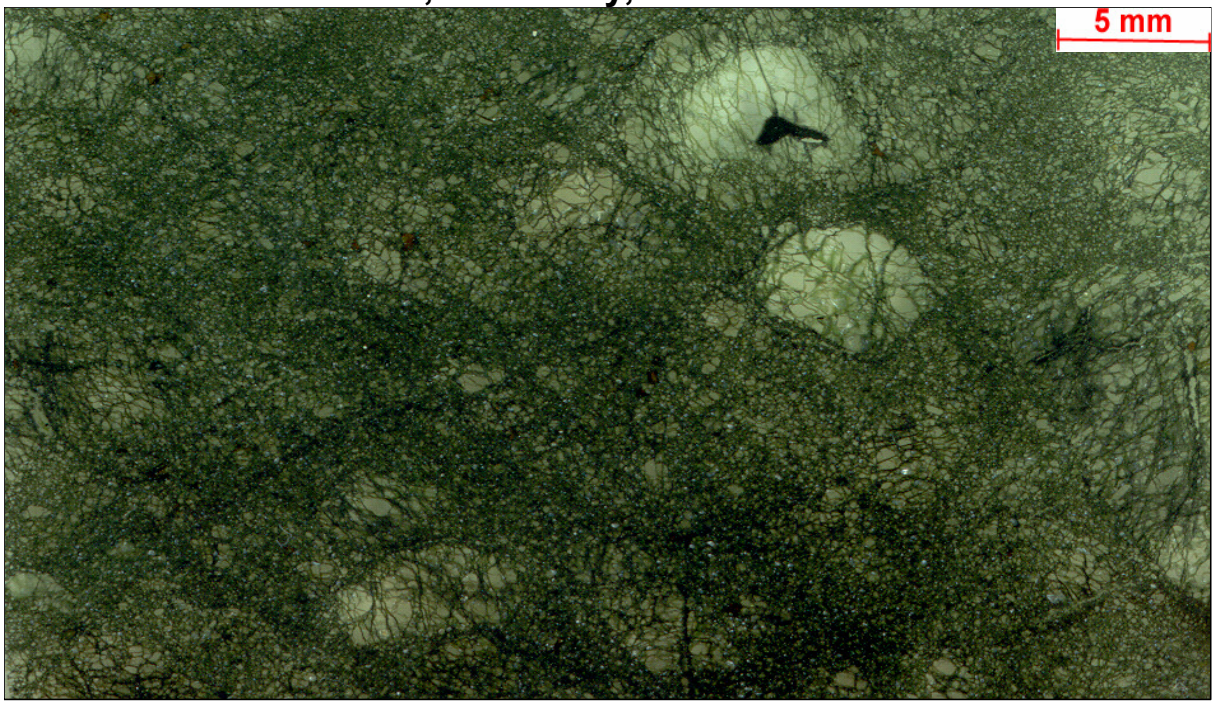

Porphyroclastic dunite xenolith with 34% olivine porphyroclasts (13 mm - 500 µm), 66% olivine neoblasts (1 mm - 50 µm) and traces of clinopyroxene, garnet, phlogopite and ilmenite.

Representative mineral major element composition [wt. %]

	ol-pc core		**ol-pc rim**		**ol-nb**			**cpx**		
SiO_2	41.73		40.50	40.62	40.39	40.55	40.38	55.92	56.56	56.42
TiO_2	<dl		<dl	0.04	<dl	<dl	0.05	0.11	0.11	0.07
Al_2O_3	<dl		<dl	<dl	<dl	<dl	0.03	0.11	0.15	0.10
Cr_2O_3	0.07		<dl	0.06	0.06	0.05	0.06	1.57	1.45	0.78
V_2O_3	<dl		0.04	<dl	<dl	<dl	<dl	0.05	0.05	<dl
BaO	nd		nd	nd	nd	nd	nd	nd	nd	nd
CaO	0.04		<dl	0.05	0.10	0.11	0.09	22.50	22.64	23.02
CoO	0.05		0.02	0.02	0.04	0.04	0.03	0.02	<dl	0.04
FeO	6.91		10.37	11.03	13.09	12.35	13.27	2.53	2.33	3.10
MgO	51.43		48.41	48.21	46.89	47.37	46.31	16.56	16.57	16.40
MnO	0.13		0.13	0.12	0.17	0.16	0.13	0.10	0.10	0.09
NiO	0.36		0.39	0.40	0.17	0.28	0.31	<dl	0.07	<dl
ZnO	<dl		<dl	<dl	<dl	<dl	<dl	<dl	<dl	<dl
K_2O	<dl		<dl	<dl	<dl	0.02	<dl	<dl	<dl	<dl
Na_2O	<dl		<dl	0.05	<dl	<dl	<dl	1.19	1.16	0.96
total	100.71		99.87	100.61	100.90	100.93	100.66	100.66	101.18	100.99
Mg/(Mg+Fe)	0.93		0.90	0.89	0.87	0.88	0.86	0.92	0.93	0.90

Representative mineral major element composition [wt. %]

	grt		**phl replacing ilm**			**ilm**		
SiO_2	43.65	43.04	39.28	38.62	39.15	0.05	0.04	0.06
TiO_2	0.31	0.22	4.29	4.07	4.03	53.08	53.41	53.01
Al_2O_3	20.28	19.65	13.02	13.53	13.28	0.19	0.20	0.19
Cr_2O_3	4.05	4.74	1.07	1.09	1.01	4.52	3.99	4.05
V_2O_3	<dl	0.05	nd	nd	nd	nd	nd	nd
BaO	nd	nd	<dl	<dl	<dl	nd	nd	nd
CaO	4.68	4.74	0.11	0.29	<dl	0.05	0.06	0.05
CoO	0.02	0.02	nd	nd	nd	nd	nd	nd
FeO	6.64	6.23	5.15	4.92	5.11	29.09	28.98	29.15
MgO	21.02	21.42	21.86	22.08	22.43	12.54	12.71	12.58
MnO	0.32	0.34	<dl	<dl	<dl	0.30	0.31	0.27
NiO	<dl	<dl	nd	nd	nd	0.23	0.22	0.24
ZnO	<dl	<dl	nd	nd	nd	0.05	0.06	0.06
K_2O	<dl	<dl	9.94	9.38	10.06	nd	nd	nd
Na_2O	0.06	0.08	0.35	0.31	0.34	nd	nd	nd
Cl	nd	nd	0.02	0.03	0.02	nd	nd	nd
F	nd	nd	0.52	0.42	0.56	nd	nd	nd
total	101.03	100.53	95.62	94.74	95.99	100.10	99.99	99.64
Mg/(Mg+Fe)	0.85	0.86	0.88	0.89	0.89	-	-	-
Ilm	-	-	-	-	-	0.50	0.49	0.49
Gk	-	-	-	-	-	0.45	0.45	0.45

Representative mineral trace element composition [ppm]

	ol-pc core			**ol-pc rim**			**ol-nb**			**cpx**		
Cr	248	257	262	255	250	251	177	194	nd	5023	5441	7445
Mn	733	752	745	746	718	750	1139	1153	1124	581	628	563
Co	125	126	125	125	124	127	170	176	178	17.5	19.2	18.3
Ni	2679	2722	2727	2712	2710	2699	2523	2718	2712	116	126	341
Cu	2.10	2.24	1.94	2.05	1.92	2.25	3.09	3.03	3.51	nd	nd	nd
Zn	46.6	47.3	47.3	46.8	48.1	52.2	103	102	96.7	13.9	14.4	12.3
Ga	0.0565	0.0696	0.0655	0.0524	0.131	0.111	0.122	0.0895	0.130	nd	nd	nd
Ti	52.6	53.9	57.0	58.2	54.4	61.0	220	235	284	556	538	695
V	5.55	5.82	5.94	5.80	5.53	5.52	3.95	3.76	5.39	256	266	221
Zr	0.191	0.194	0.207	0.201	0.203	<dl	0.372	0.448	0.541	43.3	40.7	55.9
Nb	0.143	0.120	0.120	0.136	0.144	0.163	0.0712	0.0869	0.0850	0.192	0.169	0.188
Hf	<0.0079	<0.0086	<0.0075	<0.0077	<0.022	0.0110	0.0161	0.0243	0.0227	2.00	2.26	2.86
Ta	0.0086	0.0063	0.0087	0.0074	<0.0078	0.0065	0.0140	0.0130	0.0063	0.0114	0.0129	0.0081
La	nd	nd	nd	nd	nd	nd	nd	nd	nd	4.59	4.69	7.75
Ce	<0.0026	<0.0028	<0.0030	<0.0024	<0.0077	0.0121	<0.0038	<0.0041	0.0084	18.6	19.1	31.0
Pr	nd	nd	nd	nd	nd	nd	nd	nd	nd	3.52	3.37	5.45
Nd	nd	nd	nd	nd	nd	nd	nd	nd	nd	18.8	18.3	27.0
Sm	nd	nd	nd	nd	nd	nd	nd	nd	nd	4.12	4.20	5.43
Eu	nd	nd	nd	nd	nd	nd	nd	nd	nd	1.22	1.12	1.47
Gd	nd	nd	nd	nd	nd	nd	nd	nd	nd	3.36	3.27	3.27
Tb	nd	nd	nd	nd	nd	nd	nd	nd	nd	0.338	0.377	0.365
Dy	nd	nd	nd	nd	nd	nd	nd	nd	nd	1.67	1.67	1.51
Ho	nd	nd	nd	nd	nd	nd	nd	nd	nd	0.258	0.228	0.179
Er	nd	nd	nd	nd	nd	nd	nd	nd	nd	0.468	0.458	0.441
Tm	nd	nd	nd	nd	nd	nd	nd	nd	nd	0.0417	0.0494	0.0450
Yb	nd	nd	nd	nd	nd	nd	nd	nd	nd	0.211	0.226	0.243
Lu	nd	nd	nd	nd	nd	nd	nd	nd	nd	0.0171	0.0208	0.0381
Sc	2.27	2.07	2.066	2.03	1.75	2.04	2.84	3.37	3.33	101	97.74	61.8
Rb	nd	nd	nd	nd	nd	nd	nd	nd	nd	0.0100	<dl	0.0570
Sr	<0.0036	<0.0031	<0.0029	<0.0028	0.0250	0.0349	<0.0061	0.0190	0.0305	275	282	535
Y	<0.0034	0.0046	0.0038	<0.0031	<0.0105	0.0092	0.0221	0.0245	0.0232	5.38	5.17	4.86
Ba	<0.024	<0.0184	<0.0205	<0.022	<0.061	<0.023	<0.034	<0.035	0.0280	0.344	0.292	0.206
Th	nd	nd	nd	nd	nd	nd	nd	nd	nd	0.0189	0.0238	0.0250
U	nd	nd	nd	nd	nd	nd	nd	nd	nd	0.0054	0.0007	0.0002
Li	1.22	1.20	1.15	1.22	1.06	1.54	2.56	2.60	3.89	0.324	0.285	0.221
B	0.64	0.51	0.882	0.88	0.56	0.90	1.22	0.830	0.700	nd	nd	nd
Al	54.7	53.8	62.0	58.3	60.1	69.9	47.1	40.8	64.0	nd	nd	nd
Ca	115	144	139	142	154	154	532	717	467	IST	IST	IST

Trace element composition [ppm]			
	grt		
Cr	27148	28351	nd
Mn	2714	2793	nd
Co	36.9	38.4	nd
Ni	42.4	41.8	nd
Cu	nd	nd	nd
Zn	8.99	10.7	nd
Ga	nd	nd	nd
Ti	2004	2043	1627
V	204	218	222
Zr	58.5	59.6	80.6
Nb	0.225	0.227	0.401
Hf	1.01	0.956	1.21
Ta	0.0285	0.0288	0.0337
La	0.0338	0.0245	0.110
Ce	0.381	0.296	0.802
Pr	0.177	0.144	0.243
Nd	1.82	1.82	2.45
Sm	1.53	1.53	2.11
Eu	0.637	0.659	0.856
Gd	2.27	2.29	3.47
Tb	0.346	0.353	0.537
Dy	2.36	2.30	3.86
Ho	0.503	0.513	0.815
Er	1.60	1.55	2.21
Tm	0.254	0.250	0.345
Yb	1.86	1.93	2.42
Lu	0.333	0.322	0.386
Sc	99.6	98.9	102
Rb	0.0172	<dl	nd
Sr	0.968	0.427	4.07
Y	13.6	13.5	21.4
Ba	0.0633	0.0410	0.223
Th	0.0044	0.0051	0.0012
U	0.0166	0.0177	0.0157
Li	0.0786	0.0577	0.0850
B	nd	nd	nd
Al	nd	nd	nd
Ca	IST	IST	IST

DJ0267: Fe-rich dunite xenolith, Kimberley, RSA

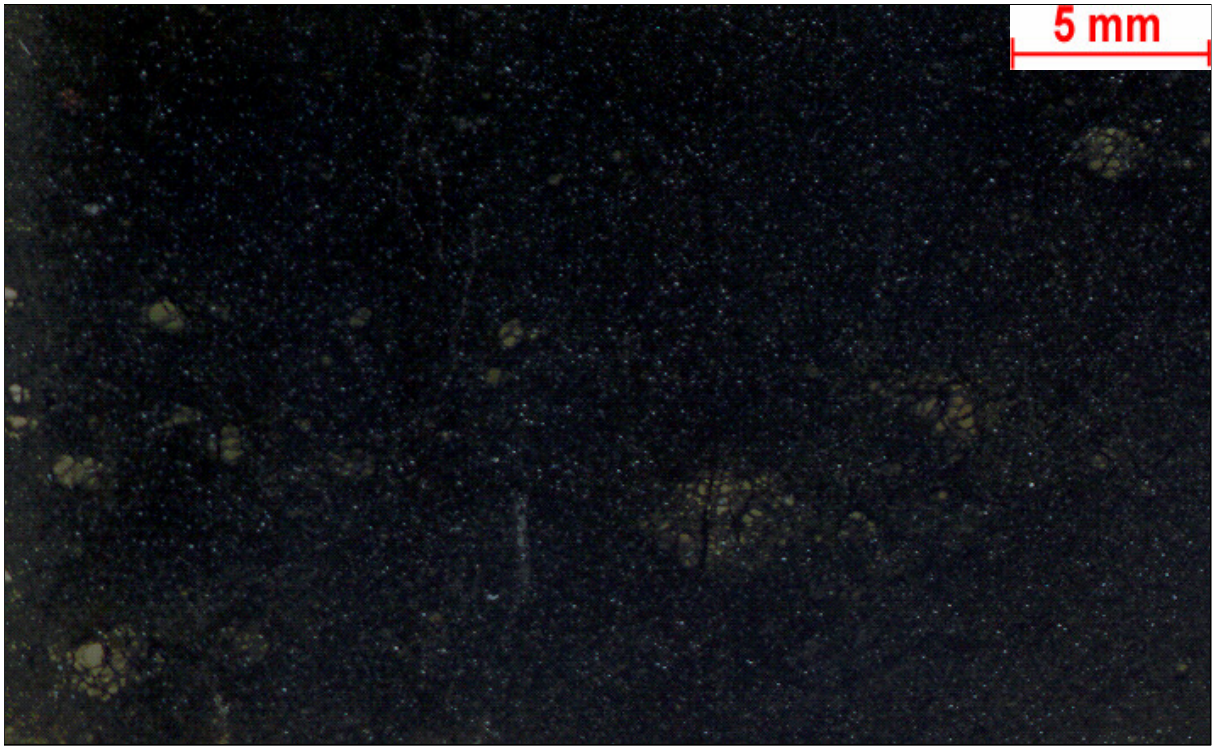

Fine-grained porphyroclastic dunite xenolith with 98% olivine (porphyroclasts 3 mm-270 µm, neoblasts 200-30 µm), 1% ilmenite (240-5 µm) and 1% phlogopite (420-140 µm).

Representative mineral major element composition [wt. %]

	ol			**phl replacing ilm**			**type II ilm**		
SiO_2	39.20	39.67	40.13	41.81	40.04	40.61	<dl	<dl	<dl
TiO_2	<dl	0.06	0.04	1.79	2.86	2.95	50.37	49.37	49.48
Al_2O_3	<dl	0.04	<dl	10.02	11.81	11.80	0.17	0.18	0.11
Cr_2O_3	<dl	<dl	0.05	0.10	1.20	0.70	6.82	7.13	6.92
V_2O_3	nd	nd	nd	nd	nd	nd	0.10	0.08	0.05
BaO	nd	nd	nd	<dl	<dl	<dl	nd	nd	nd
CaO	<dl	0.04	0.06	<dl	<dl	<dl	0.05	0.03	0.07
CoO	nd	nd	nd	nd	nd	nd	0.03	0.05	0.04
FeO	13.61	12.53	12.19	5.08	5.04	5.1	29.29	29.95	30.01
MgO	46.09	47.10	47.37	24.68	22.46	22.77	12.18	12.30	12.38
MnO	0.15	0.19	0.13	0.05	<dl	0.05	0.22	0.23	0.28
NiO	0.23	0.28	0.33	0.19	0.24	0.19	0.21	0.21	0.16
ZnO	nd	nd	nd	nd	nd	nd	<dl	<dl	<dl
K_2O	<dl	<dl	<dl	10.00	10.76	10.88	<dl	<dl	<dl
Na_2O	<dl	<dl	<dl	0.27	0.22	0.25	<dl	<dl	<dl
Cl	nd	nd	nd	0.02	0.02	0.02	nd	nd	nd
F	nd	nd	nd	1.60	0.47	0.47	nd	nd	nd
total	99.28	99.90	100.29	95.61	95.12	95.79	99.44	99.53	99.50
Mg/(Mg+Fe)	0.87	0.88	0.88	0.90	0.89	0.89	-	-	-
Ilm	-	-	-	-	-	-	0.47	0.45	0.44
Gk	-	-	-	-	-	-	0.45	0.46	0.46

Representative mineral trace element composition [ppm]

	ol			**type II ilm**		
Cr	161	146	153	49959	45893	46108
Mn	770	725	730	2172	1976	1787
Co	133	141	129	248	227	201
Ni	2156	2200	2204	2309	1871	1823
Cu	2.59	5.51	4.66	43.0	27.2	24.4
Zn	75.4	77.7	75.9	318	236	202
Ga	0.250	<0.53	<0.41	8.79	7.99	6.05
Ti	140	101	126	IST	IST	IST
V	3.32	3.70	3.06	1154	1160	1263
Zr	<0.148	0.400	<0.36	537	557	713
Nb	0.258	0.180	<0.23	809	766	823
Hf	<0.101	<0.27	<0.28	22.8	18.6	26.6
Ta	<0.049	<0.098	0.0970	123	107	113
La	nd	nd	nd	nd	nd	nd
Ce	<0.117	0.190	<0.099	nd	nd	nd
Pr	nd	nd	nd	nd	nd	nd
Nd	nd	nd	nd	nd	nd	nd
Sm	nd	nd	nd	nd	nd	nd
Eu	nd	nd	nd	nd	nd	nd
Gd	nd	nd	nd	nd	nd	nd
Tb	nd	nd	nd	nd	nd	nd
Dy	nd	nd	nd	nd	nd	nd
Ho	nd	nd	nd	nd	nd	nd
Er	nd	nd	nd	nd	nd	nd
Tm	nd	nd	nd	nd	nd	nd
Yb	<0.162	<0.55	<0.51	nd	nd	nd
Lu	nd	nd	nd	nd	nd	nd
Sc	3.11	4.43	3.88	35.5	37.9	37.1
Rb	nd	nd	nd	nd	nd	nd
Sr	0.062	<0.15	0.200	nd	nd	nd
Y	<0.065	<0.22	<0.19	0.0400	<dl	0.184
Ba	<0.52	<1.14	<0.80	<dl	<dl	<dl
Th	nd	nd	nd	<dl	0.3	<dl
U	nd	nd	nd	<dl	<dl	<dl
Li	3.34	2.86	4.13	4.49	3.04	2.74
B	<3.71	<9.65	<8.92	nd	nd	nd
Al	28.0	29.5	22.8	1419	1232	1536
Ca	704	<908.50	<852.14	387	322	360

DJ0268: Fe-rich dunite xenolith, Kimberley, RSA

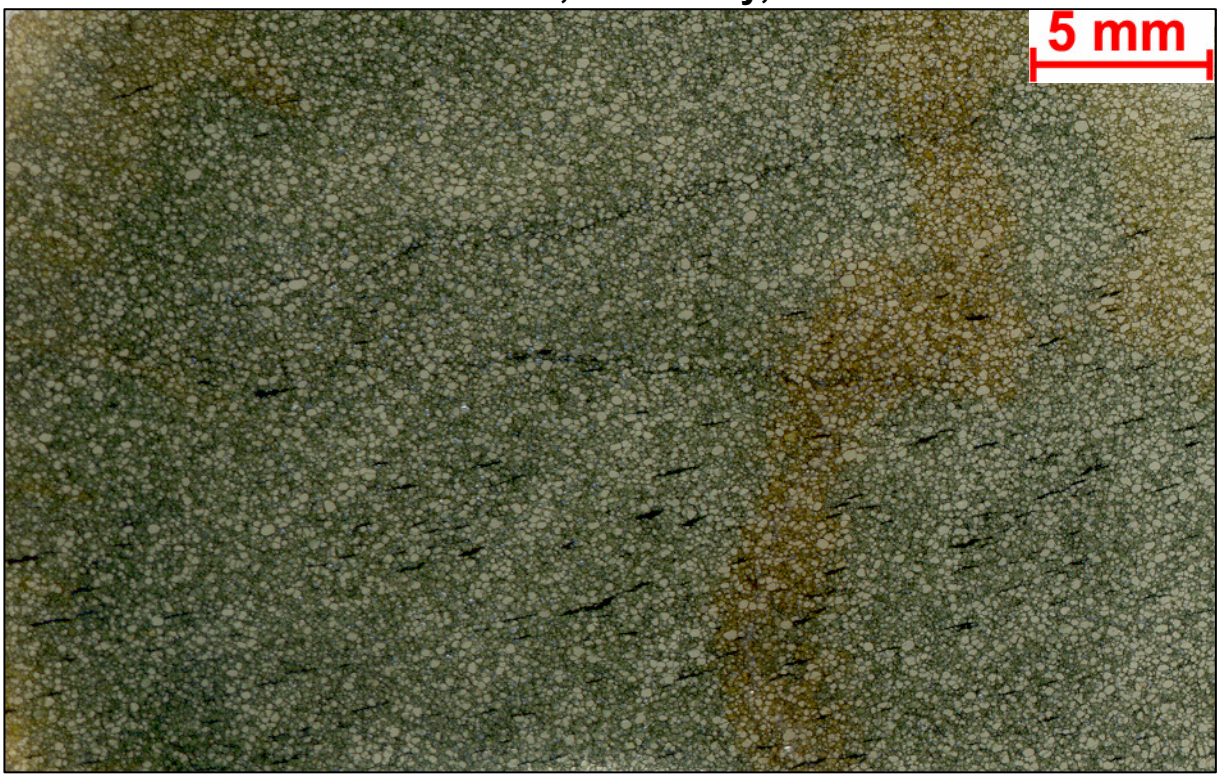

Fine-grained granular dunite xenolith with 99% olivine (200 - 15 µm) and 1% elongated ilmenite (1 mm - 5 µm).

Representative mineral major element composition [wt. %]

	ol			**type I ilm**		
SiO_2	41.01	40.61	40.69	<dl	<dl	<dl
TiO_2	0.04	0.05	0.05	48.75	48.90	48.88
Al_2O_3	0.03	<dl	<dl	0.69	0.60	0.63
Cr_2O_3	0.09	<dl	0.06	7.24	6.93	7.94
V_2O_3	<dl	<dl	<dl	<dl	<dl	<dl
BaO	nd	nd	nd	nd	nd	nd
CaO	0.05	0.07	0.06	<dl	<dl	0.04
CoO	0.03	0.05	0.04	<dl	<dl	<dl
FeO	11.45	11.50	11.59	30.57	30.84	29.54
MgO	47.55	47.61	47.59	11.84	11.74	12.40
MnO	0.14	0.12	0.18	0.21	0.21	0.17
NiO	0.33	0.35	0.37	0.25	0.24	0.25
ZnO	<dl	<dl	<dl	<dl	0.02	<dl
K_2O	<dl	<dl	<dl	nd	nd	nd
Na_2O	<dl	<dl	<dl	nd	nd	nd
Cl	nd	nd	nd	nd	nd	nd
F	nd	nd	nd	nd	nd	nd
total	100.72	100.35	100.62	99.54	99.48	99.86
Mg/(Mg+Fe)	0.88	0.88	0.88	-	-	-
Ilm	-	-	-	0.47	0.47	0.45
Gk	-	-	-	0.44	0.44	0.46

Representative mineral trace element composition [ppm]

	ol			**type I ilm**		
Cr	230	238	234	44972	44565	49350
Mn	920	961	938	1768	1917	1659
Co	145	146	143	225	230	204
Ni	2398	2404	2306	2355	2421	2236
Cu	3.05	3.21	2.85	39.9	31.3	38.5
Zn	81.3	79.1	77.6	308	266	228
Ga	0.187	0.130	0.154	15.0	16.3	15.1
Ti	297	306	297	IST	IST	IST
V	5.31	5.29	5.30	1087	1133	1178
Zr	0.191	0.226	0.234	416	475	342
Nb	0.0328	0.0137	0.0242	252	255	230
Hf	0.0110	0.0062	0.0050	12.2	13.4	11.9
Ta	0.0060	0.0018	0.0076	48.8	45.7	38.1
La	nd	nd	nd	nd	nd	nd
Ce	<dl	0.0014	0.0020	nd	nd	nd
Pr	nd	nd	nd	nd	nd	nd
Nd	nd	nd	nd	nd	nd	nd
Sm	nd	nd	nd	nd	nd	nd
Eu	nd	nd	nd	nd	nd	nd
Gd	nd	nd	nd	nd	nd	nd
Tb	nd	nd	nd	nd	nd	nd
Dy	nd	nd	nd	nd	nd	nd
Ho	nd	nd	nd	nd	nd	nd
Er	nd	nd	nd	nd	nd	nd
Tm	nd	nd	nd	nd	nd	nd
Yb	0.0072	0.0090	0.0023	nd	nd	nd
Lu	nd	nd	nd	nd	nd	nd
Sc	6.13	5.21	5.01	30.3	31.5	24.1
Rb	nd	nd	nd	nd	nd	nd
Sr	0.0058	0.0057	0.0057	nd	nd	nd
Y	0.0189	0.0290	0.0122	0.131	0.330	0.0850
Ba	<dl	0.0280	0.0057	<dl	<dl	0.200
Th	nd	nd	nd	<dl	<dl	0.0049
U	nd	nd	nd	0.0090	0.0350	0.0245
Li	2.56	2.64	2.65	3.03	2.83	2.53
B	0.930	0.910	0.810	nd	nd	nd
Al	116	120	115	4813	5304	4171
Ca	352	399	360	115	50.8	84.7

DJ0269: Fe-rich dunite xenolith, Kimberley, RSA

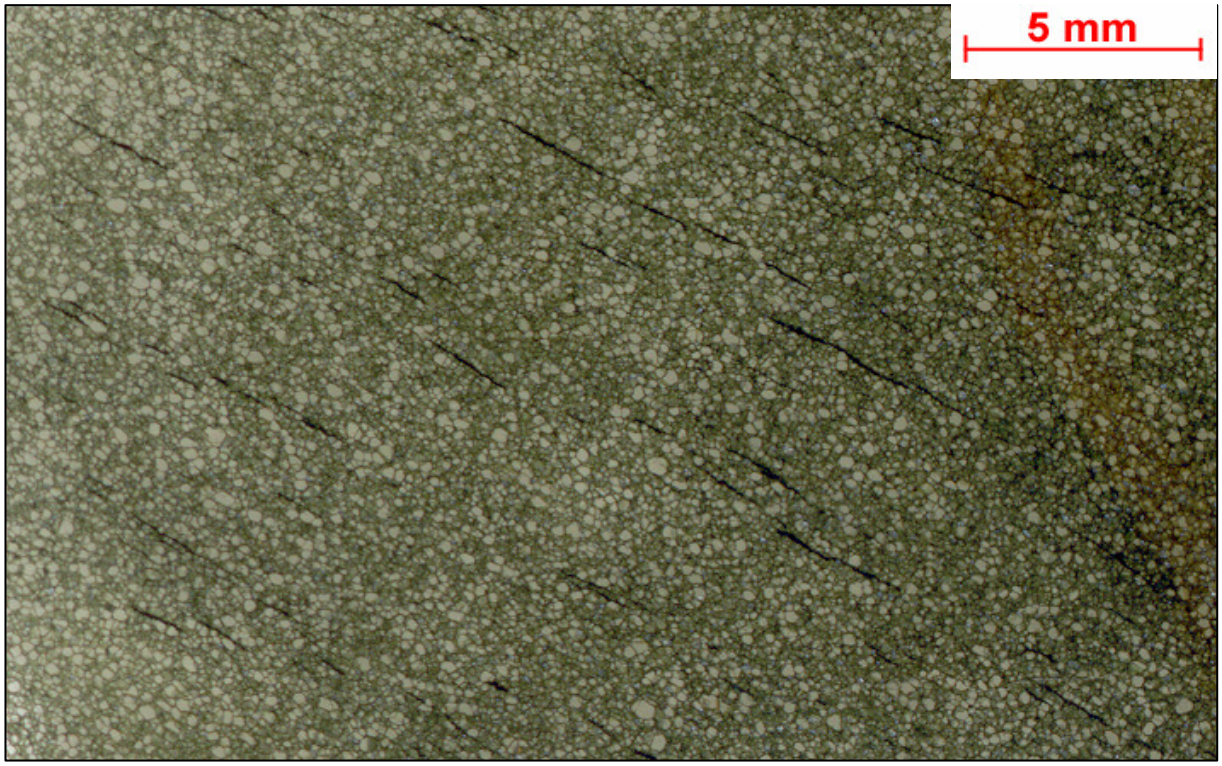

Fine-grained granular dunite xenolith with 99% olivine (660-30 µm) and 1% elongated ilmenite (3 mm - 5 µm).

Representative mineral major element composition [wt. %]

	ol			**type I ilm**		
SiO_2	39.69	39.90	40.02	<dl	<dl	<dl
TiO_2	<dl	<dl	<dl	47.93	47.90	48.19
Al_2O_3	0.03	0.03	0.05	0.68	0.53	0.51
Cr_2O_3	<dl	0.05	<dl	6.93	6.81	6.44
V_2O_3	nd	nd	nd	0.07	0.12	0.14
CaO	0.05	0.05	0.04	nd	nd	nd
CoO	nd	nd	nd	nd	nd	nd
FeO	11.97	12.17	11.42	30.66	31.06	30.81
MgO	47.46	47.85	47.80	11.87	11.59	11.73
MnO	0.12	0.13	0.12	0.19	0.21	0.20
NiO	0.35	0.35	0.35	0.24	0.20	0.25
ZnO	nd	nd	nd	nd	nd	nd
K_2O	<dl	<dl	<dl	nd	nd	nd
Na_2O	<dl	<dl	<dl	nd	nd	nd
Cl	nd	nd	nd	nd	nd	nd
F	nd	nd	nd	nd	nd	nd
total	99.66	100.54	99.80	98.57	98.42	98.28
Mg/(Mg+Fe)	0.89	0.89	0.89	-	-	-
Ilm	-	-	-	0.45	0.46	0.46
Gk	-	-	-	0.45	0.44	0.44

Representative mineral trace element composition [ppm]

	ol			**type I ilm**		
Cr	254	255	256	47666	52457	52844
Mn	1248	1246	1262	1606	1810	1711
Co	162	160	161	205	217	213
Ni	2693	2699	2725	2277	2161	2156
Cu	3.76	3.35	3.47	<dl	19.5	21.1
Zn	131	129	131	194	181	197
Ga	nd	nd	nd	15.9	14.6	17.6
Ti	291	307	289	IST	IST	IST
V	5.42	5.39	5.47	1261	1484	1397
Zr	0.224	0.233	0.223	421	801	571
Nb	0.0197	0.0289	0.0284	272	375	288
Hf	<0.01	0.0130	0.0159	15.5	22.8	15.3
Ta	<0.01	0.0054	0.0033	53.4	54.0	49.9
La	nd	nd	nd	nd	nd	nd
Ce	<0.01	<0.00	<0.00	nd	nd	nd
Pr	nd	nd	nd	nd	nd	nd
Nd	nd	nd	nd	nd	nd	nd
Sm	nd	nd	nd	nd	nd	nd
Eu	nd	nd	nd	nd	nd	nd
Gd	nd	nd	nd	nd	nd	nd
Tb	nd	nd	nd	nd	nd	nd
Dy	nd	nd	nd	nd	nd	nd
Ho	nd	nd	nd	nd	nd	nd
Er	nd	nd	nd	nd	nd	nd
Tm	nd	nd	nd	nd	nd	nd
Yb	0.0056	<0.01	<0.01	nd	nd	nd
Lu	nd	nd	nd	nd	nd	nd
Sc	5.14	5.22	5.18	26.9	40.2	35.6
Rb	<0.01	<0.01	<0.02	nd	nd	nd
Sr	<0.01	0.0059	0.0076	nd	nd	nd
Y	nd	nd	nd	<0.039	0.460	0.128
Ba	<0.02	<0.02	<0.01	<0.13	1.18	0.32
Th	nd	nd	nd	<0.0118	0.193	0.005
U	nd	nd	nd	0.0200	0.158	0.085
Li	nd	nd	nd	1.49	2.19	1.35
B	nd	nd	nd	nd	nd	nd
Al	nd	nd	nd	5755	3092	4575
Ca	319	339	324	102	<dl	94.3

DJ0270: Fe-rich dunite xenolith, Kimberley, RSA

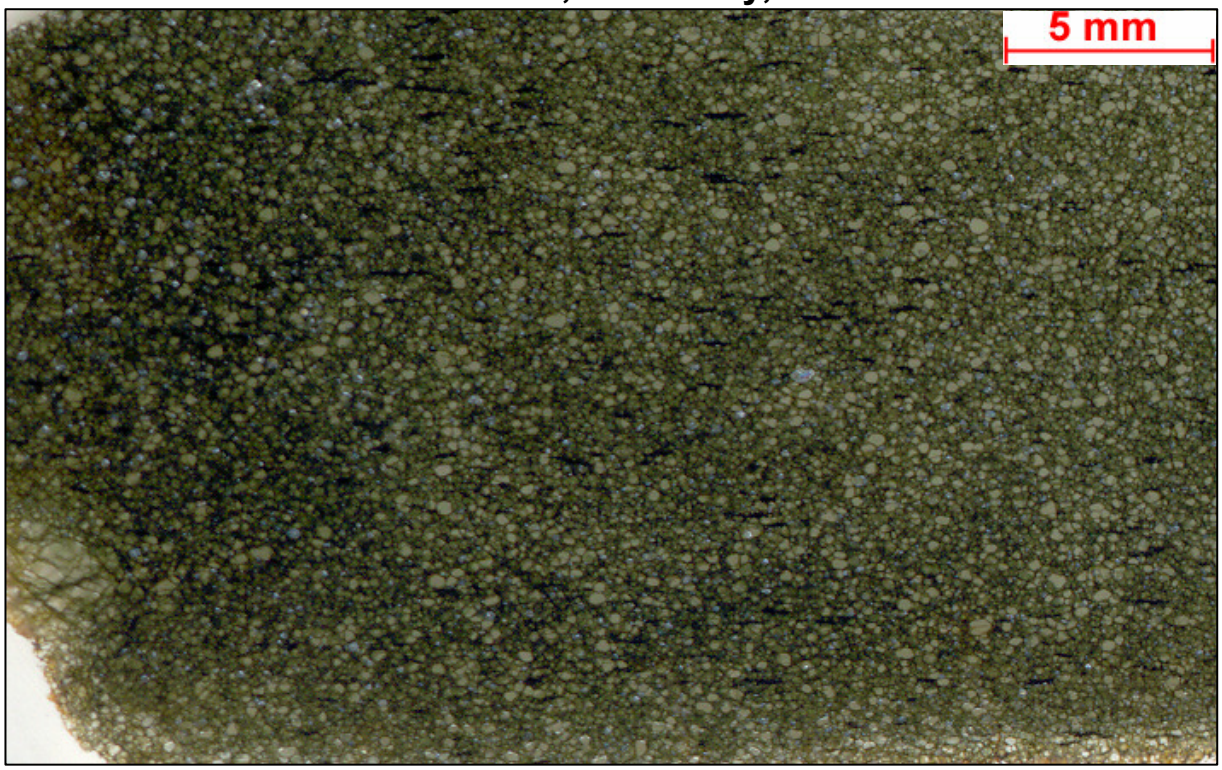

Fine-grained porphyroclastic dunite xenolith with olivine porphyroclasts (3 mm), surrounded by 98% olivine (570-70 µm) and 1% elongated ilmenite (550- 5 µm).

Representative mineral major element composition [wt. %]

	ol-pc		**ol-nb**			**type I ilm**		
SiO_2	40.03	40.05	39.61	39.65	39.47	<dl	<dl	<dl
TiO_2	0.05	<dl	<dl	<dl	<dl	48.62	47.43	47.18
Al_2O_3	<dl	<dl	<dl	<dl	<dl	0.60	0.75	0.621
Cr_2O_3	<dl	<dl	<dl	<dl	0.05	6.26	7.58	7.6
V_2O_3	nd	nd	nd	nd	nd	0.09	0.09	0.059
BaO	nd	nd	nd	nd	nd	nd	nd	nd
CaO	0.02	0.044	0.05	0.07	0.04	nd	nd	nd
CoO	nd	nd	nd	nd	nd	nd	nd	nd
FeO	10.54	10.37	11.91	11.82	12.05	30.38	30.30	30.85
MgO	49.23	49.18	47.91	47.38	47.67	11.94	11.64	11.33
MnO	0.12	0.172	0.134	0.12	0.11	0.26	0.17	0.187
NiO	0.22	0.226	0.31	0.30	0.38	0.21	0.24	0.237
ZnO	nd	nd	nd	nd	nd	nd	nd	nd
K_2O	<dl	<dl	<dl	0.01	0.01	nd	nd	nd
Na_2O	<dl	<dl	<dl	<dl	<dl	nd	nd	nd
Cl	nd	nd	nd	nd	nd	nd	nd	nd
F	nd	nd	nd	nd	nd	nd	nd	nd
total	100.21	100.04	99.93	99.35	99.77	98.36	98.20	98.06
Mg/(Mg+Fe)	0.91	0.91	0.90	0.89	0.90	-	-	-
Ilm	-	-	-	-	-	0.46	0.46	0.47
Gk	-	-	-	-	-	0.45	0.44	0.43

Representative mineral trace element composition [ppm]

	ol-pc			**ol-nb**			**type I ilm**		
Cr	59.59	74.43	70.39	221	221	229	42952	46954	51492
Mn	722	852	819	759	735	775	1590	1784	1773
Co	108	125	121	126	124	128	223	232	248
Ni	1207	1402	1357	2153	2132	2125	2309	2488	2661
Cu	1.06	1.34	1.37	2.62	3.11	2.69	43.5	40.6	39.3
Zn	62.1	70.5	76.6	71.5	69.1	72.0	222	316	255
Ga	0.0720	0.0994	0.0900	0.164	<0.097	0.119	13.3	17.1	15.8
Ti	146	165	145	226	229	242	IST	IST	IST
V	4.13	4.91	4.49	4.56	4.34	4.55	1115	1218	1255
Zr	0.347	0.320	0.310	0.112	0.156	0.158	347	544	461
Nb	0.0860	0.0900	0.1150	0.0374	0.0380	0.0490	248	282	272
Hf	0.0280	<0.0160	0.0164	0.0142	<0.022	<0.022	12.7	17.1	12.4
Ta	<0.0084	<0.0080	0.0088	<0.0093	<0.0104	<0.0090	52.5	46.3	44.6
La	nd	nd	nd	nd	nd	nd	nd	nd	nd
Ce	<0.0072	<0.0091	0.0263	<0.0078	<0.0137	<0.0076	nd	nd	nd
Pr	nd	nd	nd	nd	nd	nd	nd	nd	nd
Nd	nd	nd	nd	nd	nd	nd	nd	nd	nd
Sm	nd	nd	nd	nd	nd	nd	nd	nd	nd
Eu	nd	nd	nd	nd	nd	nd	nd	nd	nd
Gd	nd	nd	nd	nd	nd	nd	nd	nd	nd
Tb	nd	nd	nd	nd	nd	nd	nd	nd	nd
Dy	nd	nd	nd	nd	nd	nd	nd	nd	nd
Ho	nd	nd	nd	nd	nd	nd	nd	nd	nd
Er	nd	nd	nd	nd	nd	nd	nd	nd	nd
Tm	nd	nd	nd	nd	nd	nd	nd	nd	nd
Yb	<0.021	<0.022	<0.030	<0.026	<0.043	<0.021	nd	nd	nd
Lu	nd	nd	nd	nd	nd	nd	nd	nd	nd
Sc	2.26	2.65	2.38	2.70	2.76	2.64	24.0	25.4	28.2
Rb	nd	nd	nd	nd	nd	nd	nd	nd	nd
Sr	0.0343	0.0358	0.0960	<dl	<0.0151	0.0141	nd	nd	nd
Y	<0.0144	<0.0101	0.0252	<0.0128	0.0303	<dl	0.177	<0.33	<dl
Ba	0.0840	<0.093	0.1680	<0.068	<0.078	<0.082	<0.62	9.12	<1.11
Th	nd	nd	nd	nd	nd	nd	0.03	<0.135	<0.151
U	nd	nd	nd	nd	nd	nd	<0.039	<0.63	0.131
Li	1.92	2.20	2.04	2.39	2.51	2.46	2.20	3.56	3.19
B	0.860	0.540	0.650	0.430	0.570	0.690	nd	nd	nd
Al	29.1	32.4	34.7	106	105	107	5172	3538	4488
Ca	177	202	197	336	375	321	400	<388.04	539

DJ0271: grt-wehrlite xenolith, Kimberley, RSA

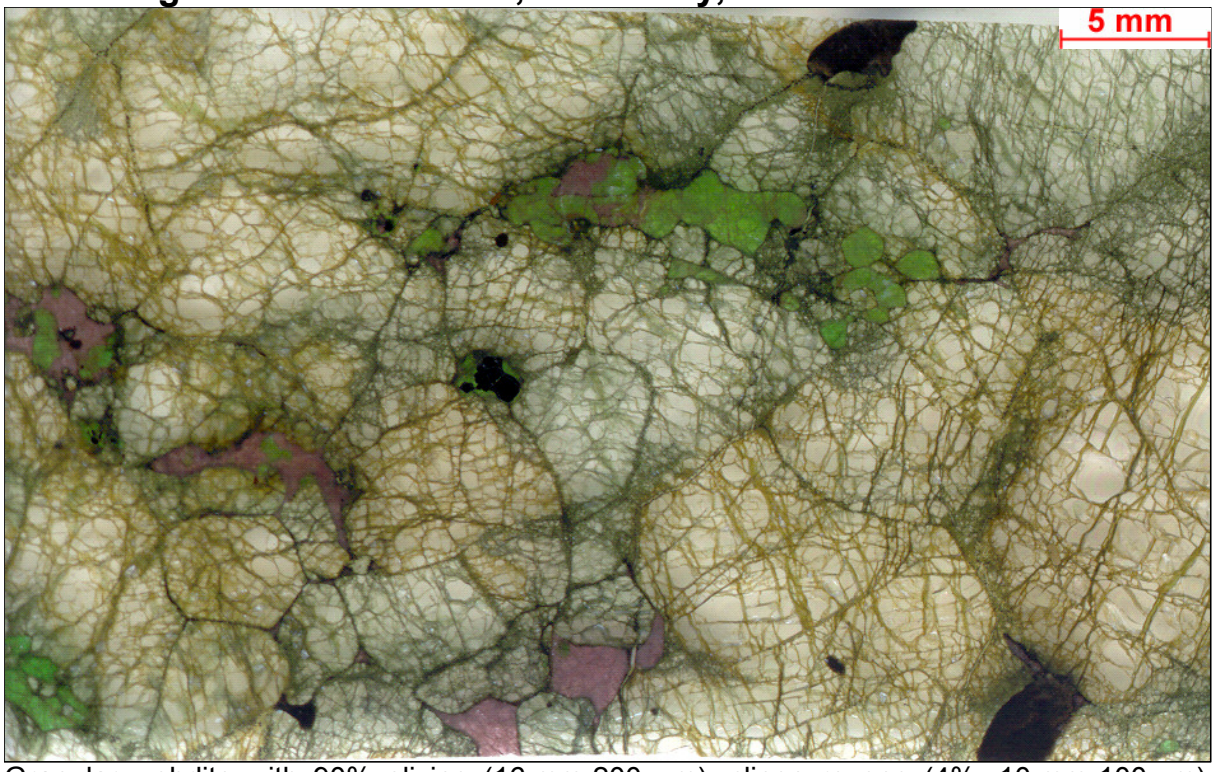

Granular wehrlite with 90% olivine (16 mm-200 µm), clinopyroxene (4%; 10 mm-100 µm), garnet (4%; 4 mm-130 µm), phlogopite (1%; 300-80 µm) and oxides (1%; 2 mm-30 µm).

Representative mineral major element composition [wt. %]

	ol			cpx			grt			phl replacing cpx	
SiO_2	40.34	40.77	40.37	54.18	53.99	54.51	40.83	40.84	40.76	40.71	39.30
TiO_2	<dl	<dl	0.06	0.42	0.44	0.35	0.58	0.58	0.58	1.69	2.86
Al_2O_3	<dl	<dl	<dl	2.78	2.87	2.52	18.42	18.20	16.72	12.39	13.57
Cr_2O_3	<dl	0.05	<dl	3.25	3.77	3.67	5.65	6.14	7.76	0.88	1.47
V_2O_3	nd	nd	nd	nd	nd	nd	nd	nd	nd	nd	nd
BaO	nd	nd	nd	nd	nd	nd	nd	nd	nd	0.06	0.06
CaO	0.04	<dl	0.04	17.80	17.55	18.06	5.28	5.49	6.05	<dl	<dl
CoO											
FeO	8.58	8.44	8.41	2.61	2.66	2.61	7.50	7.49	7.56	3.31	3.30
MgO	50.43	50.41	50.54	15.68	15.06	15.47	20.13	20.18	19.34	24.56	22.83
MnO	0.11	0.14	0.11	0.10	0.07	0.08	0.39	0.40	0.36	0.02	0.03
NiO	0.36	0.36	0.32	0.05	<dl	0.06	<dl	<dl	<dl	0.23	0.19
ZnO	nd	nd	nd	nd	nd	nd	nd	nd	nd	nd	nd
K_2O	<dl	<dl	<dl	<dl	0.03	<dl	<dl	<dl	<dl	10.35	10.02
Na_2O	<dl	0.05	<dl	2.95	3.31	2.98	0.11	0.08	0.08	0.10	0.60
Cl	nd	nd	nd	nd	nd	nd	nd	nd	nd	0.07	<dl
F	nd	nd	nd	nd	nd	nd	nd	nd	nd	0.33	0.30
total	99.86	100.22	99.85	99.82	99.75	100.31	98.88	99.40	99.21	94.69	94.52
Mg/(Mg+Fe)	0.93	0.92	0.93	0.91	0.91	0.91	0.83	0.83	0.82	0.93	0.92

Representative mineral major element composition [wt. %]

	spl			rut	ilm	
SiO_2	0.10	0.08	<dl	0.05	0.04	0.02
TiO_2	3.51	3.18	3.42	91.81	53.12	47.55
Al_2O_3	8.20	9.50	7.86	0.00	0.26	0.27
Cr_2O_3	53.89	51.04	53.18	3.94	9.17	12.13
V_2O_3	0.00	0.25	0.22	0.09	0.00	0.28
BaO	nd	nd	nd	nd	nd	nd
CaO	nd	nd	nd	nd	0.02	nd
CoO	0.02	nd	nd	nd	0.02	nd
FeO	21.49	22.10	21.50	0.18	24.17	26.02
MgO	12.53	12.79	12.60	0.02	14.13	12.14
MnO	0.19	0.27	0.20	0.00	0.18	0.14
NiO	0.14	0.20	0.18	0.00	0.30	0.31
ZnO	0.09	nd	nd	nd	0.06	nd
total	100.16	99.41	99.15	96.08	101.46	98.87
Mg/(Mg+Fe)	0.57	0.58	0.57	-	-	-
Cr/(Cr+Al)	81.51	78.28	81.95	-	-	-
Ilm	-	-	-	-	0.45	0.46
Gk	-	-	-	-	0.52	0.48

Representative mineral trace element composition [ppm]

	ol			cpx			grt		
Cr	218	233	238	26088	22218	26316	41169	39403	44125
Mn	774	811	817	717	687	702	2896	2967	3143
Co	139	127	127	20.9	20.0	22.4	nd	nd	nd
Ni	3249	2694	2658	402	393	422	63.6	61.3	67.4
Cu	2.42	1.57	1.62	nd	nd	nd	nd	nd	nd
Zn	71.7	66.2	66.3	14.4	11.0	14.1	nd	nd	nd
Ga	0.183	0.122	0.153	nd	nd	nd	17.2	16.2	16.3
Ti	188	212	215	2857	2658	2817	4510	4073	4175
V	4.97	5.67	5.90	324	329	342	284	255	258
Zr	0.333	0.273	0.319	66.9	64.0	53.1	180	141	132
Nb	0.0710	0.0780	0.1106	0.279	0.670	<dl	0.167	0.110	0.168
Hf	<0.100	0.0073	<0.0065	4.41	3.38	3.29	4.02	3.54	2.94
Ta	<0.041	0.0054	0.0057	0.0410	0.0480	<0.066	0.0141	0.0208	<0.0128
La	nd	nd	nd	1.48	2.43	1.62	0.0120	0.0165	0.0290
Ce	<0.041	<0.0025	<0.0028	5.96	8.94	6.06	0.209	0.157	0.186
Pr	nd	nd	nd	1.14	1.66	0.993	0.0743	0.0520	0.0560
Nd	nd	nd	nd	6.79	8.67	6.68	1.01	0.759	0.759
Sm	nd	nd	nd	2.01	2.50	1.67	1.09	1.16	1.12
Eu	nd	nd	nd	0.575	0.690	0.573	0.549	0.598	0.563
Gd	nd	nd	nd	1.75	1.97	1.49	2.83	2.58	2.46
Tb	nd	nd	nd	0.243	<dl	0.195	0.733	0.577	0.587
Dy	nd	nd	nd	0.900	1.04	0.990	6.30	5.55	5.67
Ho	nd	nd	nd	0.129	0.205	0.172	1.54	1.39	1.35
Er	nd	nd	nd	0.312	0.420	<dl	4.71	4.06	4.32
Tm	nd	nd	nd	0.0340	0.0560	<0.054			
Yb	nd	nd	nd	<0.114	<dl	0.189	4.13	4.08	3.64
Lu	nd	nd	nd	<0.021	<dl	0.0320	0.629	0.625	0.500
Sc	1.79	2.38	2.35	30.7	30.0	31.5	84.1	97.4	91.6
Rb	nd	nd	nd	<0.128	<0.142	<0.22	0.0430	<0.063	<0.06
Sr	<0.054	0.0060	<0.0034	103	113	107	0.330	0.198	0.257
Y	<0.058	0.0041	0.0063	3.73	3.96	3.80	36.2	34.3	32.9
Ba	<0.35	<0.0194	<0.0183	0.370	2.70	<dl	<0.089	<0.138	0.252
Th	nd	nd	nd	<0.032	0.0360	0.0860	<0.0050	<0.0121	0.0173
U	nd	nd	nd	<0.0149	<dl	<0.037	0.0128	<0.0125	<0.0137
Li	2.20	2.40	2.36	1.63	1.57	1.41	0.405	0.423	0.386
B	<2.09	0.640	0.369	nd	nd	nd	nd	nd	nd
Al	58.2	64.1	63.2	nd	nd	nd	nd	nd	nd
Ca	<155.67	187	174	IST	IST	IST	IST	IST	IST

Representative mineral trace element composition [ppm]

	spl			rut		ilm
Cr	IST	IST	IST	45566	45168	90503
Mn	1809	1768	1405	8.72	33.1	1597
Co	267	266	218	3.52	8.73	210
Ni	1637	1639	1428	31.7	46.7	3770
Cu	28.2	27.4	20.3	8.67	7.49	40.3
Zn	971	946	997	7.55	20.0	191
Ga	95.2	94.3	89.2	1.02	1.49	23.1
Ti	19784	19784	14619	IST	IST	IST
V	1454	1461	1377	1601	1545	2033
Zr	5.11	5.32	3.48	4241	4267	416
Nb	0.979	1.01	0.914	9266	9426	350
Hf	0.264	0.184	0.199	143	138	17.1
Ta	0.260	0.243	0.122	1401	1423	96.2
Sc	1.87	1.93	1.77	9.38	9.54	29.3
Rb	nd	nd	nd	nd	nd	nd
Sr	nd	nd	nd	nd	nd	nd
Y	<0.0095	<0.0110	<dl	0.0437	0.0310	<0.34
Ba	<0.075	<0.059	3.89	<0.040	<0.086	<1.71
Th	<0.0052	<0.0073	<0.0056	<0.0048	<0.0095	<0.23
U	<0.0143	<0.0059	<dl	2.93	3.02	<0.144
Li	0.967	0.921	0.589	0.585	0.440	3.85
B	nd	nd	nd	nd	nd	nd
Al	48552	48405	45939	1003	1422	5751
Ca	54.0	43.4	72.0	29.2	<40.06	<785.46

DJ0275: wehrlite xenolith, Kimberley, RSA

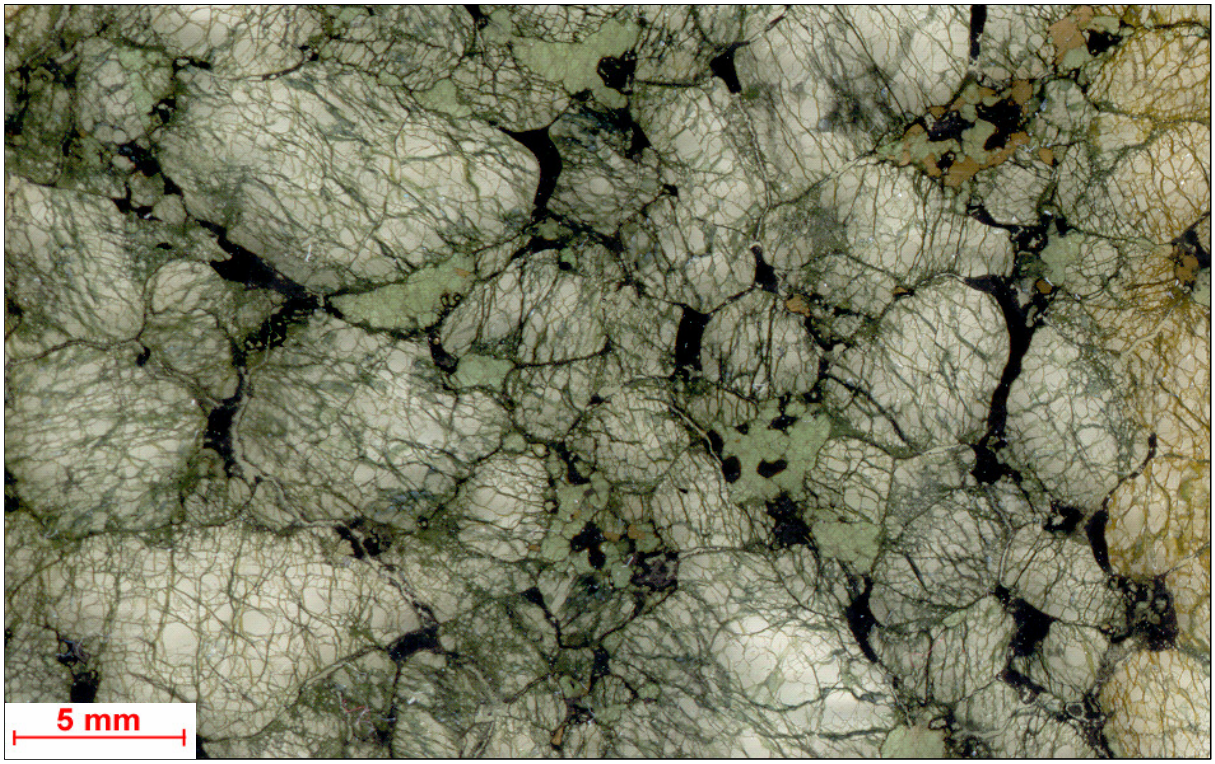

Granular coarse grained wehrlite with 94% olivine (18 mm-220 µm), 5% clinopyroxene (4 mm-200 µm) and 1% phlogopite (2 mm-150 µm) and additionally serpentine. Cpx, phl and serp form elongated patches along grain boundaries.

major elements [wt. %]	**ol**			**cpx**			**phl replacing cpx**		
SiO_2	40.18	40.33	40.29	54.79	54.87	54.80	41.57	41.69	41.32
TiO_2	<dl	<dl	<dl	0.23	0.26	0.21	0.93	0.95	0.89
Al_2O_3	<dl	<dl	0.04	0.99	1.08	1.08	11.53	11.57	11.45
Cr_2O_3	<dl	<dl	<dl	0.82	0.95	0.87	0.19	0.20	0.17
V_2O_3	nd	nd	nd	nd	nd	nd	nd	nd	nd
BaO	nd	nd	nd	nd	nd	nd	0.01	0.00	0.05
CaO	<dl	<dl	<dl	21.83	21.53	21.86	0.01	0.01	0.00
CoO	nd	nd	nd	nd	nd	nd	nd	nd	nd
FeO	11.03	10.72	10.56	2.96	3.09	3.08	3.91	3.77	3.98
MgO	48.58	48.58	48.28	16.67	16.52	16.81	25.05	25.24	25.27
MnO	0.13	0.11	0.14	0.08	0.05	0.11	0.04	<dl	<dl
NiO	0.22	0.23	0.25	<dl	0.05	<dl	0.13	0.14	0.16
K_2O	<dl	<dl	<dl	<dl	<dl	<dl	11.22	10.91	10.93
Na_2O	<dl	<dl	<dl	1.47	1.59	1.48	0.10	0.14	0.21
Cl	nd	nd	nd	nd	nd	nd	0.03	0.03	0.04
F	nd	nd	nd	nd	nd	nd	0.44	0.49	0.51
total	100.14	99.97	99.56	99.85	100.00	100.30	95.14	95.15	94.97
Mg/(Mg+Fe)	0.90	0.90	0.89	0.91	0.91	0.91	0.92	0.92	0.92

Representative mineral trace element composition [ppm]

	ol			**ol rim**			**cpx**			**phl replacing cpx**		
Cr	54.4	52.7	53.2	54.6	54.6	53.5	5633	5144	4863	1312	1237	1333
Mn	1038	1018	1020	1018	1027	991	nd	nd	nd	nd	nd	nd
Co	132	131	130	141	148	127	nd	nd	nd	nd	nd	nd
Ni	1776	1728	1721	1982	2097	1687	190	185	173	921	840	852
Cu	0.599	0.624	0.621	0.680	0.880	0.551	nd	nd	nd	nd	nd	nd
Zn	86.6	86.1	85.0	105	111	83.6	nd	nd	nd	nd	nd	nd
Ga	0.0703	0.0751	0.0947	0.0980	0.100	0.0760	nd	nd	nd	nd	nd	nd
Ti	34.1	23.1	19.5	146	141	150	1703	1661	1736	5726	5891	6079
V	4.22	4.09	4.15	4.06	4.19	4.17	407	411	385	74.5	73.5	71.9
Zr	0.280	0.254	0.241	0.408	0.386	0.371	113	109	120	2.61	4.28	3.05
Nb	0.506	0.615	0.519	0.213	0.293	0.214	0.243	0.272	0.228	5.65	5.49	6.21
Hf	0.0083	0.0099	0.0059	<0.035	<0.042	0.0087	7.18	7.38	7.90	0.111	0.166	0.114
Ta	0.0203	0.0200	0.0193	0.0211	0.0178	0.0140	0.0218	0.0219	0.0237	0.480	0.492	0.512
La	nd	nd	nd	nd	nd	nd	2.54	1.79	2.12	<0.0039	<0.0052	0.0181
Ce	<0.0022	<0.00243	<0.00231	<0.0136	<0.0155	0.0029	11.0	7.29	8.74	<dl	0.0124	0.0575
Pr	nd	nd	nd	nd	nd	nd	2.25	1.48	1.85	0.0017	<0.00236	0.0027
Nd	nd	nd	nd	nd	nd	nd	12.7	8.54	10.7	<dl	<0.024	0.0289
Sm	nd	nd	nd	nd	nd	nd	3.38	2.48	2.87	<0.0070	<0.0171	0.0095
Eu	nd	nd	nd	nd	nd	nd	1.01	0.729	0.865	0.0051	0.0145	<0.0088
Gd	nd	nd	nd	nd	nd	nd	2.69	2.01	2.56	0.0101	<0.0118	<0.0113
Tb	nd	nd	nd	nd	nd	nd	0.336	0.271	0.317	0.0026	<0.00186	0.0004
Dy	nd	nd	nd	nd	nd	nd	1.53	1.38	1.63	<0.0051	<0.0088	<0.0060
Ho	nd	nd	nd	nd	nd	nd	0.196	0.194	0.215	0.0038	0.0029	0.0023
Er	nd	nd	nd	nd	nd	nd	0.388	0.372	0.435	<0.0036	<0.0089	0.0046
Tm	nd	nd	nd	nd	nd	nd	0.0421	0.0356	0.0423	0.0031	<0.00102	<0.00098
Yb	nd	nd	nd	nd	nd	nd	0.186	0.184	0.194	<0.0074	<0.0102	<0.0044
Lu	nd	nd	nd	nd	nd	nd	0.0179	0.0222	0.0170	0.0012	0.0005	<0.00092
Sc	2.30	2.20	2.17	2.24	1.99	2.14	55.6	59.1	54.2	2.86	2.82	2.98
Rb	nd	nd	nd	nd	nd	nd	<0.0086	0.0361	0.0122	764	738	657
Sr	<0.0038	<0.0030	<0.0029	<0.0181	<0.024	0.0036	155	122	123	2.48	2.10	2.64
Y	<0.0033	0.0035	<0.0031	<0.0143	<0.0184	0.0034	4.62	4.28	4.75	<0.0054	0.0071	<0.0114
Ba	<0.0213	<0.0181	<0.0156	<0.136	<0.149	<0.0178	0.0910	0.488	0.0470	116	116	115
Th	nd	nd	nd	nd	nd	nd	0.0160	0.0187	0.0159	0.0157	0.0071	0.0140
U	nd	nd	nd	nd	nd	nd	0.0030	0.0030	0.0036	<0.00164	0.0071	0.0025
Li	2.28	2.22	2.25	1.99	2.08	2.10	nd	nd	nd	nd	nd	nd
B	0.551	0.434	0.340	0.970	<0.77	0.589	nd	nd	nd	nd	nd	nd
Al	13.6	12.4	12.7	13.2	13.2	13.0	nd	nd	nd	nd	nd	nd
Ca	152	135	139	111	131	138	IST	IST	IST	142	176	276

DJ0276: wehrlite xenolith, Kimberley, RSA

Porphyroclastic wehrlite with coarse-grained, well rounded 46% olivine porphyroclasts (15 mm-300 µm), surrounded by 50% fine grained olivine neoblasts (230-15 µm) and schlieren of 3% clinopyroxene (3 mm-250 µm) 1% phlogopite (3 mm-160 µm) and ilmenite (600-5 µm).

Representative mineral major element composition [wt. %]

	ol-pc			**ol-nb**			**cpx**			**phl replacing cpx**	
SiO_2	40.15	40.21	40.32	40.04	40.28	40.32	54.34	54.47	54.39	41.44	41.34
TiO_2	<dl	<dl	<dl	<dl	<dl	<dl	0.28	0.30	0.30	1.17	1.17
Al_2O_3	<dl	<dl	<dl	<dl	<dl	<dl	1.38	1.49	1.47	11.94	11.93
Cr_2O_3	<dl	<dl	<dl	<dl	<dl	<dl	0.93	1.16	2.47	0.25	0.25
V_2O_3	nd	nd	nd	nd	nd	nd	nd	nd	nd	nd	nd
BaO	nd	nd	nd	nd	nd	nd	nd	nd	nd	0.07	0.07
CaO	0.04	<dl	0.03	0.03	0.03	<dl	21.00	20.71	20.10	0.00	0.05
CoO	nd	nd	nd	nd	nd	nd	nd	nd	nd	nd	nd
FeO	10.69	10.85	10.71	10.68	10.74	10.64	3.16	3.30	2.92	3.96	3.91
MgO	48.69	48.38	48.33	48.95	48.81	48.50	16.60	16.33	15.94	24.64	24.64
MnO	0.09	0.08	0.18	0.10	0.11	0.14	0.08	0.07	0.09	0.03	0.01
NiO	0.19	0.27	0.27	0.19	0.21	0.22	0.02	0.02	0.04	0.07	0.10
K_2O	<dl	<dl	<dl	<dl	<dl	<dl	0.01	0.00	0.01	10.94	10.74
Na_2O	<dl	<dl	<dl	<dl	<dl	<dl	1.71	1.78	2.23	0.15	0.14
Cl	nd	nd	nd	nd	nd	nd	nd	nd	nd	0.06	0.04
F	nd	nd	nd	nd	nd	nd	nd	nd	nd	0.52	0.55
total	99.85	99.79	99.85	99.99	100.18	99.82	99.52	99.63	99.95	95.23	94.95
Mg/(Mg+Fe)	0.90	0.90	0.89	0.91	0.90	0.90	0.90	0.90	0.91	0.92	0.92
Ilm	-	-	-	-	-	-	-	-	-	-	-
Gk	-	-	-	-	-	-	-	-	-	-	-

Representative mineral trace element composition [ppm]

	ol-pc			**ol-nb**			**cpx**		
Cr	62.4	61.9	75.6	57.5	55.5	55.0	6672	11047	6339
Mn	952	948	969	872	862	849	605	594	609
Co	135	135	136	142	140	143	20.0	19.6	21.0
Ni	1603	1626	1648	1739	1650	1679	189	192	216
Cu	1.02	1.05	1.12	<0.86	1.49	1.67	nd	nd	nd
Zn	83.6	85.6	85.9	87.2	89.3	88.0	12.3	13.1	13.3
Ga	0.119	0.112	0.114	<0.182	0.147	0.201	nd	nd	nd
Ti	196	190	208	165	155	154	1930	1975	1874
V	4.86	4.79	4.86	4.34	4.1	4.24	408	383	391
Zr	0.378	0.363	0.351	0.431	0.370	0.420	89.5	92.7	88.4
Nb	0.146	0.133	0.169	<0.096	<0.060	0.123	0.202	0.194	0.255
Hf	0.0113	<0.0131	<0.0123	<0.141	<0.117	<0.127	5.62	5.72	4.98
Ta	0.0099	0.0071	0.0091	<0.068	<0.040	<0.045	0.0221	0.0137	<0.049
La	nd	nd	nd	nd	nd	nd	2.42	2.06	2.38
Ce	<0.0044	0.0057	<0.0057	<0.064	<0.041	<0.055	10.1	8.91	10.1
Pr	nd	nd	nd	nd	nd	nd	1.95	1.79	1.96
Nd	nd	nd	nd	nd	nd	nd	11.2	10.0	10.1
Sm	nd	nd	nd	nd	nd	nd	3.15	2.55	3.27
Eu	nd	nd	nd	nd	nd	nd	0.879	0.828	1.02
Gd	nd	nd	nd	nd	nd	nd	2.63	2.20	2.65
Tb	nd	nd	nd	nd	nd	nd	0.297	0.276	0.248
Dy	nd	nd	nd	nd	nd	nd	1.54	1.31	1.52
Ho	nd	nd	nd	nd	nd	nd	0.206	0.190	0.246
Er	nd	nd	nd	nd	nd	nd	0.411	0.358	0.343
Tm	nd	nd	nd	nd	nd	nd	nd	nd	nd
Yb	nd	nd	nd	nd	nd	nd	0.172	0.126	<0.22
Lu	nd	nd	nd	nd	nd	nd	0.0137	0.0199	<0.052
Sc	2.79	2.85	2.48	2.17	2.7	1.72	44.7	48.1	41.0
Rb	nd	nd	nd	nd	nd	nd	<0.0154	<0.0170	<0.176
Sr	0.0047	0.0055	<0.0052	<0.100	<0.064	<0.062	137	151	136
Y	0.0057	<0.0058	0.0101	<0.098	<0.053	<0.057	4.73	4.19	4.35
Ba	<0.037	<0.033	<0.036	<0.55	<0.45	<0.39	<0.044	0.0610	<0.48
Th	nd	nd	nd	nd	nd	nd	0.0137	0.0166	<0.045
U	nd	nd	nd	nd	nd	nd	<0.0035	0.0041	<0.043
Li	2.35	2.30	2.39	2.25	1.56	1.60	0.502	0.640	<1.26
B	0.456	0.700	1.46	<3.30	<2.27	<2.52	nd	nd	nd
Al	23.1	22.7	23.8	19.3	19.0	20.7	nd	nd	nd
Ca	154	128	150	<249.65	<170.87	<189.36	IST	IST	IST

GB0402: Fe-rich dunite xenolith, Kimberley, RSA

Porphyroclastic dunite with 55% coarse olivine porphyroclasts (3.5 – 1.3 mm) surrounded and merging into fine-grained olivine neoblasts (42%; 400 - 55 µm), with 2% phlogopite (750 - 20 µm) and 1% spinel and ilmenite (10 - 5 µm).

Representative mineral major element composition [wt. %]

	ol-pc			**ol-pc**	**ol-nb**			**phl**	
SiO_2	40.81	39.99	40.02	40.46	40.47	40.71	40.40	39.42	39.48
TiO_2	0.02	0.02	0.02	<dl	0.04	0.05	0.03	3.42	3.31
Al_2O_3	<dl	<dl	<dl	<dl	<dl	0.03	<dl	12.51	12.34
Cr_2O_3	<dl	<dl	<dl	<dl	<dl	0.08	0.04	0.64	0.45
V_2O_3	<dl	<dl	<dl	<dl	<dl	<dl	<dl	nd	nd
BaO	nd	nd	nd	nd	nd	nd	nd	<dl	<dl
CoO	<dl	0.05	0.02	0.04	0.02	0.05	0.03	nd	nd
CaO	<dl	<dl	<dl	<dl	0.10	0.06	0.07	<dl	<dl
FeO	11.86	13.34	12.97	11.77	12.58	12.36	12.90	5.17	5.97
MgO	47.37	47.03	46.61	47.54	47.06	47.08	46.80	23.86	24.07
MnO	0.23	0.22	0.18	0.17	0.15	0.14	0.15	<dl	<dl
NiO	0.34	0.14	0.14	0.28	0.39	0.34	0.17	nd	nd
ZnO	<dl	<dl	<dl	<dl	<dl	<dl	0.05	nd	nd
K_2O	<dl	<dl	<dl	<dl	<dl	<dl	<dl	9.95	9.94
Na_2O	<dl	0.04	<dl	<dl	<dl	0.05	<dl	0.40	0.41
Cl	nd	nd	nd	nd	nd	nd	nd	<dl	<dl
F	nd	nd	nd	nd	nd	nd	nd	0.81	0.71
total	100.63	100.82	99.97	100.26	100.81	100.93	100.64	96.18	96.68
Mg/(Mg+Fe)	0.88	0.88	0.87	0.88	0.87	0.87	0.87	0.89	0.88
Cr/(Cr+Al)	-	-	-	-	-	-	-	-	-
Ilm	-	-	-	-	-	-	-	-	-
Gk	-	-	-	-	-	-	-	-	-

Representative mineral major element composition [wt.

	spl		**ilm**		
SiO_2	0.07	0.08	<dl	<dl	<dl
TiO_2	16.08	4.00	52.35	53.35	53.00
Al_2O_3	1.91	1.05	0.10	0.11	0.14
Cr_2O_3	22.63	54.81	1.66	1.87	1.87
V_2O_3	nd	nd	0.11	0.07	0.11
BaO	nd	nd	nd	nd	nd
CoO	<dl	0.03	0.05	0.07	0.05
CaO	<dl	<dl	0.12	0.09	0.08
FeO	47.10	29.39	30.48	30.15	31.21
MgO	9.58	8.77	12.95	13.33	12.58
MnO	0.27	0.20	0.29	0.39	0.35
NiO	0.36	0.16	0.13	0.13	0.12
ZnO	0.08	0.10	<dl	<dl	<dl
K_2O	nd	nd	<dl	<dl	<dl
Na_2O	nd	nd	<dl	<dl	<dl
Cl	nd	nd	nd	nd	nd
F	nd	nd	nd	nd	nd
total	98.07	98.60	98.25	99.55	99.51
Mg/(Mg+Fe)	0.35	0.42	-	-	-
Cr/(Cr+Al)	0.89	0.97	-	-	-
Ilm	-	-	0.45	0.45	0.48
Gk	-	-	0.46	0.47	0.44

Representative mineral trace element composition [ppm]

	ol			**ol-pc**	**ol-nb**		
Cr	34.7	38.5	31.0	217	222	253	236
Mn	1886	1899	1924	1381	1408	1277	1409
Co	155	155	160	173	175	179	175
Ni	1264	1272	1295	2613	2800	3045	2700
Cu	<dl	<dl	<0.71	<dl	2.52	<dl	3.99
Zn	146	158	155	143	149	142	134
Ga	nd	nd	nd	nd	nd	nd	nd
Ti	116	119	111	269	218	233	206
V	2.46	2.44	2.20	4.72	4.02	4.09	3.42
Zr	0.639	0.616	0.522	0.291	<0.14	0.228	0.201
Nb	0.733	0.871	0.734	0.0617	0.0589	<0.04	0.0250
Hf	0.0210	<0.02	0.0205	0.0121	<0.04	<0.04	0.0135
Ta	0.0519	0.0828	0.0378	0.0034	<0.01	<0.01	<0.00
La	nd	nd	nd	nd	nd	nd	nd
Ce	<dl	0.0094	<0.00	0.0141	<0.04	0.0134	<0.00
Pr	nd	nd	nd	nd	nd	nd	nd
Nd	nd	nd	nd	nd	nd	nd	nd
Sm	nd	nd	nd	nd	nd	nd	nd
Eu	nd	nd	nd	nd	nd	nd	nd
Gd	nd	nd	nd	nd	nd	nd	nd
Tb	nd	nd	nd	nd	nd	nd	nd
Dy	nd	nd	nd	nd	nd	nd	nd
Ho	nd	nd	nd	nd	nd	nd	nd
Er	nd	nd	nd	nd	nd	nd	nd
Tm	nd	nd	nd	nd	nd	nd	nd
Yb	<0.01	<0.02	<0.01	<0.02	<0.06	<0.04	0.0085
Lu	nd	nd	nd	nd	nd	nd	nd
Sc	5.62	5.68	5.89	5.44	4.99	5.12	5.37
Rb	<dl	<0.03	<0.03	<0.02	<0.10	<0.08	<0.03
Sr	<dl	0.0241	<0.01	0.0392	<0.14	0.0382	0.0203
Y	nd	nd	nd	nd	nd	nd	nd
Ba	<dl	0.183	<0.05	<0.03	<0.53	0.200	<0.03
Th	nd	nd	nd	nd	nd	nd	nd
U	nd	nd	nd	nd	nd	nd	nd
Li	nd	nd	nd	nd	nd	nd	nd
B	nd	nd	nd	nd	nd	nd	nd
Al	nd	nd	nd	nd	nd	nd	nd
Ca	119	101	106	392	341	351	350

KP0403: Fe-rich dunite xenolith, Kimberley, RSA

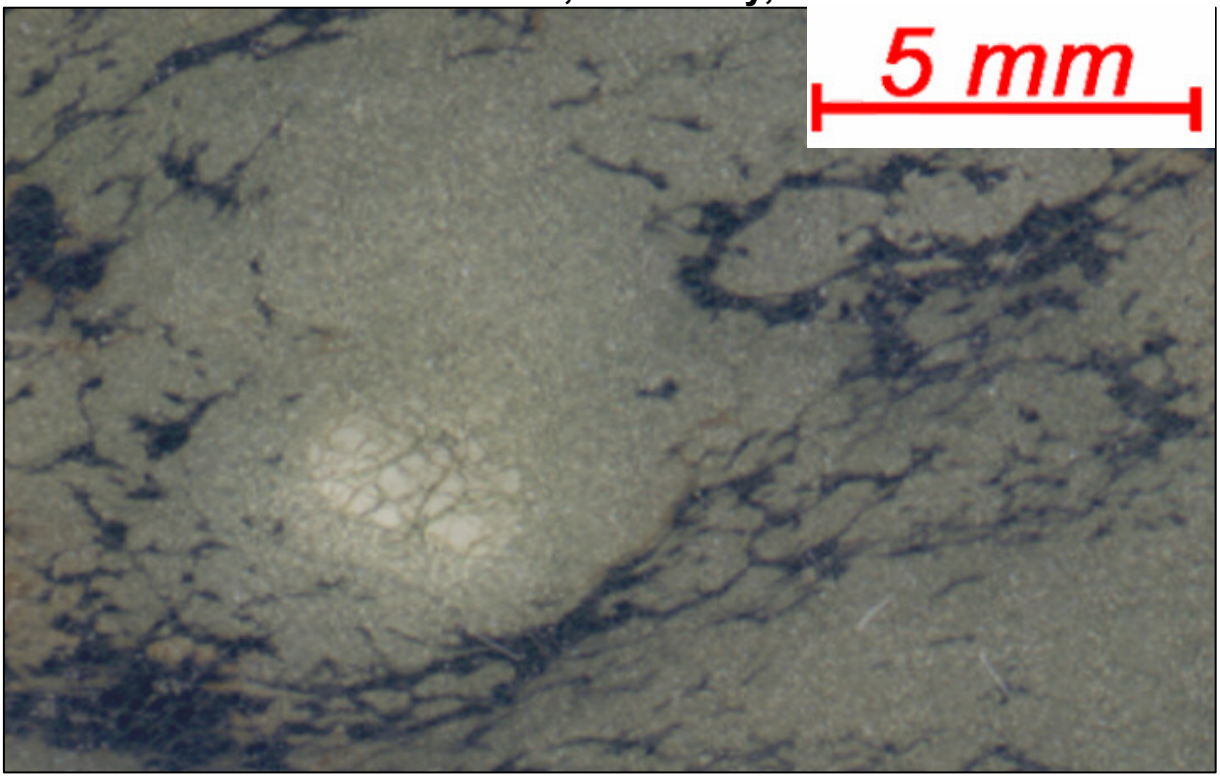

Porphyroclastic dunite with 1% olivine porphyroclasts (1.3 mm) surrounded byolivine neoblasts (76%; 360 - 44 µm), with 1% phlogopite (44- 15 µm) and 22% spinel and ilmenite (3 mm - 20 µm).

Representative mineral major element composition [wt. %]

	ol-pc		ol-nb			phl			spl		
SiO_2	40.56	40.95	40.72	40.59	40.59	39.82	39.54	39.26	0.08	0.08	0.07
TiO_2	0.03	<dl	0.03	0.02	<dl	2.76	3.23	2.96	6.67	5.68	6.18
Al_2O_3	<dl	<dl	<dl	<dl	<dl	13.57	14.20	13.82	10.90	11.17	12.92
Cr_2O_3	0.05	0.03	<dl	0.07	0.06	1.40	1.60	1.34	38.06	39.78	39.49
V_2O_3	<dl	0.04	<dl	<dl	<dl	nd	nd	nd	0.28	0.27	0.23
BaO	nd	nd	nd	nd	nd	0.22	0.15	0.23	nd	nd	nd
CoO	0.02	0.04	0.03	0.05	0.02	nd	nd	nd	0.06	0.05	0.09
CaO	0.04	0.03	0.04	0.05	0.04	<dl	<dl	<dl	<dl	<dl	<dl
FeO	11.79	11.76	11.76	12.23	12.05	4.88	5.18	4.86	32.05	30.68	29.71
MgO	47.85	47.73	47.76	46.74	47.38	23.80	23.07	23.33	11.66	11.53	11.66
MnO	0.17	0.14	0.13	0.15	0.14	0.00	0.00	0.00	0.16	0.21	0.18
NiO	0.16	0.15	0.12	0.38	0.37	nd	nd	nd	0.27	0.29	0.25
ZnO	0.07	<dl	<dl	<dl	<dl	nd	nd	nd	0.11	0.07	0.15
K_2O	<dl	<dl	<dl	<dl	<dl	10.00	9.96	9.66	<dl	<dl	<dl
Na_2O	<dl	<dl	<dl	<dl	<dl	0.39	0.45	0.43	<dl	<dl	<dl
Cl	nd	nd	nd	nd	nd	0.03	0.03	0.03	nd	nd	nd
F	nd	nd	nd	nd	nd	0.51	0.49	0.43	nd	nd	nd
total	100.73	100.86	100.59	100.28	100.66	97.38	97.89	96.35	100.30	99.81	100.93
Mg/(Mg+Fe)	0.88	0.88	0.88	0.87	0.88	0.90	0.89	0.90	0.49	0.50	0.49
Cr/(Cr+Al)	-	-	-	-	-	-	-	-	0.70	0.70	0.67

Major element composition [wt. %]

	ilm		
SiO_2	<dl	0.04	<dl
TiO_2	47.20	47.04	46.49
Al_2O_3	0.98	1.19	1.07
Cr_2O_3	8.88	9.08	9.38
V_2O_3	0.07	0.04	0.04
CoO	0.01	<dl	0.02
CaO	0.02	<dl	<dl
FeO	31.20	30.64	31.42
MgO	11.33	11.31	11.22
MnO	0.14	0.14	0.13
NiO	0.21	0.26	0.24
ZnO	0.28	0.19	0.30
total	100.32	99.93	100.31
Ilm	0.45	0.45	0.44
Gk	0.43	0.43	0.43

Representative mineral trace element composition [ppm]

	ol			ol-nb			phl			spl		
Cr	37.4	32.5	33.9	256	292	306	9405	9351	7368	IST	IST	IST
Mn	1232	1220	1103	972	964	930	nd	nd	nd	1735	1819	1671
Co	133	135	123	180	178	169	nd	nd	nd	303	384	373
Ni	1300	1327	1188	2876	2885	2788	1356	1457	1234	3089	3270	3086
Cu	<0.47	1.00	1.05	3.47	3.56	4.11	nd	nd	nd	63.3	65.1	60.6
Zn	93.1	101	101	119	115	104	nd	nd	nd	<dl	1556	1862
Ga	nd	nd	nd	nd	nd	nd	nd	nd	nd	118	110	121
Ti	103	94.6	96.8	165	124	250	19868	15380	13083	39366	45889	34153
V	3.03	2.97	3.09	4.38	5.06	9.16	127	129	121	1287	1580	1369
Zr	0.534	0.566	<dl	0.750	0.314	<dl	5.75	7.58	7.00	<dl	14.2	10.5
Nb	0.301	0.301	0.396	0.145	0.0841	0.216	14.5	12.2	8.63	<dl	<dl	0.780
Hf	<0.012	0.0238	0.0128	0.0440	<0.012	<dl	0.580	<0.48	0.850	1.01	0.550	<0.78
Ta	0.0299	0.0200	0.0375	0.0360	0.0117	0.0281	3.06	1.11	1.17	<dl	1.33	<0.31
La	nd	nd	nd	nd	nd	nd	<0.107	<0.187	0.26	nd	nd	nd
Ce	<0.0030	0.0244	<dl	0.195	<0.025	<dl	0.197	0.190	0.500	nd	nd	nd
Pr	nd	nd	nd	nd	nd	nd	nd	nd	nd	nd	nd	nd
Nd	nd	nd	nd	nd	nd	nd	<0.51	1.10	0.690	nd	nd	nd
Sm	nd	nd	nd	nd	nd	nd	<0.47	<0.77	<0.70	nd	nd	nd
Eu	nd	nd	nd	nd	nd	nd	0.190	<0.27	0.0280	nd	nd	nd
Gd	nd	nd	nd	nd	nd	nd	0.430	<1.01	<0.37	nd	nd	nd
Tb	nd	nd	nd	nd	nd	nd	nd	nd	nd	nd	nd	nd
Dy	nd	nd	nd	nd	nd	nd	nd	nd	nd	nd	nd	nd
Ho	nd	nd	nd	nd	nd	nd	nd	nd	nd	nd	nd	nd
Er	nd	nd	nd	nd	nd	nd	nd	nd	nd	nd	nd	nd
Yb	<0.0120	0.0034	0.0160	0.0380	<0.0116	0.0260	nd	nd	nd	nd	nd	nd
Lu	nd	nd	nd	nd	nd	nd	<0.074	<0.112	<0.086	nd	nd	nd
Sc	5.27	4.85	4.90	5.62	5.59	5.53	<1.56	3.19	3.23	<5.95	4.39	<4.90
Rb	<0.020	0.0309	<dl	<0.073	0.0670	<dl	652	615	514	nd	nd	nd
Sr	<0.0067	0.112	<dl	0.260	0.175	<dl	27.5	29.2	25.6	nd	nd	nd
Y	nd	nd	nd	nd	nd	nd	<0.112	<0.18	<0.144	<0.45	<0.092	<0.28
Ba	<0.0236	0.207	<dl	<0.55	0.650	<dl	520	451	448	<3.94	0.560	2.35
Th	nd	nd	nd	nd	nd	nd	<0.081	<0.150	0.119	<1.59	<0.044	<0.229
U	nd	nd	nd	nd	nd	nd	<0.058	<0.087	<0.098	<4.53	0.0420	<0.23
Li	nd	nd	nd	nd	nd	nd	3.25	1.76	1.11	<4.16	1.45	<1.89
Al	nd	nd	nd	nd	nd	nd	nd	nd	nd	75990	80262	92835
Ca	157	228	2677	448	343	999	<927.33	<1380.94	<953.64	<899.42	<126.49	<652.74

Trace elements [ppm]

	ilm		
Cr	68052	64272	69525
Mn	1411	1389	1356
Co	221	206	217
Ni	2361	2100	2261
Cu	33.3	27.6	30.9
Zn	177	146	156
Ga	21.2	18.8	20.9
Ti	IST	IST	IST
V	1630	1567	1598
Zr	545	516	508
Nb	418	424	406
Hf	18.3	18.3	18.1
Ta	61.7	75.6	67.3
La	nd	nd	nd
Ce	nd	nd	nd
Pr	nd	nd	nd
Nd	nd	nd	nd
Sm	nd	nd	nd
Eu	nd	nd	nd
Gd	nd	nd	nd
Tb	nd	nd	nd
Dy	nd	nd	nd
Ho	nd	nd	nd
Er	nd	nd	nd
Yb	nd	nd	nd
Lu	nd	nd	nd
Sc	30.5	32.5	30.4
Rb	nd	nd	nd
Sr	nd	nd	nd
Y	0.0850	0.0880	0.0990
Ba	<0.162	<0.103	<0.114
Th	<0.0153	<0.0106	0.0066
U	0.0470	0.0365	0.0417
Li	<0.23	1.86	2.00
Al	7571	6607	7548
Ca	<94.46	71.3	60.9